DARTMOUTH COLLEGE

Thayer School of Engineering

Hanover, New Hampshire

MAGNETOPAUSE STRUCTURE FROM SATELLITE OBSERVATIONS

FINAL TECHNICAL REPORT

NASA GRANT NSG 7292

October 3, 1979

Bengt U. Ö. Sonnerup
Professor of Engineering
Principal Investigator

RADIOPHYSICS LABORATORY

Thayer School of Engineering

DARTMOUTH COLLEGE

Hanover, New Hampshire 03755

MAGNETOPAUSE STRUCTURE FROM SATELLITE OBSERVATIONS

FINAL TECHNICAL REPORT

NASA GRANT NSG 7292

Grant period: Oct 1, 1976 - Sept 30, 1977
(Suppl. #1): Oct 1, 1977 - Sept 30, 1978

Prepared by

Bengt U. Ö. Sonnerup
Professor of Engineering
Principal Investigator

for

National Aeronautics and Space Administration

Scientific and Technical Information Facility

P.O. Box 33, College Park, Maryland 20740

MAGNETOPAUSE STRUCTURE FROM SATELLITE OBSERVATIONS

The scientific results of the study are described in the following publications, and preprints, all of which are reproduced in this report:

1. OGO-5 Magnetopause Structure and Classical Reconnection (B. U. Ö. Sonnerup and B. G. Ledley), J. Geophys. Res., 84, 399-405, 1979.

2. Magnetic Field Reconnection (B. U. Ö. Sonnerup), Chapter III.1.2 in Solar System Plasma Physics, L. T. Lanzerotti, C. F. Kennel, and E. N. Parker, eds., North Holland Publ. Co., pp. 45-108, 1979.

3. Transport Mechanisms at the Magnetopause (B. U. Ö. Sonnerup), in Proceedings of Chapman Conf. on Magnetospheric Substorms and Related Plasma Processes, Los Alamos, Oct. 1978, S.-I. Akasofu, ed., 24 pages; to appear Astrophysics and Space Sci. Library, D. Reidel Publ. Co.

4. Electromagnetic Structure of the Magnetopause and Boundary Layer (B. U. Ö. Sonnerup and B. G. Ledley), in Proceedings of Chapman Conf. on Magnetospheric Boundary Layers, Alpbach, June 1979; European Space Agency Special Publication ESA SP-148, pp. 401-411, August 1979.

5. Structure of Jupiter's Magnetopause (B. U. Ö. Sonnerup, E. J. Smith, B. T. Tsurutani, and J. H. Wolfe), preprint, 33 pages; to be submitted to J. Geophys. Res., 1979.

6. Tearing Modes at the Magnetopause (B. U. Ö. Sonnerup and J. B. Greenly), preprint, 28 pages; to be submitted to J. Geophys. Res., 1979.

Hanover, October 3, 1979

Bengt Sonnerup

Bengt U. Ö. Sonnerup
Professor of Engineering
Principal Investigator

Ogo 5 Magnetopause Structure and Classical Reconnection

B. U. Ö. SONNERUP

Dartmouth College, Hanover, New Hampshire 03755

B. G. LEDLEY

Goddard Space Flight Center, Greenbelt, Maryland 20771

The observations made during one unusual crossing of the magnetopause by the satellite Ogo 5 are compared with the classical reconnection model developed by Levy, Petschek, and Siscoe. The magnetic field observations appear to be generally consistent with this MHD model, although allowance must be made for the fact that the estimated magnetopause thickness was no more than 3.5 ion gyrodiameters. The nature of the finite gyroradius effects in such thin structures is discussed.

INTRODUCTION

More than a decade ago, *Levy et al.* [1964] proposed a magnetohydrodynamic (MHD) model for steady state magnetic field reconnection at the magnetopause which has served as the focus for most subsequent attempts to observationally verify or deny the occurrence of this process near the subsolar point. A great deal of indirect evidence has been found which is compatible with the assumption of dayside reconnection [e.g., *Burch*, 1974]. However, on the whole, direct evidence bearing on the occurrence of dayside reconnection has been more negative than positive. Minimum variance determinations of the magnetic field component perpendicular to the magnetopause [*Sonnerup*, 1976] show that a measurable component is present in a significant number of magnetopause crossings, in agreement with the reconnection model. However, other aspects of the magnetic field structure of the magnetopause predicted by the MHD model are seen only rarely. In general, magnetopause conditions appear to be highly time and/or space variable making the comparison with a steady state theoretical model difficult. The most negative piece of evidence so far has been the absence of energized protons in the plasma boundary layer observed just inside the magnetopause [*Haerendel et al.*, 1978]. As first emphasized by *Heikkila* [1975], energization of the plasma at the magnetopause is an unavoidable consequence of all reconnection models.

It is the purpose of this paper to present the magnetic field record of a single magnetopause crossing which agrees in essential parts with the predictions of the MHD model by Levy et al. and where deviations from that model may be explained in terms of the finite gyroradii of protons. We find the agreement between theory and observation to be sufficiently remarkable to warrant a detailed discussion of this single crossing even though it is an uncommon case. However, it is to be emphasized at the outset that we do not consider this crossing to provide incontrovertible evidence for the occurrence of reconnection, and certainly not for the importance of that process, at the magnetopause. Interconnection of field lines on the two sides of the magnetopause in this crossing is established by the presence of a nonzero normal magnetic field. But reconnection requires in addition that an electric field $E_{\parallel}$ tangential to the magnetopause be present. To prove the occurrence of reconnection, either $E_{\parallel}$ must be measured directly or else the particles energized in this field must be detected. *Mozer et al.* [1978] claim to have detected a substantial nonzero value of $E_{\parallel}$, but it remains to be established whether these results are valid and reproducible.

THE LEVY-PETSCHEK-SISCOE MODEL

A brief review of the main features of the steady state MHD reconnection model is in order. A schematic of the flow and field geometry is shown in Figure 1. Except in the immediate vicinity of the reconnection region, at the center of the figure, the magnetopause consists of a large-amplitude intermediate wave front (Alfvén wave; rotational discontinuity) across which the component of the magnetic field tangential to the front changes direction abruptly. When the magnetosheath field is antiparallel to the earth's field, as assumed in Figure 1, the direction change is by 180°, but in principle the angle change is arbitrary. Simple MHD theory of a one-dimensional steady wave-front structure indicates that the tangential field component rotates with constant magnitude from the magnetosheath to the magnetosphere direction. Since the field normal to the front remains constant, the total magnetic field magnitude is preserved during the field rotation.

MHD theory makes no prediction concerning the sense of rotation of the tangential field. However, kinetic models of the rotational discontinuity, to be discussed at a later point in this paper, indicate that structures of thickness comparable with an ion gyroradius have the electron whistler polarization. But the normal magnetic field component, along which the wave propagates, has opposite sense north and south of the reconnection region, pointing toward the earth in the former case, away from it in the latter (see Figure 1). Thus the electron-whistler polarization implies that when observed by a satellite crossing from the magnetosphere into the magnetosheath, say, the actual sense of rotation of the tangential field vector in a thin magnetopause structure would be clockwise north and counterclockwise south of the reconnection region, assuming the observer is facing the sun.

The magnetosheath plasma flows across the magnetopause at a speed equal to the Alfvén speed based on the normal field component, preserving its density and temperature. As the plasma crosses the magnetopause, the intense magnetic forces, $\mathbf{j} \times \mathbf{B}$, increase its velocity component tangential to that surface by an amount approximately equal to twice the Alfvén speed, based on the tangential field component. Thus the plasma just inside the magnetopause flows nearly tangential to the magnetopause in two high-speed jets directed away from the reconnection region. On the side facing the earth, these jets are terminated by narrow expansion fans of the slow MHD mode

Paper number 8A0981.
0148-0227/79/008A-0981$01.00

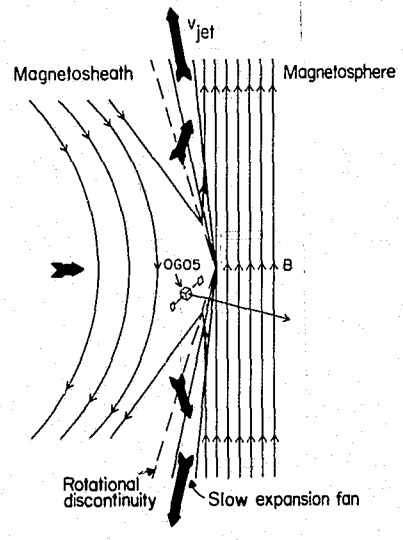

Fig. 1. The Levy-Petschek-Siscoe model of magnetopause reconnection. Inbound crossing of Ogo 5 just south of the reconnection line is shown.

and centered at the reconnection line. As the plasma in the jets flows across these fans, it expands isentropically, i.e., its pressure, density, and temperature gradually decrease to zero, while the magnetic field and the flow speed tangential to the magnetopause increase. The model which in the simple form described above assumes a vacuum magnetosphere, has been analyzed quantitatively by *Yang and Sonnerup* [1977].

Figure 2 shows schematic polar plots of the predicted behavior of the tangential and normal magnetic fields during crossings of the magnetopause and slow expansion fan north and south of the reconnection region when the magnetosheath field is antiparallel to the magnetospheric field. The orientation of the mutually orthogonal axes, labeled B_1, B_2, and B_3, is as follows. The B_1 axis is approximately due north, the B_2 axis is due west, and the B_3 axis is normal to the magnetopause and pointing away from the earth.

Observed Magnetopause Structure

The magnetic field observations to be discussed here were made from the satellite Ogo 5 during the large magnetosphere erosion event on March 27, 1968 [*Aubry et al.*, 1970; 1971], during which the magnetopause traveled inward with the satellite for a period of approximately 2 hours. The total number of clearly identifiable magnetopause crossings during this event exceeded 20, occurring at low solar magnetospheric latitudes in the midmorning sector of the magnetosphere. The structure of these crossings varied greatly, usually bearing little resemblance to the theoretical structure described in the previous section. The crossing to be discussed here is therefore exceptional. It was also studied by *Aubry et al.* [1971; Figure 15], who arrived at conclusions rather different from those to be given here.

A time plot of the magnetic field data from the GSFC magnetometer during the crossing is shown in Figure 3. The magnetic field is presented in terms of its magnitude $|\mathbf{B}|$, solar magnetospheric latitude, θ, and longitude, φ. The crossing from the magnetosheath into the magnetosphere was extremely rapid, the entire magnetopause region being traversed in about 4 s. Presumably this unusually short time is caused by rapid motion of the magnetopause past the satellite. It gives confidence that the satellite may have nearly captured a snapshot of the local magnetic structure of the magnetopause.

The magnetic data for this crossing have been subjected to minimum variance analysis [*Sonnerup and Cahill*, 1967] in order to determine the principal axes of the variance ellipsoid, defined by the matrix

$$M_{\alpha\beta} = \overline{B_\alpha B_\beta} - \overline{B}_\alpha \overline{B}_\beta$$

In this formula an overbar denotes an average over the data set. Also, B_α and B_β ($\alpha, \beta = 1, 2, 3$) are the Cartesian components of an individual measured field vector. The principal axes and the associated unit vectors $\mathbf{N}_1$, $\mathbf{N}_2$, and $\mathbf{N}_3$ correspond to the directions of maximum, intermediate, and minimum variance (λ_1, λ_2, and λ_3) in the corresponding field components, B_1, B_2, and B_3, respectively. When the component B_3 of the field along $\mathbf{N}_3$ remains nearly constant during a crossing and when, additionally, $\lambda_3 \ll \lambda_2$, one may interpret $\mathbf{N}_3$ as the vector normal to the magnetopause and B_3 as the normal magnetic field component. Such an interpretation is not entirely unique but it is consistent with a locally one-dimensional model of the magnetopause structure. In such a model the normal magnetic field component must remain constant as a direct consequence of $\nabla \cdot \mathbf{B} = 0$. Adopting this interpretation, the orientation of the right-handed orthogonal triad ($\mathbf{N}_1$, $\mathbf{N}_2$, $\mathbf{N}_3$) relative to the magnetopause is then approximately as described in the caption of Figure 2.

Results from the minimum variance analysis of five nested data segments within the magnetopause crossing in Figure 3 are shown in Table 1, along with the estimated error ΔB_3 in $\overline{B}_3$, the average value of B_3, and $\Delta \mathbf{N}_3$ in the orientation of $\mathbf{N}_3$, as discussed by *Sonnerup* [1971], *Sonnerup and Ledley* [1974], and *Sonnerup* [1976]. Note that the error estimates do not include systematic errors caused, for example, by spacecraft fields or by changes in the orientation of the boundary during the crossing.

It is seen that the results from all five data segments are consistent in all essential respects. As expected, the estimated errors are large for the innermost data segment 1. However, for the outermost segment 5 they are very small. The high accuracy results principally from the large separation between the smallest and the intermediate eigenvalue, λ_3 and λ_2, respectively. If the estimated vector error in the magnetopause nor-

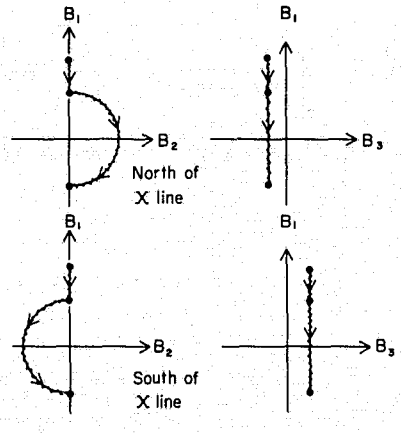

Fig. 2. Predicted polar plots of the magnetic field during magnetopause crossings north and south of the reconnection line. The field components B_1, B_2, and B_3 are directed along the orthogonal right-handed unit vector triad $\mathbf{N}_1$, $\mathbf{N}_2$, $\mathbf{N}_3$. The vectors $\mathbf{N}_1$ and $\mathbf{N}_2$ are tangential to the magnetopause and due approximately north and west, respectively, while $\mathbf{N}_3$ is normal to the magnetopause and points away from the earth.

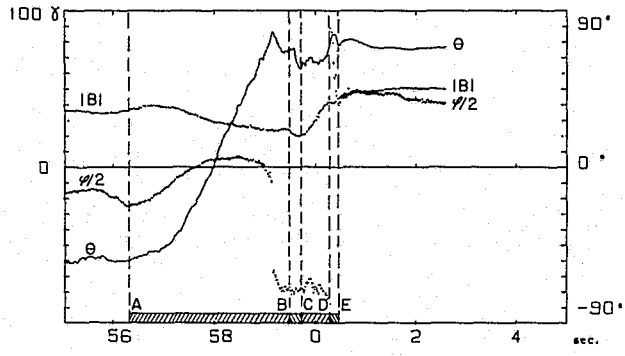

Fig. 3. Time record of the magnetic field during Ogo 5 inbound magnetopause crossing on March 27, 1968, at 1818:58 UT. The magnitude $|B|$ of the field vector and its solar magnetospheric latitude angle θ and longitude angle φ are shown ($\theta > 0$ for fields with a northward component, $\varphi > 0$ for fields with an eastward component). The sampling rate is 56 complete field vector measurements per second. The interval A-E consisting of 240 points comprises data segment 5 in Table 1. Approximate satellite location (GSM): $X \simeq 55000$ km, $Y \simeq -47000$ km, $Z \simeq 4000$ km.

mal vector $\mathbf{N}_3$ is denoted by $\Delta\mathbf{N}_3$ it is seen that $|\Delta\mathbf{N}_3 \cdot \mathbf{N}_1| = 0.01$ rad and $|\Delta\mathbf{N}_3 \cdot \mathbf{N}_2| = 0.03$ rad for data segment 5. Furthermore, $\bar{B}_3 = 8.1 \pm 0.4\ \gamma$ ($1\ \gamma = 1$ nT) for that segment.

We conclude that the minimum variance method in this case yields a very accurate determination of the magnetopause normal vector $\mathbf{N}_3$ and of the average field component $\bar{B}_3$ along it. We also conclude that $\bar{B}_3$ is significantly different from zero, a result also obtained by *Aubry et al.* [1971], using data from the UCLA magnetometer on board Ogo 5. The value of $\bar{B}_3$ obtained by the latter authors was $+12\ \gamma$. The reasons for the difference between this result and the value $+8\gamma$ obtained in our study are not known. However, for nearly half of the magnetopause crossings during the March 27, 1968, event the minimum variance analysis, applied to the zero level corrected GSFC data, yielded normal magnetic field components $|\bar{B}_3| < \Delta B_3$, a result that we think is not random and would be unlikely to occur if large zero level errors or spacecraft fields contaminated the data. The total zero level correction, obtained by comparison with the GSFC rubidium vapor magnetometer, was about 2.5 γ; the spacecraft field is unknown but was about 1 γ during preflight testing. On this basis we are confident that measurement errors contributed less than 2 γ to the total uncertainty in the values of $\bar{B}_3$ determined from the GSFC data. We also emphasize that the differences between the UCLA and GSFC measurements are too small to have a significant influence on the results to be discussed in this paper.

In order to compare the observed magnetopause structure to the predictions of the Levy-Petschek-Siscoe model in Figure 2 we present the data in the principal axis system $\mathbf{N}_1, \mathbf{N}_2, \mathbf{N}_3$, as polar plots of B_1 versus B_2 and B_1 versus B_3. The result is shown in Figure 4. It is seen that the observations bear a striking similarity to the theoretical prediction for a crossing south of the reconnection region. Points A and E correspond to the magnetosheath and the magnetosphere, respectively. The segment A-B in the left-hand diagram in Figure 4 may represent the rotational discontinuity in which the tangential field vector rotates by approximately 180°. Note that the field magnitude does not remain constant during the rotation. The interval B-C, where the tangential field undergoes little direction and magnitude change, may correspond to the traversal of the narrow wedge of uniform flow and field immediately on the magnetospheric side of the rotational discontinuity. The interval C-D may correspond to the slow expansion fan in which the field magnitude increases with little change in field direction. The segment D-E, in which the field magnitude remains more or less constant but the field direction adjusts to the final magnetospheric orientation at E, has no counterpart in the MHD model.

Note that the polar plot of the tangential field in Figure 15 of *Aubry et al.* [1971] shows only a portion of the field rotation (A-B). Mainly on the basis of the changing field magnitude in the rotation, these authors concluded that (A-B) was not a rotational discontinuity.

The time durations of the various portions of the crossing are listed in Table 2. It is seen that the segment A-B occupies the largest portion of the total crossing time. On the basis of the normal vector orientations, *Aubry et al.* [1971, Figure 16] have interpreted this crossing and one occurring about 2 min earlier [see *Aubry et al.*, 1971, Figure 13] as being the result of a broad indentation in the magnetopause, traveling tailward along the surface with a speed comparable with the magnetosheath flow speed, V_0. In such a model the angle between the flow vector, taken to be tangential to the average magnetopause, and $\mathbf{N}_3$ is about 55°. Thus the thickness δ of any portion of the magnetic field record of duration Δt is

$$\delta = V_0(\cos 55°)\Delta t$$

The last column in Table 2 lists the thicknesses of the various magnetopause segments calculated from this formula and with $V_0 = 200$ km/s. On this basis, it is seen that the total thickness of the entire magnetopause region is about 470 km, an estimate that exceeds the one given by Aubry et al. by a factor of 2. This discrepancy derives from the use of different total crossing time Δt.

With a proton gyroradius of about 70 km, say, the entire crossing is no more than 3–4 gyrodiameters thick. The individual features B-C, C-D, and D-E have thicknesses less than this gyroradius but much greater than the electron gyroradius. In such circumstances one might expect considerable deviations

TABLE 1. Results of Minimum Variance Analysis of the GSFC Magnetic Data From the Ogo 5 Magnetopause Crossing on March 27, 1968, 1818:58 UT

Segment	Number of **B** Vectors	Eigen Values, γ^2			Normal Field	Error in $\mathbf{N}_3$	
		λ_1	λ_2	λ_3	$\bar{B}_3 \pm \Delta B_3, \gamma$	$\Delta\mathbf{N}_3 \cdot \mathbf{N}_1$	$\Delta\mathbf{N}_3 \cdot \mathbf{N}_2$
1	48	76	1.5	0.15	3.4 ± 3.4	0.02	0.13
2	96	267	23	0.58	10.0 ± 1.2	0.02	0.06
3	144	463	83	1.3	8.1 ± 0.7	0.02	0.04
4	192	570	124	1.6	8.0 ± 0.5	0.02	0.03
5	240	722	130	1.9	8.1 ± 0.4	0.01	0.03

The five nested data segments are centered at 65938239 ms UT.
Fifty-six vector samples per second.

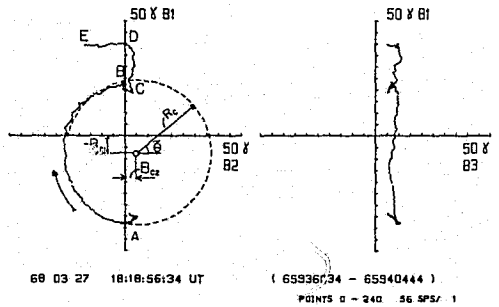

Fig. 4. Polar plots of the observed magnetic field for the Ogo 5 magnetopause crossing on March 27, 1968, at 1818:58 UT. Format is the same as that in Figure 2, and the curves should be compared with the predicted curves for a crossing south of the reconnection line. The dashed circular arc, of radius R_c and centered at (B_{c_1}, B_{c_2}), represents the best fit of (10) to the data segment A-B. Data segment 5 in Table 1 is plotted. The components of the vectors $\mathbf{N}_1$, $\mathbf{N}_2$, and $\mathbf{N}_3$ on the GSM Cartesian axes (X, Y, Z) are (−0.3794, 0.1470, 0.9135), (−0.8467, −0.4532, −0.2787), and (0.3730, −0.8792, 0.2964), respectively.

from simple MHD theory. The principal observed discrepancies are (1) the field magnitude does not remain constant during the 'rotational discontinuity' (A-B) and (2) there is a field direction change (D-E) at the inner edge of the 'slow expansion fan' (C-D). These effects are discussed in the next two sections.

Structure of the Rotational Discontinuity

By considering the conservation laws across a rotational discontinuity, *Hudson* [1970, 1971, 1973] has shown that in a plasma with nonisotropic pressure the magnetic field magnitude and the plasma state need not remain unchanged across the discontinuity. On the other hand, the quantity $(p_\perp + B^2/2\mu_0)$ does remain constant, from which we conclude that in the present case the pressure $p_\perp$ perpendicular to the magnetic field must increase by $\Delta p_\perp = 3.6 \times 10^{-10}$ N/m² as the magnetosheath plasma flows across the rotational discontinuity. At a nominal density of 30 particles per cubic centimeter such a pressure increase would correspond to an increment $\Delta T_\perp = 0.9 \times 10^6$ °K in the perpendicular temperature $T_\perp$, which does not seem unreasonable. In reality the density as well as the temperature would change across such a discontinuity.

Unless particle reflections from the downstream side are important, an increase in the perpendicular pressure across a rotational discontinuity requires nonadiabatic particle behavior and may occur as a result of the scattering of particles off fluctuating electromagnetic fields or as a result of steep magnetostatic field gradients. Hudson's analysis does not yield any information about the internal structure of a rotational discontinuity, but neither of the above effects is likely to be important unless the thickness of the discontinuity is small as it is indeed observed to be in the present case. Unfortunately, no adequate self-consistent theory seems to exist for rotational discontinuities with thickness of the order of the ion gyrodiameter. However, even if such a theory did exist, it would probably not be directly applicable to the present case. Indeed, it is unlikely that even Hudson's jump conditions should be used across the segment A-B. The reason is that the extreme proximity of the slow expansion fan (segment C-D in Figure 4) to the rotational discontinuity (A-B) is bound to influence the structure of both. Some ions will spend part of a gyro orbit in the rotational discontinuity and another part in the expansion fan, so that conditions in the segment B-C do not approach the gyrotropic equilibrium assumed in deriving Hudson's jump conditions.

Clearly then, it is not justifiable to treat the various segments of the crossing as separate entities. Nevertheless, it is useful to consider the following 'pseudotheory' which probably contains the essential ingredients which influence the magnetic structure of a thin rotational discontinuity.

Let us adopt a one-dimensional model of the rotational discontinuity in which

$$\mathbf{B} = (B_1(x_3), B_2(x_3), B_3)$$

$$\mathbf{E} \simeq 0$$

and in which the plasma flows across the current layer from the magnetosheath into the magnetosphere. The frame of reference chosen for this analysis is such that the flow is exactly antiparallel to the magnetic field on both sides of the discontinuity. In the satellite frame this is not the case, and in that frame $\mathbf{E} \neq 0$. However, nonrelativistically, the magnetic field is the same in both frames. Note that the x_3 axis points from the magnetosphere outward into the magnetosheath, so that the plasma flow has a component in the negative x_3 direction. We also assume the electrons to be cold so that they move through the magnetopause by sliding exactly along the magnetic field lines. In other words, we assume that the electron length scales and drifts are unimportant in establishing the structure of the field rotation (A-B). It then follows that the electron current may be written

$$\mathbf{j}_e = ne v_e \mathbf{B}/|\mathbf{B}| \qquad (1)$$

where n, v_e, and $\mathbf{B}$ are the local electron density, electron speed, and magnetic field, respectively, and where e is the magnitude of the electron charge. Conservation of electrons yields

$$j_{e_3} = nev_eB_3/|\mathbf{B}| = \text{const} = n_0ev_0B_3/|\mathbf{B}_0| \qquad (2)$$

when n_0, v_0 and $\mathbf{B}_0$ are the electron density, electron velocity, and magnetic field, respectively, in the magnetosheath. Note that B_3 is constant, that the number density of protons is everywhere the same as that of electrons, and that the velocity v_0 in the magnetosheath is common to protons and electrons, so that the net current in the x_3 direction vanishes. Equation (2) may be solved for $nev_e/|\mathbf{B}|$, and when the result is substituted into (1) there results

$$\mathbf{j}_e = n_0ev_0\mathbf{B}/|\mathbf{B}_0| \qquad (3)$$

The proton current is more complicated to deal with. For layers that are much thicker than the proton gyroradius the proton motion consists of the guiding centers sliding along the field lines, thus effectively canceling the electron current given above, but with first-order drifts across the field lines which

TABLE 2. Time Duration Δt and Thickness δ of Various Segments of the Magnetopause Crossing

Segment	Δt, s	δ, km
A–B	3.12	358
B–C	0.24	28
C–D	0.56	64
D–E	0.20	23
A–E	4.12	473

See Figures 3 and 4.
The thickness is calculated from the formula $\delta = V_0(\cos 55°)\,\Delta t$ with $V_0 = 200$ km/s.

then account for the net current. Structures of this type have been analyzed by *Su and Sonnerup* [1968]. For layers of thickness comparable with the ion gyroradius, one expects only a partial cancellation of the electron current plus a drift current parallel to the layer which is much larger than that described by first-order orbit theory and which exhibits much less detailed spatial structure across the layer. Denoting the latter current by j_p and accounting for the partial cancellation of the electron current by the factor k ($0 < k \leq 1$), the two nontrivial components of Ampère's law become

$$\mu_0 j_1 = -\frac{\partial B_2}{\partial x_3} = \mu_0(j_{p_1} + kn_0ev_0B_1/|\mathbf{B}_0|)$$
$$\mu_0 j_2 = \frac{\partial B_1}{\partial x_3} = \mu_0(j_{p_2} + kn_0ev_0B_2/|\mathbf{B}_0|) \tag{4}$$

where μ_0 is the permeability of free space. These two equations may be combined into the complex form

$$\frac{dB_t}{dx_3} + i\alpha\mu_0 B_t = -i\mu_0 j_{pt} \tag{5}$$

where $i \equiv (-1)^{1/2}$, $\alpha \equiv kn_0ev_0/|\mathbf{B}_0|$, and

$$B_t = B_1 + iB_2$$
$$j_{pt} = j_{p1} + ij_{p2} \tag{6}$$

If we consider j_{pt} as a known nonhomogeneous term in the linear equation (5) for B_t, we find the following solution to that equation:

$$B_t = (\exp -i\alpha\mu_0 x_3)\left\{B_{mt} - \mu_0 i\int_0^{x_3} j_{pt}(x)(\exp i\alpha\mu_0 x)\,dx\right\} \tag{7}$$

where B_{mt} is the complex field at $x_3 = 0$.

The following observations should be made concerning the formula (7):

1. The complex exponential multiplying the right-hand side describes rotational behavior of the magnetic field vector in the B_1B_2 plane with a nonconstant field magnitude given by the parentheses. The sense of the rotation of the field vector is the same as the one observed in the magnetopause crossing examined in this paper. It also agrees with earlier observations [*Sonnerup and Cahill*, 1968; *Sonnerup and Ledley*, 1974] and with the theory of *Su and Sonnerup* [1968]. Clearly, this polarization is the direct result of the electron current flowing along the magnetic field.

2. The rotation of the field vector is periodic rather than aperiodic. Thus the solution obtained describes an infinite stationary wave rather than an isolated rotational discontinuity. However, by assuming that approximately one half period of this wave can be used to describe the structure of a rotational discontinuity in which the field rotates by 180°, one obtains a thickness δ given by

$$\delta \simeq \frac{\pi}{\mu_0\alpha} = \pi\frac{|\mathbf{B}_0|}{\mu_0 n_0 ev_0 k} = \pi\frac{v_{A_0}}{v_0}\frac{\lambda_i}{k} \tag{8}$$

where v_{A_0} is the Alfvén speed in the magnetosheath and λ_i is the ion inertial length, i.e.,

$$\lambda_i = (m_i/\mu_0 n_0 e^2)^{1/2} \tag{9}$$

Since apart from the correction factor for nonisotropic pressure, $v_0 \simeq v_{A_0}$, one concludes that the lower limit for the thickness of the rotational discontinuity is of the order of $\pi\lambda_i$, i.e., about 132 km for $n_0 = 30$ cm^{-3}. This occurs when $k = 1$. As k decreases below unity, the thickness gradually increases. For $n_0 \simeq 30$ cm^{-3} the thickness $\delta_{AB} = 358$ km given in Table 2 is obtained with $k = 0.37$.

It may be added that the greatest difficulty in developing self-consistent Vlasov theory or two-fluid theory of the rotational discontinuity is associated with obtaining aperiodic solutions. Exact solutions for infinite wave trains have been known for a number of years [*Bell*, 1965; *Lutomirski and Sudan*, 1966; *Sonnerup and Su*, 1967; *Abraham-Shrauner and Feldman*, 1977]. The only known aperiodic solutions are those obtained by *Eastwood* [1972, 1974] by numerical integration of the Vlasov-Maxwell equations. They are restricted to the firehose limit so that no net flow of the plasma across the layer takes place. Further, the magnetic field component B_2 is identically zero. An aperiodic adiabatic solution again with zero net flow but with $B_2 \neq 0$ has been given by *Francfort and Pellat* [1976]. Oblique cold plasma whistler soliton solutions are also known [e.g., *Kellogg*, 1964], but these only allow field rotations of exactly 2π.

3. One may attempt to make further use of (7) by assuming the complex proton current to be approximately constant and equal to $\bar{j}_{pt}$ in the rotational discontinuity. One then finds

$$B_t = -\bar{j}_{pt}/\alpha + (B_m + \bar{j}_{pt}/\alpha)\exp(-i\alpha\mu_0 x_3) \tag{10}$$

In the B_1B_2 plane this formula is represented by a circle of radius $R_c = (B_m + \bar{j}_{pt}/\alpha)$ centered at $B_{c_1} = -\bar{j}_{p_1}/\alpha$, $B_{c_2} = -\bar{j}_{p_2}/\alpha$. The best fitting circle, shown by a dashed curve in Figure 4, is centered at $B_{c_1} = -8\ \gamma$, $B_{c_2} = +5\ \gamma$, so that with $\alpha \equiv kn_0ev_0/|\mathbf{B}_0|$ and $|\mathbf{B}_0| = 39\ \gamma$

$$\bar{j}_{p_1} = 0.21\, n_0ev_0k$$
$$\bar{j}_{p_2} = -0.13\, n_0ev_0k \tag{11}$$

In the field given by (10) the curvature drift current derived from first-order orbit theory may be shown to be

$$j_{p_{\text{drift}}} \equiv j_{p_1} + ij_{p_2} = \frac{nm_iv_{\parallel}^2B_3^2}{B^4}R_c\alpha\mu_0\exp(-i\alpha\mu_0 x_3) \tag{12}$$

where $v_{\parallel}$ is the ion velocity along $\mathbf{B}$ and the angle $\tilde{\theta} = \alpha\mu_0 x_3$ is shown in Figure 4. In calculating the average proton current $\bar{j}_p$ from this expression by integration over x_3, it is seen that $\bar{j}_{p_1}$ and $\bar{j}_{p_2}$ are proportional to the averages of $(\cos\tilde{\theta})/B^4$ and $(-\sin\tilde{\theta})/B^4$, respectively. Thus it is seen that $\bar{j}_{p_2}$ is negative regardless of the variation of B^4 with $\tilde{\theta}$, while $\bar{j}_{p_1} = 0$ when $B_{c_1} = 0$, and $\bar{j}_{p_1} > 0$ when $B_{c_1} < 0$. We conclude that the directions of the proton current components given in (11) are compatible with the directions expected from the first-order curvature current. The magnitude of the first-order drift current is far less than that given by (11), which is not surprising. Computer simulations of particle orbits in thin rotational discontinuities show that protons may become semitrapped and execute meanderlike orbits with very large displacements parallel to the layer.

The present model in which j_{pt} is constant within the layer and then changes abruptly to zero at the edges is by necessity crude. Thus we do not wish to overemphasize the importance of the detailed agreement between the circle and the measured segment (A-B) in Figure 4.

4. It would appear that the present model does not preclude the occurrence of an electric field E_3 along the x_3 direction within the current layer. Such a field may be produced by miniscule deviations from charge neutrality in the layer. It leads to $\mathbf{E} \times \mathbf{B}/B^2$ drifts of both electrons and ions but not to any additional currents. *Su and Sonnerup* [1968] have shown

that in the approximation of first-order orbit theory, $E_3 \neq 0$ must occur in a rotational discontinuity in a hot plasma.

EDGE CURRENT

Given the extreme thinness of the segment C-D (see Table 2), it would be unreasonable to expect the MHD theory of slow expansion fans to represent accurately the structure of this portion of the magnetopause. In the interpretation offered in this paper the reason for the small thickness is that the crossing occurred very close to the reconnection line. In this low-latitude region of space, one might also expect finite gyroradius effects at the magnetospheric edge of the expansion fan: the protons will penetrate approximately a proton gyroradius further into the magnetospheric field than the electrons. Since in the reconnection model the plasma in the expansion fan is moving away from the reconnection line nearly parallel to the magnetopause, a proton current due south would occur at the inner edge of the expansion fan C-D in Figure 4. This current is expected to induce a magnetic field component along the negative B_2 direction on the magnetospheric side, as is indeed observed in segment D-E. The magnitude of this field component is seen to be $\Delta B_2 \simeq 21\ \gamma$. In the edge-current model described above we have

$$\Delta B_2 = \tfrac{1}{2}\mu_0 n_D e v \delta_{DE} \tag{13}$$

where δ_{DE} is the thickness of the segment D-E and it has been assumed that the particle density n of the streaming plasma rises linearly from zero at the magnetospheric edge (point E in Figure 4) to the value n_D at the point D.

The small difference in field magnitude between points A (39 γ) and E (44 γ) indicates that a substantial amount of magnetospheric plasma is also present. However, this plasma is nearly stagnant and does not contribute substantially to the edge current. With $\delta_{DE} = 23$ km and $v = 900$ km/s, the latter number being taken from the compressible magnetopause reconnection model of *Yang and Sonnerup* [1977], (13) yields $n_D = 10\ \text{cm}^{-3}$. For a very thick expansion fan (C-D), one might expect $n_D \simeq 0$. However, in view of the thinness of the entire fan and edge current layer, $\delta_{CD} + \delta_{DE} \simeq 87$ km, a density of 10 cm^{-3} at point D does not seem unreasonable.

Parker (1967*a*, *b*) has discussed the generation of a transverse magnetic field component in the magnetopause when the plasma is streaming along the field. This effect, which has been analyzed quantitatively by *Su and Sonnerup* [1971, Figure 4], is in all essential respects equivalent to the edge effect discussed here.

It should also be noted that the above discussion is relevant only very near the reconnection line. At higher latitudes the magnetic field configuration is such that the magnetosheath electrons may penetrate deeper into the magnetosphere than the protons, simply by flowing along the magnetic field lines (see Figure 1). Such a situation would lead to an induced field ΔB_2 of the opposite sign.

CONCLUSION

As is evident from the previous discussion, it is not entirely appropriate to analyze the present crossing in terms of separate MHD structures such as a rotational discontinuity and a slow expansion fan separated by a wedge of uniform flow and field. The total thickness of the crossing is too small for such a procedure to be acceptable, and the crossing should be considered as a single unit. For example, the 'expansion fan' segment (C-D) appears to be a recovery from the weak magnetic field at the inner edge (B) of the rotational segment (A-B) rather than an actual increase in field magnitude above the magnetosheath level as is assumed in the Petschek model. Nevertheless, if one asks what magnetopause structure should be expected at a location south of, but very near, the reconnection line of a standard MHD reconnection model, then one answer, a reasonable one, would be in terms of a structure of the type discussed in this paper. In other words, the observed crossing may be thought of as an embryonic Petschek-type structure which at larger distances from the reconnection line evolves into a full-fledged MHD magnetopause reconnection configuration.

The preceding arguments do not imply that one should think of reconnection as occurring in a quasi-steady fashion over the entire frontside of the magnetosphere. Rather, it is tempting to suggest that reconnection was confined to the tailward-convecting magnetopause indentation associated with this crossing and the one immediately preceding it (which, however, had a much smaller normal magnetic field component, $B_3 = -2.7\ \gamma$) and that the indentation itself was the direct result of local erosion of the magnetosphere caused by reconnection.

Finally, it is noted that the magnetopause structure observed for the crossing discussed here appears sufficiently laminar so that it would be worthwhile to attempt a self-consistent particle field simulation of this structure on the computer. Such a simulation would give a valuable check of the magnetopause thickness and it would indicate whether a time-independent equilibrium is in fact possible.

Acknowledgments. This research was supported by the National Aeronautics and Space Administration under grant NSG 7292 and by the Atmospheric Research Section, National Science Foundation, under grant ATM74-08223A01 to Dartmouth College.

The Editor thanks S. W. H. Cowley and P. D. Hudson for their assistance in evaluating this paper.

REFERENCES

Abraham-Schrauner, B., and W. C. Feldman, Nonlinear Alfvén waves in high-speed solar wind streams, *J. Geophys. Res., 82,* 618, 1977.

Aubry, M. P., C. T. Russell, and M. G. Kivelson, On inward motion of the magnetopause preceding a substorm, *J. Geophys. Res., 75,* 7018, 1970.

Aubry, M. P., M. G. Kivelson, and C. T. Russell, Motion and structure of the magnetopause, *J. Geophys. Res., 76,* 1673, 1971.

Bell, T. F., Nonlinear Alfvén waves in a Vlasov plasma, *Phys. Fluids, 8,* 1829, 1965.

Burch, J. L., Observations of interactions between interplanetary and geomagnetic fields, *Rev. Geophys. Space Phys., 12,* 363, 1974.

Eastwood, J. W., Consistency of fields and particle motion in the 'Speiser' model of the current sheet, *Planet. Space Sci., 20,* 1555, 1972.

Eastwood, J. W., The warm current sheet model and its implications on the temporal behavior of the geomagnetic tail, *Planet. Space Sci., 22,* 1641, 1974.

Francfort, P., and R. Pellat, Magnetic merging in collisionless plasmas, *Geophys. Res. Lett., 8,* 433, 1976.

Haerendel, G., G. Paschmann, N. Sckopke, H. Rosenbauer, and P. C. Hedgecock, The frontside boundary layer of the magnetosphere and the problem of reconnection, *J. Geophys. Res., 83,* 3195, 1978.

Heikkila, W. J., Is there an electrostatic field tangential to the dayside magnetopause and neutral line?, *Geophys. Res. Lett., 2,* 154, 1975.

Hudson, P. D., Discontinuities in an anisotropic plasma and their identification in the solar wind, *Planet. Space Sci., 18,* 1611, 1970.

Hudson, P. D., Rotational discontinuities in an anisotropic plasma, *Planet. Space Sci., 19,* 1693, 1971.

Hudson, P. D., Rotational discontinuities in an anisotropic plasma, II, *Planet. Space Sci., 21,* 475, 1973.

Kellogg, P. J., Solitary waves in cold collisionless plasma, *Phys. Fluids, 7,* 1555, 1964.

Levy, R. H., H. E. Petschek, and G. L. Siscoe, Aerodynamic aspects of the magnetospheric flow, *AIAA J., 2,* 2065, 1964.

Lutomirski, R. F., and R. N. Sudan, Exact nonlinear electromagnetic whistler modes, *Phys. Rev., 147,* 156, 1966.
Mozer, F. S., R. B. Torbert, U. V. Fahleson, C.-G. Fälthammar, A. Gonfalone, A. Pedersen, and C. T. Russell, Direct observation of a tangential electric field component at the magnetopause, submitted to *Geophys. Res. Lett.*, 1978.
Parker, E. N., Confinement of a magnetic field by a beam of ions, *J. Geophys. Res., 72,* 2315, 1967*a*.
Parker, E. N., Small-scale nonequilibrium of the magnetopause and its consequences, *J. Geophys. Res., 72,* 4365, 1967*b*.
Sonnerup, B. U. Ö., Magnetopause structure during the magnetic storm of September 24, 1961, *J. Geophys. Res., 76,* 6717, 1971.
Sonnerup, B. U. Ö., Magnetopause and boundary layer, in *Physics of Solar Planetary Environments* edited by D. J. Williams, p. 541, AGU, Washington, D. C., 1976.
Sonnerup, B. U. Ö., and L. J. Cahill, Jr., Magnetopause structure and attitude from Explorer 12 observations, *J. Geophys. Res., 72,* 171, 1967.
Sonnerup, B. U. Ö., and L. J. Cahill, Jr., Explorer 12 observations of the magnetopause current layer, *J. Geophys. Res., 73,* 1757, 1968.
Sonnerup, B. U. Ö., and B. G. Ledley, Magnetopause rotational forms, *J. Geophys. Res., 79,* 4309, 1974.
Sonnerup, B. U. Ö., and S.-Y. Su, Large amplitude whistler waves in a hot collision-free plasma, *Phys. Fluids, 10,* 462, 1967.
Su, S.-Y., and B. U. Ö. Sonnerup, First-order orbit theory of the rotational discontinuity, *Phys. Fluids, 11,* 851, 1968.
Su, S.-Y., and B. U. Ö. Sonnerup, On the equilibrium of the magnetopause current layer, *J. Geophys. Res., 76,* 5181, 1971.
Yang, C.-K., and B. U. Ö. Sonnerup, Compressible magnetopause reconnection, *J. Geophys. Res., 82,* 4, 1977.

(Received July 7, 1978;
revised August 28, 1978;
accepted September 8, 1978.)

CHAPTER III.1.2

MAGNETIC FIELD RECONNECTION

Bengt U.Ö. SONNERUP

Radiophysics Laboratory, Dartmouth College, Hanover, New Hampshire 03755, USA

Solar System Plasma Physics. Volume III
Edited by L.T. Lanzerotti, C.F. Kennel and E.N. Parker

Contents

1. Introduction

Magnetic-field reconnection has been proposed as a basic energy-conversion process which may occur in many parts of the universe. Its primary function in the cosmic scheme is to prevent the build up of excessive amounts of magnetic energy in association with intense electric current sheets formed in highly conducting plasmas. The reconnection process is thought to cause a relaxation of such configurations, either partially or completely, and either continuously or sporadically, toward their lowest energy (current-free) state. The magnetic energy released during reconnection is converted into kinetic and internal energy of the plasma. The process causes the transfer of magnetic flux and plasma from topological cells with excessive flux to cells deficient in flux. This fact provides the basis for a precise definition of reconnection to be given in subsect. 3.4. Reconnection is also often referred to as magnetic field merging or magnetic field annihilation but, as will be seen, the three terms should not be used synonymously.

Figures 1–5 show examples of cosmic current sheets where reconnection may occur. Figure 1 represents the field produced by two photospheric dipoles which gradually move toward each other [94]. In the absence of reconnection, a current sheet of increasing length forms between the dipoles in the highly conducting solar

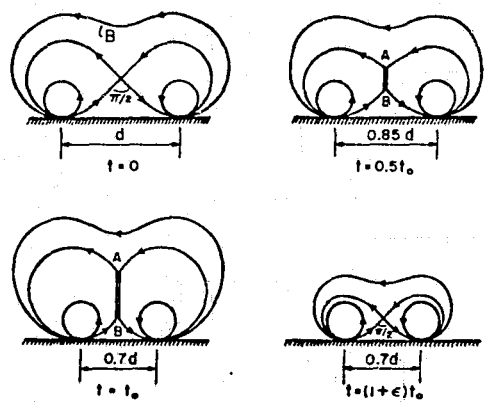

Fig. 1. Qualitative time sequence for two dipoles moving toward each other on the solar surface. A current sheet A–B develops during time $0 < t < t_0$. Rapid reconnection sets in at $t = t_0$ and relaxes the configuration toward a potential field in the short time ϵt_0.

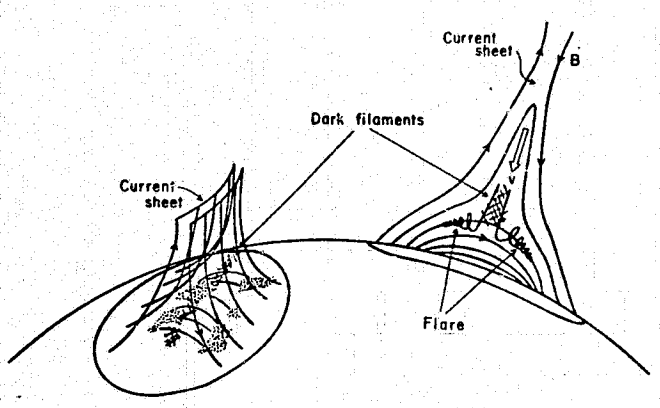

Fig. 2. Current-sheet formation caused by stretching of magnetic loop on the sun (after Carmichael [14]).

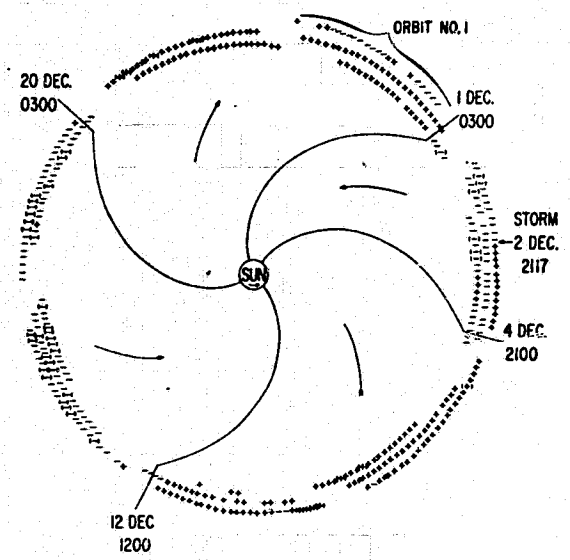

Fig. 3. Sector structure of the interplanetary magnetic field in the ecliptic plane as observed by IMP-1 in 1963. Positive and negative signs indicate the direction of the measured interplanetary magnetic field away and toward the sun, respectively (Wilcox and Ness [123]). The regions of inward and outward fields are separated by a current sheet which intersects the ecliptic along the four spiral lines. (Copyright by American Geophysical Union, 1965.)

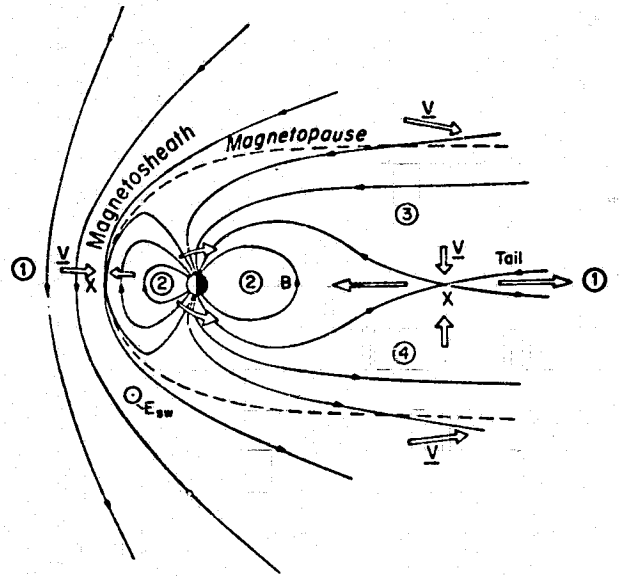

Fig. 4. The earth's magnetosphere with magnetosheath magnetization due south.

atmosphere above them. If reconnection suddenly sets in, the magnetic field may relax toward a potential one, as indicated in the last picture of the sequence. This represents a possible, perhaps even plausible, mechanism for a solar flare [57,92]. Figure 2 illustrates current-sheet formation caused by the stretching of magnetic loops on the sun during rapid plasma ejection [14]. Fig. 3 shows interplanetary magnetic sectors with different polarity [123] separated by a current sheet. Figure 4 shows the magnetopause current layer, formed as the solar wind presses the interplanetary magnetic field against the terrestrial field, as well as the tail current sheet, resulting directly from tangential stresses exerted by the solar wind on the magnetic field in the two tail lobes. The topology shown in the figure was first proposed by Dungey [32]. Figure 5 shows the magnetic field configuration expected for a rapidly spinning planetary magnetosphere such as that of Jupiter [48,67].

All of the above examples, and many possible other ones, such as supernova remnants [70], accretion disks [76], and galactic dynamos [87], illustrate cosmic situations in which magnetic field reconnection may occur. However, we do not know with certainty that the process does in fact take place in any or all of these geometries. And if it does take place, we still do not know much in detail about its

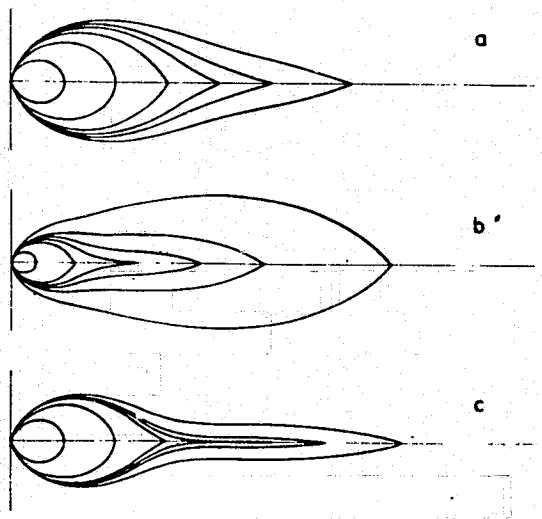

Fig. 5. Magnetic field configurations for a rapidly spinning magnetosphere containing low-energy plasma (Gleeson and Axford [48]). (Copyright by American Geophysical Union, 1976)

dynamics. Are both continuous and sporadic reconnection possible, and if so, what are the plasma parameters and geometries in which these two modes are to be expected? What are the conditions for onset of reconnection? What is the energy conversion rate? In spite of twenty years of theoretical effort, recently summarized in a brilliant manner by Vasyliunas [118], as well as several laboratory experiments [10,31,84,85,114] and computer experiments [4,42,43], no universal agreement exists concerning the answers to most of these basic questions. Even in the most recent literature, opinions about the cosmic occurrence of the process range from full acceptance [118] to outright rejection [2,3]. On the other hand, there is conclusive evidence that reconnection occurs in tokamaks and other fusion devices as an end product of the resistive tearing-mode instability [120 -122].

One of the difficulties with the cosmic reconnection research effort to date is that to a large extent it has lacked the detailed integration of theoretical and experimental work essential to the effective advancement of our knowledge concerning the process. On the one hand, an extensive but rather abstract body of theoretical work exists [118], concerned primarily with the steady-state process and utilizing the fluid description. The latter is likely to be inadequate for the analysis of certain critical aspects of the process. On the other hand, laboratory experiments [10,11] indicate the importance of sporadic reconnection. However,

the plasma parameters in these experiments are sufficiently different from those prevailing in most cosmic applications so as to pose serious difficulties in the application of the laboratory results in cosmos. A wealth of indirect observational evidence in the terrestrial magnetosphere, both at the magnetopause and in the tail, suggests that if the process occurs, it is likely to do so sporadically rather than continuously. In current observational magnetospheric work, the reconnection process is often invoked to account for a great variety of observations but with little effort to check theoretical predictions in detail or to consider alternate interpretations. The result is that the observational case for the occurrence of the process in the magnetosphere is not as solid as it might be. For other astrophysical applications, the situation is even worse.

On balance, our best opportunity for learning about reconnection as a viable cosmic energy conversion process is likely to be in the earth's magnetosphere. It is difficult to account for the overall dynamic behavior of the magnetosphere without invoking time-dependent transfer of magnetic flux from closed to open field lines and vice versa. And such transfer is one of the principal features of the reconnection process. The magnetosphere offers the unique advantage of permitting in situ plasma and field observations with probes that are much smaller than relevant plasma length scales. Thus an intense magnetospheric observational program with a focus on reconnection, coupled with a theoretical effort aimed at the geometries and plasma parameters prevailing at the magnetopause and in the magnetotail would seem to have high potential for success. What is learned about reconnection in the magnetosphere may then be applied to other cosmic systems which do not permit in situ observations. It is seen that a research effort focused on magnetospheric reconnection is likely to lead to significant advances in our understanding of many other astrophysical and cosmic problems.

It is the purpose of this chapter to provide a concise qualitative summary of the present state of reconnection theory and observations, with special reference to the earth's magnetosphere, and to bring into focus a number of specific problems and questions concerning the reconnection process in its magnetospheric application which should be studied both theoretically and observationally. The organization of the paper is as follows. First, a number of basic concepts are introduced via a qualitative discussion of steady two-dimensional reconnection in sect. 2, and of possible nonsteady and/or three-dimensional configurations in sect. 3. With this background, the more detailed technical discussion in subsequent sections can be presented in a compact fashion. Specifically, sect. 4 deals with the external flow region, which is usually described in terms of the fluid approximation. Section 5 discusses one-fluid and two-fluid approaches to the plasma dynamics in the diffusion region, which is the site of the field reconnection process itself, and in which plasma microinstabilities are likely to be important. Section 6 discusses possible mechanisms for the generation of finite resistivity in the diffusion region and for the onset of reconnection. Section 7 contains a brief summary of present observational evidence for or against magnetospheric reconnection. Finally, sect. 8 provides a summary of out-

standing problems along with certain recommendations concerning the organization of future reconnection studies.

Three comments should be made about the scope of the chapter. First, it does not attempt to provide a historical perspective. Rather it is organized to elucidate basic physical principles and recent significant approaches to the development of adequate theories of cosmic reconnection. Second, the paper does not attempt to cover all direct and indirect evidence for or against reconnection in the magnetosphere, on the sun, or elsewhere in cosmos. Third, the paper does not deal with applications in tokamaks and other laboratory devices where the physical boundary conditions are such that spatially periodic behavior results. It should be stressed, however, that vigorous interaction between fusion plasma physicists and cosmic physicists on the problem of reconnection is likely to be of substantial benefit to both groups.

2. Plane steady-state reconnection: a qualitative picture

In order to develop an understanding of certain basic features of magnetic field reconnection, it is desirable first to examine the simplest possible qualitative model of the process. To this end, consider the two-dimensional time-independent

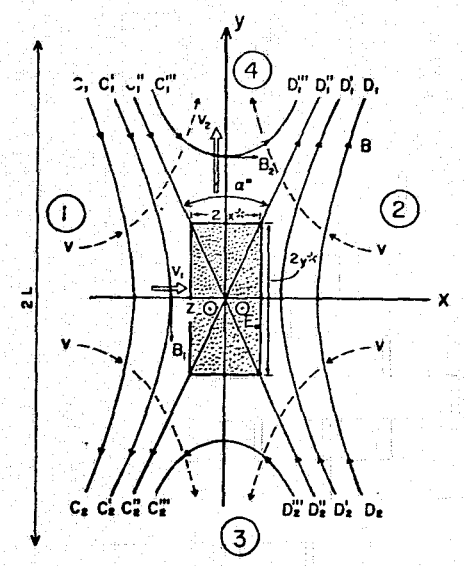

Fig. 6. Basic plane reconnection configuration. Solid lines are magnetic field lines: dashed lines are streamlines. The shaded region at the center is the diffusion region.

electromagnetic field configuration shown in fig. 6. The magnetic field $\boldsymbol{B}$ is confined to the xy plane and has a hyperbolic (X-type) null point at the origin. An electric field of the form $\boldsymbol{E} = E_0\hat{\boldsymbol{z}}$ is present along the direction perpendicular to the plane of the figure. Since $\nabla \times \boldsymbol{E} = 0$ in a steady state, and since partial derivatives with respect to z are assumed to be zero, it follows that E_0 is independent of x and y, i.e., the electric field is uniform. This electromagnetic field is imagined to be imbedded in an electrically conducting fluid or plasma. In the following subsections we examine several aspects of this physical model: flux transport, external plasma dynamics, nature of the region around the magnetic null point, and electromagnetic energy conversion. The treatment is qualitative. More detailed discussion of existing analyses is presented in later sections of the chapter.

2.1. Flux transport

It is well known [8,83] that $\boldsymbol{E} \cdot \boldsymbol{B} = 0$ is a sufficient condition for the flux transport velocity $\boldsymbol{v}_E = \boldsymbol{E} \times \boldsymbol{B}/B^2$ to move points which are on a given magnetic field line at one instant in such a way that they remain linked by a field line at all later times. For example, points which at a certain instant are located on field lines C_1C_2 and D_1D_2 in fig. 6 will move in such a way that at a later time they are located on field lines $C_1'C_2'$ and $D_1'D_2'$, respectively. Thus, a set of points, originally located on a field line and subsequently moving with $\boldsymbol{v}_E$, may be thought of as representing a "moving field line". This fact explains the use of the term flux transport velocity for $\boldsymbol{v}_E$. Note that the reconnection process may be discussed entirely without reference to moving field lines and that indeed the latter concept might become invalid if substantial electric fields parallel to the magnetic field should develop. However, in the present simple model no such parallel fields occur except in the region very near the magnetic null. The use of the concept of moving field lines is then just another way of referring to the electric field E_0. In this model, the use of the term "reconnection" to describe the process is best understood in terms of moving field lines. As the lines C_1C_2 and D_1D_2 move with $\boldsymbol{v}_E$ toward each other through positions $C_1'C_2'$ and $D_1'D_2'$ they ultimately reach location $C_1''C_2''$ and $D_1''D_2''$ where the lines meet at the origin. The surfaces through these lines and perpendicular to the plane of the figure are called separatrices, because they separate families of field lines of different topological origin. When the lines have reached this critical position, they appear to be cut and reconnected so that at still later times they are connected as $C_1'''D_1'''$ and $C_2'''D_2'''$, as shown in the figure. It is evident that the reconnection may be thought of as leading to a transport of magnetic flux from flux cells ① and ② across the separatrices into cells ③ and ④.

2.2. External plasma dynamics

Up to this point the description of the reconnection process has contained no reference to plasma dynamics. Indeed, the process may well have been imagined to

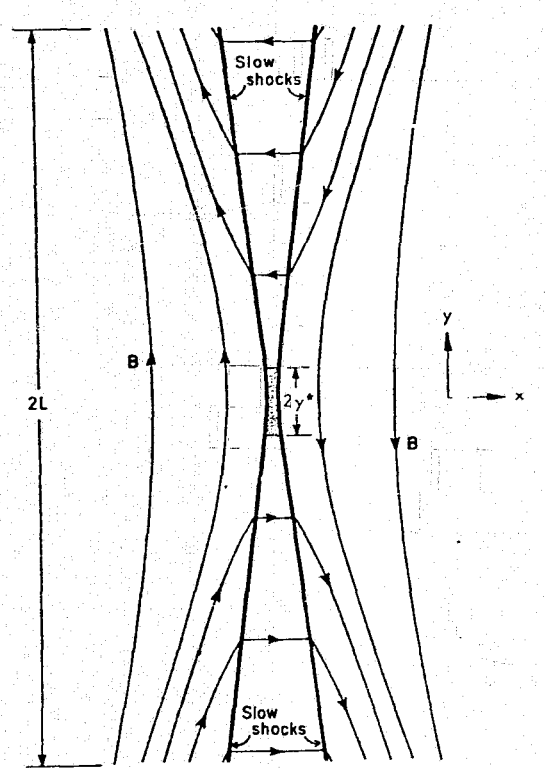

Fig. 7. Configuration of slow MHD shocks in the reconnection geometry (after Petschek [90]).

occur in a vacuum. In such an instance, or if the field configuration is imbedded in a weakly conducting plasma, few restrictions exist on the magnitude of E_0, i.e., on the magnitude of v_E. And the magnetic field will be equal to, or nearly equal to, a vacuum configuration with an angle α of nearly $\frac{1}{2}\pi$ between the intersecting separatrices at the origin. The coupling between the electromagnetic field and the plasma is weak or absent. But in virtually all cosmic applications of interest, the field configuration in fig. 6 would be imbedded in a plasma of high electrical conductivity. Indeed, in many cases Coulomb collisions may be considered entirely absent and the conductivity, if such a term is to be used, is associated with plasma turbulence and/or inertial and gyro effects, occurring near the magnetic null. Away

from that point, the coupling between the B field and the plasma is strong and the plasma dynamics of the process will have dramatic effects in determining the detailed magnetic field configuration and perhaps in limiting the magnitude of the electric field E_0. We now outline some basic features of the plasma dynamics of the reconnection process.

First, it is observed that in a collision-free plasma the guiding centers of charged particles move with some velocity v_D under the influence of the electromagnetic field in fig. 6. In the drift approximation, which is expected to be valid, except in the immediate vicinity of the origin, the component of v_D parallel to the xy plane and perpendicular to B is identical with the flux transport velocity v_E. Thus, in that plane, and as long as $E \cdot B = 0$, the magnetic field lines may be thought of as moving with the plasma or vice versa. We note that the simplified magnetohydrodynamic description also yields this result in the limit of an infinite electrical conductivity. The region away from the magnetic null in which plasma and fields move together is referred to as the convection region. Qualitatively the plasma motion is the one shown by the velocity arrows in fig. 6. Plasma approaches the origin along the positive and negative x axes and leaves along the positive and negative y axes. The motion may be the result of an external electric field E_0 applied between capacitor plates at $z = \pm h$. Alternatively, E_0 may be a polarization field created by an impressed plasma flow, specified in terms of a prescribed inflow rate at large $|x|$ values, say. The details of the overall flow and field configuration will depend on these and other boundary conditions in a manner discussed in subsect. 4.1. However, all MHD models are expected to have in common the occurrence of large-amplitude standing waves in which the plasma is accelerated into the exit flow along the $\pm y$ direction, as shown in fig. 7. In incompressible analyses, these waves are Alfvén waves: in compressible flow they are slow shocks approaching the switch-off limit. The occurrence of these standing wave patterns is related to the fact that the propagation speed of these modes is very small in directions nearly perpendicular to the magnetic field. Thus, by arranging the angle between the wave normal and the upstream magnetic field to be sufficiently near 90°, the wave front can remain stationary even for very small inflow speeds along the $\pm x$ direction. The set of waves divides the flow field into two inflow regions and two outflow regions. These regions do not coincide exactly with the four flux cells in fig. 6. Because the separatrices are located upstream of the standing waves, parts of cells ③ and ④ overlap the inflow regions.

The standing waves contain concentrated electric currents, directed along the z axis, as shown in fig. 7. The $j \times B$ force associated with these currents serves two purposes: it balances the difference in perpendicular momentum and in pressure of the plasma across the shock, and it accelerates the plasma in a direction tangential to the shock. It should be emphasized that currents are by no means confined to flowing only in the wave fronts. Distributed currents j_z may occur throughout the flow field. In particular, as will be shown in subsect. 4.1, the current distribution in the inflow region may influence the reconnection process in a crucial way.

An approximate balance of the magnetic shear stress at the shock and the exit momentum flow * yields

$$\rho_1 v_1 v_2 \simeq B_1 B_z/\mu_0 \tag{2.1}$$

where ρ_1 is the plasma density in the inflow. Further, v_1, B_1 and v_2, B_2, are inflow and outflow speeds and magnetic fields, respectively. They are related via

$$E_0 = v_1 B_1 = v_2 B_2 . \tag{2.2}$$

If v_1 is eliminated between eqs. (1) and (2), we find

$$v_2 \simeq B_1/(\mu_0 \rho_1)^{1/2} \equiv v_{A_1} \tag{2.3}$$

and

$$M_{A_1} \equiv v_1/v_{A_1} \simeq B_2/B_1 . \tag{2.4}$$

Thus it appears that, regardless of the inflow speed, the exit speed v_2 is always of the order of the Alfvén speed v_{A_1}, based on inflow conditions. Also, for fixed B_1, the magnitude of the magnetic field B_2 in the exit flow increases with increasing Alfvén number M_{A_1} in the inflow. When $M_{A_1} = 0$, $B_2 = 0$ and the configuration reduces to a current sheet. When $M_{A_1} \simeq 1$ the two fields are approximately equal, i.e., $B_2 \simeq B_1$.

In steady-state reconnection models, the inflow Alfvén number M_{A_1} is commonly used as a measure of the reconnection rate.

For very small values of M_{A_1}, and in a collisionless plasma, the plasma ejection along the $\pm y$ axis, postulated in the model in fig. 6, may become gradually replaced by an ejection at $z = -h$ and $z = +h$, respectively, of electrons and positive ions meandering in the current layer, as suggested by Alfvén [1] and discussed further by Cowley [23]. The charge separation effects in that case lead to an electric field E_z which is a function of the coordinate z. This limit will not be dealt with in the present paper.

2.3. Region near the magnetic null

The preceding discussion has dealt with plasma motion away from the magnetic neutral point at the origin in fig. 6. Let us now briefly consider the region immediately adjacent to that point. As the origin is approached, the flux transport velocity v_E tends to infinity. Thus it is evident that the plasma can no longer move with

* In this calculation it is assumed that the plasma has a negligible velocity component along the y direction as it enters the shock. This assumption is not always valid. See subsects. 4.1 and 4.2.

v_E in the xy plane. In fact, as the plasma approaches the origin from both sides it must be brought to rest for symmetry reasons. In hydrodynamic terms, the magnetic neutral point is also a double stagnation point. The region in which the plasma velocity deviates significantly from v_E is referred to as the diffusion region; its dimensions are denoted by $2x^*$ and $2y^*$ as indicated in fig. 6. In this region finite conductivity effects of some type must come into play, allowing the current density to remain finite at the null point for $E_0 \neq 0$. Three main possibilities exist.

(i) In a collisional plasma with large but finite electrical conductivity σ, the half width x^* of the diffusion region is expected to adjust itself in such a way that a balance is established between the rate of magnetic flux convected into the diffusion region and the rate of diffusion of the flux through the semistagnant plasma in the diffusion region. The ratio of these two transport rates is measured by the magnetic Reynolds number $R_m \equiv \mu_0 \sigma v_1 x^*$. Thus we expect $R_m \simeq 1$, i.e., x^* is of the order of the resistive length:

$$x^* \simeq (\mu_0 \sigma v_1)^{-1} . \tag{2.5}$$

We note that x^* decreases with increasing conductivity and increasing v_1. Since $v_1 = v_E = E_0/B_1$, B_1 being the magnetic field at $(x = \pm x^*, y = 0)$, increasing v_1 corresponds to increasing E_0, assuming B_1 to remain fixed.

(ii) In a collision-free plasma one might expect the value of x^* to be determined instead by the scale of the particle orbits near the null point. Four such scales may be of relevance: the electron and ion gyroradii and the electron and ion inertial lengths. Further discussion of these scales is presented in sect. 5. An equivalent electrical conductivity may be imagined in this case, such that the effective residence time of a particle (an electron or an ion) replaces the usual collision time τ in the expression $\sigma = ne^2\tau/m$ (m = particle mass). This residence time is found to be inversely proportional to v_1 so that $x^* \sim (\mu_0 \sigma v_1)^{-1}$ becomes independent of v_1 and hence of E_0 for fixed B_1. For further discussion, see subsect. 6.1.

(iii) In each of the above two cases, the current density or the gradients in the diffusion region may become sufficiently large to cause plasma microinstabilities. The resulting plasma turbulence will lead to a reduction in the effective conductivity, as discussed in subsect. 6.2.

Whether the plasma dynamics in the diffusion region is described in a continuum fashion, i.e., by use of an effective conductivity, or in terms of individual particle orbits near the magnetic null point, it is easy to see that the net current I in the diffusion region will be along the positive z axis so that $E \cdot I > 0$. Thus the diffusion region, along with the entire shock system, acts as a dissipator of electromagnetic energy.

We note that the overall conservation of mass in the diffusion region yields

$$\rho_1 v_1 y^* = \rho_2 v_2 x^* , \tag{2.6}$$

which may be combined with eqs. (2.2) and (2.4) to yield

$$M_{A_1} \equiv v_1/v_{A_1} \simeq B_2/B_1 \simeq (\rho_2/\rho_1)(x^*/y^*). \tag{2.7}$$

Assuming the density ratio ρ_2/ρ_1 to vary only moderately with M_{A_1}, we see that the diffusion region is very elongated along the y axis for small M_{A_1} values. Additionally, in a collisional plasma the thickness x^* increases with decreasing M_{A_1}, as shown by eq. (2.5):

$$x^* \simeq (\mu\sigma v_{A_1})^{-1}(M_{A_1})^{-1}. \tag{2.8}$$

Combining eqs. (2.7) and (2.8) it appears that $x^* \sim M_{A_1}^{-1}$, $y^* \sim M_{A_1}^{-2}$ in a collisional plasma [case (i)] while $x^* \sim$ const., $y^* \sim M_{A_1}^{-1}$ in a collision-free case dominated by inertial resistivity [case (ii)].

Finally, we estimate the separatrix angle α in the outflow (see fig. 6). Near the magnetic null point we may write:

$$B_x = ay; \quad B_y = bx; \tag{2.9}$$

where a and b are positive constants, and the angle $\alpha = 2\tan^{-1}(a/b)^{1/2}$. Estimating $ay^* \simeq B_2$ and $bx^* \simeq B_1$ we find by use of eq. (2.7)

$$\alpha = 2\tan^{-1}(B_2x^*/B_1y^*)^{1/2} \simeq 2\tan^{-1}[(x^*/y^*)(\rho_2/\rho_1)^{1/2}]$$

$$\simeq 2\tan^{-1}[(\rho_1/\rho_2)^{1/2}M_{A_1}], \tag{2.10}$$

indicating that the range of Alfvén numbers M_{A_1} from zero to $(\rho_2/\rho_1)^{1/2}$ corresponds to an α range of zero to $\frac{1}{2}\pi$. The latter value corresponds to $b = a$, i.e. to a current-free state, because $j_z = (b-a)/\mu_0$.

2.4. Energy conversion

The reconnection model described in this section serves as a steady-state converter of electromagnetic energy into plasma kinetic and internal energy. For example, the rate of electromagnetic energy flow into and out of the diffusion region may be estimated as follows:

$$\text{inflow} = 8y^*hE_0B_1/\mu_0; \quad \text{outflow} = 8x^*hE_0B_2/\mu_0;$$

where the diffusion region has been taken to be a rectangular box with sides $2y^*$, $2x^*$ and $2h$. Thus the net rate of inflow of electromagnetic energy is

$$W_{em} = (8y^*hE_0B_1/\mu_0)(1 - x^*B_2/y^*B_1)$$

which upon use of eqs. (2.2) and (2.7) may be written

$$W_{em} \simeq 16y^*h(B_1^2/2\mu_0)\,v_{A_1}M_{A_1}(1 - M_{A_1}^2\,\rho_1/\rho_2). \tag{2.11}$$

It is evident from this approximate expression that the energy conversion rate has a maximum at some value of the reconnection rate M_{A_1} intermediate between 0 and a maximum value, which in the present approximate set of relations appears to be $M_{A_1} = (\rho_2/\rho_1)^{1/2}$. Note that $W_{em} = 0$ both for $M_{A_1} = 0$ and for $M_{A_1} = (\rho_2/\rho_1)^{1/2}$. For the latter value of M_{A_1}, the configuration near the null is current-free and symmetric ($b = a$; $\alpha = \frac{1}{2}\pi$). In such circumstances one may expect $(\rho_2/\rho_1)^{1/2} \simeq 1$. Thus $M_{A_1} \simeq 1$ appears as a theoretical upper limit for the reconnection rate (based on plasma conditions at $x = x^*$, $y = 0$). It is, however, by no means assured that boundary conditions at large distances or plasma processes in the diffusion region will always permit this upper limit to be reached.

The net rate of increase of kinetic energy of the plasma may be expressed as follows

$$W_{ke} \simeq \rho_1 v_1\, 8y^*h(\tfrac{1}{2}v_2^2 - \tfrac{1}{2}v_1^2) \simeq 8y^*h(B_1^2/2\mu_0)\,v_{A_1}M_{A_1}(1 - M_{A_1}^2) \tag{2.12}$$

and conservation of energy requires the difference $W_{em} - W_{ke}$ to be the rate of increase of the internal energy of the plasma, W_i. This latter rate may include thermal as well as nonthermal parts, for example in the form of run-away electrons.

The analysis given above applies to the diffusion region. But usually only a minute part of the total energy conversion occurs there, the main part taking place in the shocks. In approximate terms, the formulae (2.11) and (2.12) may be modified to be valid for the entire reconnection geometry by replacing y^* by L, where $2L$ is the height of the total configuration, as shown in fig. 6. Also, all quantities bearing the subscript 1 (which are evaluated at $x = x^*$, $y = 0$) should be replaced by quantities bearing the subscript ∞, i.e. they should be evaluated at $x \gg x^*$, $y = 0$. Depending on the nature of the boundary conditions, the inflow may be such that $M_{A\infty}$ differs significantly from M_{A_1} (see subsects. 4.1 and 4.2).

The phrase magnetic field annihilation has been used to describe the reconnection process. In the light of the preceding discussion, this term appears appropriate only in the limit of small M_{A_1} values where the magnetic field B_2 in the exit flow is small (or absent as in Alfvén's model, mentioned earlier [1,23]). Henceforth, annihilation will refer to situations where M_{A_1} is sufficiently small so that the diffusion region occupies the entire length of the current sheet, i.e., $y^* \geqslant L$. By combination of eqs. (2.7) and (2.8) this is seen to occur for $0 < M_{A_1} \leqslant [(\rho_2/\rho_1)/(\mu_0\sigma v_{A_1}L)]^{1/2}$.

In reconnection, energy conversion occurs on a time scale comparable to the Alfvén wave time $\tau_A = L/v_{A_1}$ (assuming the inflow regions to extend to $|x| \simeq L$), while in annihilation the scale is $(\tau_A\tau_D)^{1/2}$, τ_D being the time for purely resistive decay of a current sheet i.e., $\tau_D = \mu_0\sigma L^2$. τ_D is enormous in most cosmic applications, so that reconnection rather than annihilation is required to account for the rapid energy release in solar flares, geomagnetic substorms, etc.

3. Flux transfer in time-dependent and three-dimensional configurations

The two-dimensional steady reconnection model outlined in sect. 2 is useful as a vehicle for introducing certain basic aspects of reconnection. But it appears likely that in any real cosmic applications of the process, three-dimensional and temporal effects are important, perhaps even dominant. For this reason it is useful to consider briefly a few reconnection configurations which incorporate these effects. To date, the plasma dynamics associated with such geometries has not been dealt with in a substantial way, so that the discussion is confined mainly to the electromagnetic field topology and flux transfer aspects of the process. In the following subsections we describe the two-dimensional but time-dependent double inverse pinch configuration, a simplified steady-state three-dimensional magnetopause topology and a possible three-dimensional time-dependent magnetotail configuration. Finally, in subsect. 3.4, a general definition of reconnection is given.

3.1. Plane time-dependent geometry

A plane vacuum magnetic field geometry associated with the double inverse pinch laboratory experiments [10] is shown in fig. 8. The X type magnetic null point is again located at the origin. The magnetic field is maintained by the currents I in the two metal rods at the center of flux cells ① and ②, and a return current $2I$, flowing in the plasma along an outer envelope, which coincides with the outermost field lines in flux cell ③. In the experiments, the current I increases with time so

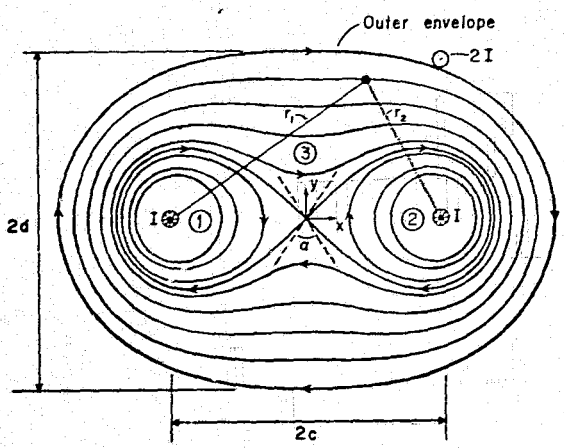

Fig. 8. Field configuration in double inverse pinch experiment (after Bratenahl and Baum [11]).

that magnetic flux is generated continually at the two rods, i.e., in cells ① and ②. If we assume for a moment that no plasma is present, the flux in cell ③ increases proportionately so that magnetic flux may be thought of as being transported from the rods into cells ① and ② and from there across the separatrix into cell ③. It is of interest to calculate the electric field responsible for this flux transport. The vector potential for the vacuum configuration is given by

$$A = -\hat{z}\frac{\mu_0 I}{2\pi}\ln\left[\frac{c^2+d^2}{r_1 r_2}\right] = \hat{z}A_z(x, y, t) \tag{3.1}$$

where the rod separation is $2c$, the minor diameter of the return-current envelope is $2d$, and the radii r_1 and r_2 are measured from the two rods as shown in fig. 8. Note that $A = 0$ at the envelope. In the experiment, the current I and the envelope diameter both increase with time: in a more general case, the rod separation might be imagined to depend upon time also. But for our purposes it suffices to consider the time variation of the current I and the diameter d. Then, the electric field is

$$E = -\frac{\partial A}{\partial t} = \hat{z}\frac{\mu_0 \dot{I}}{2\pi}\ln\left[\frac{c^2}{r_1 r_2}\right] + \hat{z}\frac{\mu_0 I}{2\pi}\left[\frac{2d\dot{d}}{c^2+d^2}\right]$$

$$= -\hat{z}\frac{\dot{I}}{I}A_z(x, y, t) + \hat{z}\frac{\mu_0 I}{2\pi}\left[\frac{2d\dot{d}}{c^2+d^2}\right].$$

Since at each instant A_z remains constant on a magnetic field line, the instantaneous electric field has the same value on a given field line but its value changes from one line to another. In particular, on the separatrix it has the value

$$E_z = \frac{\mu_0 \dot{I}}{2\pi}\ln\left(1+\frac{d^2}{c^2}\right) + \frac{\mu_0 I}{2\pi}\left[\frac{2d\dot{d}}{c^2+d^2}\right]. \tag{3.2}$$

Thus for increasing current I and diameter d, E_z is positive as required for flux transport into cell ③.

In the presence of a plasma, the field configuration is modified as follows. The electric field now drives plasma currents in the vicinity of the magnetic null line, causing a field deformation of the type shown by the dashed lines in fig. 8. The separatrix intersection angle α falls below its vacuum value of $\frac{1}{2}\pi$. These effects imply an excess of magnetic flux in cells ① and ②, a deficiency in cell ③, compared to the vacuum configuration, which is the lowest energy state. Thus, a certain amount of free magnetic energy is stored in the system. However, at the same time a considerable amount of flux transport into cell ③ takes place. That is, reconnection occurs continuously *. The principal difference between the present case and the steady-state model in sect. 2 is the spatial nonuniformity of the instantaneous electric field. This effect occurs because in the nonsteady case some of the flux

* By contrast, ref. [15] analyzes a hyperbolic-field collapse, where α decreases from $\frac{1}{2}\pi$ to 0, without any reconnection.

transported in the xy plane is being deposited locally, causing a field magnitude increase at each point. Associated with this flux accumulation, a plasma compression must also occur. But this would appear to be a relatively minor effect so that the steady model in sect. 2 may provide an adequate instantaneous description of the flow away from the rods and the return envelope. Thus the essential qualitative features of the reconnection flow may be obtained by examination of a sequence of steady-state configurations.

Impulsive flux transfer events are observed in the double inverse pinch experiments. It appears that, as the magnetic field and associated plasma currents near the null point grow, anomalous resistivity associated with ion sound turbulence sets in abruptly with an associated rapid increase of electric field and decrease of currents at the null point. The net result is a much more rapid flux transfer into cell ③ and an associated relaxation of the entire magnetic field configuration toward its potential form with the separatrix intersection angle α increasing toward $\frac{1}{2}\pi$. Evidently the stored free magnetic energy described in the previous paragraph is being rapidly converted into plasma energy. These events occur on a time scale much shorter than that associated with I. Hence it is unlikely that they may be described, even approximately, by a sequence of steady-state configurations. But the conditions for onset of such an event may perhaps be identified by examination of such a sequence.

3.2. Steady three-dimensional geometry

A three-dimensional magnetic-field configuration of interest for steady-state magnetopause reconnection is obtained by the superposition of a dipole and a uniform field of arbitrary direction . This topology, shown in one cross section in fig. 9, has been discussed extensively in the literature [24,32,127]. Two hyperbolic magnetic null points X_1 and X_2 are formed in the plane containing the dipole moment vector and the uniform field vector. A basic topological property of such a null point is that many field lines enter it forming a separatrix surface and two single field lines leave it along directions out of that surface, or vice versa. The separatrix surfaces associated with X_1 and X_2 intersect along a circular ring located in a plane through the two points and perpendicular to the plane of fig. 9. This ring is referred to alternatively as a singular line, a reconnection or merging line, a critical line, an X line, or a separator line. At a chosen point on the ring the magnetic field does not vanish in general, but it is directed along the ring. Only at X_1 and X_2 is the field intensity zero. If the uniform field is exactly antiparallel to the dipole field a degenerate situation arises in which the magnetic field vanishes at each point on the ring.

A schematic picture of the two separatrix surfaces is shown in fig. 10, in a configuration that may be appropriate for magnetopause reconnection. The upper part of the figure shows a view in the antisolar direction of field lines on the separatrix surface associated with the null point X_2: the lower part shows the same view of

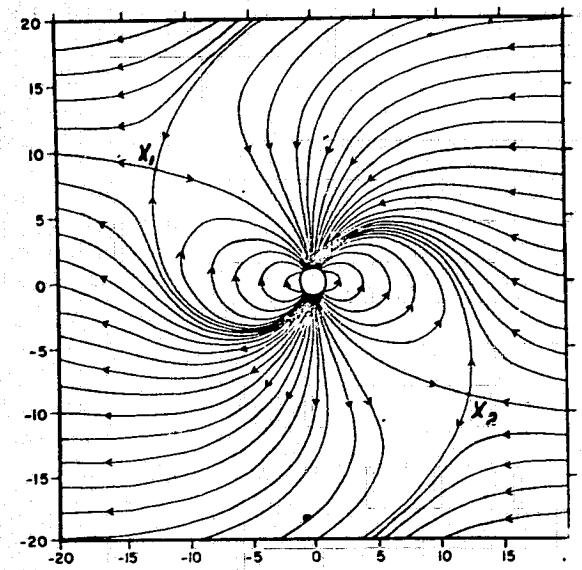

Fig. 9. Field lines in the plane of the neutral points X_1 and X_2 for a uniform magnetic field and a dipole field (Cowley [24]). Dipole moment vector at right angles to the uniform field. (Copyright by American Geophysical Union, 1973)

the X_1 separatrix. The total picture is an overlay of the two diagrams with the reconnection line connecting X_1 and X_2. Part of the solar-wind electric field E_{sw} is impressed across the configuration and must be sustained along the reconnection line. Thus, in the vicinity of that line a strong electric field component is present along the magnetic field. Unless special circumstances exist, such parallel electric fields do not arise in highly conducting plasmas. However, it is believed that the field lines on the separatrix and its immediate vicinity bend to become nearly parallel to the reconnection line extremely close to that line, as shown in fig. 10. Thus parallel electric fields occur only within the diffusion region which surrounds the reconnection line and in which finite resistivity effects permit their presence. Fig. 10 suggests that it may be possible to study reconnection in this geometry by use of a locally two-dimensional model which is then applied to each short segment of the reconnection line. Such a model will be similar to that discussed in sect. 2, but with an added magnetic field component $B_z(x, y)$. Thus the reconnection of fields that are not antiparallel is obtained. Further discussion of such geometries is given in subsect. 4.4. The dynamics of the motion near the points X_1 and X_2 has not been studied to date. It may well be that these points mark the end points of a reconnection line segment on the front lobe of the magnetopause surface.

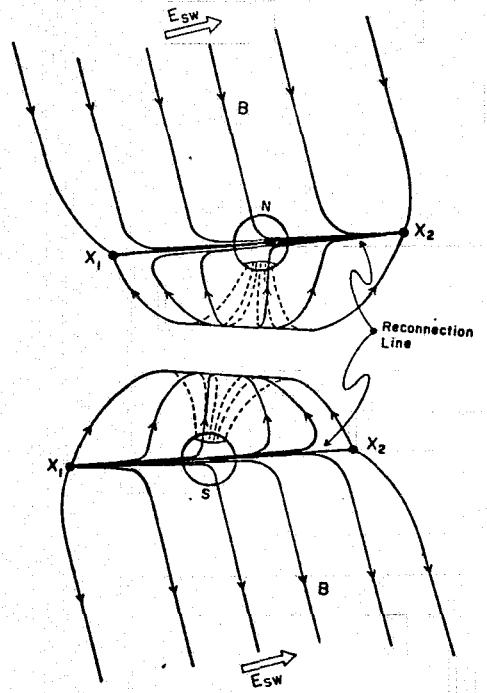

Fig. 10. Schematic of separatrix surfaces for magnetopause reconnection. Lower figure shows separatrix of the null point X_1; upper figure that of X_2. The two figures are to be superimposed.

Referring to fig. 4, which represents a cut through the earth's magnetosphere in the noon–midnight meridional plane, it is seen that reconnection at the magnetopause, as described above, serves to transport magnetic flux from the interplanetary cell ① and from the front-lobe magnetospheric cell ② into the polar cap cells ③ and ④.

3.3. Time-dependent three-dimensional geometry

As a final example of reconnection geometries of cosmic interest, consider the magnetic-field topology associated with the formation of a reconnection bubble in the geomagnetic tail. The evolution of the field geometry in the noon–midnight meridional plane is shown in fig. 11. Note the formation of an X type and an O

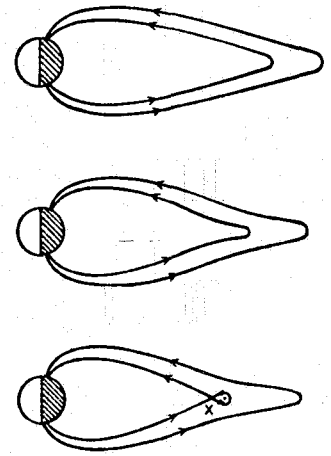

Fig. 11. Formation of reconnection bubble in the geomagnetic tail. Schematic of field configuration in the noon-midnight meridional plane.

type neutral point. The bubble originally has a very small longitudinal dimension. As it grows in size in the noon–midnight plane, it also occupies an increasing longitude sector. The actual three-dimensional magnetic field topology of such a bubble is not known, but it may be represented schematically by an X type and an O-type null line as in fig. 12. The points A, X, B and O in that figure all emerge at the same place at the time of onset of reconnection. Subsequently they move apart as the reconnection process continues and the bubble grows. An electric field exists along the reconnection line AXB but none, or almost none, along the O line AOB.

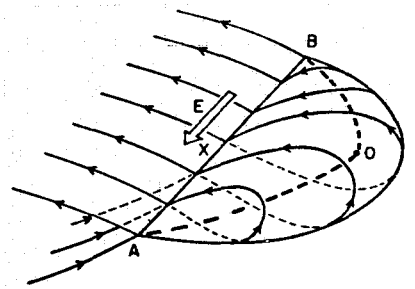

Fig. 12. Three-dimensional sketch of reconnection bubble with the reconnection line along AXB and an O-type magnetic null line along AOB.

This field presumably has an inductive and an electrostatic part which tend to cancel along AOB while adding along AXB.

3.4. Definitions

On the basis of the preceding discussion we now formalize the definition of several terms, used in the magnetic-field reconnection literature:

(i) A separatrix is a surface in space which separates magnetic field lines belonging to different topological families. By necessity the separatrix is everywhere tangential to the magnetic field. The field lines constituting the surface originate at a hyperbolic neutral point in the field.

(ii) A separator is the line of intersection between two separatrices or the line of intersection of one separatrix with itself. The separator is also called reconnection line, merging line, or X line. The terms neutral line, singular line, or critical line should be avoided, since they may refer to the O-type topology as well.

(iii) The diffusion region is a plasma channel, surrounding the separator, in which resistive diffusion, caused by collisional processes, turbulence, or intertial effects, is important. In a highly conducting plasma, the diffusion region is imbedded in a much larger convection region, in which magnetized plasma moves toward and away from the separator, in the inflow and outflow regions, respectively, and in which dissipative effects are confined to shocks.

(iv) Magnetic-field reconnection is said to occur when an electric-field component E_0 (induced or electrostatic) is present along a separator or a macroscopic portion thereof. It is proposed that the term magnetic-field annihilation be reserved for the case where the separator has degenerated (for dynamic puposes *) to a surface (e.g., the surface separating two half spaces containing antiparallel uni-directional fields). The term magnetic-field merging may be taken to encompass both reconnection and annihilation.

(v) The local instantaneous reconnection rate at a chosen point on a separator is measured by the instantaneous magnitude of the electric-field component E_0 along that line. It is desirable to express this rate in a nondimensional form by dividing the electric field by the product of a characteristic velocity and a characteristic magnetic field. The latter two quantities may be taken to be the Alfvén speed v_{A_r} and magnetic field B_r at a chosen reference point, denoted by the subscript r, in the inflow, such as $(x_r = x^*, y_r = 0)$ or $(x_r = L, y_r = 0)$. Since E_0/B_r represents a characteristic flow speed, the dimensionless reconnection rate takes the form of an Alfvén number:

$$M_0 = (E_0/B_r)/v_{A_r}.$$

In steady, two-dimensional ($B_z = 0$, $\partial/\partial z = 0$), models the electric field E_0 is

* See comments in subsects. 2.4 and 6.1.

constant throughout the xy plane so that $E_r = E_0$. With the reference point in the convection region, and on the x axis where $B_z = 0$, E_0/B_r is then the plasma flow speed toward the separator at the reference point and M_0 is the local Alfvén number, $M_0 = M_{A_r}$. In nonsteady flow, the electric field at the reference point, E_r, in general differs from E_0, and $M_0 \neq M_{A_r}$.

Vasyliunas [118] has defined magnetic merging as "the process whereby plasma flows across a surface that separates regions containing topologically different magnetic field lines"; he takes the magnitude of that flow as a measure of the merging rate. For reconnection in a highly conducting plasma, such that $R_m \equiv \mu_0 \sigma v L \gg 1$, the two definitions are essentially equivalent. However, the one adopted here, in terms of an electric field component along the separator works also for flows at arbitrary R_m. It corresponds to the occurrence of flux rather than plasma transport across the separatrix, because flux transport is but an alternate way of referring to the electric field *. Note also that for the degenerate case of magnetic field annihilation there is no plasma flow across a separatrix. There is, however, an electric field and a corresponding magnetic flux transport.

4. The convection region

The plasma dynamics in the regions away from the immediate neighborhood of the reconnection line usually is described by use of continuum equations. Nonsteady solutions have not been found to date, which describe rapid configuration changes such as might be associated with impulsive flux transfer events in the double inverse pinch experiment (for a circuit model, see Bratenahl and Baum, [11]). Three-dimensional solutions also have not been obtained. Hence the discussion in the present section is confined to steady-state plane reconnection.

The incompressible assumption corresponds to the limit $\beta \to \infty$, where β is the ratio of plasma pressure to magnetic pressure. While this limit is invalid in most cosmic applications, it has the advantage of yielding simple analysis. Thus it provides an opportunity to study certain basic features of the reconnection flow without undue mathematical complications. We first describe two incompressible reconnection flows with fundamentally different behavior. Certain compressibility effects are considered in the second subsection. The third subsection discusses asymmetric reconnection configurations, perhaps applicable to the magnetopause. The fourth subsection deals with the reconnection of magnetic fields that are not antiparallel, a common situation at the magnetopause. Finally, a partial single-particle model is discussed briefly.

* This equivalence is seen most clearly [119] by casting Faraday's law into the form of a conservation equation, viz., in subscript notation, $\partial B_i/\partial t + \partial/\partial x_j (\epsilon_{ijk} E_k) = 0$, where ϵ_{ijk} is the antisymmetric (Levi–Civita) unit tensor.

4.1. Two incompressible symmetric flow models

Figure 13, reproduced from Vasyliunas [118], shows a field and flow map for a reconnection model initially analyzed by Petschek [90] and subsequently considerably refined and improved by Vasyliunas. The model contains a set of four Alfvén discontinuities which in compressible flow may be identified as slow-mode shocks and across which the plasma is accelerated into the exit flow regions. Note that the plasma flow converges toward the x axis in the inflow and that the magnetic field intensity decreases on that axis for decreasing $|x|$ values. As pointed out by Vasyliunas, this behavior is characteristic of fast-mode expansion of the plasma as it

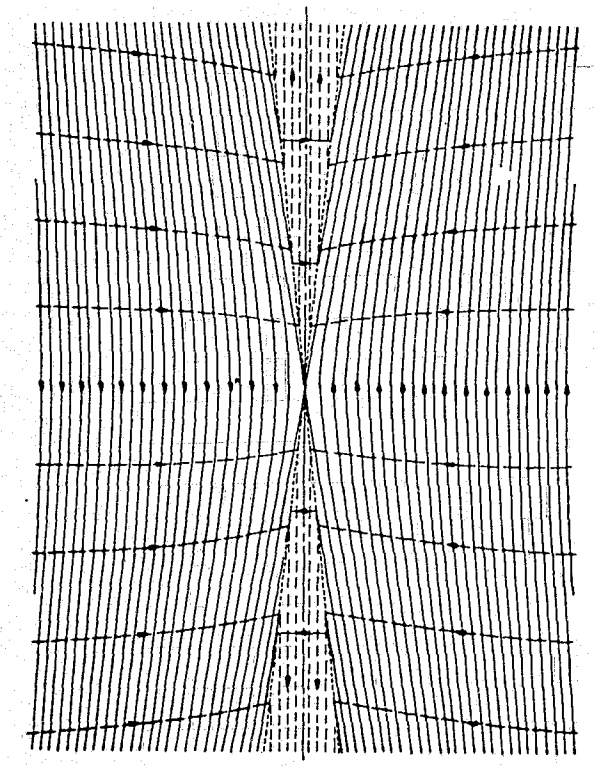

Fig. 13. Petschek's reconnection model with $M_{A\infty} = 0.1$. Magnetic field lines (solid lines) and streamlines (broken lines) are shown. (Vasyliunas [118].) Fast-mode expansion in the entry flow (Copyright by American Geophysical Union, 1975.)

approaches the reconnection line. Because the fast-mode propagation speed is infinite in the incompressible limit, such expansion is by necessity an elliptic effect, that is, no standing expansion wavelets are possible. The maximum reconnection rate in this model corresponds to an Alfvén number M_{A_1} of about one in the inflow just adjacent to the diffusion region. But because of the increase in flow speed and decrease in magnetic field associated with the fast-mode expansion, the Alfvén number, $M_{A\infty}$, at large distances upstream is considerably less than unity. Values in the range $0.05 < M_{A\infty} < 0.2$ for the maximum rate are obtained (see ref. [118], fig. 12). Recently, Soward and Priest [110] have reexamined Petschek's reconnection geometry by use of an asymptotic approach, valid away from the reconnection line. Their analysis in all essential respects supports the conclusions summarized above.

Fig. 14, also taken from ref. [118], shows a flow and field map for a different

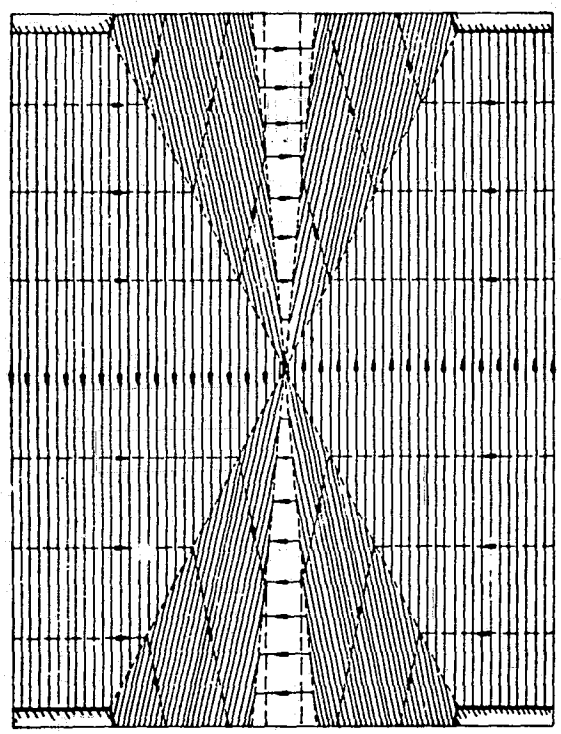

Fig. 14. Slow-mode reconnection model with $M_{A_1} = 0.5$. (Vasyliunas [118].) Slow-mode expansion in the inflow is concentrated to waves from four external corners. (Copyright by American Geophysical Union, 1975)

model [103], which is the sole nonsingular member of the similarity solutions derived by Yeh and Axford [131]. This model contains a second set of Alfvén discontinuities located upstream of the slow shocks and originating at external corners in the flow, as shown in the figure. These discontinuities represent the incompressible limit of slow-mode expansion fans centered at the external corners. They cause a large deflection of the plasma flow away from the x axis and a substantial increase in field magnitude. It is now generally agreed that these discontinuities will not occur in any real situation. Rather they represent a suitable mathematical lumping of slow-mode expansion effects in the inflow. The maximum reconnection rate in this model * is $M_{A1} = (1+\sqrt{2})$. On the x axis this value remains constant, independent of $|x|$. However, this is a result of the lumping of the slow-mode effects. In a model where these effects are spread over the inflow region the value of M_A on the x axis will decrease with decreasing $|x|$ in association with a decrease in plasma velocity and an increase in magnetic field. Thus, in reality it is unlikely that the inflow into the diffusion region can occur at M_{A1} as high as $(1+\sqrt{2})$; more likely that value corresponds to the maximum $M_{A\infty}$ at large $|x|$ values. Further discussion of this point is given in subsects. 4.2 and 5.1.

The two models discussed above represent two extreme sets of conditions in the inflow: pure fast-mode and pure slow-mode expansion. In any real application both effects may be present. Vasyliunas [118] has pointed out that from a mathematical viewpoint the difference between the two models is related to the boundary conditions at large distances from the reconnection line. Far upstream, the fast-mode model is essentially current free and has a nearly uniform flow and magnetic field, while the slow-mode model contains substantial currents which bend the magnetic field lines and cause a deflection of the flow away from the x axis. Vasyliunas has further suggested that the former state of affairs may obtain when a demand for magnetic flux originates at the current sheet itself (the yz plane) or in the exit flow, as may be the case in the geomagnetic tail, while the latter set of conditions may correspond to externally forced inflow such as at the magnetopause. In this context, it is worth noting that slow-mode expansion effects have been argued [132] to be present outside the subsolar magnetopause regardless of whether or not reconnection occurs there.

4.2. Compressible symmetric models

A detailed compressible analysis of the external region of Petschek's reconnection geometry is not available at present. On the other hand, the slow-mode expansion model has been extended to include compressibility effects. An isothermal analysis was given by Yeh and Dryer [130]. But the isothermal assumption leads to

* The estimates given in sect. 2, viz., $v_2 \simeq v_{A_1}$ and $(v_1)_{max} \simeq v_{A_1}$, assumed a negligible flow component along the y axis as the plasma enters the shock. Such a component is present in this model, the result being that the exit flow speed v_2 and the maximum inflow speed $(v_1)_{max}$ both exceed v_{A_1} by a factor $(1+\sqrt{2})$.

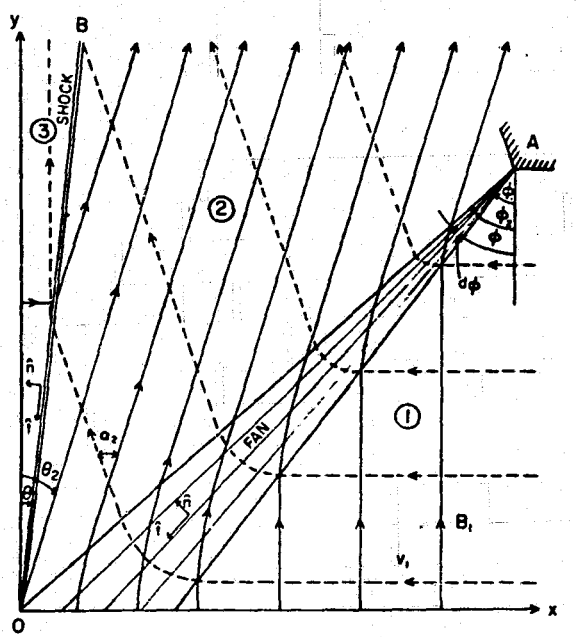

Fig. 15. One quarter of a symmetric compressible slow-mode magnetic-field reconnection model for $M_{A1} = 0.7$ and $\beta_1 \equiv 2\mu_0 p_1/B_1^2 = 5$ (Yang and Sonnerup [125]). (Reprinted by permission from C.K. Yang and B.U.O. Sonnerup and the University of Chicago Press. Copyright by the American Astonomical Society, 1976.)

unacceptable entropy variations with decreasing entropy across the shocks and increasing entropy across the expansion waves. More recently, an analysis has been performed by Yang and Sonnerup [125], which assumes isentropic flow in the inflow and uses the ordinary jump relations for slow shocks. It is found that the expansion-wave discontinuities in the incompressible solution do indeed dissolve into slow expansion fans centered at the external corners in the flow (see fig. 15). It might be thought that the reflection of these fans in the x axis, and the subsequent interaction of the reflected waves with the shocks, shown schematically in fig. 16, may be treated exactly by the method of characteristics. However, it is found that the flow from region ① in the figure, across the last expansion wavelet and the innermost portion of the shock, cannot be dealt with without the inclusion of elliptic (fast-mode) effects. This is extrememly difficult to do. Thus, in the main part of their work, Yang and Sonnerup, after calculating the isentropic plasma and field changes across the fans, considered them to be lumped into a single discontinuity, i.e., they ignored the reflection altogether. While such a procedure is

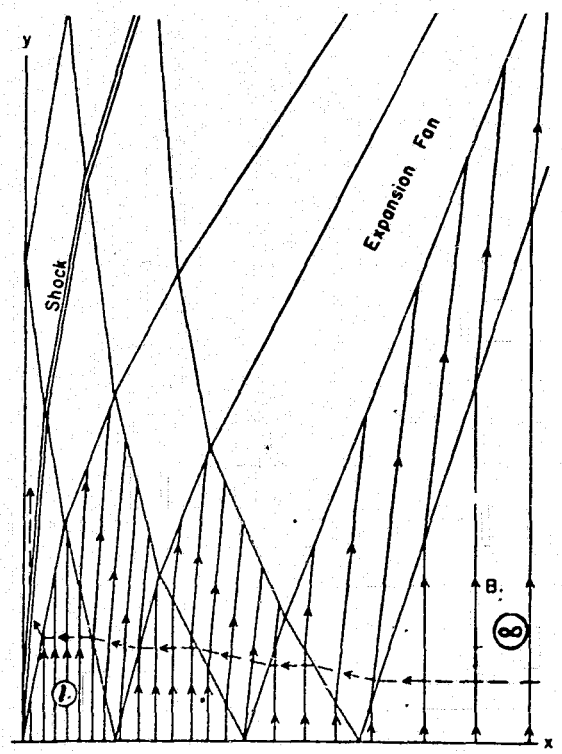

Fig. 16. Schematic showing "reflection" of slow-mode expansion fan in the x axis (Yang and Sonnerup [125]). [Copyright by American Astronomical Society (University of Chicago Press, 1976)]

perhaps justified in a first attempt to study compressibility effects in the external flow, it nevertheless seriously limits the usefulness of the resulting solutions. The width of the slow expansion fans in the inflow increases dramatically with increasing compressibility, i.e., with decreasing values of $\beta_1 \equiv 2\mu_0 p_1/B_1^2$, so that for $\beta_1 \simeq 1$ the lumping of the fan into a single discontinuity is difficult to defend. Furthermore, except perhaps for very large β values, conditions immediately outside the diffusion region are not adequately represented so that the solution may not be used to provide external boundary conditions for compressible matched diffusion-region analyses. However, the analysis is valid at large distances from the origin, and it is of interest to examine its predictions concerning flow and plasma conditions in the exit regions. When conditions typical of geomagnetic tail reconnection are

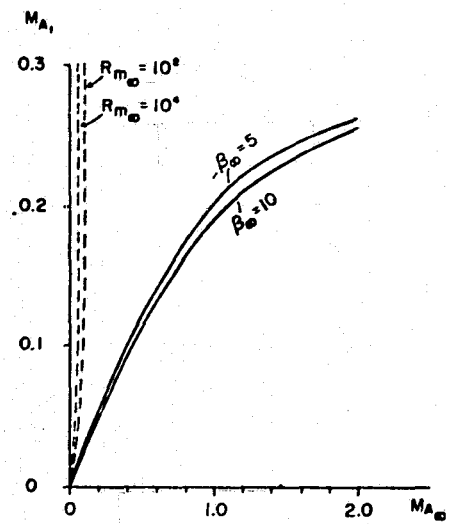

Fig. 17. Relationship between the inflow Alfvén numbers M_{A_∞}, far upstream, and M_{A_1}, adjacent to the diffusion region. Solid curves refer to slow-mode expansion model [125], dashed curves to the Soward–Priest [110] analysis of the fast-mode expansion model.

substituted, flow speeds in the range of 1000 km sec^{-1} are calculated, in rough agreement * with observed proton speeds in the tail during energy-release events [39,63]. The analysis also predicts exit flow speeds considerably greater than the fast-mode propagation speed so that standing transverse fast shocks may be present in the two exit flow regions, causing a decrease in flow speed and an associated increase in plasma density, temperature, and in the exit magnetic field.

Yang and Sonnerup [125] also calculated the change in plasma and flow properties along the x axis in fig. 16, caused by the reflection of the slow expansion fan, but ignoring the elliptic effects mentioned earlier. The solid curve in fig. 17 shows the resulting relationship between the Alfvén numbers M_{A_1} and M_{A_∞}, in regions (1) and (∞) of fig. 16, respectively. For comparison, the corresponding relationship for the fast-mode model, developed by Soward and Priest [110], is shown by the dashed curves. It is evident that the different distant boundary conditions for the fast-mode and the slow-mode models may lead to profoundly different inflow conditions into the diffusion region for the two models.

* The agreement is however not sufficiently detailed to support this particular reconnection configuration over others.

4.3. Asymmetric models

A qualitative reconnection model for the asymmetric flow and field conditions existing at the magnetopause was first described by Levy et al. [72,91]. In this model, shown in fig. 18, the magnetosheath plasma is assumed to carry with it a compressed interplanetary magnetic field which is due south so that a field reversal results at the magnetopause (see fig. 4). In impinging on the earth's field, the plasma encounters a wave system consisting of an intermediate wave (rotational discontinuity; large amplitude Alfvén wave) followed by a narrow slow expansion

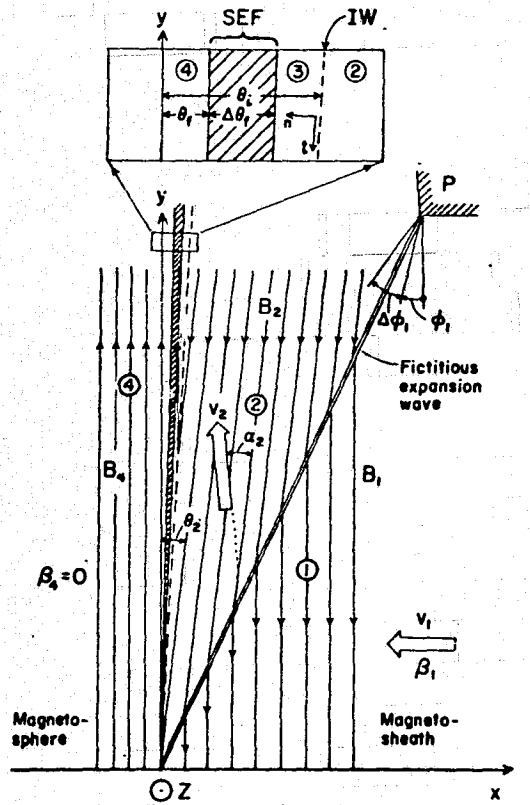

Fig. 18. Upper half of compressible slow-mode model of magnetopause reconnection for M_{A_1} = 0.2 and $\beta_1 = 2\mu_0 p_1/B_1^2 = 2$. The intermediate wave (IW) marking the magnetopause is shown as a dashed line. The slow mode expansion fan (SEF) is shaded. (Yang and Sonnerup [126].) (Copyright by American Geophysical Union, 1977.)

fan. The intermediate wave, which marks the magnetopause, accomplishes the field direction reversal and an associated plasma acceleration parallel to the magnetopause and away from the reconnection line. The magnetic-field magnitude remains constant across this wave but it then increases to its higher magnetospheric value in the slow expansion fan across which the plasma pressure also is reduced to match the pressure in the magnetosphere, taken to be equal to zero in the model. The quantitative details of this model have not been worked out for fast-mode expansion in the inflow. But for the incompressible slow-mode expansion model, various types of asymmetries in the flow and field have been analyzed [26,82,106]. Certain compressible counterparts of these geometries have been studied by Yang [124] by use of the procedure of lumping slow-mode effects in the inflow, discussed in subsect. 4.2. In particular, the case of vacuum conditions in the magnetosphere has been reported in detail [126]. A typical resulting field and flow configuration is as shown in fig. 18. The model predicts the following features of the magnetic field: (i) a small magnetic field component normal to the magnetopause; (ii) rotational behavior of the magnetic-field component tangential to the magnetopause; (iii) a gradual increase in magnetic field intensity inside the magnetopause. In terms of plasma flow, the model predicts: (i) flow of magnetosheath plasma normal to and across the magnetopause with speed equal to the Alfvén speed based on the normal magnetic field component; (ii) tangential acceleration of the plasma to speeds of

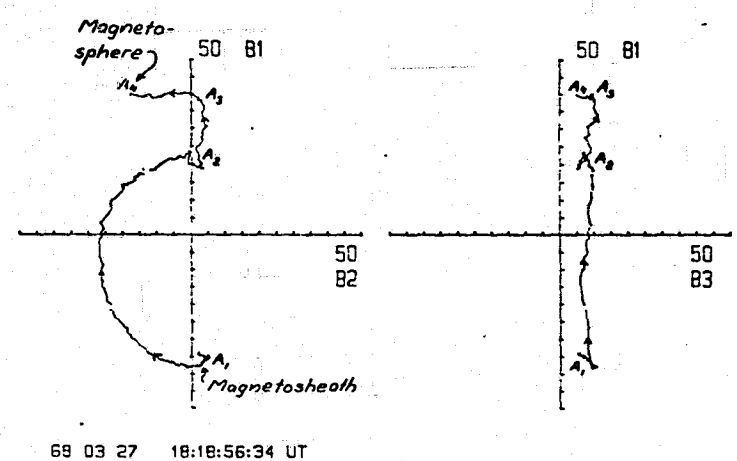

Fig. 19. Polar plots of magnetic field at the magnetopause. Left hand figure shows the field components B_1 and B_2 tangential to the magnetopause during an OGO-5 crossing; right hand figure shows the nearly constant magnetic-field component B_3 normal to the magnetopause. The field is given in units of γ (1γ = 1nt). Intermediate wave or rotational discontinuity is segment A_1–A_2 of the left-hand trace: the slow expansion fan is segment A_2–A_3. The segment A_3–A_4 may be caused by a finite gyroradius effect not contained in the MHD model.

the order of 500–750 km sec^{-1} as it crosses the magnetopause; (iii) no change in plasma density or temperature as it crosses the magnetopause; (iv) an isentropic decrease in density and temperature and an associated velocity increase as the plasma expands in the slow expansion fan inside the magnetopause. To date, the predicted plasma behavior has not been observed. At various times some but usually not all of the predicted magnetic signatures have been seen [108]. An example is shown in fig. 19.

4.4. Reconnecting fields forming an arbitrary angle

In his original paper on reconnection, Petschek [90] observed that in incompressible two-dimensional reconnection flow, a constant magnetic field component B_z could be added to any solution without changing the flow or magnetic field configuration in the xy plane (refer to fig. 6). Thus, it is possible to generate solutions that describe the reconnection of fields that form an arbitrary angle. This provides a link between the traditional cosmic reconnection models and the problems of reconnection in nearly force-free field configurations, such as the tokamak [120–122]. This procedure has provided the basis of a number of attempts to describe the dependence of the cross-magnetospheric electric potential difference on magnetosheath field direction, assuming the former to be caused by magnetopause reconnection [49,58,59,107]. The result of these geometrical analyses is that the potential should have a principal angle dependence given by the function *

$$f(\theta) = \frac{(B_0/B_i - \cos\theta)^2}{1 + (B_0/B_i)^2 - 2(B_0/B_i)\cos\theta}, \tag{4.1}$$

where θ denotes the angle between the tangential field B_i in the magnetosphere and B_0 in the magnetosheath. For $\cos\theta \geq B_0/B_i$ no reconnection occurs ** and $f(\theta) \equiv 0$. Observations [13] indicate a low energy injection rate from the solar wind into the magnetospheric ring current system when $\theta < \frac{1}{2}\pi$, a result which appears compatible with eq. (4.1). Observations [12] of the magnetosperic cusp location as a function of θ also are in qualitative agreement with this equation.

Recently, Cowley [25,28] has pointed out that incompressible solutions exist in which B_z is a function of x and y. Thus the assumption underlying eq; (4.1), of one and the same value of B_z on the magnetospheric and the magnetosheath side of a typical magnetopause reconnection model, may be invalid. It is noted that this assumption corresponds to a situation where the net current in the magnetopause (and in the diffusion region) is parallel to the separator.

In the incompressible MHD approximation the equations describing the flow and

* In ref. [49] the functional dependence is $[f(\theta)]^{1/2}$.

** If the magnetosheath field magnitude exceeds the magnetosphere field, the subscripts o and i are to be interchanged.

field in the xy plane are completey uncoupled from the differential equations for the velocity component v_z and for B_z. However, as pointed out by Cowley [25], an indirect coupling exists via the requirement that the line integral $\oint \boldsymbol{E} \cdot d\boldsymbol{l} = 0$ for any closed loop which encircles the diffusion region. This requirement poses an additional constraint on the shape of the diffusion region, a constraint that does not arise when $B_z = 0$, or $B_z = \text{const.}$, and that does not appear to be automatically satisfied by the diffusion region of plane reconnection geometries. Thus it is not clear at the present time whether Cowley's criticism of eq. (4.1) has a firm foundation in incompressible MHD theory. But even if it doesn't, the use of a constant B_z in the real compressible magnetopause flow situation to construct reconnection geometries for arbitrary θ values remains hypothetical. Further theoretical study of this problem requires detailed analysis of compressible external and diffusion-region flows and appropriate matching of these flows at the edge of the diffusion region.

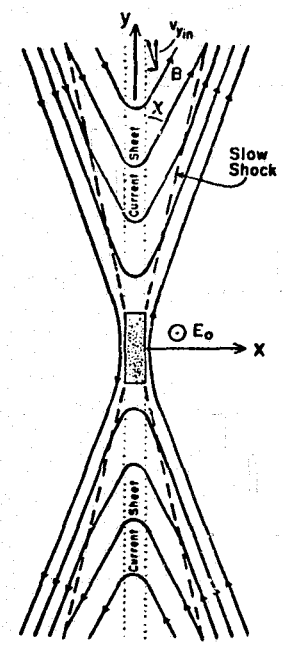

Fig. 20. Hill's [59] collisionless reconnection model. The magnetic-field change across the slow shock becomes weak for $\beta \equiv 2\mu_0 p/B^2 \to 0$ with the principal field reversal occurring in a current layer at $x = 0$.

4.5. Collisionless model

No complete or nearly complete collisionless models for the external reconnection region have been developed to date. But certain partial results have been obtained by Hill [59]. He suggests that for small β values the principal field reversal is accomplished by a current sheet located on the y axis, as shown in fig. 20, with only a small amount of field-line bending at the slow shocks. Hill does not treat the flow and field configurations in the inflow or in these weak shocks. Rather he assumes that, away from the magnetic null point at the origin, the field lines form an angle χ with the current sheet. He then proceeds to discuss the properties of the sheet. One-dimensional self-consistent Vlasov equilibria of such sheets have been obtained numerically by Eastwood [36,37]; an approximate analytic theory using the adiabatic invariant [34,65,104] associated with the meandering particle orbits in the sheet has also been given [38]. However, the result primarily used by Hill is obtained directly from the overall stress balance at the sheet, without reference to the sheet structure: in a frame of reference sliding along the y axis (see fig. 20) with a speed such that the reconnection electric field E_0 vanishes, the usual firehose limit must apply. Assuming the magnetic moment of individual particles to be preserved, Hill shows that for inflow along the x axis * this condition may be expressed as a local reconnection rate

$$E_0/v_A B = (1-\alpha)^{1/2} \sin\chi \cos\chi, \tag{4.2}$$

where $v_A \equiv B/(\mu_0\rho)^{1/2}$ and B are the Alfvén speed and magnetic field, respectively, in the region adjacent to the current sheet. Further, the anisotropy factor α of the incident particles is defined by

$$\alpha = 2\mu(p_\parallel - p_\perp)_{in}/B^2. \tag{4.3}$$

Note that $\alpha = 0$ corresponds to isotropic pressure, $\alpha = 1$ to firehose conditions (taking account of the fact that the total plasma density ρ is twice the density, ρ_{in}, of the incident particles).

The preceding result is incomplete in that the angle χ must be a function of the reconnection rate. Also, the rate should refer to conditions on the x axis in the inflow region. Equation (4.2) is nevertheless interesting because it suggests that pressure anisotropy in the incoming plasma may be an important factor. In particular, it appears that reconnection may cease altogether for $\alpha = 1$.

Using the same approach, Hill has also considered the case of reconnection of fields of unequal magnitude and with a constant B_z component present. He obtains the formula (4.1) for the angular dependence of the reconnection potential.

* Hill's analysis also includes an unspecified velocity component v_y of the incoming particles, which we have set equal to zero.

The particle energization in a model of Hill's type is seen to be the direct result of inertia and gradient drifts in the current sheet, moving positive ions in the direction of the reconnection electric field, electrons in the opposite direction. It is also important to note that the energized plasma will be streaming out nearly parallel to the y axis, i.e., for small angles χ, nearly parallel to the magnetic field on both sides of the current sheet. By contrast, the symmetric fluid dynamical models yield an exit plasma flow that is perpendicular to the weak magnetic field in the two exit flow regions (see figs. 13 and 14 below).

5. Fluid description of the diffusion region

A complete theoretical treatment of the reconnection problem requires not only a self-consistent solution for the external flow, but also an internal, or diffusion-region solution which describes the essential dissipative physical processes operating in that region, and which joins smoothly to the external solution. In the present section we review attempts to describe the diffusion region in terms of continuum equations which incorporate effects of plasma microinstabilities, if any, by means of an effective conductivity σ.

A brief discussion of one-fluid theories is given in subsect. 5.1. In magnetospheric applications of reconnection, the collisional resistive length $(\mu_0\sigma v_1)^{-1}$ is much smaller than relevant inner plasma scales, such as the electron inertial length. Thus one-fluid theory is directly applicable only if turbulent processes generate an effective resistive length which exceeds these inner scales. But even if that condition is not met, one-fluid theory serves the important purpose of providing an opportunity for a careful mathematical treatment in one region of plasma-parameter space.

The two-fluid description of the diffusion region is dealt with in subsects. 5.2 and 5.3. The former discusses the importance of the electron inertial length in determining the width $2x^*$ of the diffusion region when no collisional or turbulent resistivity is present. In the latter section, the importance of Hall currents and of the ion-inertial length and gyroradius are discussed.

5.1. One-fluid models

Detailed studies of the flow and field configuration in the diffusion region, using one-fluid magnetohydrodynamics, have utilized two approaches: series expansion around the magnetic null point, and development of integral or "lumped" equations for the entire diffusion region. Additionally, certain exact solutions exist.

Series expansions have been given by Priest and Cowley [93] and by Cowley [27]. They found that in incompressible flow, and assuming analytic behavior at the null point, a plasma velocity of the form $v_x = -k_1 x$, $v_y = k_1 y$ to lowest order yields a magnetic field behavior of the form $B_x = k_2 y^3$, $B_y = k_3 x$, i.e., the field lines touch at the neutral point, rather than cross at an angle $\alpha \neq 0$. The latter

type of configuration may however be obtained by assuming a third-order, rather than a first-order zero in $v_x(x)$ at $x = 0$. Furthermore, Yeh [128] has shown that the flow and field behavior near the null point need not be analytic. Logarithmic terms are possible in the expansion. Whether or not such terms are in fact present can be determined only by matching of the series expansion solution to an appropriate external solution, which has not yet been done. It also appears that the inclusion of compressibility effects will invalidate the above-mentioned result of Priest and Cowley. Finally, Cowley [27] has shown that series expansions yielding a non-constant field $B_z(x, y)$ are possible. But the question of whether such solutions may be matched to corresponding external solutions with non-constant B_z (see ref. [25]) has not been resolved.

The first lumped analysis of the diffusion region was performed by Parker [86] with application to Sweet's resistive current-sheet model [113] of a solar flare. The analysis yielded the following expression for the reconnection rate in incompressible flow:

$$M_{A_1} \simeq (\mu_0 \sigma v_{A_1} y^*)^{-1/2}. \tag{5.1}$$

This result is obtained directly from eqs. (2.5) and (2.7) with $\rho_2 = \rho_1$. Originally, the formula was used with y^* replaced by L, the half-length of the current sheet. It then describes field annihilation (see subsect. 2.4) and yields a value of M_{A_1} that is far too small to account for an energy-release time of the order of 10^3 sec in a solar flare, or for the observed potential difference of 20–100 kV across the terrestrial magnetosphere. Later Petschek [90] used the formula (5.1), now with $2y^*$ representing the height of the diffusion region and with $y^* \ll L$, to describe the diffusion-region flow in his model. The basic point made by Petschek is that eq. (5.1) determines, not the reconnection rate, but the height y^* of the diffusion region. In agreement with the discussion in subsect. 2.3, y^* is then seen to be proportional to $M_{A_1}^{-2}$.

A more detailed lumped analysis was performed by Sonnerup [103] in an attempt to develop a diffusion region solution for the slow-mode reconnection geometry in fig. 14. The treatment is incomplete because it does not take account of the momentum balance. Additional criticism has been offered by Vasyliunas [118] on the basis that the model implicitly assumes an abrupt switch from finite to infinite electrical conductivity at the outer edge of the diffusion region. Considering the extreme simplification of the external flow in this model, with slow expansion effects lumped into a single discontinuity (see subsect. 4.1 and fig. 14), this latter criticism is probably not of serious consequence. The following qualitative results of the analysis are likely to remain valid for the slow-mode reconnection model in fig. 14:

(i) A relationship exists between M_{A_1} and the magnetic Reynolds number $R_y \equiv \mu_0 \sigma v_{A_1} y^*$ which is of the form given by Parker, eq. (5.1), for small values of M_{A_1}, and which yields $R_y = 0$ for $M_{A_1} = (1 + \sqrt{2})$. Thus, the dimensions of the diffusion region shrink toward zero as M_{A_1} approaches its maximum value.

(ii) When the slow-mode expansion in the inflow is concentrated into discontinuities as in fig. 14, the increase in magnetic field and decrease in flow speed, described in subsects. 4.1 and 4.2 must occur in the outer portions of the diffusion region. Thus, as the origin is approached along the $\pm x$ axis, the magnetic field first increases then decreases to zero while $|v_x|$ decreases montonically to zero. Thus, in the outer portion of the diffusion region the field behaves almost in a frozen-in manner. This may account for the large diffusion region width x^* found in the analysis [103,118].

Two exact solutions exist which describe flow near the magnetic null point. Yeh [129], obtained shock-free similarity solutions by assuming resistivity and viscosity to increase linearly with distance from the origin. It is not clear how such assumptions can be reconciled with an exterior solution in which dissipative effects are confined to shocks. A different type of exact solution has been discussed by Priest and Sonnerup [95,109]. It describes an incompressible two or three-dimensional MHD resistive stagnation-point flow at a current sheet. The field lines are straight and parallel to the current sheet. Thus, purely resistive magnetic field annihilation without reconnection occurs, as illustrated in fig. 21. These solutions represent a

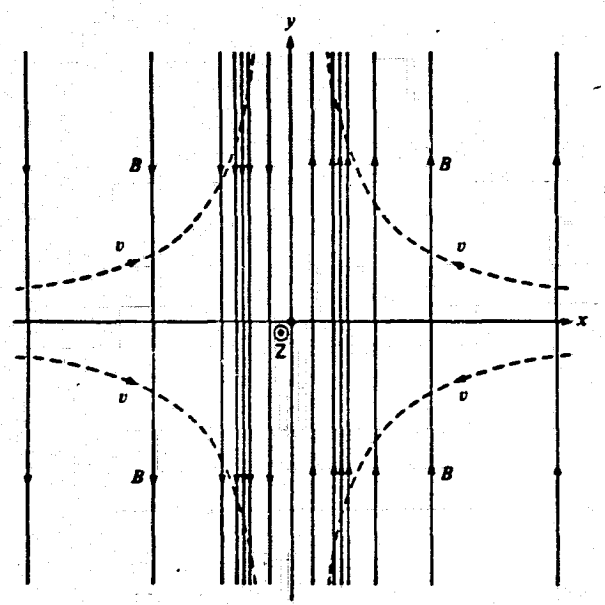

Fig. 21. Magnetic field lines and streamlines for stagnation point flow, $v = (-k_1 x, k_2 y, k_3 z)$, at a current sheet. The diffusion–dominated region is shaded (Sonnerup and Priest [107]).

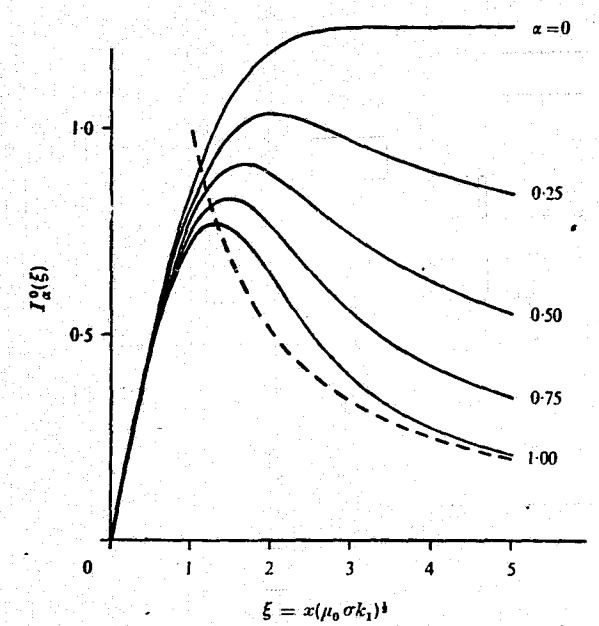

Fig. 22. Nondimensional magnetic-field profiles $I_\alpha^0 = B_y E_0^{-1} (\mu_0\sigma/k_1)^{-1/2}$ for the configuration in fig. 21 in the resistive limit ($\alpha = k_2/k_1$; $k_3 = k_1 - k_2$). Plane stagnation point flow for $\alpha = 1$, axisymmetric flow for $\alpha = \frac{1}{2}$. The frozen field profile for $\alpha = 1$ is shown by dashed line (Sonnerup and Priest [109]).

generalization of a case studied by Parker [88]. The resulting magnetic field profiles are shown in fig. 22. Three features are of interest. First, the characteristic width of the current layer is of the order of the resistive length as expected. Second, the frozen field condition applies at large $|x|$ values and leads to a gradual increase in the field magnitude $|B_y|$ as $|x|$ and $|v_x|$ decrease. As resistivity effects become increasingly important $|B_y|$ reaches a maximum and then decreases to zero at $x = 0$. This is precisely the behavior described in (ii) above. Third, a nonconstant value of B_z is possible.

5.2. Two-fluid effects: electron scale lengths

In the two-fluid description of an electron–proton plasma, the ordinary Ohm's law is replaced by a generalized form (see, e.g., Rossi and Olbert [96]).

$$E + v \times B = \frac{j}{\sigma} + \frac{m_e}{ne^2}\left[\frac{\partial j}{\partial t} + \nabla \cdot (jv + vj)\right] - \frac{1}{ne}\nabla \cdot \mathbf{P}_e + \frac{1}{ne} j \times B. \qquad (5.2)$$

As pointed out by Vasyliunas, the terms on the right-hand side may introduce a variety of plasma scale lengths into the problem. The first term yields the resistive length $\lambda_r = (\mu_0\sigma v_1)^{-1}$; the second set of terms yields the electron inertial length $\lambda_e = (m_e/\mu_0 ne^2)^{1/2}$; the off-diagonal parts of the electron stress tensor term $\mathbf{P}_e$ yield the electron gyroradius; the last term, describing the Hall effect, yields $(v_A/v_1)\lambda_i$ where $\lambda_i = (m_i/\mu_0 ne^2)^{1/2}$ is the ion inertial length. The importance of the diagonal terms in $\mathbf{P}_e$ has not been studied: with isotropic pressure and isentropic flow, these terms are cancelled identically by an electrostatic field.

To illustrate the effects of the electron inertia terms we now generalize the stagnation-point flows discussed by Sonnerup and Priest [109] to include two-fluid effects. Assuming incompressible flow and diagonal stress tensors for ions and electrons, the flow and fields are of the form:

$$v = -\hat{x}k_1 x + \hat{y}k_2 y + \hat{z}k_3 z; \qquad B = \hat{y}B_y(x) + \hat{z}B_z(x); \qquad (5.3)$$

where the quantities k_1, k_2 and k_3 are constants such that $k_1 = k_2 + k_3$. These assumptions lead to a Bernoulli-type pressure integral

$$p = p_0 - \tfrac{1}{2}\rho(k_1^2x^2 + k_2^2y^2 + k_3^2z^2) - (2\mu_0)^{-1}(B_y^2 + B_z^2)$$

of the momentum equation, and to the following components of the induction equation [the curl of eq. (5.2)]:

$$\lambda_e^2 k_1 x B_y''' + (k_2\lambda_e^2 - 1/\mu_0\sigma) B_y'' - k_1 x B_y' - k_2 B_y = 0,$$

$$\lambda_e^2 k_1 x B_z''' + (k_3\lambda_e^2 - 1/\mu_0\sigma) B_z'' - k_1 x B_z' - k_3 B_z = 0. \qquad (5.4)$$

It is seen that only the electron-inertial length and the resistive length appear in eqs. (5.4). The Hall current term in eq. (5.2) is curl-free and is cancelled exactly by a Hall electric field $E_x(x)$. Thus the ion inertial length does not appear. The solutions of eqs. (5.4) in the resistive limit are illustrated in fig. 22. In the inertial limit, the odd solutions are shown in fig. 23 for various values of $\alpha \equiv k_2/k_1$. As expected, the width of the magnetic-field reversal region is now of the order of the electron inertial length regardless of the flow rate. Further, it is observed that for $\alpha = 1$, i.e., for plane flow, the current density is logarithmically infinite at $x = 0$, a conclusion also drawn by Coroniti and Eviatar [22]. Thus some form of plasma microinstability or other effect by necessity must be present to reduce the current density to a finite value.

The off-diagonal terms in the electron pressure tensor will provide a finite electron gyroradius correction to the preceding results. When the electron gyroradius greatly exceeds λ_e, it will replace the electron inertial length as the minimum width of the layer [118]. However, a detailed calculation of these effects is difficult because the appropriate form of the off-diagonal pressure tensor terms is not known

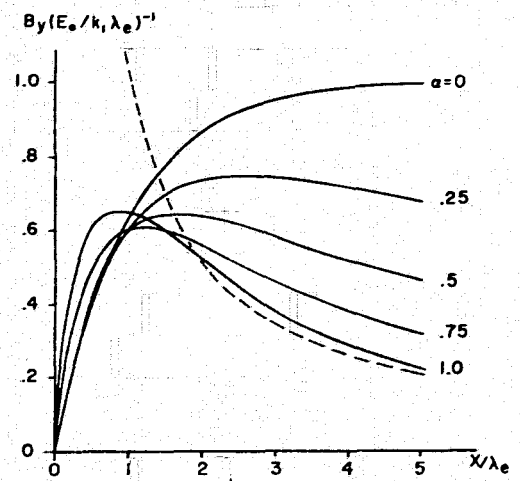

Fig. 23. Nondimensional magnetic-field profiles for the configuration in fig. 21 in the electron-inertial limit [$\alpha = k_2/k_1; k_3 = k_1 - k_2; \lambda_e = (m_e/\mu_0 ne^2)^{1/2}$]. Plane stagnation-point flow for $\alpha = 1$; axisymmetric flow for $\alpha = \frac{1}{2}$. The frozen field profile for $\alpha = 1$ is shown by dashed line.

in a field reversal region of width comparable to the orbit scale.

Vasuliunas [118] pioneered the study of electron inertial effects in the diffusion region. In an approximate lumped analysis which neglected compressibility (later included by Coroniti and Eviatar [22]), off-diagonal stress tensor elements, and Hall-current effects, he showed that the diffusion region in the inertial limit (i.e., neglecting resistivity) is hyperbolic in shape with width

$$x^*(y) \simeq (M_{A_1}^2 y^2 + \lambda_e^2)^{1/2}. \tag{5.5}$$

The exact analysis given here in all essential respects confirms Vasyliunas' results for small values of $M_{A_1}^2 y^2/\lambda_e^2$. It also provides magnetic field profiles $B_y(x)$ whereas Vasyliunas neglected B_y within the diffusion region. Note that the formula (5.5) yields $x^*(0) \simeq \lambda_e$; $y^* \simeq \lambda_e/M_{A_1}$, in agreement with the behavior quoted in subsect. 2.3. [between eqs. (2.8) and (2.9)].

5.3. Two-fluid effects: ion scale lengths

It is not clear how a diffusion region of the small physical dimensions implied by eq. (5.5) can be joined to an external solution with slow shocks of thickness [20] comparable to, or greater than, the ion inertial length. Thus we are led to ask why

the ion inertial length and the ion gyroradius did not appear in the previous analysis. The former is introduced via the Hall current term $\boldsymbol{j} \times \boldsymbol{B}/ne$ in eq. (5.2). It may be cancelled by a Hall electric field only when it is curl free, which was the case for the stagnation-point in subsect. 5.2. The ion gyroradius as introduced via the off-diagonal terms in the ion pressure tensor. We now demonstrate that in plane reconnection flow these effects imply the presence of Hall-current components j_x and j_y as well as a macroscopic flow $v_z(x, y)$ and a field component $B_z(x, y)$. Assuming $\partial/\partial z \equiv 0$ and omitting electron inertia and pressure terms for brevity, the z components of the momentum and induction equations are, respectively:

$$\rho v_x \frac{\partial v_z}{\partial x} + \rho v_y \frac{\partial v_z}{\partial y} = -\left(\frac{\partial}{\partial x} P_{xz} + \frac{\partial}{\partial y} P_{yz}\right) + \frac{1}{\mu_0}\left(B_x \frac{\partial B_z}{\partial x} + B_y \frac{\partial B_z}{\partial y}\right); \tag{5.6}$$

$$\left(B_x \frac{\partial v_z}{\partial x} + B_y \frac{\partial v_z}{\partial y}\right) - \left(v_x \frac{\partial B_z}{\partial x} + v_y \frac{\partial B_z}{\partial y}\right) = -\frac{1}{\mu_0 \sigma} \nabla^2 B_z$$

$$+ \frac{1}{ne}\left(B_x \frac{\partial j_z}{\partial x} + B_y \frac{\partial j_z}{\partial y}\right); \tag{5.7}$$

where the particle density n and the conductivity σ have been assumed constant. In the second equation, the Hall term (the last term on the right) is seen to be of the form $(\boldsymbol{B} \cdot \nabla j_z)/ne$, i.e., it vanishes only when the current j_z remains constant along a field line. Otherwise it becomes a driving term in the second equation forcing values of v_z and B_z different from zero. Similarly, in the first equation it appears that the stress terms will usually force values of v_z and B_z different from zero. These terms are expected to introduce the ion gyroradius as a characteristic length into the problem. However, it is difficult to discuss these effects in detail, because the form of the stress terms in a thin field-reversal region is not known. Thus, we confine attention to the Hall current term, $(\boldsymbol{B} \cdot \nabla j_z)/ne$. While this term vanishes in the stagnation-point flow discussed in the previous section (and indeed along the x axis of any configuration), it cannot vanish throughout the diffusion region. We may estimate the magnitude of B_z by approximately equating the third term on the left and the second term on the right in eq. (5.7):

$$v_x \, \partial B_z/\partial x \sim (1/ne) B_x \, \partial j_z/\partial x.$$

With $v_x \sim v_1, B_x \sim B_2 \sim B_1 M_{A_1}, j_z \sim B_1/\mu_0 x^*$ and $\partial/\partial x \sim 1/x^*$ we then find

$$B_z/B_1 \sim \lambda_i/x^*,$$

where $\lambda_i \equiv (m_i/\mu_0 ne^2)^{1/2}$ is the ion inertial length. Thus it appears that values of x^* much less than λ_i would give rise to unacceptably high values of B_z. A similar comparison between the terms $B_x \partial v_z/\partial x$ and $(ne)^{-1} B_x \partial j_z/\partial x$ yields $v_z/v_{A_1} \sim \lambda_i/x^*$.

Again, $x^* \ll \lambda_i$ leads to an unacceptable result. Vasyliunas [119] has pointed out that off-diagonal electron pressure tensor terms, not shown in eq. (5.7), may possibly cancel the Hall term. However, there seems to be no obvious physical reason to expect such a cancellation. And problems with the off-diagonal stress tensor terms P_{xz} and P_{yz} in eq. (5.6) would still remain.

Detailed analysis of the effects described above is not available at present. However, a nonvanishing field component $B_z(x, y)$ would imply the presence of Hall currents $j_x = \mu_0^{-1}\,\partial B_z/\partial y$ and $j_y = -\mu_0^{-1}\,\partial B_z/\partial x$ in the diffusion region. The expected current flow and field pattern is shown schematically in fig. 24. The behavior of the B_y and B_z components indicated in the figure should be easy to identify in magnetic-field vector measurements from a satellite which crosses the diffusion region at the magnetopause or in the geomagnetic tail.

The reason for the appearance of the Hall current component j_x with the direction shown in fig. 24 may be understood by noting that for $\sigma \simeq \infty$ the generalized Ohm's law [eq. (5.2)] implies that apart from electron-inertia and gyroradius effects the magnetic field is frozen into the electron component of the plasma. Thus the electrons flowing toward $x = 0$ are brought to rest over a distance of the

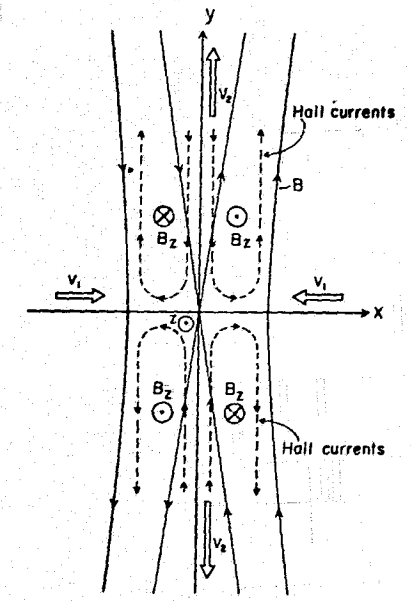

Fig. 24, Schematic picture of Hall current loops in the diffusion region. Also shown is the transverse magnetic field $B_z(x, y)$ induced by these currents.

order of the electron inertial length or the electron gyroradius. If the ions are similarly brought to rest over a distance comparable to the ion inertial length or the ion gyroradius, a relative motion of electrons and ions results, leading to currents j_x in the direction shown in the figure. Charge conservation then implies the presence of j_y as shown.

The z component of the force $\boldsymbol{j} \times \boldsymbol{B}$ associated with the Hall currents also leads to an acceleration of the plasma in the $\pm z$ direction. This effect is caused by drift and meandering motion of the ions in the current sheet. It may be interpreted as an ion current in the layer. Indeed, if $x^* \sim \lambda_i$, the principal current component j_z is carried by the ions; if $x^* \sim \lambda_e$ it is carried by the electrons.

It is evident that in the absence of plasma resistivity (classical or turbulent) the electron length scales must play a significant role in the diffusion region structure. But from the preceding discussion it appears possible that the ion length scales may determine the overall width $2x^*$ of the diffusion region while the electron length scales give the size of the detailed structures of j_x, j_y, and j_z near $x = 0$. From the preceding discussion, it is concluded that, even without plasma turbulence, the electromagnetic structure of the diffusion region may be far more complicated than previously assumed.

6. Non-fluid effects in the diffusion region

In magnetospheric and interplanetary applications of the reconnection process, collisional resistive effects in the diffusion region are negligible. Thus an effective resistivity in that region must derive either from inertia effects or from plasma turbulence. The former effects were dealt with in subsects. 5.2 and 5.3 from a fluid point of view. However, to develop a physical understanding of inertial phenomena in the diffusion region, it is useful to obtain an approximate expression for the effective inertial conductivity. This is done in subsect. 6.1. Subsection 6.2 examines plasma instabilities which may generate steady-state turbulence in the diffusion region, but with details provided only for the ion-acoustic instability. Subsection 6.3 discusses several threshold effects that might be of importance for the onset of reconnection and for the identification of situations in which reconnection may not occur. Particle acceleration in nonsteady reconnection is discussed in subsect. 6.4.

It will become quickly apparent that most of the material in this section is speculative in nature. Different processes may occur in different applications. It appears that no systematic effort has been made to sort out which mechanisms dominate in different parts of plasma parameter space.

In reading the present section, it will be useful to refer to the typical values of several physical parameters given in table 1.

6.1. Inertial resistivity

The concept of inertial resistivity was first discussed, in the context of magnetic field reconnection, by Speiser [108]. The basic idea is that a particle spends only a

Table 1
Physical paramaters for various reconnection sites

Quantity	Laboratory (argon plasma)	Solar flare (pre-flare state) I	Solar flare (pre-flare state) II	Magneto-pause	Magneto-tail	Interpl. sector boundary
Number density n_1 (m^{-3})	1.5×10^{20}	10^{21}	10^{15}	2×10^{7}	10^{6}	5×10^{6}
Ion temperature T_{i_1} (K)	10^{4}	10^{4}	10^{6}	10^{6}	10^{7}	5×10^{5}
Temperature ratio T_{e_1}/T_{i_1}	1	1	1	0.5	0.1	1
Magnetic field B_1 (Weber m^{-2})	1	5×10^{-2}	10^{-2}	3×10^{-8}	1.5×10^{-8}	5×10^{-9}
$\beta_{i_1} = 2\mu_0 n_1 k T_{i_1}/B_1^2$	5.2×10^{-5}	0.14	3.5×10^{-4}	0.8	1.5	3.5
$\lambda_{coll} = (\mu_0 \sigma_{coll} v_1)^{-1}$ (m)	7.8×10^{-3}	0.40	2.0×10^{-6}	1.3×10^{-4}	4.2×10^{-5}	8.0×10^{-4}
$\lambda_{turb} = (\mu_0 \sigma_{turb} v_1)^{-1}$ (m)	5.9×10^{-2}	0.20	0.94	2.5×10^{5}	5.6×10^{5}	1.9×10^{6}
$\lambda_e = (m_e/\mu_0 n_1 e^2)^{1/2}$ (m)	4.3×10^{-4}	1.7×10^{-1}	1.7×10^{-1}	1.2×10^{3}	5.3×10^{3}	2.4×10^{3}
$\lambda_i = (m_i/\mu_0 n_1 e^2)^{1/2}$ (m)	1.2×10^{-1}	7.3×10^{-3}	7.2	5.1×10^{4}	2.3×10^{5}	10^{5}

Notes: (1) Weber/m^2 = 10^4 G = 10^8 γ.
(2) $\sigma_{coll}^{-1} = 6.5 \times 10^3 \ln \Lambda / T_{e_1}^{3/2}$ (Spitzer [112]).
(3) σ_{turb} is given by eq. (6.12).
(4) $v_1 = 0.1 v_{A_1} = 0.1\, B_1/(\mu_0 n_1 m_i)^{1/2}$.

finite amount of time in the diffusion region and thus can pick up only a finite amount of energy from the electric field $E_0 \hat{z}$. The inertial conductivity is written as

$$\sigma_{inert} = \bar{n} e^2 \bar{\tau}/m, \tag{6.1}$$

where $\bar{n}$ is the average particle density in the diffusion region and $\bar{\tau}$ is the effective time available for acceleration in the electric field. The formula (6.1) may be used with either the electron mass $m = m_e$ or the ion mass $m = m_i$ depending on whether the diffusion region current is principally an electron current or an ion current. Both cases may be treated the same way so that the particle mass m will be left without a subscript.

The average displacement, $\overline{\Delta z}$, along the electric field E_0, of a particle in the diffusion region may be obtained from a simple mass balance over a box of dimensions $2x^* \times 2y^* \times \overline{\Delta z}$:

$$2n_1 v_1 2y^* \overline{\Delta z} = \bar{n} \bar{v}_z 2x^* 2y^* = 2n_2 v_2 2x^* \overline{\Delta z} \tag{6.2}$$

where $\bar{v}_z$ is the average particle speed along the electric field $E_0 \hat{z}$, and $\bar{v}_z = \overline{\Delta z}/\bar{\tau}$. As before, the subscripts 1 and 2 refer to conditiosn at the points $(x^*, 0)$ and $(0, y^*)$, respectively. From the first equality in eq. (6.2) we thus obtain

$$\bar{\tau} \simeq \bar{n} x^*/n_2 v_1. \tag{6.3}$$

When this expression for $\bar{\tau}$ is substituted into eq. (6.1) there results

$$\sigma_{inert} = \bar{n}^2 e^2 x^*/n_1 v_1 m. \tag{6.4}$$

Thus the inertial conductivity is very high for low reconnection speeds, v_1, i.e., when the configuration approaches a current sheet. This is the behavior referred to in subsect. 2.3.

Expressing the basic balance of field convection and diffusion as $\mu_0 \sigma_{inert} v_1 x^* = 1$, which is valid for small reconnection rates *, we find

$$x^* = (n_1/\bar{n})\, \lambda_1 \tag{6.5}$$

where λ_1 is the inertial length $\lambda_1 = (m/\mu_0 n_1 e^2)^{1/2}$. For $m = m_e$ this result is in agreement with Vasyliunas' formula [eq. (5.5)]. See also Coroniti and Eviatar [22]. But the calculation gives no clue as to whether the electron or the ion inertial length is to be used.

It should be realized that the value of x^* given by eq. (6.5) represents a lower

* With inertial resistivity, pure field annihilation is found to occur for $0 < M_{A_1} < \lambda_1/L$ (compare subsect. 2.4). "Small reconnection rates" implies $\lambda_1/L < M_{A_1} << 1$.

limit. The calculation assumed the time $\bar{\tau}$ available for free acceleration in the electric field to be equal to the residence time of a particle within the control box. In reality $\bar{\tau}$ must always be less than the residence time because the magnetic field does not vanish within the entire box. Thus the inertial conductivity is less than that given by eq. (6.4) and x^* is correspondingly larger than in eq. (6.5). When diamagnetic currents become important, i.e., for $\beta_1 = 2\mu_0 p_1/B_1^2 > 1$, it may be shown that x^* gradually approaches a magnitude of the order of the gyroradius instead.

The previous estimate of x^* applies only for small values of the reconnection rate. To understand this fact, we note that the expression $\mu_0 \sigma v_1 x^* = 1$, which was used in obtaining eq. (6.5), derives directly from Ohm's law in the approximate form $j_z = \sigma E_0 = \sigma v_1 B_1$ with $j_z \simeq \mu_0^{-1} \partial B_y/\partial x \simeq B_1/\mu_0 x^*$. For large reconnection rates it becomes important to incorporate the term $\boldsymbol{v} \times \boldsymbol{B}$ in the electric field, as well as the curvature term $\partial B_x/\partial y$ in the expression for j_z. The latter effect leads to a multiplicative factor $(1 - M_{A_1}^2 \rho_1/\rho_2)$ on the right-hand side of eq. (6.5) [see eq. (6.7) below] so that the size of the diffusion region decreases toward zero as the reconnection rate approaches its maximum value. Thus, for large reconnection rates, the required width of the diffusion region may be substantially less than the relevant plasma scale (the inertial length or gyroradius, depending on β_1). It is difficult to reconcile such a situation with the nature of the particle orbits in that region. Therefore, it is conceivable that steady-state reconnection with inertial resistivity as the dominant effect in the diffusion region is not possible for large reconnection rates.

The average electrostatic particle energization in the diffusion region may be obtained directly from the first equality in eq. (6.2):

$$\bar{\mathcal{E}} = e\overline{\Delta z} E_0 = \bar{n} e \bar{v}_z x^* E_0/n_1 v_1 . \tag{6.6}$$

But we also have $\bar{n} e \bar{v}_z = \bar{j}_z = \bar{\mu_0}^{-1} (\partial B_y/\partial x - \partial B_x/\partial y)$. Approximating $\partial B_y/\partial x$ by B_1/x^*, $\partial B_x/\partial y$ by B_2/y^*, noting that $B_2/B_1 = v_1/v_2 \simeq \rho_2 x^*/\rho_1 y^*$ we find

$$j_z = \bar{n} e \bar{v}_z \simeq (B_1/\mu_0 x^*)[1 - (\rho_1/\rho_2) M_{A_1}^2] \tag{6.7}$$

and from eq. (6.6)

$$\bar{\mathcal{E}} \simeq \frac{B_1^2}{\mu_0 n_1} [1 - (\rho_1/\rho_2) M_{A_1}^2] , \tag{6.8}$$

where the relations $E_0 = v_1 B_1$ and $v_1/v_2 \simeq v_1/v_{A_1} = M_{A_1}$ have been used. This formula agrees with eq. (2.11). Maximum acceleration occurs for small reconnection rates and densities: for magnetospheric conditions $\bar{\mathcal{E}} \sim 1$–10 keV. It is emphasized that eq. (6.8) represents the average energy gain. A small number of particles moving nearly along the reconnection line may gain larger amounts of energy in the electric field E_0.

6.2. Plasma turbulence

A variety of plasma instabilities may serve to generate plasma turbulence in the diffusion region and an associated turbulent conductivity σ_{turb}. We now discuss such effects in an assumed quasi-steady state of reconnection. Onset effects are dealt with in subsect. 6.3

The tearing instability, either in its collisional resistive version [45,97,117] or in the collision-free electron-inertial version [17,30,44,61,69] has been studied intensely in the context of reconnection. It generates a pattern of alternating X type and O type magnetic neutral lines in a current sheet. But most analyses of this instability pertain to current sheets with a vanishing magnetic-field component B_x perpendicular to the sheet. In other words, in the present application either the reconnection rate M_{A_1} is very small or the magnetic field lines at the null point are "touching" rather than "crossing", as discussed in subsect. 5.1. Schindler [99] has pointed out that for $B_x \neq 0$ the collisionless tearing instability may still proceed as long as the gyro-period $\tau_g = 2\pi m/eB_x$ of a particle in the field B_x exceeds the instability growth time $\tau_0 \simeq (x^*/v_{th})(x^*/R_L)^{3/2}$ where v_{th} is the thermal speed and R_L the gyroradius. This condition may be applied either to electrons (electron tearing) or ions (ion tearing). In rough terms, non-gyrotropic behavior of the particles is required for these instabilities to be possible. While the nature or existence of steady-state tearing turbulence does not appear to have been established, one cannot exclude the possibility that such turbulence could be of importance in the diffusion region [19,21,47].

Parker [89] has suggested that interchange instability may serve to enhance the flow rates in Sweet's [113] current sheet model. In the geomagnetic tail, the instability would be driven, not in the diffusion region itself, but rather by the pressure gradient and field curvature in the near-earth section of the tail plasma sheet (see fig. 4). A detailed analysis, including the impeding effects of the ionosphere, has been given recently by Kan and Chao [66]. It indicates growth times of the order of a few hours with ionospheric coupling, a few minutes without such coupling. The situation relative to the level of steady-state turbulence is not clear.

Huba et al. [64] have proposed that the lower-hybrid-drift instability may provide anomalous resistivity in the diffusion region. It appears that the threshold for this instability is sufficiently low to permit the diffusion region width to be of the order of the ion inertial length.

Haerendel [50] has discussed the possibility that the electron–cyclotron drift instability, which has a current threshold somewhat less than that of the ion–acoustic instability, may generate turbulence in a diffusion region of width $2x^*$ equal to a few electron-inertial lengths. However, its importance has been questioned by Coroniti and Eviatar [22] on the basis that the gyrocoherence required by the instability may not be available in the diffusion region. They also note that when the electron drift speed exceeds the threshold for the ion–acoustic instability the electron–cyclotron drift mode goes over nonlinearly to the ion–acoustic one.

The ion–acoustic instability has been proposed [9,22,41,101] as a likely agent for the generation of turbulence in the diffusion region. It will be dealt with in some detail in the remainder of this subsection. This is done for illustrative purposes and not as an indicator of a universal preference for this particular mechanism. On the other hand, the ion–acoustic instability appears in fact to occur in laboratory reconnection experiments [9,85]. But it is probably not relevant to magnetospheric reconnection.

For a current-driven instability such as the ion–acoustic one to occur, the current density in the diffusion region must exceed a certain minimum value, corresponding to a critical current velocity v_c, i.e., $j > \bar{n}ev_c$. If Hall currents are present, as discussed in subsect. 5.3, the total current must be considered. Here we shall confine attention to the component j_z. According to eq. (6.7) we then find

$$j_z = \frac{B_1}{\mu_0 x^*}\left[1 - \frac{\rho_1}{\rho_2} M_{A_1}^2\right] \geqslant \bar{n}ev_c \tag{6.9}$$

where, for the ion–acoustic instability

$$v_c = (kT_i/m_e)^{1/2}/f(T_e/T_i). \tag{6.10}$$

Combination of eqs. (6.9) and (6.10) yields

$$x^*/\lambda_e \leqslant (2/\beta_i)^{1/2}\,[1 - (\rho_1/\rho_2)\,M_{A_1}^2]\,f(T_e/T_i), \tag{6.11}$$

where $\beta_i \equiv 2\mu_0 \bar{n} kT_i/B^2$. The function $f(T_e/T_i)$ is shown in fig. 25. It is seen that $f(T_e/T_i)$ is of the order unity for $T_e \simeq T_i$ so that for small M_{A_1}, and for β_i of order unity or less, the critical diffusion region width is of the order of the electron inertial length. For large values of β_i, x^* must be considerably less than λ_e suggesting that only a sub-portion of the diffusion region may contain ion–acoustic turbulence

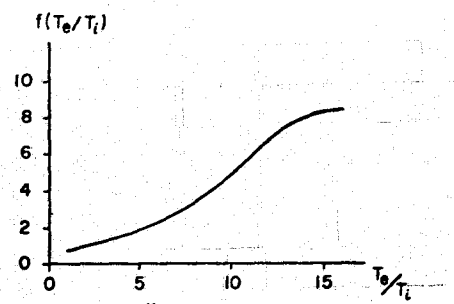

Fig. 25. Function $f(T_e/T_i) = (kT_i/m_e)^{1/2}/v_c$ where v_c is the critical current velocity for onset of ion-acoustic instability (after Fredricks [40]).

(compare the logarithmic singularity in j_z at $x = 0$, discussed in subsect. 5.2). Coroniti and Eviatar [22] indicate $\beta < 5$ as a condition for their analysis to remain valid. For greater β values, the size of the turbulent region approaches the wavelength of the ion–acoustic turbulence. For M_{A_1} of order unity the diffusion region must also be very small for ion–acoustic turbulence to occur.

For high temperature ratios T_e/T_i, the instability may occur for x^* considerably larger than λ_e but probably not as large as λ_i (see fig. 25). A large temperature ratio may perhaps be generated temporarily by electron run-away in a current sheet at the onset of reconnection (see next subsection). For example, in the double inverse pinch experiment the collisional resistive length considerably exceeds λ_e (see table 1), so that run-away must occur to initiate the ion–acoustic instability. But it appears unlikely that a large temperature ratio T_e/T_i could be sustained on a steady basis in a diffusion region of width much greater than λ_e since in most of such a region the run-away would have to occur transverse to a strong magnetic field. We conclude that steady-state ion–acoustic turbulence, driven by the current component j_z, is unlikely to be important unless the diffusion region width, $2x^*$, is of the order of the electron inertial length. At the same time it is observed that the Hall current component j_y discussed in subsect. 5.3 (fig. 24) may be sufficiently intense to drive the instability in parts of a diffusion region of total width comparable to the ion inertial length.

Coroniti and Eviatar [22] have examined the question of the turbulent saturation of the ion–acoustic instability in detail. They conclude that the current velocity will remain close to the threshold value given by eq. (6.10). The resulting weak steady-state turbulence is adjusted to give the value of turbulent conductivity required to satisfy $\mu_0 \sigma_{turb} v_1 x^* \simeq 1$ with x^* given by the equality in eq. (6.11). On the other hand, common estimates of the effective electrical conductivity associated with the ion–acoustic instability, in a state of turbulent saturation, such as (see, e.g., refs. [40,115])

$$\sigma_{turb} = \frac{\bar{n}e^2}{m_e}\left[\frac{10^2}{\omega_{pe}}\,\frac{(kT_i/me)^{1/2}}{j/ne}\left(\frac{T_i}{T_e}\right)^{1/2}\right], \tag{6.12}$$

where $\omega_{pe} = (\bar{n}e^2/\epsilon_0 m_e)^{1/2}$, give a much too low value of the conductivity, even at the critical current velocity $j/\bar{n}e = v_c$. In other words, with reasonable reconnection speeds and with x^* satisfying eq. (6.11), one finds $\mu_0 \sigma_{turb} v_1 x^* \ll 1$, which is impossible in a steady state. In table 1, this fact is manifested by the inequality $\lambda_{turb} \gg \lambda_e$, where λ_{turb} is the turbulent resistive length.

6.3. Onset of rapid reconnection

There is ample observational evidence relating to solar flares, to the earth's magnetotail, and to the double inverse pinch experiment, to indicate that occasionally rapid reconnection is switched on in an abrupt, almost explosive manner. At the

earth's magnetopause, if reconnection actually occurs there, the switch-on appears more gentle and may be a direct consequence of the interplanetary field turning southward so that the angle between the reconnecting fields exceeds some critical value (compare subsect. 4.4). It is natural to assume that the more explosive events might be associated with a plasma instability and/or an abrupt decrease in the effective conductivity in a current sheet or in the diffusion region of a slowly reconnecting configuration. Five such possibilities, all speculative at present, are mentioned below:

(i) *Thermal instability.* It has been proposed [16,19,56] that the flash phase of a solar flare may be associated with a thermal instability. For example, explosive solutions of the electron energy equation, i.e., solutions which yield an infinite temperature in a finite time, are known to occur when collisional Joule dissipation dominates the equation. This instability is not relevant for magnetospheric applications or for the upper solar atmosphere (case II, in table 1).

(ii) *Beta threshold.* It may be hypothesized [106] that, in a collision-free plasma, reconnection is suppressed for high β_1 values but may occur for small β_1. Thus, any current sheet in which β_1 decreases gradually from some initially large value may be converted to a rapidly reconnecting configuration when a critical β_1 value is reached. In the geomagnetic tail, an abrupt decrease in β_1 value occurs if the plasma sheet in which the tail current sheet is imbedded shrinks to a thickness equal to the current sheet thickness. On the other hand, at the subsolar magnetopause, Lees [71] and Zwan and Wolf [132] have described a magnetosheath plasma depletion mechanism (by escape along the magnetic field lines) which would tend to maintain a value of β_1 of order unity or less. The β_1 threshold is not relevant to the double-inverse pinch laboratory experiment, and probably not to solar flares because β_1 is small in these applications (table 1).

(iii) *Current threshold.* Assume that a current sheet with little or no reconnection gradually thins from an initial width of an ion gyroradius or more toward the electron inertial length, in response to an increased external total pressure, $p_1 + B_1^2/2\mu_0$. In this process the current density in the sheet increases gradually. When the threshold for onset of current-driven plasma instabilities is reached, e.g., for the ion–acoustic instability, when eq. (6.11) is satisfied, a reduction in effective electrical conductivity takes place in the layer. If this reduction occurs sufficiently rapidly, the inductance of the system will allow us to consider the current density initially to remain essentially unchanged. Instead an inductive electric field $E_z(x, t)$ is developed within the sheet to maintain the current density. The magnitude of this electric field is larger, the larger the conductivity reduction.

For a turbulent conductivity of the size used by Coroniti and Eviatar [22], E_z is of the size usually estimated for steady-state reconnection. This electric field, which is initially confined to the current sheet, is subsequently spread by fast-mode expansion waves propagating outward from the sheet as the configuration converts itself to one of steady or quasi-steady reconnection.

If the conductivity is reduced to the level given by eq. (6.12), E_z may be one or two orders of magnitude larger than typical steady-state values. Smith [102] has pointed out that the width $2x^*$ of the current sheet must then increase. As pointed out in subsect. 6.2, for reasonable flow rates we find $\mu_0\sigma v_1 x^* \ll 1$ when $x^* \simeq \lambda_e$ and with σ given by eq. (6.12). Thus an increase in x^* occurs in order to bring $\mu_0\sigma v_1 x^*$ toward unity as required in a steady state. The rate $-\partial B/\partial t$ associated with the increase in x^* is the principal source of E_z. But the main result of the increase in x^* is that condition (6.11) ultimately is violated so that the ion–acoustic instability is quenched. Smith [102] proposes that the process may then repeat itself. A state of pulsating reconnection is established. See also Bratenahl and Baum [11]. While the above arguments were given in terms of the ion–acoustic instability, other mechanisms may produce similar effects.

(iv) *Tearing threshold.* In a collision-free current sheet with a vanishing normal magnetic field component, electron tearing should be normally present, unless it is supressed by some agent such as pressure anisotropy [18] or velocity shear [60]. With a nonvanishing normal magnetic field component B_x, a threshold for the onset of collision-free tearing does exist, as mentioned in subsect. 6.2. If $|B_x|$ is originally large, no tearing occurs. But as $|B_x|$ gradually decreases it may set in when the gyroperiod in B_x exceeds the growth time. Schindler [99,100] has noted that this threshold may be exceeded for ions (but not electrons) in the geomagnetic tail current sheet during the thinning of that sheet which occurs in the expansive phase of the geomagnetic substorm. Since the tail at this time has free energy available for dissipation, the ultimate result of the onset of ion tearing should be large-scale relaxation (via reconnection) of the tail towards a state of minimum free energy, rather than merely the generation of tearing turbulence in the sheet. Further development of the ion-tearing instability theory has been given by Galeev and Zeleny [46,47].

(v) *Interchange instability.* An abrupt onset of interchange turbulence in the geomagnetic tail [66,89] may occur if the ionosphere becomes decoupled from the tail plasma sheet by the development of electric fields parallel to the magnetic lines of force.

6.4. Particle acceleration

One of the most important, and at the same time most poorly understood, aspects of magnetic-field reconnection is its presumed ability to accelerate particles to high energies. Observations in the magnetospheric tail indicate the occurrence of energetic electron and proton bursts [6,68,116] during times when reconnection may be going on. And it should be remembered that our ability to observe reconnection on the sun and in the far reaches of cosmos depends critically on the generation of energetic particles and on the electromagnetic radiation they subsequently produce.

Particle acceleration may occur either in turbulent small-scale electric fields or in

the large-scale reconnection electric field E_z. Both types of acceleration are expected to be operative principally in high-current regions: the diffusion region and the shocks. To discuss turbulent acceleration one must understand the nature of the dominant micro-processes in these regions. Since no such understanding is at hand, the discussion in this section is confined to particle acceleration in the large-scale reconnection electric field.

In many, but not all, cosmic applications, the total potential difference associated with a steady reconnection electric field is sufficiently high to account in principle for observed particle energies. However, it is only in the small diffusion region that particles have the opportunity to move along the electric field for any considerable distance. And even there, most particles have short residence times and undergo a correspondingly small energization, as shown by eq. (6.8). Thus, steady-state reconnection does not appear to be an effective mechanism for the acceleration of particles to very high energies [105]. Additionally, in applications such as the geomagnetic tail it is necessary to account for particle energies which exceed the steady-state cross-tail voltage by an order of magnitude or more. One is therefore led to consider the possibility of particle acceleration during nonsteady reconnection [116]. Two possible advantages are gained. First, the inductive electric fields may, in principle at least, become much stronger than the quasistatic ones during steady reconnection. Second, the nonconservative nature of E permits acceleration within more localized regions of space. For example, betatron acceleration to high energy may occur in a small region of space where the particles experience a large increase in magnetic field intensity. By contrast electrostatic acceleration requires particles to move large distances along the separator.

The lack of nonsteady reconnection models prevents a detailed analysis of particle acceleration. But the simple model given below may serve as an illustration of how electron energization might occur in the diffusion region. A resistively decaying one-dimensional current sheet, perhaps generated as described in subsect. 6.3, may be crudely described by

$$B = \begin{cases} \hat{y} B_1 x/x^* & |x| < x^* \\ \hat{y} B_1 |x|/x & |x| > x^* \end{cases} \tag{6.13}$$

where the sheet width x^* is an increasing function of time and B_1 is the constant field outside the sheet. Assuming no inflow into the sheet, the associated electric field is

$$E = \hat{z} \tfrac{1}{2} B_1 (1 - x^2/x_*^2)\, \mathrm{d}x^*/\mathrm{d}t . \tag{6.14}$$

The direction of this field is such that it drives the particles toward the center of the current sheet ($x = 0$). A particle accelerating freely at $x = 0$ in this electric field may be shown to gain an amount of energy given by

$$\Delta \mathcal{E} = mc^2 \{ [1 + (eB_1 \Delta x^*/2mc)^2]^{1/2} - 1 \}, \tag{6.15}$$

provided it doesn't leave the system (at $z = \pm h$) during the time it takes the current sheet to widen by Δx^*. In the geomagnetic tail $B_0 \simeq 20$nt, and for $\Delta x^* = 500$ km eq. (6.15) predicts a possible energy gain of 1.07 MeV for electrons (protons would gain a similar amount of energy only if $\Delta x^* \sim 15000$ km). Since an electron in this energy range traverses the entire tail in less than a second, it would appear that an unreasonably large value of $\mathrm{d}x^*/\mathrm{d}t$ is needed. But this is not necessarily so. If the widening current sheet is located along the separator AXB of the reconnection bubble in fig. 12, electrons may be accelerated as they move from A to B along the separator AXB. They may then return from B to A by gradient drift in the vicinity of the O type neutral line BOA where the electric field vanishes. Subsequently they reenter the acceleration region at A. By cycling electrons through this loop many times the energy gains predicted by eq. (6.15) may be achieved even for small values of $\mathrm{d}x^*/\mathrm{d}t$.

The illustrative example discussed above emphasizes that it may be necessary to consider three-dimensional time-dependent configurations in order to account for particle acceleration in the reconnection process. For further illustrative calculations, see refs. [56,116].

7. Magnetospheric evidence

Much of the observational evidence concerning the possible occurrence of reconnection in the magnetosphere has been summarized by Burch [12]. Relevant references may be found in his paper and are not, for the most part, repeated here.

A large amount of evidence exists indicating a relationship of various magnetospheric activity indices to the southward component of the interplanetary magnetic field. Also, spatial asymmetries in a variety of polar-cap processes appear to be correlated with the orientation of the interplanetary magnetic field. Such evidence is compatible with, but does not prove, the occurrence of reconnection at the magnetopause. This body of observations will not be discussed here. Instead, we focus, in subsect. 7.1, on observations relating directly to the transfer of magnetic flux from closed to open field lines, and vice versa, in the magnetosphere. If such transfer in fact occurs, reconnection of some form must take place. If not, there is no need for it. Subsect. 7.2 contains a brief discussion of direct measurements of magnetic field and plasma in the vicinity of what may have been reconnection sites.

7.1. Flux transfer evidence

The case for the occurrence of flux transfer in the magnetosphere from closed to open field lines is based on four sets of observations, discussed below:

(i) *Existence of open field lines in the tail.* Anderson and Lin [5] have studied the shadowing effects on solar electrons ($\mathcal{E} > 20$ keV), produced by the moon when it is located in the geomagnetic tail. They provide persuasive evidence that a substan-

tial amount of magnetic flux in the two tail lobes occurs on open field lines, i.e., on lines that intersect the earth's surface in one place only. But the observations do not establish how large a fraction of the tail flux is on open lines at a given distance from the earth. Thus, it is not known for a fact how large a fraction of the earth's polar-cap field lines, i.e., lines emerging at latitudes above the auroral oval, that are open. A popularly held view is that all are open. But Heikkila [53], questioning the soundness of this view, has drawn attention to observations my McDiarmid et al. [77,78] which indicate the common occurrence of trapped particle pitch-angle distributions in the day-side cusp region as well as poleward of discrete auroral arcs.

(ii) *Flux erosion from the front-lobe magnetosphere.* The magnetopause is observed to move closer to the earth when the interplanetary field develops a southward component. At the same time, the dayside polar cusp moves to lower latitudes. These effects cannot be accounted for by simple compression of the magnetosphere. Maezawa [79] has estimated that flux on closed field lines is removed from the magnetosphere front lobe in an amount estimated at about 10^8 weber during a typical event. Either this flux is transferred to open field lines in the polar cap by dayside magnetopause reconnection or it is moved into the tail while remaining on closed field lines. In the latter case, the flux might be added to the lobe of closed field lines in the tail or it might possibly be placed on open field lines by reconnection at the tail magnetopause. The popularly held view is that the flux is transferred to open flux by reconnection somewhere on the dayside magnetopause.

(iii) *Flux addition in the open tail lobes.* A substantial body of evidence indicates that the magnetic field intensity in the tail starts to increase shortly after the onset of a southward component of the interplanetary magnetic field while at the same time the asymptotic tail cross-section increases [80]. The observed concurrent gradual thinning of the tail plasma sheet (which is believed to contain the closed tail field lines) argues against these effects being caused by an increase of flux on closed field lines in the tail. Rather they indicate an increase of flux on open field lines in the two tail lobes by an amount estimated at $1-2.5 \times 10^8$ weber. If the auroral oval (and the dayside cleft) is associated with the separatrix between closed and open field lines, the motion of this oval to lower latitudes following the southward turning of the interplanetary field [62] supports this interpretation. But the evidence, while strong, is not conclusive. If closed field lines occur in the tail outside (i.e., above and below) the plasma sheet, the flux on open field lines could conceivably remain unchanged.

(iv) *Polar cap electric fields and convection.* Electric field measurements [55] in the polar ionosphere indicate an average voltage difference across the polar cap of the order of 65 kV, corresponding to a magnetic flux transport across the cap from dayside to nightside at a rate of about 2×10^8 weber/h [80]. Ion flow measurements [52] over the polar cap show flow patterns that carry particles and, unless $\boldsymbol{E} \cdot \boldsymbol{B} \neq 0$, magnetic flux poleward across the dayside cleft in a narrow longitude

sector. Most but not all of the flow in the cap region occurs near the equatorward edge of the cap adjacent to an abrupt flow reversal, below which the return flow to the dayside occurs. While the exact location of the separatrix between closed and open field is not known, it is difficult to locate it in such a way that these results do not imply a transfer of flux from closed to open field lines.

In spite of the ambiguities in the interpretation of the observations listed above, their mutual consistency in terms of flux transfer rates is impressive and lends credence to the idea that flux transfer from closed to open field lines does occur in the magnetosphere. However, a far greater body of simultaneous observations by satellites at different locations in the magnetosphere needs to be examined in order to establish the validity of the idea in a conclusive manner. It is noted that on the average, any flux transfer from closed to open field lines must be balanced by a reverse transfer from open to closed lines. Tail reconnection, occurring sporadically in connection with the expansive phase of magnetic substorms, is thought to accomplish this latter transfer but conclusive evidence is not available (see subsect. 7.2).

7.2. *Measurements near reconnection sites*

In a strict sense, direct evidence for reconnection consists of in situ observations of the hyperbolic magnetic field configuration associated with a separator and an electric field along that line. The electric field observation may convincingly be replaced by the observation of plasma energized in the reconnection process (compare subsects. 2.4 and 4.2).

Hones et al. [63] have reported observations of proton fluxes and of magnetic fields in the geomagnetic tail at geocentric distances in the range of 25–32 earth radii. They have found substorm events in which tailward proton flows at speeds up to 1000 km/sec and an associated southward component of the magnetic field occurred during the storm expansion phase, followed by earthward flow and a northward field component during recovery. Such observations are consistent with a separator moving tailward past the satellite. However, evidence concerning the magnetic-field component perpendicular to the tail current sheet is not entirely convincing unless the field is measured near the center of the sheet, which was not the case. And recently Lui et al. [74,75] have challenged observations purporting to show the formation of a near earth reconnection line during substorms. Observations of proton jetting in the tail [39], of energetic particle bursts [6,68,98], and of lunar shadow patterns of electron fluxes [73], while generally compatible with tail reconnection, nevertheless cannot be claimed to provide unambiguous proof of the occurrence of the process.

At the dayside magnetopause, magnetic field components perpendicular to the magnetopause have been observed [108], although not as a permanent feature not even when the magnetosheath field opposes the terrestrial one. The narrow jets of energized plasma, predicted by magnetopause reconnection models (e.g., fig. 19)

and flowing nearly tangential to the magnetopause, have no been seen *, even though satellites such as HEOS 2 have had the right position and attitude to observe them [50,51]. These facts along with recent observations of a plasma boundary layer inside the dayside magnetopause [29,35] suggest that magnetopause reconnection, if it occurs, may be more sporadic and more localized than originally expected. Furthermore, the possibility of reconnection in the cusps and elsewhere on the magnetopause surface, rather than near the sub-solar point, needs to be examined [50].

The absence of observations of plasma energized by dayside reconnection has led Heikkila [54] to suggest that no such reconnection occurs, i.e., that the magnetopause is an electrostatic equipotential. This suggestion is difficult to reconcile with the presence of magnetic field components perpendicular to the magnetopause, unless one is willing to accept potential differences of the order of 50 kV along field lines extending from the magnetopause into the solar wind; or unless one argues that such perpendicular components are never present over any substantial part of the dayside magnetopause.

8. Summary and recommendations

In this paper we have given a reasonably detailed description of the present status of our understanding of reconnection. The picture that emerges is of a process, simple in concept but extremely complicated and multifaceted in detail. Nonlinear magnetohydrodynamic processes in the external flow region, governed by distant boundary conditions, are coupled to non-linear microscopic plasma processes in the diffusion region in a manner not clearly understood. And it appears that reconnection may operate in entirely different ways for different plasma parameters and for different external boundary conditions. Steady reconnection may be allowed in some cases, forbidden in others, with intermediate situations involving impulsive or pulsative events.

On the whole, our theoretical and empirical knowledge of reconnection is poor. Yet the process plays a key role in solar-flare theory as well as in our present concept of the dynamic magnetosphere. And it appears as an unwanted feature in tokamaks and other fusion configurations. These facts, along with the potential importance of reconnection in other parts of the cosmos, amply justify vigorous research efforts related to reconnection in the following five areas: solar-flare and astrophysical observations, magnetospheric observations, laboratory experiments, computer simulation, and analytical model building. The first area, while extremely important, is too broad to be commented upon here. In the remaining areas the following recommendations are made:

* However, a layer of energetic electrons of unknown origin has been discovered outside the tail magnetopause [7,81].

(i) *Magnetospheric observations and experiments* should include:
(1) A coordinated program to establish (or deny) the occurrence of flux transfer across separatrix surfaces, and to study other global consequences of reconnection;
(2) Direct observations of magnetic field, plasma, energetic particles, and fluctuating as well as steady electric fields, near magnetospheric reconnection sites. Multi-satellite missions are needed to separate spatial and temporal effects;
(3) Perhaps active experiments, such as the release of barium clouds near reconnection sites.

(ii) *Laboratory experiments.* The observation of impulsive flux transfer events and of ion-acoustic turbulence in the double inverse pinch experiment illustrates the importance of such experiments in shaping our understanding of reconnection. Yet, (excluding fusion devices) the double inverse pinch appears to be the only operating reconnection experiment in the US today. A substantially expanded laboratory program is needed with four principal goals:
(1) Simulation of solar-flare reconnection;
(2) Simulation of magnetospheric reconnection;
(3) Study of basic plasma processes of importance in reconnection, such as slow shocks and anomalous resistivity;
(4) Exploration of reconnection in plasma heating devices.

(iii) *Computer simulation* provides a potentially very powerful tool for the study of reconnection. Magnetohydrodynamic codes, and ultimately self-consistent particle-fields codes should be developed. It is particularly important to build into such simulations the effects of inertial and anomalous resistivity in the diffusion region.

(iv) *Analytical models* of reconnection should emphasize the following interrelated problems:
(1) Nonsteady and three-dimensional effects;
(2) Plasma processes in the diffusion region;
(3) Particle acceleration;
(4) Reconnection of fields that are not antiparallel.

It is through vigorous activities in the aforementioned areas, and effective interaction between scientists involved in them, that our understanding of the reconnection process may be most rapidly advanced. To bring about such a state of affairs, two proposals are made:
(A) That a special working group be assembled with the charge of promoting effective research on all aspects of the reconnection problem and with membership drawn from the five research areas discussed above.
(B) That NASA and other funding agencies develop coordinated programs of support for reconnection research.

The importance of the reconnection concept is such that we can ill afford the present somewhat haphazard approach to its study.

Acknowledgments

Research supported by the National Science Foundation under Grant ATM 74-08223 A01 and by the National Aeronautics and Space Administration under Grant NSG 7292 to Dartmouth College.

The author has benefitted from comments on the paper by: P.J. Baum, A. Bratenahl, W.J. Heikkila, F.W. Perkins, E.R. Priest and V.M. Vasyliunas. Conversations with A. Bratenahl and W.J. Heikkila have enlightened the author on many aspects of reconnection and its possible application in the magnetosphere.

Note added in proof

Several developments relating to reconnection have occurred after the completion of this paper. New computer models have been reported [133,137,139,144]. Laboratory experiments [142] simulating the flow of magnetized plasma past the magnetosphere have revealed magnetic field configurations suggestive of reconnection in the tail as well as at the dayside magnetopause (sometimes at the sub-solar point, sometimes in the cusps). Space experiments [140] have revealed the presence of a substantial electric field tangential to the dayside magnetopause. An analytical model of resistive current layer decay has been developed [138]. Mathematical studies of plasma motion near magnetic null points [135,143] have been reported. And an exact compressible MHD model of the convection region flow, based on fig. 14, has been developed [136]. It contains intermediate, rather than fast or slow waves in the inflow regions. Finally, the ion tearing mode has been studied further [134] and its existence has been called into question [141].

References

[1] Alfvén, H., Some properties of magnetospheric neutral surfaces, J. Geophys. Res. 73 (1968) 4379.
[2] Alfvén, H., Electric current structure of the magnetosphere, in Physics of the Hot Plasma in the Magnetosphere (B. Hultquist and L. Stenflo eds.) (New York, 1975).
[3] Alfvén, H., On frozen-in field lines and field-line reconnection, J. Geophys. Res. 81 (1976) 4019.
[4] Amano, K. and T. Tsuda, Reconnection of magnetic field lines by clouds – in clouds-in-cells plasma model, J. Geomagn. Geoelec. (Japan) 29 (1977) 9.
[5] Anderson, K.A. and R.P. Lin, Observations of interplanetary field lines in the magnetotail, J. Geophys. Res. 74 (1969) 3953.
[6] Baker, D.N. and E.C. Stone, Observations of energetic electrons in the earth's magnetotail: Plasma sheet and fireball observations, J. Geophys. Res. 82 (1977) 1532.
[7] Baker, D.N. and E.C. Stone, The magnetopause electron layer along the distant magnetotail, Geophys. Res. Lett. 4 (1977) 133.
[8] Birmingham, T.J., Field line motion in the presence of finite conductivity, in Cosmic Plasma Physics, (K. Schindler ed.) (Plenum Press, New York, 1972).
[9] Bratenahl, A. and C.M. Yeates, Experimental study of magnetic flux transfer at the hyperbolic neutral point, Phys. Fluids 13 (1970) 2696.

[10] Bratenahl, A. and P.J. Baum, Impulsive flux transfer events and solar flares, Geophys. J. Royal. Astr. Soc. 46 (1976) 259.
[11] Bratenahl, A. and P.J. Baum, On flares, substorms, and the theory of impulsive flux transfer events, Solar Phys. 47 (1976) 345.
[12] Burch, J.L., Observations of interactions between interplanetary and geomagnetic fields, Revs. Geophys. and Space Phys. 12 (1974) 363.
[13] Burton, R.K., R.L. McPherron and C.T. Russell, The terrestrial magnetosphere: a half-wave rectifier of the interplanetary electric field, Science 189 (1975) 717.
[14] Carmichael, H., A process for solar flares, AAS-NASA Symposium on solar flares, (W.N. Hess ed.) (NASA SP-50, 1964) p. 451.
[15] Chapman, S. and P.C. Kendall, Liquid instability and energy transformation near a magnetic neutral line: a soluble non-linear hydromagnetic problem, Proc. Roy. Soc. A 271 (1963) 435.
[16] Coppi, B., Remarks on sequence-of-plasma-instabilities models of solar flares, Astrophys. J. 195 (1975) 545.
[17] Coppi, B., G. Laval and R. Pellat, Dynamics of the geomagnetic tail, Phys. Rev. Lett. 16 (1966) 1207.
[18] Coppi, B. and M.N. Rosenbluth, Model for the earth's magnetic tail, in Stability of Plane Plasmas, (Spec. Publ. 36, Eur. Space Res. Org., Paris, 1968).
[19] Coppi, B. and A.B. Friedland, Processes of magnetic energy conversion and solar flares, Astrophys. J. 169 (1971) 379.
[20] Coroniti, F.V., Laminar wave train structure of collisionless magnetic slow shocks, Nuclear Fusion 11 (1971) 261.
[21] Coroniti, F.V., On the nonlinear evolution of the collisionless tearing mode, Phys. Rev. Lett. 38 (1977) 1355.
[22] Coroniti, F.V. and A. Eviatar, Magnetic-field reconnection in a collisionless plasma Astrophys. J. Suppl. 33 (1977) 189.
[23] Cowley, S.W.H., A self-consistent model of a simple magnetic neutral sheet system surrounded by a cold collisionless plasma, Cosmic. Electrodynamics 3 (1973) 448.
[24] Cowley, S.W.H., A qualitative study of the reconnection between the earth's magnetic field and an interplanetary field of arbitrary orientation, Radio Sci. 8 (1973) 903.
[25] Cowley, S.W.H., On the possibility of magnetic fields and fluid flows parallel to the X-line in a re-connexion geometry, J. Plasma Phys. 12 (1974) 319.
[26] Cowley, S.W.H., Convection-region solutions for the re-connexion of antiparallel magnetic fields of unequal magnitude in an incompressible plasma, J. Plasma Phys. 12 (1974) 341.
[27] Cowley, S.W.H., Magnetic field-line reconnexion in a highly conducting incompressible fluid: Properties of the diffusion region, J. Plasma Phys. 14 (1975) 475.
[28] Cowley, S.W.H., Comments on the merging of nonantiparallel magnetic fields, J. Geophys. Res. 81 (1976) 3455.
[29] Crooker, N.U., Explorer 33 entry layer observations, J. Geophys. Res. 82 (1977) 515.
[30] Cross, M.A. and G. Van Hoven, High conductivity magnetic tearing instability, Phys. Fluids 19 (1976) 1591.
[31] Dailey, C.L., H.A. Davis and R.H. Lovberg, An experimental investigation of magnetic field annihilation, Bull. Am. Phys. Soc. 17 (1972) 1011.
[32] Dungey, J.W., Interplanetary magnetic field and the auroral zones, Phys. Rev. Letters 6 (1961) 47.
[33] Dungey, J.W., The structure of the exosphere or adventures in velocity space, in Geophys., The Earth's Environment, (C. De Witt, J. Hieblot, and L. Le Beau eds.) (Gordon and Breach, New York, 1963) p. 503.
[34] Dungey, J.W., Waves and particles in the magnetosphere, in Physics of the Magnetosphere, (R.L. Carovillano, J.F. McClay and H.R. Radoski eds.) (D. Reidel, Dordrecht, Netherlands, 1968) p. 218.

[35] Eastman, T.E., E.W. Hones Jr., S.J. Bame and J.R. Asbridge, The magnetospheric boundary layer: Site of plasma, momentum and energy transfer from the magnetosheath into the magnesphere, Geophys. Res. Lett. (1976) 685.
[36] Eastwood, J.W., Consistency of fields and particle motion in the Speiser model of the current sheet, Planet. Space Sci. 20 (1972) 1555.
[37] Eastwood, J.W., The warm current-sheet model and its implications on the temporal behavior of the geomagnetic tail, Planet. Space Sci. 22 (1974) 1641.
[38] Francfort, Ph. and R. Pellat, Magnetic merging in collisionless plasmas, Geophys. Res. Lett. 3 (1976) 433.
[39] Frank, L.A., K.L. Ackerson and R.P. Lepping, On hot tenuous plasmas, fireballs and boundary layers in the earth's magnetotail, J. Geophys. Res. 81 (1976) 5859.
[40] Fredricks, R.W., Electrostatic heating of solar wind ions beyond 0.1 AU, J. Geophys. Res. 74 (1969) 2919.
[41] Friedman, M. and S.M. Hamberger, On the neutral point region in Petschek's model of magnetic field annihilation, Astrophys. J. 152 (1968) 667.
[42] Fukao, S. and T. Tsuda, On the reconnection of magnetic lines of force, J. Plasma Phys. 9 (1973) 409.
[43] Fukao, S. and T. Tsuda, Reconnexion of magnetic lines of force: evolution in incompressible MHD fluids, Planet. Space Sci. 21 (1973) 1151.
[44] Furth, H.P., The mirror instability for finite particle gyroradius, Nuclear Fusion Suppl. Pt. 1 (1962) 169.
[45] Furth, H.P., J. Killeen and M.N. Rosenbluth, Finite resistivity instabilities of a sheet pinch, Phys. Fluids 6 (1963) 459.
[46] Galeev, A.A. and L.M. Zeleny, The role of plasma processes in the dynamics of magnetospheric substorms, Paper presented at International Symposium on Solar-Terrestrial Physics, Boulder, Colorado, June 1976.
[47] Galeev, A.A. and L.M. Zeleny, Magnetic reconnection in a space plasma, (Academy of Sciences of the USSR, Space Research Institute, Moscow, 1977) Report D-249.
[48] Gleeson, L.J. and W.I. Axford, An anlytic model illustrating the effects of rotation on a magnetosphere containing low-energy plasma, J. Geophys. Res. 81 (1976) 3403.
[49] Gonzalez, W.D. and F.S. Mozer, A quantitative model for the potential resulting from reconnection with an arbitrary interplanetary magnetic field, J. Geophys. Res. 79 (1974) 4186.
[50] Haerendel, G., Microscopic plasma processes related to reconnection, J. Atm. Terr. Phys. 40 (1977) 343.
[51] Haerendel, G., G. Paschmann, N. Sckopke, H. Rosenbauer and P.C. Hedgecock, The frontside boundary layer of the magnetosphere and the problem of reconnection, J. Geophys. Res. 83 (1978) 3195.
[52] Heelis, R.A., W.B. Hanson and J.L. Burch, Ion convection velocity reversals in the dayside cleft, J. Geophys. Res. 81 (1976) 3803.
[53] Heikkila, W.J., Magnetospheric plasma regions and boundaries, in Physics of the Hot Plasma in the Magnetosphere (B. Hultquist and L. Stenflo eds.) (Plenum Publ. Co., New York, 1975) p 69.
[54] Heikkila, W.J., Is there an electrostatic field tangential to the dayside magnetopause and neutral line?, Geophys. Res. Lett. 2 (1975) 154.
[55] Heppner, J.P., High latitude electric fields and the modulations related to interplanetary magnetic field parameters, Radio Sci. 8 (1973) 933.
[56] Heyvaerts, J. and E.R. Priest, Thermal evolution of current sheets and flash phase of solar flares, Solar Phys. 47 (1976) 223.
[57] Heyvaerts, J., E.R. Priest and D. Rust, An emerging flux model for the solar flare phenomenon, Astrophys. J. 216 (1977) 123.

[58] Hill, T.W., A three-dimensional model of magnetic merging at the magnetopause, Radio Sci. 8 (1973) 915.
[59] Hill, T.W., Magnetic merging in a collisionless plasma, J. Geophys. Res. 80 (1975) 4689.
[60] Hofmann, I., Resistive tearing modes in a sheet pinch with shear flow, Plasma Phys. 17 (1975) 143.
[61] Hoh, F.C., Stability of sheet pinch, Phys. Fluids 9 (1966) 277.
[62] Holzworth, R.H. and C.-I. Meng, Mathematical representation of the auroral oval, Geophys. Res. Lett. 2 (1975) 377.
[63] Hones, E.W., Jr., S.J. Bame and J.R. Asbridge, Proton flow measurements in the magnetotail plasma sheet made with Imp 6, J. Geophys. Res. 81 (1976) 227.
[64] Huba, J.D., N.T. Gladd and K. Papadopoulos, The lower-hybrid-drift instability as a source of anomalous resistivity for magnetic field line reconnection, Geophys. Res. Lett. 4 (1977) 125.
[65] Janicke, L., Adiabatic Invarianz im Mittel bei räumlicher Feldumkehr, thesis, (Institut für Plasmaphysik der Kernforchungsanlage, Jülich, 1965).
[66] Kan, J.R. and J.K. Chao, Magnetic field reconnection enhanced by interchange stability, J. unpublished manuscript (1976).
[67] Kennel, C.F. and F.V. Coroniti, Possible origin of time variability in Jupiter's outer magnetosphere, Geophys. Res. Lett. 4 (1977) 215.
[68] Kirsch, E., S.M. Krimigis, E.T. Sarris, R.P. Lepping and T.P. Armstrong, Possible evidence for large transient electric fields in the magnetotail from oppositely directed anisotropies of energetic protons and electrons, Geophys. Res. Lett. 4 (1977) 137.
[69] Laval, G., R. Pellat and M. Vuillemin, in Plasma Physics and Controlled Fusion Research-Culham, II (1965) 259.
[70] Layzer, D. and J.R. Burke, On the acceleration of ultrarelativistic electrons and nuclei in nonthermal radio sources, Astrophys. J. 157 (1969) 1169.
[71] Lees, L., Interaction between the solar plasma wind and the geomagnetic cavity, AIAA J. 2 (1964) 1576.
[72] Levy, R.H., H.E. Petschek and G.L. Siscoe, Aerodynamic aspects of the magnetospheric flow, AIAA J. 2 (1964) 2065.
[73] Lin, R.P., K.A. Anderson, J.E. McCoy and C.T. Russell, Observations of magnetic merging and the formation of the plasma sheet in the earth's magnetotail, J. Geophys. Res. 82 (1977) 2761.
[74] Lui, A.T., C.-I. Meng and S.-I. Akasofu, Search for the magnetic neutral line in the near-earth plasma sheet, I, Critical reexamination of earlier studies on magnetic field observations, J. Geophys. Res. 81 (1976) 5934.
[75] Lui, A.T., C.-I. Meng and S.-I. Akasofu, Search for the magnetic neutral line in the near earth plasma sheet, II, Systematic study of IMP 6 magnetic field observations, J. Geophys. Res. 82 (1977) 1547.
[76] Lynden-Bell, D., Galactic nuclei as collapsed old quasars, Nature 223 (1969) 690.
[77] McDiarmid, I.B., J.R. Burrows and E.E. Budzinski, Average characteristics of magnetospheric electrons (150 eV–200 keV) at 1400 km, J. Geophys. Res. 80 (1975) 73.
[78] McDiarmid, I.B., J.R. Burrows and E.E. Budzinski, Particle properties in the day side cleft, J. Geophys. Res. 81 (1976) 221.
[79] Maezawa, K., Dependence of the magnetopause position on the southward interplanetary magnetic field, Planet. Space Sci. 22 (1974) 1443.
[80] Maezawa, K., Magnetotail boundary motion associated with geomagnetic substorms, J. Geophys. Res. 80 (1975) 3543.
[81] Meng, C.-I. and K.A. Anderson, A layer of energetic electrons ($E > 40$ keV) near the magnetopause, J. Geophys. Res. 75 (1970) 1827.
[82] Mitchell, H.G., Jr. and J.R. Kan, Merging of magnetic fields with field-aligned plasma flow components, submitted to J. Plasma Phys. (1977).

[83] Newcomb, W.A., Motion of magnetic lines of force, Ann. Phys. 3 (1958) 347.
[84] Ohyabu, N.S., Okamura and N. Kawashima, Strong ion heating in a magnetic neutral point discharge, Phys. Fluids 17 (1974) 2009.
[85] Overskei, D. and P.A. Politzer, Plasma turbulence in the vicinity of a magnetic neutral point, Phys. Fluids 19 (1976) 683.
[86] Parker, E.N., The solar flare phenomenon and the theory of reconnection and annihilation of magnetic fields, Astrophys. J. Suppl. Series. 8 (1963) 177.
[87] Parker, E.N., The origin of magnetic fields, Astrophys. J. 160 (1970) 383.
[88] Parker, E.N., Comments on the reconnection rate of magnetic fields, J. Plasma Phys. 49 (1973).
[89] Parker, E.N., The reconnection rate of magnetic fields, Astrophys. J. 180 (1973) 247.
[90] Petschek, H.E., Magnetic field annihilation, AAS–NASA Symposium on the Physics of Solar Flares, (W.N. Hess ed.) (NASA SP-50, 1964) p 425.
[91] Petschek, H.E., The mechanism for reconnection of geomagnetic and interplanetary field lines, in the Solar Wind (R.J. Mackin Jr. and M. Neugebauer eds.) (Pergamon Press, New York, 1966) p 257.
[92] Priest, E.R., The solar flare phenomenon, Physics of Solar–Planetary Environments (D.J. Williams ed.) (Am. Geophys. U., 1976) p 144.
[93] Priest, E.R. and S.W.H. Cowley, Some comments on magnetic-field reconnection, J. Plasma Phys. 14 (1975) 271.
[94] Priest, E.R. and M.A. Raduu, Preflare current sheets in the solar atmosphere, Solar Phys. 43 (1975) 177.
[95] Priest, E.R. and B.U.Ö. Sonnerup, Theories of magnetic field annihilation, Geophys. J.R. Astr. Soc. 41 (1975) 405.
[96] Rossi, B. and S. Olbert, Introduction to the physics of space (McGraw-Hill, New York, 1970).
[97] Rutherford, P.H., Nonlinear growth of the tearing mode, Phys. Fluids 16 (1973) 1903.
[98] Sarris, E.T. and W.I. Axford, Energetic protons at the plasma sheet boundary, Geophys. Res. Lett., 4 (1977).
[99] Schindler, K., A theory of the substorm mechanism, J. Geophys. Res. 79 (1974) 2803.
[100] Schindler, K., Large scale plasma processes in the solar system, Physics of Solar Planetary Environments (D.J. Williams ed.) (Am Geophys. U., 1976). p 798.
[101] Smith, D.F. and E.R. Priest, Current limitation in solar flares, Astrophys. J. 176 (1972) 487.
[102] Smith, D.F., Current instability in reconnecting current sheets, J. Geophys. Res. 82 (1977) 704.
[103] Sonnerup, B.U.Ö., Magnetic-field re-connexion in a highly conducting incompressible fluid, J. Plasma Phys. 4 (1970) 161.
[104] Sonnerup, B.U.Ö., Adiabatic particle orbits in a magnetic null sheet, J. Geophys. Res. 76 (1971) 8211.
[105] Sonnerup, B.U.Ö., Magnetic field reconnection and particle acceleration, High Energy Phenomena on the Sun, Symposium Proceedings, (NASA–GSFC Doc. X-639-73-193, 1973) p 357.
[106] Sonnerup, B.U.Ö., The reconnecting magnetosphere, in Magnetospheric Physics (B.M. McCormac ed.) (D. Reidel, Dordrecht, Holland, 1974) p 23.
[107] Sonnerup, B.U.Ö., Magnetopause reconnection rate, J. Geophys. Res., 79 (1974) 1546.
[108] Sonnerup, B.U.Ö., Magnetopause and boundary layer, Physics of Solar–Planetary Environments (D.J. Willia ns ed.) (Am. Geophys. U., 1976) p 541.
[109] Sonnerup, B.U.Ö. and E.R. Priest, Resistive MHD stagnation point flows at a current sheet, J. Plasma Phys. 14 (1975) 283.
[110] Soward, A.M. and E.R. Priest, Fast magnetic-field reconnection, Phil. Trans. Roy Soc. London, A, 284 (1977) 369.

[111] Speiser, T.W., Conductivity without collisions or noise, Planet. Space Sci. 18 (1970) 613.
[112] Spitzer, L., Jr., Physics of fully ionized gases (Interscience, New York, 1964).
[113] Sweet, P.A., The neutral point theory of solar flares, in Electromagnetic Phenomena in Cosmical Physics, (B. Lehnert ed.) (Cambridge U. Press, 1958) p 123.
[114] Syrovatskii, S.I., A.G. Frank and A.Z. Khodzhaev, Development of a current layer when plasma moves in a magnetic field with a neutral line, Soviet Physics, JETP Lett. 15 (9172) 94.
[115] Tamao, T., Anomalous electrical conductivity for the field-line merging current, Report of Ionosphere and Space Res. in Japan 29 (1975) 140.
[116] Tsurutani, B.T., B.E. Goldstein and A. Bratenahl, Acceleration of energetic particles of the outer regions of planetary magnetospheres: inferences from laboratory and space experiments, Planet. Space Sci. 24 (1976) 995.
[117] VanHoven, G. and M.A. Cross, Energy release by magnetic tearing: The nonlinear limit, Phys. Rev. A7 (1973) 1347.
[118] Vasyliunas, V.M., Theoretical models of magnetic field line merging, Revs. Geophys. Space Phys. 13 (1975) 303.
[119] Vasyliunas, V.M., private communication (June, 1977).
[120] Waddell, B.V., M.N. Rosenbluth, D.A. Monticello and R.B. White, Nonlinear growth of the $m = 1$ tearing mode, Nuclear Fusion, 16 (1976) 528.
[121] White, R.B., D.A. Monticello, M.N. Rosenbluth and B.V. Waddell, Nonlinear tearing modes in tokamaks, paper presented at Sixth International Conference on Plasma Physics and Controlled Nuclear Fusion, Berchtesgaden, W. Germany, Oct. 1976 (Princeton Plasma Physics Laboratory Report PPL 1282, 1976).
[122] White, R.B., D.A. Monticello, M.N. Rosenbluth and B.V. Waddell, Saturation of the tearing mode, Phys. Fluids 20 (1977) 800.
[123] Wilcox, J.M. and N.F. Ness, Quasi-stationary corotating structure in the interplanetary medium, J. Geophys. Res. 70 (1965) 5793.
[124] Yang, C.-K., Compressible magnetic field reconnection, thesis (Dartmouth College, Hanover, NH., June 1976).
[125] Yang, C.-K. and B.U.Ö. Sonnerup, Compressible magnetic field reconnection: a slow wave model, Astrophy. J. 206 (1976) 570.
[126] Yang, C.-K. and B.U.Ö. Sonnerup, Compressible magnetopause reconnection, J. Geophys. Res. 82 (1977) 4.
[127] Yeh, T., Day-side reconnection between a dipolar geomagnetic field and a uniform interplanetary field, J. Geophys. Res. 81 (1976) 2140.
[128] Yeh, T., Diffusive hydromagnetic flow in the vicinity of a neutral point, Astrophys. J. 207 (1976) 837.
[129] Yeh, T., Reconnection of magnetic field lines in viscous conducting fluids, J. Geophys. Res. 81 (1976) 4524.
[130] Yeh, T. and M. Dryer, On the reconnection of magnetic field lines in compressible conducting fluids, Astrophys. J. 182 (1973) 301.
[131] Yeh, T. and W.I. Axford, On the re-connexion of magnetic field lines in conducting fluids, J. Plasma Phys. 4 (1970) 207.
[132] Zwan, B.J. and R.A. Wolf, Depletion of solar wind plasma near a planetary boundary, J. Geophys. Res. 81 (1976) 1636.
[133] Cheng, A.F., Paper on magnetic field annihilation in a decaying one-dimensional current sheet presented at NASA-JPL Astrophysics Workshop, Snowmass, Co. (1978).
[134] Galeev, A.A., F.V. Coroniti and M. Ashour-Abdalla, Explosive tearing mode reconnection in the magnetospheric tail, UCLA preprint PPG-339 (1978).
[135] Grad, H., Reconnection of magnetic lines in an ideal fluid, Courant Inst. Math. Sci., New York Univ., preprint C00-3077-152 MF-92 (1978).

[136] Hameiri, E., Compressible magnetic-field reconnexion, Courant Inst. Math. Sci., New York Univ., preprint (1978).
[137] Hayashi, T. and T. Sato, Magnetic reconnection: acceleration, heating, and shock formation, J. Geophys. Res. 83 (1978) 217.
[138] Kirkland, K.B. and B.U.Ö. Sonnerup, Self similar resistive decay of a current sheet in a compressible plasma, submitted to J. Plasma Phys. (1977).
[139] Leboeuf, J.N., T. Tajima, C.F. Kennel and J.M. Dawson, Global simulation of the time-dependent magnetosphere, Geophys. Res. Lett. 5 (1978) 609.
[140] Mozer, F.S., R.B. Torbert, U.V. Fahleson, C.-G. Fälthammar, A. Gonfalone, A. Pedersen and C.T. Russell, Direct observation of a tangential electric field component at the magnetopause, Geophys. Res. Lett. 4 (1978).
[141] Pellat, R., About "reconnection" in a collisionless plasma, paper presented at COSPAR meeting Innsbruck, Austria (1978).
[142] Podgorny, I.M., E.M. Dubinin and Yu.N. Potanin, The magnetic field on the magnetospheric boundary from laboratory simulation data, Geophys. Res. Lett. 4 (1978) 207.
[143] Rosenau, P., On three-dimensional flow with neutral points, I., Courant Inst. Math. Sci., New York Univ., preprint (1978).
[144] Ugai, M. and T. Tsuda, Magnetic field-line reconnection by localized enhancement of resistivity, J. Plasma Phys. 17 (1977) 337.

TRANSPORT MECHANISMS AT THE MAGNETOPAUSE

Bengt U. Ö. Sonnerup[1]
Max Planck Institut für Physik und Astrophysik, Institut für extraterrestrische Physik, 8046 Garching b. München, West Germany

ABSTRACT

Mass, momentum, and energy transferred from the solar wind and magnetosheath into the magnetosphere must cross the boundary of the earth's magnetic field, the magnetopause. This paper reviews the possibilities for convective and diffusive transport across the boundary and discusses the dependence of such processes on the orientation of the interplanetary magnetic field. It is first shown that, in the absence of transport processes, the magnetosheath magnetic field just outside the magnetopause always builds up to a dynamically significant level. The possibility of macroscopic plasma flow (convection) across the magnetopause is then discussed both for the case of a vanishing and a nonvanishing magnetic field component normal to the boundary. In the former case, convective flow does not appear possible, unless substantial electric fields occur parallel to the magnetic field. The latter case includes exactly field-aligned flows as well as magnetic-field reconnection. Particular attention is given to the problem of particle energization during reconnection. Finally, a brief discussion is given of diffusion processes and the constraints placed upon them by existing observations. It is shown that the efficiency of diffusive as well as convective transfer should be expected to have a strong dependence on the angle θ between the magnetospheric and the magnetosheath magnetic fields with a maximum for $\theta = \pi$, a minimum for $\theta = 0$.

1. INTRODUCTION

All mass, momentum, and energy transferred from the solar wind to the magnetosphere must cross the magnetopause. The processes whereby such transfer takes place are poorly understood at present, and they constitute one of the most important unsolved problems in magnetospheric physics. It is the purpose of this paper to provide a brief qualitative review of possible transfer mechanisms and the extent to which they are able to explain plasma and field observations near the dayside magnetopause. The nature of these observations has been discussed recently by Eastman and Hones (1979), Paschmann et al. (1979), and by

Russell and Elphic (1979). A study of the magnetic structure of the magnetopause may be found in Sonnerup (1976). In the present paper, particular attention will be paid to the question of how the transfer rates may be modulated by the orientation of the interplanetary magnetic field.

Traditionally, transfer processes are classified in three groups:

(i) Transport by convection, i.e., in the present application, by direct macroscopic flow of plasma across the magnetopause.

(ii) Transport by diffusion, i.e., by processes that are considered microscopic on the temporal and spatial scales of interest.

(iii) Transport by radiation, i.e., by waves propagating across the magnetopause.

The last of these categories is rather special because it involves no mass transfer. Apart from the electromagnetic radiation, there may also be momentum and energy transfer across the magnetopause via compressive MHD waves, as pointed out by Axford (1964). This topic and the related one of the Kelvin-Helmholtz instability, while important, are beyond the scope of the present paper.

The distinction between convection and diffusion, depends on one's definition of the terms macroscopic and microscopic. In other words, it depends on the space and time resolution available (or desired). Turbulent transport may be considered a diffusive process, described by an effective "eddy" diffusivity, if one is concerned only with time and space scales long compared to the correlation times and correlation lengths of the turbulence. With higher temporal and spatial resolution, it should be properly considered a convective process. For the purposes of this paper, time scales shorter than a few proton gyroperiods and length scales shorter than a few proton gyroradii must be considered microscopic. (The gyroperiod and gyroradius of a 1kV proton in a 50nt field are 1.3 sec and 92 km, respectively.)

The paper is organized as follows. First, a discussion is given of the "ideal" or nontransfer state of the magnetosphere with focus on the magnetic field near the magnetopause. This is an appropriate starting point, for the transport across the magnetopause usually appears to be sufficiently modest so as to be considered a small perturbation on the nontransfer state. Furthermore, well established correlations between various geomagnetic effects and the interplanetary magnetic field (e.g., Burch, 1974), indicate the importance of understanding the nature of the magnetosheath magnetic field immediately outside the magnetopause.

Second, a presentation is given of existing convective transfer mechanisms by which plasma flows directly across the magnetopause, usually under the influence of an electric field parallel to that

surface. The cases where the magnetic field component normal to the magnetopause vanishes and does not vanish are considered separately.

Third, a brief summary is given of diffusive processes that may be operative at the magnetopause and the constraints placed on them by existing observations of the plasma boundary layer immediately inside the magnetopause.

2. THE NONTRANSFER STATE

The problem of ideal flow past the magnetosphere was dealt with in great detail in the sixties (e.g., Spreiter and Alksne, 1969). In general, the approach was to calculate the magnetopause shape and the flow configuration under the assumption that the interplanetary magnetic field plays no dynamic role other than that of rendering the plasma a continuum. The magnetic field configuration outside the magnetopause was calculated afterwards (Alksne and Webster, 1970) by use of the frozen field condition. The point to be made here is that, no matter how weak the interplanetary field, such a procedure always leads to a violation of the basic assumption that the Maxwell stresses may be ignored. We illustrate this point by considering ideal steady axisymmetric supersonic flow past a blunt-nosed impenetrable and perfectly diamagnetic object, as shown in Figure 1. In each meridional plane, the streamlines in such a flow are given by $\psi(R,\Theta) = \text{const.}$, where $\psi(R,\Theta)$ is Stokes' stream function and the notation in the figure is used.[2]

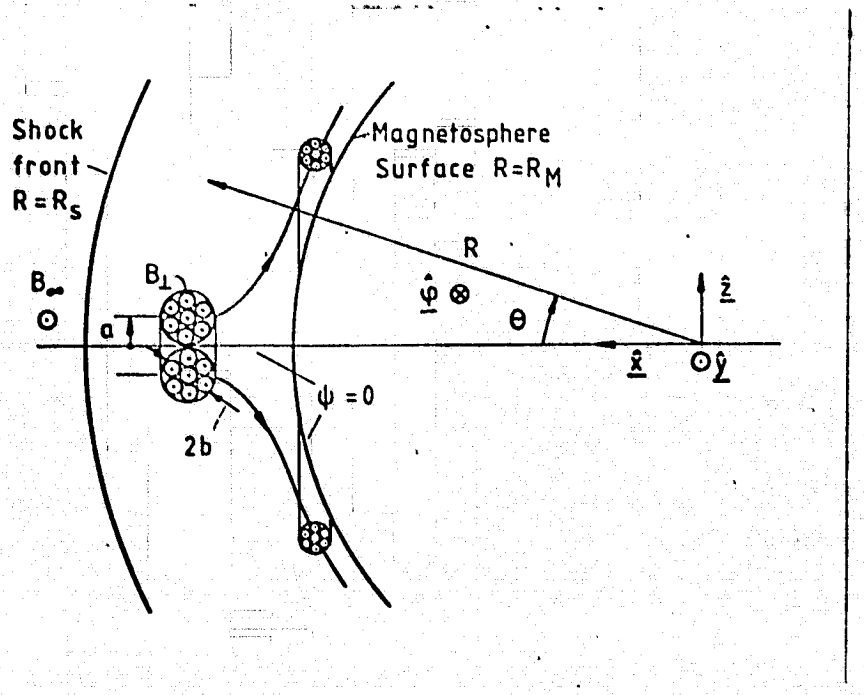

Figure 1. Ideal MHD flow past an impenetrable diamagnetic object.

The velocity $\underline{v}$ is given by

$$\underline{v} = (\underline{\nabla}\psi \times \hat{\underline{\phi}})/\rho R\sin\Theta \tag{1}$$

ρ being the density and $\hat{\underline{\phi}}$ a unit vector in the azimuthal direction.

The frozen magnetic field condition

$$\underline{E} + \underline{v} \times \underline{B} = 0 \tag{2}$$

with

$$\underline{E} = -\underline{\nabla}\Phi \tag{3}$$

implies that not only the magnetic field lines but also the streamlines are equipotentials. Since each streamline lies along the intersection between a meridional plane, ϕ = const., and an axisymmetric stream surface, ψ = const., the electrostatic potential may be written $\Phi = \Phi(\psi,\phi)$. The functional form of this latter expression may be evaluated in the region upstream of the bow shock (subscript ∞) where the flow and field are uniform. With $\underline{B}_\infty = \hat{\underline{y}}B_\infty$, say, we find

$$\Phi_\infty = -v_\infty B_\infty z = -v_\infty B_\infty R\sin\Theta\sin\phi \tag{4}$$

But the stream function for uniform flow with speed v_∞ is

$$\psi_\infty = -\tfrac{1}{2}\rho_\infty v_\infty R^2\sin^2\Theta \tag{5}$$

so that

$$\Phi_\infty = -v_\infty B_\infty\sqrt{-2\psi_\infty/(\rho_\infty v_\infty)}\sin\phi \tag{6}$$

One concludes from Equation (6) that the potential distribution in the entire flow field must be given by

$$\Phi(R,\Theta,\phi) = -B_\infty\sqrt{-2v_\infty\psi/\rho_\infty}\,\sin\phi \tag{7}$$

By use of the frozen field condition, the component of the magnetic field perpendicular to the flow velocity vector may now be written as

$$\underline{B}_\perp \equiv \underline{B} - \underline{v}(\underline{v}\cdot\underline{B})/v^2 = \underline{\nabla}\Phi \times \underline{v}/v^2 \tag{8}$$

The component of $\underline{B}$ along $\underline{v}$ is not of interest here, but it may be obtained from $\underline{\nabla} \cdot \underline{B} = 0$.

The stream function ψ vanishes on the axis (see Equation (5) for $\Theta = 0$) and since the streamline along the axis splits at the forward stagnation point and then covers the entire surface of the object, we conclude that ψ vanishes on that surface. In calculating $\underline{\nabla}\Phi$, with Φ given by Equation 7, a factor $\psi^{-\frac{1}{2}}$ will be generated. Thus when $\underline{\nabla}\Phi$ is substituted into Equation (8), $\underline{B}_\perp$ becomes infinite at $\psi = 0$, i.e., on

the entire surface of the blunt object (Alksne and Webster, 1970). The only exception occurs if $\rho = 0$ on the surface; this possibility will be discussed below.

As an example, the magnetic field intensity on the axis ($\Theta = 0$) has been calculated as a function of position using Lighthill's well-known constant-density solution for hypersonic flow past a sphere (see Hayes and Probstein, 1959) for which the stream function in the region between the shock and the sphere is given by

$$\psi = [\rho_\infty v_\infty (R_s \sin\theta)^2/(30\varepsilon^3)][3(1-\varepsilon)^2(R/R_s)^4 - 5(1-4\varepsilon)(R/R_s)^2 + 2(1-\varepsilon)(1-6\varepsilon)(R_s/R)] \quad (9)$$

Here R_s is the shock radius (the radius of the sphere, R_M, is obtained by solving the equation $\psi = 0$) and

$$\varepsilon \equiv (\gamma-1)/(\gamma+1) \quad (10)$$

γ being the ratio of specific heats at constant pressure and constant volume. The resulting $B_\perp$ field distribution along the stagnation streamline is shown in Figure 2.

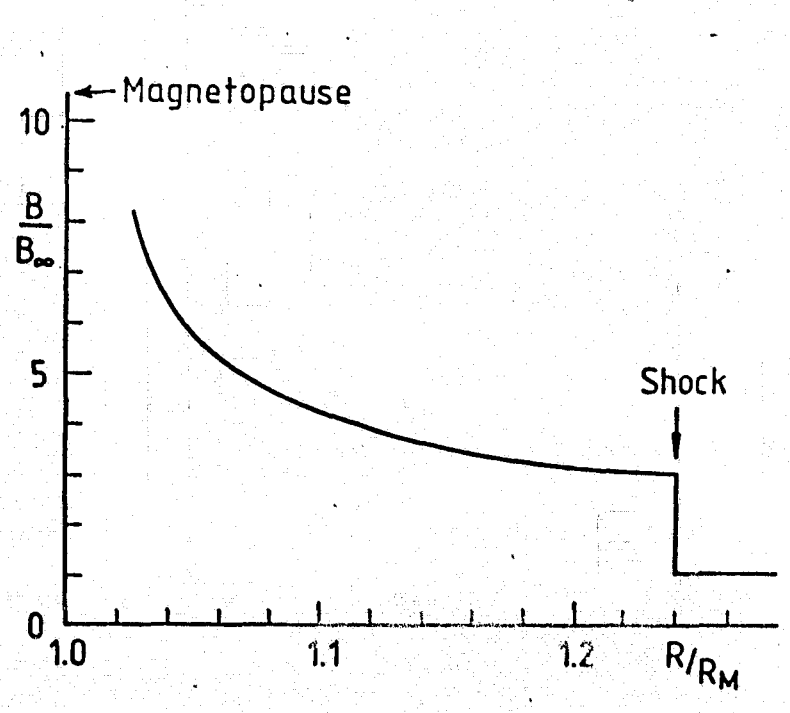

Figure 2. Magnetic field as a function of position R/R_M on the stagnation streamline (the x axis) for Lighthill's solution with $\gamma = 2$.

One may understand the infinite value of the surface magnetic field in the following manner. Consider a plasma torus of major and minor radius a and b, respectively, moving towards the sphere as shown in Figure 1. As it approaches the stagnation point it must expand its circumference $2\pi a$ enormously in order to allow the object to pass through. In this process the mass of the torus is preserved so that

$$\rho(2\pi a)(\pi b^2) = \text{const.} \tag{11}$$

At the same time, the magnetic flux trapped within the cross sectional area πb^2 is also conserved:

$$B_\perp(\pi b^2) = \text{const.} \tag{12}$$

The ratio of these two expressions is

$$B_\perp/(\rho a) = \text{const.} \tag{13}$$

Unless ρ decreases proportionately to the increase in a as the torus expands past the object, one concludes that $B_\perp$ must increase. In the limit of an infinitely small torus threading the stagnation streamline the fractional increase in a and hence in $B_\perp$ becomes infinite as the torus expands and moves along the surface of the object.

One concludes from the preceding result that in ideal MHD flow the original assumption of negligible Maxwell stresses can never be true in the magnetosheath flow near the magnetopause. The net effect of the action of these stresses must be either to decrease the density to zero at the surface of the object, as suggested by Lees (1964) and further developed by Zwan and Wolf (1976), or to change the flow topology in such a way that $B_\perp$ may remain finite. A substantial decrease in density immediately outside the magnetopause has in fact been seen (Crooker and Siscoe, 1975; Paschmann et al., 1979). Nevertheless, the density does not go to zero so that the dilemma remains.

An example of a topological change is shown in Figure 3. The flow ceases to be axisymmetric and a stagnation line, parallel to the local magnetic field, forms on the nose of the object. At the two ends of the stagnation line the magnetic field has null points from which magnetic null lines emerge.

The formation of stagnation lines aligned with $\underline{B}$ and magnetic null lines aligned with $\underline{v}$ may be predicted directly from the frozen magnetic field condition in the form

$$(\underline{B}/\rho) \cdot \underline{\nabla v} = \underline{v} \cdot \underline{\nabla}(\underline{B}/\rho) \tag{14}$$

If $\underline{v} = 0$ and $\underline{B} \neq 0$, $\rho \neq 0$, at a certain point on the surface of the diamagnetic object then $\underline{B} \cdot \underline{\nabla v} = 0$ there. Thus $\underline{v}$ remains zero if one moves along the surface in the direction of $\underline{B}$. Similarly, if $\underline{B} = 0$ and $\underline{v} \neq 0$, $\rho \neq 0$, at some point, then $\underline{v} \cdot \underline{\nabla}(\underline{B}/\rho) = 0$ there. Thus $\underline{B}$

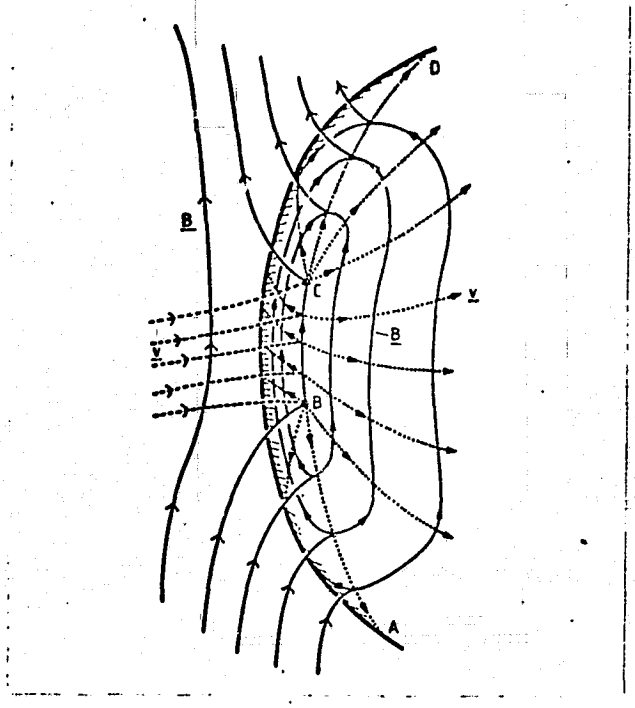

Figure 3. Magnetosheath field and flow on the subsolar magnetopause. Streamlines are dotted, magnetic field lines solid. The line segment B-C is a stagnation line at which each incoming streamline splits. The line segments A-B and C-D are magnetic null lines at which each incoming magnetic field line splits. The points B and C have $\underline{B} = 0$ and $\underline{v} = 0$.

remains zero if one moves along $\underline{v}$. It may be predicted qualitatively that the length of the stagnation line increases with decreasing β_∞ value, β_∞ being the ratio of plasma to magnetic pressure in the solar wind.

The flow near the stagnation region in Figure 3 is organized to be predominantly perpendicular to the magnetic field. The main result of this geometry is that the torus-shaped plasma element in the preceding discussion must be replaced by a chain-link shaped one which threads all of the magnetosheath stream lines joining the stagnation line. The fractional increase in circumference of such an element is finite as it expands to allow passage of the object through it. Thus the cross section of the chain-link will remain finite and, with a constant magnetic flux trapped in that cross section, the magnetic field will also remain finite.

The implications of ideal MHD flow past a diamagnetic object are described above. In the real case of solar-wind flow past the magnetosphere, deviations from the frozen-field condition at the magnetopause may obscure the effects shown in Figure 3 either partially or

completely. If in reality there exist conditions such that the front side of the magnetosphere remains essentially impenetrable to the magnetosheath field and plasma (the "ground-state" magnetosphere) then some of the features shown in the figure should be relevant. On the other hand, if field line interconnection across the magnetopause is important, the field topology will be quite different.

The basic prediction of the MHD theory for flow past an impenetrable object is that the magnetic field immediately outside the magnetopause builds up until it becomes dynamically significant. Potentially it therefore becomes sufficiently strong to exercise a controlling influence on the transfer processes at the magnetopause. Without such processes a β value of the plasma of order unity or less should be expected in the stagnation region just outside the magnetopause. On the other hand, observations of large β values would be a clear indication of a substantial violation of the frozen magnetic field condition, presumably in association with strong transfer across the magnetopause. Both small and large β values have in fact been reported (see Paschmann et al., 1979). It is of interest to note that the smallest value occurred when the magnetosheath field was due north, suggesting that the transfer may be a minimum for this field direction.

3. CONVECTIVE TRANSFER

In order to discuss the possibility of convective transfer across the magnetopause we adopt a simple one-dimensional time-independent model of the local magnetopause structure. In such a model, Maxwell's equations require the normal component of the magnetic field and the tangential component of the electric field to remain constant across the layer. Denoting the magnetosheath and magnetosphere sides by subscripts 1 and 2, respectively, we find

$$B_{n_1} = \underline{B}_1 \cdot \hat{\underline{n}} = \underline{B}_2 \cdot \hat{\underline{n}} = B_{n_2} \equiv B_n \tag{15}$$

$$\underline{E}_{t_1} = \underline{E}_{t_2} = \underline{E}_t \tag{16}$$

where the subscripts n and t refer to components normal and tangential to the magnetopause surface. The unit vector $\hat{\underline{n}}$ is perpendicular to that surface and points away from the earth.

We shall explore the consequences of the assumption that the electric field has no component along the magnetic field, i.e.,

$$\begin{aligned} \underline{E}_1 \cdot \underline{B}_1 &= \underline{E}_t \cdot \underline{B}_{t_1} + E_{n_1} B_n = 0 \\ \underline{E}_2 \cdot \underline{B}_2 &= \underline{E}_t \cdot \underline{B}_{t_2} + E_{n_2} B_n = 0 \end{aligned} \tag{17}$$

For given $\underline{E}$ and $\underline{B}$, the normal flow velocity on either side of the magnetopause may be written

$$v_n = \hat{n} \cdot (\underline{E}_t \times \underline{B})/B^2 + \hat{n} \cdot \underline{v}_{\parallel} \qquad (18)$$

where $\underline{v}_{\parallel}$ is the velocity along $\underline{B}$.

The model described above does not require the actual magnetopause to be stationary or smooth. It may be applied locally to a wavy and rapidly moving and deforming current layer as long as the frozen magnetic field condition holds on the two sides. (This condition does not have to be, and generally is not, valid within the magnetopause structure itself.) However, when used to interpret satellite magnetic and electric field observations during magnetopause crossings, the possibility of time aliasing must be considered.

Observations of the magnetopause (Sonnerup, 1976) indicate the importance of examining both the case $B_n = 0$ and the case $B_n \neq 0$.

4. THE CASE $B_n = 0$

We now examine the possibility of plasma convection across the magnetopause when the normal magnetic field component is vanishingly small. It then follows from Equation (17) that $\underline{E}_t$ must be perpendicular to $\underline{B}_{t1} = \underline{B}_1$, as well as to $\underline{B}_{t2} = \underline{B}_2$. For $\underline{E}_t \neq 0$ this is clearly possible only if $\underline{B}_{t1}$ and $\underline{B}_{t2}$ are either parallel or antiparallel, i.e., if $\underline{B}_1 = k\underline{B}_2$, where k is a positive or negative factor. Thus we have the following cases:

(i) $\underline{B}_1 \neq k\underline{B}_2$. Either $\underline{E}_t = 0$, in which case $v_{n1} = v_{n2} = 0$ so that no convection occurs, or there is an electric field component parallel to the magnetic field on at least one side of the magnetopause. In general, this parallel electric field would have a magnitude comparable to the field $\underline{E}_t$. It is questionable whether such a field can be sustained in a quasisteady state and on spatial scales sufficiently large to be classified as macroscopic.

(ii) $\underline{B}_1 = k\underline{B}_2$; $k < 0$. The magnetic fields on the two sides of the magnetopause are antiparallel. The case $k = -1$ has been discussed by Alfvén (1968) and by Cowley (1973). The prediction is that a voltage difference $\Delta\Phi = B^2/(\mu\, Ne)$ can be sustained along the magnetopause surface (and perpendicular to the magnetic field). For $B = 50$ nt, $N = 10^7 m^{-3}$, we find $\Delta\Phi = 1.24$ kV. This result should be compared to the typical value of 50 kV for the observed potential difference across the polar cap. It would appear that Alfvén's mechanism cannot explain the observations.

(iii) $\underline{B} = k\underline{B}_2$; $0 < k < 1$. If $\underline{E}_t \neq 0$ then the magnetopause must be identified with a fast MHD shock. Since this is certain not to be the case, we conclude that $\underline{E}_t = 0$ so that plasma convection across the magnetopause does not occur.

(iv) $\underline{B} = k\underline{B}_2$; $k > 1$. The magnetopause would then be a reverse fast shock, which does not exist. Again, no plasma convection across the magnetopause is possible.

(v) $\underline{B}_1 = \underline{B}_2$. In this case, no restriction occurs on the tangential electric field $\underline{E}_t$ except that it be perpendicular to the magnetic field. From a local viewpoint, an arbitrarily large plasma flow may occur across the magnetopause. This is the case assumed by Alfvén (e.g., 1958) in his theory of the geomagnetic storm. In this situation the magnetopause cannot be identified locally as a current sheet. Rather, it is defined in a global sense by the fact that the field lines on its two sides have different topological origins. On the magnetopause surface itself, the field lines converge to the two magnetically neutral lines, shown in Figure 3. Unless $\underline{E} \cdot \underline{B} \neq 0$, this topological feature will lead to a short circuiting along $\underline{B}$ of any transverse electric field in the equatorial plane. Since magnetic substorm activity correlates positively with the southward, not the northward, component of the interplanetary magnetic field, it appears that the short circuiting along the field lines may be remarkably efficient, a fact that needs to be taken into account in local models of plasma flow across the magnetopause (e.g., Cole, 1974; Formisano et al., 1978; Lemaire and Roth, 1978).

In summary, it appears that, unless the condition $\underline{E} \cdot \underline{B} = 0$ is violated, the case $B_n = 0$ leads to the classic signatures of a tangential discontinuity and does not offer any hope for convective plasma entry across the magnetopause. And abandonment of $\underline{E} \cdot \underline{B} = 0$ is not a step that can be taken lightly. To be sure, the electric field along $\underline{B}$ is not identically equal to zero. Voltage differences comparable to the average particle energy may be easily sustained along the magnetic field lines. But the proton energy is of the order of 1kV or less, which is insignificant compared to a 50kV potential difference across the polar cap. Various reconnection geometries, to be discussed in the next section, bypass this difficulty by admitting large potential drops only along singular field lines where the X-type field topology permits of such voltage drops without the generation of enormous currents.

5. THE CASE $B_n \neq 0$

When the normal magnetic field B_n is finite, Equations (17) do not place a constraint on the value of the tangential electric field $\underline{E}_t$. Rather, for given $\underline{E}_t$ the two equations may be used to solve for E_{n1} and E_{n2}, the normal electric field components on the two sides of the magnetopause. The plasma convection speed across the magnetopause is given by Equation (18) which shows that the parallel velocity may now yield a convective flow across the magnetopause even when $\underline{E}_t = 0$. In such a case we have interconnection of the field lines across the magnetopause but no reconnection. When $\underline{E}_t \neq 0$ reconnection occurs. Both cases are discussed below.

Equations (17) and (18) describe the kinematics of the flow across the magnetopause. The dynamics consists of the balancing of the Maxwell stresses (the $\underline{I} \times \underline{B}$ force, $\underline{I}$ being the Chapman-Ferraro current per unit width) against the change in particle momentum as the plasma crosses the current layer. It is dealt with most conveniently by transforming to a local coordinate system S' which moves along the magnetopause at a velocity $\underline{v}_0$ such that the electric fields $\underline{E}_1$ and $\underline{E}_2$ are transformed away. The relationship between $\underline{v}_0$ and $\underline{E}_t$ is:

$$\underline{E}_t + \underline{v}_0 \times \hat{\underline{n}} B_n = 0 . \tag{19}$$

For the case of antiparallel fields of equal magnitude, B_t, ($\underline{B}_{t_1} = -\underline{B}_{t_2}$), see Figure 4a, the momentum balance becomes

$$2B_n B_t/\mu_0 = -2\rho v_n v_t' \tag{20}$$

where $\pm v_t'$ is the tangential flow speed in the frame S'. By use of the trigonometric relations

$$\left.\begin{aligned} B_n &= B\sin\delta \\ B_t &= B\cos\delta \end{aligned}\right\} \qquad \left.\begin{aligned} v_n &= -v_{\|}' \sin\delta \\ v_t' &= v_{\|}' \cos\delta \end{aligned}\right\} \tag{21,22}$$

which follow directly from the geometry in Figure 4a and in which $v_{\|}'$ is the flow speed along $\underline{B}$ in the frame S', one finds

$$v_{\|}' = B/\sqrt{\mu_0 \rho} \equiv v_A \tag{23}$$

In other words, the flow speed along $\underline{B}$ is equal to the Alfvén speed and the current layer itself should be identified as a large amplitude Alfvén wave or rotational discontinuity. A more general analysis which permits of arbitrary orientations and magnitudes of $\underline{B}_{t_1}$ and $\underline{B}_{t_2}$, and associated nonisotropic and unequal pressure tensors and unequal densities on the two sides of the magnetopause, may be found in Hudson (1970). The result is that the flow speed on either side is equal to the modified Alfvén speed $\tilde{v}_A \equiv v_A[1-(p_{\|} - p_{\perp})\mu_0/B^2]^{-\frac{1}{2}}$. For simplicity we pursue only the case of isotropic pressure and antiparallel fields here.

We now return to the magnetospheric frame of reference by means of the transformation velocity $\underline{v}_0$ which we first assume to lie in the plane of Figure 4a so that the electric field $\underline{E}_t$ is perpendicular to that plane. Expressing the transformation speed as a fraction of the Alfvén speed, $v_0 \equiv rv_A$, we then find

$$E_t = rv_A B_n \tag{24}$$

For small values of the angle δ in Figure 4a the downward flow velocities are

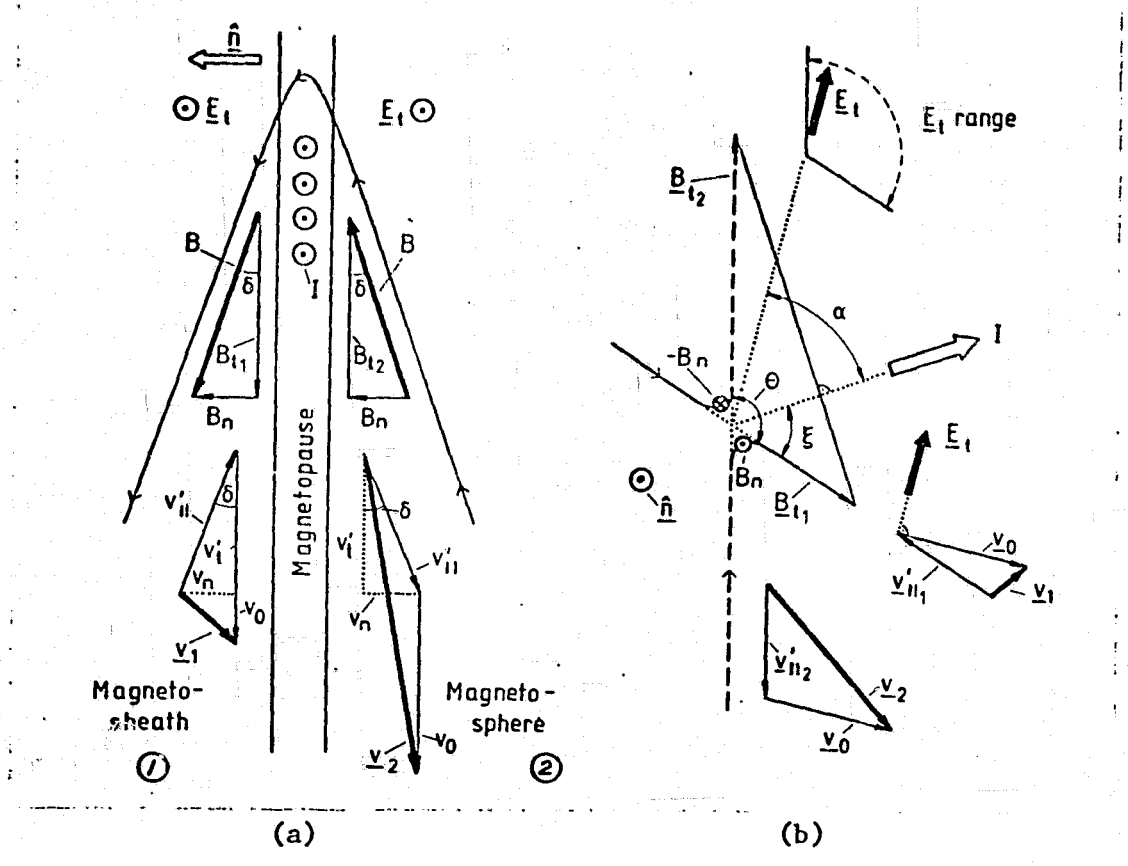

Figure 4. (a) Geometrical interpretation of particle energization during reconnection. In a frame of reference such that $\underline{E} = 0$ the flow is along $\underline{B}$; the flow speed is $v'_{\parallel} = v_A$. In the magnetospheric frame, the electric field is $\underline{E}_t$; the velocity changes from $\underline{v}_1$ to $\underline{v}_2$ as the plasma crosses the magnetopause. The figure represents a side view of the magnetopause. (b) Particle energization when $\underline{B}_{t_1}$ and $\underline{B}_{t_2}$ form an arbitrary angle θ, and the electric field $\underline{E}_t$ forms an angle α with the net magnetopause current vector I. The figure represents a view of the magnetopause from the sun.

$$v_1 \cong (r-1)v_A$$
$$v_2 \cong (r+1)v_A \qquad (25)$$

and the change in energy of a particle of mass m is

$$\Delta\mathcal{E} = \frac{1}{2} m(v_2^2 - v_1^2) \cong 2rmv_A^2 = 2rB^2/\mu_0 N \qquad (26)$$

where N is the particle density. This formula applies also to particles which are reflected at, rather than transmitted through the magnetopause. When $\Delta\mathcal{E}$ is multiplied by the particle flux into the magnetopause, $f = Nv_A B_n/B$, there results

$$f\Delta\mathcal{E} = (2rB^2/\mu_0 N)(Nv_A B_n/B) = (2B/\mu_0)E_t = \underline{E}_t \cdot \underline{I} \qquad (27)$$

In other words, the power supplied to the particles per unit area of the magnetopause is exactly equal to the rate of dissipation of electromagnetic energy per unit area. Thus, the energization is exactly the one discussed by Heikkila (1975,1978) by use of Poynting's theorem.

We examine the meaning of Equations (24)-(27) for different r values:

(i) $r < 0$. In this case, $\underline{E}_t \cdot \underline{I} < 0$ and the particles lose energy in crossing the magnetopause. This case has been occasionally invoked for the front lobe of the magnetosphere with the reconnection site in one of the polar cusps rather than in the equatorial plane. The electric field $\underline{E}_t$ is then opposite to the interplanetary electric field.

(ii) $r = 0$. In this case $\underline{E}_t = 0$ and no particle energization occurs. The plasma crosses the magnetopause by flowing exactly along the magnetic lines of force with the Alfvén speed. It is the case of interconnection of field lines without reconnection. Such flows could conceivably occur on parts of the magnetospheric front lobe. Flow velocity reversals across the magnetopause have been seen (Paschmann et al., 1979) but it has not been established whether cases occur where the flow is exactly field aligned and Alfvénic.

(iii) $0 < r < 1$. The electric field $\underline{E}_t$ is now parallel to the Chapman-Ferraro current $\underline{I}$. Particles are energized and reconnection occurs. A reversal of the tangential component of the flow still occurs at the magnetopause.

(iv) $r = 1$. In this case the plasma inflow is perpendicular to the magnetopause. For $N = 10^7 m^{-3}$, $B = 50$nt we find $\Delta\mathcal{E} = 2.5$ kV, while for $N = 3 \times 10^7 m^{-3}$, $B = 35$ nt, $\Delta\mathcal{E} = 400$ V. The energization per particle is substantial and it may be argued (Heikkila, 1975) that it should be easily observable.

(v) $r > 1$. In this case no flow reversal occurs across the magnetopause. The particle energization is greater than in (iv) by a factor r.

It is an interesting fact that the energization given by Equation (26) is independent of the magnitude of the electric field E_t, even though the mechanism of energization must be the displacement of the particles along the electric fields in the magnetopause. The explanation is as follows. Equation (24) shows that small values of E_t correspond to small values of B_n. But for small B_n values the drift displacement of individual particles along E_t is large. As E_t increases, B_n must also increase proportionately. The result is a smaller drift displacement in a larger electric field such that the total voltage

change experienced by a particle is independent of both E_t and B_n. What does occur as E_t and B_n increase is that the inflow rate, f, of plasma increases with increasing E_t so that more particles are energized per unit time and unit area.

The derivation of Equation (26) emphasizes that the particles energized are the particles responsible for maintaining the momentum balance in the current layer. For example, if this balance were maintained by a small number of escaping radiation belt particles then the density N in Equation (26) should be the small density of these particles. The energization per particle would be correspondingly large. However, in MHD theories of reconnection it is the magnetosheath ions which maintain the momentum balance and are energized. The energy gain of electrons is smaller by the mass ratio m_e/m_i. It is here that the reconnection concept, applied at the magnetopause, faces its most formidable observational test. Three years ago, Heikkila (1975) pointed out that no observations available at that time indicated the presence of such energized protons just inside the magnetopause. More recent studies of the plasma boundary layer (Paerendel et al., 1978; Eastman and Hones, 1979; Paschmann et al., 1979) also have failed to reveal convincing evidence of proton energization. On the other hand, Mozer et al., (1979) have reported direct measurements of substantial tangential fields $\underline{E}_t$. It is also noted that an energetic electron layer has been found outside the magnetopause (Meng and Anderson, 1970,1975; Baker and Stone, 1977,1978). However, it is difficult to construct a model in which these particles are the ones responsible for the momentum balance in the magnetopause.

Heikkila (1978) has examined a large number of ways of accounting for the discrepancy between MHD reconnection theory and observations. He found them all wanting and concluded that reconnection on the dayside magnetopause does not occur. Yet, there are compelling reasons, in particular the observed flux erosion of the magnetospheric front lobe when the interplanetary field has a southward component (e.g., Aubry et al., 1970; Holzer and Slavin, 1978,1979), which make it difficult to discard reconnection. Below we examine several ways of avoiding Heikkila's conclusion:

(a) Equation (26) represents an upper limit on the energization in two ways. First, it represents a maximum, because $\underline{E}_t$ was chosen to be parallel to the net current $\underline{I}$ in the magnetopause so that the electromagnetic dissipation rate $\underline{E}_t \cdot \underline{I}$ is a maximum. Although no conclusive proof is available, there are strong theoretical arguments (Cowley, 1974,1976) indicating that other directions of $\underline{E}_t$ may be possible. For the case $\underline{B}_{t_1} = -\underline{B}_{t_2}$, $\underline{E}_t$ may even be perpendicular to $\underline{I}$ so that the dissipation rate is zero. The transformation velocity $\underline{v}_0$ in Figure 4a is then perpendicular to the plane of the figure and the particle velocity is equal to $(v_0^2 + v_A^2)^{\frac{1}{2}}$ on both sides of the magnetopause. A second point is that the energization is less when the two fields $\underline{B}_{t_1}$ and $\underline{B}_{t_2}$ are not antiparallel. Figure 4b shows a combination of the two effects.

It also suggests the range of directions of the electric field for which reconnection-like flows occur, i.e., flows in which perpendicular magnetic flux B_n is transported away from the reconnection line (which has been tacitly assumed to be parallel to $\underline{E}_t$). The calculation of the particle energization for an arbitrary configuration is a straightforward geometrical task.

Except for the extreme case $\underline{B}_{t_1} = -\underline{B}_{t_2}$ mentioned above, there is no possibility of removing all of the particle acceleration associated with dayside reconnection in this manner. But the two effects discussed here may help reduce the energization to the point where it could have been overlooked.

(b) If the magnetopause is partly reflective,[3] energized particles will appear on both sides of the current layer. Thus the full energization is not discovered by comparing particle energies inside and outside the magnetopause. Rather it becomes necessary to separate the particles on the magnetosheath side into incident and reflected populations before the energization can be established. It should be added that such a model of the magnetopause would contain an abrupt density change so that the internal boundary layer has significantly lower density than the magnetosheath. A completely reflective magnetopause may be contemplated too (Sonnerup, 1976) but momentum conservation then requires the two fields $\underline{B}_{t_1}$ and $\underline{B}_{t_2}$ to be exactly antiparallel (or possibly exactly parallel).

Again, reflection effects do not remove the energization of particles. But they do provide a set of circumstances in which it may have been overlooked.

(c) The energy gained by the ions in the reconnection electric field may be transferred to the electrons, or possibly to plasma waves, by some internal magnetopause process. The nature of this process is unknown. However, as a simple example, assume that the magnetopause structure, viewed in the frame S', contains a normal electric field E'_{no}. Equation (20) assumes no such field to be present. If E'_{no} is directed outward from the earth, then, in the frame S', the ions will be decelerated, the electrons accelerated, as they cross the magnetopause, while the energies of reflected particles will remain unchanged. Since the potential increase across the magnetopause cannot exceed the incident energy of the transmitted ions it is easy to show that their exit energy in the magnetospheric frame can be less than that given by Equation (26) by a factor of at most $4r/(2r-1)$. However, if part of the incident ion population is reflected, a situation may now arise where the average ion energy outside the magnetopause is greater than that inside. Energized electrons will appear in a layer inside the magnetopause. It is not clear in what circumstances an electric field E'_{no} could occur self-consistently in the magnetopause. One requirement would be that in the absence of E'_{no} the magnetopause appeared substantially more reflective to electrons than to ions.

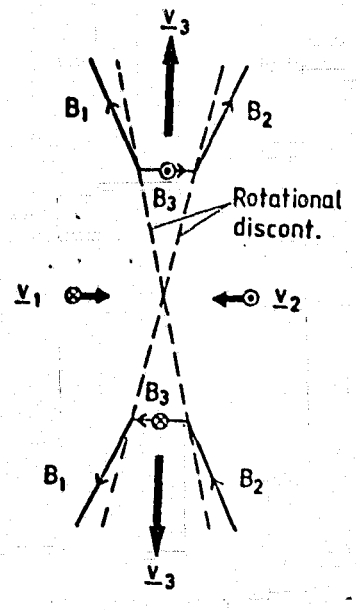

Figure 5. Magnetic field reconnection without plasma energization. Magnetopause is the wedge-shaped region between the two rotational discontinuities. Quantities in this region are denoted by subscript 3. Note that $|\underline{B}_3| = |\underline{B}_1| = |\underline{B}_2|$ and $|\underline{v}_3| = |\underline{v}_1| = |\underline{v}_2|$.

(d) Reconnection geometries do exist in which the reconnection component $\underline{E}_t$ of the electric field is directed along the net current $\underline{I}$ but where no particle energization occurs. Figure 5 shows an example of such a geometry. The magnetopause is wedge-shaped and contains a strong magnetic field perpendicular to the plane of the figure. At the two edges of the magnetopause, rotational discontinuities deflect the flows incident from both sides without change of the particle speed. In the inflow regions the flow is predominantly perpendicular to the plane of the figure while in the outflow (i.e., in the magnetopause) the flow vector lies in that plane. From the point of view of the Poynting-vector flux, the inflow of electromagnetic energy from both sides is exactly balanced by an outflow in the wedge shaped magnetopause regions so that no conversion of electromagnetic to particle energy occurs. Mathematical details of such models may be extracted from the work of Cowley (1974).

There is no observational information that would exclude the possibility of a wedge shaped magnetopause. And the magnetopause often contains a transverse field of magnitude comparable to $\underline{B}_{t_1}$ and $\underline{B}_{t_2}$. But the model does not predict a plasma boundary layer inside the magnetopause. Rather, the magnetopause and the boundary layer coincide, and plasma is fed into this layer from both sides.

(e) In the light of existing observations of the magnetopause structure it seems likely that reconnection, if it occurs at the

magnetopause, is a patchy and highly time-dependent process. Assume that, on the average, reconnection signatures may be seen over an area equivalent to a strip of width $\Delta = 1R_E$ on the front lobe of the magnetosphere. With a normal magnetic field component $B_n = 5\text{-}10nt$ such a strip can reconnect a sufficient amount of flux to replenish the tail flux in a few hours. The probability P of a satellite encountering a reconnection patch is equal to the area of the strip divided by the area of the entire front lobe. With a magnetospheric cross sectional radius of $R_T = 15R_E$ one then finds $P = \pi R_T \Delta / 2\pi R_T^2 = 1/30$. When instrumental limitations of the plasma experiments are folded into the picture it seems possible that reconnection could occur even though a clear signature of it has not yet been seen[4] in the plasma data.

It should be remembered that various magnetic signatures compatible with reconnection, such as the presence of nonvanishing value of B_n and rotational behavior of the tangential magnetic field in the magnetopause, have been seen (e.g., Sonnerup, 1976; Sonnerup and Ledley, 1974,1979). Sonnerup and Ledley (1979) suggest that patchy reconnection should produce indentations in the magnetopause. Such indentations, when swept along the magnetopause, lead to rapid multiple boundary crossings. Thus it may be that the search for the plasma signatures of reconnection should focus on, or at least include, multiple crossings. Such crossings were excluded in a recent study of IMP6 data by Eastman and Hones (1979).

In summary, it seems that a combination of some of the effects (a)-(e) may be able to account for the discrepancy between classical reconnection theory and presently available observations. Better data, supplied by the ISEE and other experiments, and more detailed intercomparison of magnetic field, electric field, and plasma data are needed before one can assess the importance of plasma convection across the magnetopause (with or without reconnection) in a reliable way.

Recent laboratory experiments by Podgorny et al., (1978) and Dubinin et al., (1978) seem to establish the possibility of two topologically distinct magnetospheres, depending on the ratio of flow speed to Alfvén speed in the incoming flow. For low values of that ratio and a southward interplanetary field, a Dungey type configuration (Dungey, 1961) is established with magnetopause reconnection in the equatorial plane. For high values an entirely different geometry is observed with a "visor", containing closed field line loops, covering the front lobe of the magnetosphere. It is suggested here that in the real magnetosphere this visor has a thickness comparable to the ion gyroradius (as it did in the experiment) and that it represents the dayside magnetopause of a closed magnetosphere. If this interpretation is reasonable, then the magnetosphere with a southward interplanetary field would have two states: fully open for low values of the ratio of flow speed to Alfvén speed, closed for high values of that ratio, the latter being the normal situation. A suggestion to this effect has been made by Sonnerup (1965). It is also in accord with the work of Cassen and Szabo (1970), who observed that viscous boundary layer solutions in

field-aligned flow cease to exist below a certain critical ratio of flow speed to Alfvén speed. They suggested a "disrupted" magnetopause in such circumstances.

The patchy reconnection discussed above would appear as a perturbation on the closed state. The question then remains whether the fully open configuration ever occurs. It would seem possible that it does during magnetic storms that involve large southward interplanetary fields. Sonnerup (1971) has reported one possible direct observation of the reconnection line in the equatorial plane during a magnetic storm.

6. ENERGY DISSIPATION

It is of interest to consider briefly the expression for the electromagnetic energy dissipation rate per unit area during reconnection. Using the notation in Figure 4b we find

$$\mathcal{P} \equiv \underline{E}_t \cdot \underline{I} = E_t I \cos\alpha \tag{28}$$

where α is the angle between $\underline{E}_t$ and $\underline{I}$ and the magnetopause current per unit length is

$$I = (B_{t_1}/\mu_0)\sqrt{1+(B_{t_2}/B_{t_1})^2-2(B_{t_2}/B_{t_1})\cos\theta}$$
$$\rightarrow (2B_{t_1}/\mu_0)\sin(\theta/2) \tag{29}$$

Here θ is the angle between $\underline{B}_{t_1}$ and $\underline{B}_{t_2}$. For $B_{t_2} = B_{t_1}$, i.e., when the field magnitudes are equal, the last member of the equality results. Below, the last member in each formula for $\mathcal{P}$ refers to this case. At present, the electric field magnitude E_t and angle α cannot be predicted from theory. However, it is of interest to explore the consequences of two reasonable sets of assumptions concerning these quantities.

Assume that we take $\underline{E}_t$ to be proportional to the unperturbed interplanetary electric field vector so that $E_t = K v_\infty B_\infty$ (where $B_\infty = \sqrt{B_Y^2 + B_Z^2}$ in solar magnetospheric coordinates[1] and v_∞ is the solar wind speed) and $\alpha = 90 - \xi$. (The angle ξ is defined in Figure 4b.) In that case

$$\mathcal{P} = K_1 v_\infty B_\infty (B_{t_1}/\mu_0)(1-B_{t_2}/B_{t_1}\cos\theta)$$
$$\rightarrow (2K_1 v_\infty B_\infty^2/\mu_0)(B_{t_1}/B_\infty)\sin^2\theta/2 \quad (\pi/2<\theta<\pi) \tag{30}$$

The coefficient K_1 may be a function of θ as well. It is not clear precisely how B_{t_1}/B_∞ or θ should be related to conditions upstream in the solar wind. But it is evident that the power input will be a strong function of $\theta/2$ with a maximum when B_{t_1} is antiparallel to B_{t_2} ($\theta=\pi$;

the interplanetary field is due south). This model also gives $\mathcal{P} = 0$ for $0<\theta<\pi/2$. In other words, it gives a "rectifier" type of behavior (Burton et al., 1975).

Another possibility is to insist that the electric field $\underline{E}_t$ is along the current $\underline{I}$ and that its magnitude is determined by a Petschek type upper limit on reconnection (see Sonnerup, 1974):

$$E_t = K_2 v_{A_\perp} B_{t_1} \sin\xi \qquad (K_2 \simeq 0.1\text{-}0.2) \tag{31}$$

where $v_{A_\perp} = B_{t_1}\sin\alpha/\sqrt{\mu_0 \rho_1}$

We then find

$$\mathcal{P} = \frac{K_2}{\mu_0}\frac{B_{t_1}^3}{\sqrt{\mu_0\rho_1}}\,\frac{(1-B_{t_2}/B_{t_1}\cos\theta)^2}{\sqrt{1+(B_{t_2}/B_{t_1})^2-2(B_{t_2}/B_{t_1})\cos\theta}} \rightarrow [2K_2 B_{t_1}^3/(\mu_0\sqrt{\mu_0\rho_1})]\sin^3(\theta/2) \tag{32}$$

In this case too, a very strong dependence on the angle $\theta/2$ is predicted.

From empirical considerations Perreault and Akasofu (1978) propose that the total energy input into the magnetosphere is[5]

$$\sim v_\infty B_\infty \sin^4(\tilde{\theta}/2) \tag{33}$$

where $\tilde{\theta} = \pi/2 - \tan^{-1}(B_Z/B_Y)$.

It is unlikely that any of the preceding expressions, which describe only the magnetopause dissipation, can be cast into this form. But, assuming $\tilde{\theta}$ and θ to be proportional, the reconnection process seems to agree with the observational result that the power input depends strongly on the angle $\tilde{\theta}$ with maximum input at $\tilde{\theta} = \pi$ and zero in put at $\tilde{\theta} = 0$ (or possibly for $\tilde{\theta}$ less than some minimum value).

7. DIFFUSION

The reconnection model is not the only one to yield a strong dependence of the energy input on the angle θ between the fields on the two sides of the magnetopause. In a purely resistive magnetopause the electromagnetic power dissipation rate per unit area is

$$= \eta[I]I^2 \tag{34}$$

where $\eta[I]$ is the resistivity, assumed to be a function of the current I. With the expression (29) for the current, and for $B_{t_1} = B_{t_2}$, we find

$$\mathcal{P} \rightarrow (2B_{t_1}/\mu_0)^2 \sin^2(\theta/2)\,\eta[(2B_{t_1}/\mu_0)\sin(\theta/2)] \tag{35}$$

If η increases rapidly with increasing current as it may when the resistive effects are produced by current or gradient driven microinstabilities, we find the electromagnetic dissipation rate to be a very strong function of θ with a minimum at $\theta = 0$ and a maximum at $\theta = \pi$.

In a diffusion dominated situation, most of the energy input into the magnetosphere is in the form of mechanical and thermal energy of the particles which diffuse across the magnetopause. The electromagnetic portion given above is small. However, presumably this latter energy goes into the establishment of the microturbulence which in turn allows particles to diffuse across the magnetopause. Thus $\mathcal{P}$ becomes the controlling factor for the diffusion so that its θ dependence governs the total mass and energy flow across the magnetopause.

The detailed nature of the microinstabilities operative in the magnetopause is not known. Eviatar and Wolf (1968) have suggested two-stream ion cyclotron instability, Huba et al., (1977) have proposed the lower-hybrid drift instability, and Hasegawa and Mima (1978) have calculated diffusion coefficients in the presence of kinetic Alfvén wave turbulence. On the basis of these results it appears reasonable to assume that effective kinematic viscosities ν in the required range of 10^9–5×10^9 m^2/s (Axford, 1964) can be generated via microinstabilities in the magnetopause.

The hydrodynamic Reynolds number based on a flow speed $v = 100$ km/s, a magnetopause thickness $h = 200$ km, and a kinematic viscosity $\nu = 10^9$ m^2/s, is $Re \equiv vh/\nu = 20$. A sheet jet in ordinary hydrodynamics becomes turbulent at $Re = 30$. When account is taken of the stabilizing effects of the sheared magnetic field at the magnetopause, and of the fact that the flow is strongly accelerated, it appears unlikely that hydrodynamic turbulence and the associated eddy diffusivity is important near the subsolar point. (In the tail magnetopause, it may well be dominant.)

Dayside plasma boundary layer observations reveal a bewildering array of possible structures (Eastman and Hones, 1979; Paschmann et al., 1978) including situations where little or no boundary layer is seen. The statement that such a layer is present implies that magnetosheath-like plasma is seen inside the inner edge of the magnetopause. Often this plasma layer is much thicker than the current layer. If such a situation is to be explained by diffusive processes then the diffusion coefficient for mass must be much greater than that for current. Such differences are not uncommon for molecular diffusion phenomena (e.g., momentum diffusivity greatly exceeds heat diffusivity in laminar flow of oil); they may occur in a plasma as a result of microinstabilities as well. Hasegawa and Mima (1978) find that kinetic Alfvén waves yield a diffusion coefficient for electrons that is much greater than that for the current. Papadopolous (private communication, 1978) has suggested that the unequal thicknesses of the current and the plasma layer may be accounted for by a turbulent wave field generated by the intense currents in the magnetopause and then spreading to the

adjacent boundary-layer region allowing effective mass diffusion there.

On the other hand, in turbulent hydrodynamic boundary layers the diffusivities for mass, momentum, and energy are approximately equal. Similarly, in the magnetopause application, if eddy diffusivity associated with gross hydrodynamic turbulence provided the dominant transport mechanism, then the magnetopause current layer would be as thick as the boundary layer and the two layers would occupy the same region in space.

On the basis of the discussion given here, we conclude that diffusion produced by plasma microturbulence may not be ruled out as an important, occasionally even dominant, transport process at the dayside magnetopause. Large-scale hydrodynamic turbulence appears to be a less likely agent, at least near the subsolar point. It must be pointed out, however, that the boundary layer is sometimes observed to have features which are difficult to explain on the basis of diffusion. For example, extremely steep density gradients have been seen at the magnetopause, followed by a nearly constant density in the boundary layer with another sharp drop-off in density at the inner edge of that layer (Paschmann et al., 1979).

ACKNOWLEDGEMENT

The research was supported in part by the National Aeronautics and Space Administration under grant NSG 7292, and by the Atmospheric Research Section, National Science Foundation under grant ATM 74-08223A01 to Dartmouth College. Support from the Max Planck Gesellschaft during the author's visit to the Institute for Extraterrestrial Physics in Garching is gratefully acknowledged.

NOTES

1. On leave from Dartmouth College, Hanover, N.H. 03755, U.S.A.

2. The polar angle Θ is not to be confused with the angle θ between the magnetospheric and the magnetosheath field.

3. Another possibility, leading to similar results, is that particles of magnetospheric origin flow outwards across the magnetopause.

4. After completion of this paper, a few ISEE magnetopause crossings have been found with substantially enhanced plasma flow speeds near the magnetopause (Paschmann, private communication, 1979).

5. Rossberg (this conference) has shown improved correlation when $B_\infty^2 = B_Y^2 + B_Z^2$ rather than $B_\infty^2 = B_X^2 + B_Y^2 + B_Z^2$.

REFERENCES

Alfvén, H.: 1958, Tellus 10, p. 104.

Alfvén, H.: 1968, J. Geophys. Res. 73, p. 4379.

Alksne, A.Y. and Webster, D.L.: 1970, Planet. Space Sci. 18, p. 1203.

Aubry, M.P., Russell, C.T. and Kivelson, M.G.: 1970, J. Geophys. Res. 75, p. 7018.

Axford, W.I.: 1964, Planet. Space Sci. 12, p. 45.

Baker, D.N. and Stone, E.N.: 1977, Geophys. Res. Lett. 4, p. 133.

Baker, D.N. and Stone, E.N.: 1978, J. Geophys. Res. 83, p. 4327.

Burch, J.L.: 1974, Revs. Geophys. Space Phys. 12, p. 363.

Burton, R.K., McPherron, R.L. and Russell, C.T.: 1975, Science 189, p. 717.

Cassen, P. and Szabo, J.: 1970, Planet. Space Sci. 18, p. 349.

Cole, K.D.: 1974, Planet. Space Sci. 22, p. 1075.

Cowley, S.W.H.: 1973, Cosm. Electrodyn. 3, p. 448.

Cowley, S.W.H.: 1974, J. Plasma Phys. 12, p. 319.

Cowley, S.W.H.: 1976, J. Geophys. Res. 81, p. 3455.

Crooker, N.U. and Siscoe, G.L.: 1975, J. Geophys. Res. 80, p. 4368.

Dubinin, E.M., Podgornyi, I.M. and Potanin, Y.N.: 1978, Cosmic Research 16, p. 66.

Dungey, J.W.: 1961, Phys. Rev. Lett. 6, p. 47.

Eastman, T.E. and Hones, E.W., Jr.: 1979, J. Geophys. Res. 84, p. 2019.

Eviatar, A. and Wolf, R.A.: 1968, J. Geophys. Res. 73, p. 5561.

Formisano, V., Domingo, V. and Wenzel, K.-P.: 1978, J. Atm. Terr. Phys. 40, p. 279.

Haerendel, G., Paschmann, G., Sckopke, N., Rosenbauer, H. and Hedgecock, P.C.: 1978, J. Geophys. Res. 83, p. 3195.

Hasegawa, A. and Mima, K.: 1978, J. Geophys. Res. 83, p. 1117.

Hayes, W.D. and Probstein, R.F.: 1959, Hypersonic Flow Theory, Academic Press, New York, p. 158.

Heikkila, W.J.: 1975, Geophys. Res. Lett. 2, p. 154.

Heikkila, W.J.: 1978, J. Geophys. Res. 83, p. 1071.

Holzer, R.E. and Slavin, J.A.: 1978, J. Geophys. Res. 83, p. 3831.

Holzer, R.E. and Slavin, J.A.: 1979, J. Geophys. Res. 84, p. 2573.

Huba, J.D., Gladd, N.T. and Papadopoulos, K.: 1977, Geophys. Res. Lett. 4, p. 125.

Hudson, P.D.: 1970, Planet. Space Sci. 18, p. 1611.

Lees, L.: 1964, AIAA J. 2, p. 1576.

Lemaire, J. and Roth, M.: 1978, J. Atm. Terr. Phys. 40, p. 331.

Meng, C.-I. and Anderson, K.A.: 1970, J. Geophys. Res. 75, p. 1827.

Meng, C.-I. and Anderson, K.A.: 1975, J. Geophys. Res. 80, p. 4237.

Mozer, F.S., Torbert, R.B., Fahleson, U.V., Fälthammar, C.-G., Gonfalone, A., Pedersen, A. and Russell, C.T.: 1979, Geophys. Res. Lett. 6, p. 305.

Paschmann, G., Sckopke, N., Haerendel, G., Papamastorakis, I., Bame, S.J., Asbridge, J.R., Gosling, J.T., Hones, E.W., Jr. and Tech, E.R.: 1978, Space Sci. Revs. 22, p. 717.

Perreault. P.D. and Akasofu, S.-I.: 1978, Geophys. J. Roy. Astr. Soc. 54, p. 547.

Podgorny, I.M., Dubinin, E.M. and Potanin, Yu.N.: 1978, Geophys. Res. Lett. 5, p. 207.

Russell, C.T. and Elphic, R.C.: 1978, Space Sci. Revs. 22, p. 681.

Sonnerup, B.U.Ö.: 1965, J. Geophys. Res. 70, p. 1051.

Sonnerup, B.U.Ö.: 1971, J. Geophys. Res. 76, p. 6717.

Sonnerup, B.U.Ö.: 1974, J. Geophys. Res. 79, p. 1546.

Sonnerup, B.U.Ö.: 1976, Physics of Solar Planetary Environments (D.J. Williams, ed.), Am. Geophys. Union, p. 541.

Sonnerup, B.U.Ö. and Ledley, B.G.: 1974, J. Geophys. Res. 79, p. 4309.

Sonnerup, B.U.Ö. and Ledley, B.G.: 1979, J. Geophys. Res. 84, p. 399.

Spreiter, J.R. and Alksne, A.Y.: 1969, Rev. Geophys. Space Phys. 7, p. 11.

Zwan, B.J. and Wolf, R.A.: 1976, J. Geophys. Res. 81, p. 1636.

ELECTROMAGNETIC STRUCTURE OF THE MAGNETOPAUSE AND BOUNDARY LAYER

B. U. Ö. Sonnerup[1]

Max-Planck-Institut
für extraterrestrische Physik
8046 Garching, W. Germany

B. G. Ledley

Goddard Space Flight Center
Greenbelt, MD 20771, USA

ABSTRACT

After a review of the properties and predictions of the closed and open models of the magnetopause, OGO-5 magnetometer data are used to illustrate various observed signatures of the magnetopause current layer and the adjacent plasma boundary layer. Among the topics touched upon are: fluctuations, diamagnetic effects, and field-aligned currents in the boundary layer; one-dimensionality of the magnetopause; presence and absence of a magnetic field component perpendicular to the magnetopause; finite ion gyroradius effects. A brief summary is given of existing Vlasov theory for the description of tangential, rotational and contact discontinuities. Special attention is paid to the tangential momentum balance and the jump conditions at a rotational discontinuity. Finally, a discussion is given of low frequency fluctuations with emphasis on the signatures of the tearing mode.

Keywords: Magnetopause, Boundary Layer, Tangential Discontinuity, Rotational Discontinuity, Tearing Mode

1. INTRODUCTION

The magnetopause is the thin layer in space which marks the outer boundary of the earth's magnetic field. Immediately outside the magnetopause one finds the streaming solar-wind plasma of the magnetosheath and its imbedded interplanetary magnetic field of time-variable direction, draped around the magnetosphere. Immediately inside, the magnetic-field direction is less variable and is in large measure controlled by the earth. The magnetopause itself is an electric current layer which adjusts the magnetic field direction and magnitude from the magnetosheath to the magnetospheric state, in accordance with Ampère's law. Inside the magnetopause one finds a highly time-variable layer of streaming plasma of magnetosheath origin, at the inner edge of which the magnetic field may undergo further, usually much smaller, changes in magnitude and direction. This layer is referred to as the boundary layer.

The present paper attempts to briefly summarize what is known, and not known, both observationally and theoretically, about the electromagnetic structure of the magnetopause and boundary layer regions. Over the years, a substantial body of observational facts has accumulated concerning the magnetic structure (Ref. 1-14). Direct measurements of the DC electric fields near the magnetopause are far more difficult and results have started to emerge only very recently (Ref. 15; also A. Pedersen, this conference). Fluctuating electric and magnetic fields have been studied only to a limited extent (Ref. 9, 16-17). The existence of the plasma boundary layer has been established relatively recently (Ref. 18-26). The properties of this layer have been observed in fair detail (see review by G. Paschmann, this volume) but its generation and relationship to the adjoining magnetopause remain obscure. From a theoretical viewpoint, the electromagnetic and plasma structures of the magnetopause and boundary layer are of course inextricably intertwined. Thus, the theoretical discussion to be given will, by necessity, deal with both aspects.

There are three major scientific reasons for study of the magnetopause and boundary layer: (i) From the point of view of solar-planetary physics, it is essential to understand the transfer of mass, momentum, and energy from the solar wind, across the magnetopause, into the magnetosphere. Included among possible processes are diffusion due to micro- and macroturbulence as well as convective entry in association with magnetic-field reconnection. (ii) Current sheets appear to play an important role in many cosmic systems. Any physical understanding of the structure of, and dynamical processes in, the thin collision-free magnetopause current layer may be directly used in other cosmic contexts. In particular, if we can learn to understand the reasons for the occurrence, or absence of occurrence, of reconnection at the magnetopause, and in the former case, if we can establish the efficiency and physical manifestations of that process, then our level of understanding of the conversion of magnetically stored energy in cosmos into plasma kinetic and thermal energy will be significantly advanced. (iii) The magnetopause provides an excellent opportunity for plasma physicists to develop and test theories for linear and nonlinear micro- and macroprocesses in current-carrying collision-free plasmas.

The magnetometer data presented in the paper were obtained with the Goddard Space Flight Center fluxgate magnetometer (J. Heppner, principal investigator) onboard the satellite OGO-5.

[1]Permanent address: Dartmouth College, Hanover, NH 07355, USA.

2. GLOBAL CONSIDERATIONS

For given interplanetary and magnetospheric conditions the time-average magnetopause and boundary-layer structures presumably vary in an organized manner with location. For example, it appears that the boundary layer thickness increases systematically with increasing distance from the subsolar point (Ref. 21). However, because of unknown, usually rapid, radial motion of the local magnetopause, the absolute thicknesses of the current layer and boundary layer have been difficult to assess precisely (for a summary, see Ref. 27), at least before the ISEE mission. Furthermore, structural changes associated with changing interplanetary and magnetospheric conditions often obscure effects associated with different locations on the magnetospheric surface. Since no systematic observational studies exist which separate all of these effects, we resort to a simpler approach: only structures on the front lobe of the magnetosphere will be considered, during conditions where there is a large and relatively abrupt change in field direction at the magnetopause, making it easily identifiable in the magnetic data. It must be remembered that there are many recorded instances where these conditions are not met.

The closed and open models of the magnetosphere have played, and continue to play, an important role in the interpretation of observed magnetopause structures. The former has its origin in the work of Chapman and Ferraro (Ref. 28). Note that in its modern form, this model does not imply a tail of finite length but merely a vanishingly small magnetic field component B_n normal to the magnetopause. The latter model, in a simple form, was introduced by Dungey (Ref. 29). For our purposes, its most important property is that $B_n \neq 0$.

Recently, these two conceptual models have been put on a firmer physical basis by the laboratory simulation experiments of Podgorny and coworkers (Ref. 30). They have shown that for antiparallel fields on the two sides of the magnetopause the open configuration occurs for flow speeds comparable to, or less than, the Alfvén speed while a configuration similar to the closed model (but with a disproportionately thick magnetopause, presumably resulting from the large ion gyroradius in the experiment) occurs at high flow speeds. In the real case, the solar-wind flow speed is large compared to the Alfvén speed so that one might normally expect the closed model, perturbed by those micro- and macroprocesses, including small-scale "patchy" reconnection, which may operate in the real magnetopause but perhaps not in the simulated one. Because of imperfect scaling, the conditions for which a transition between the two models occurs may be substantially different in the laboratory and in the real case. Thus, one cannot exclude the possibility that the Dungey model occurs in nature.

In the closed model the plasma boundary layer inside the magnetopause must be formed either by local diffusion of magnetosheath plasma across the magnetopause or by nonlocal entry, e.g., at the cusps. In the open model, the plasma flows directly across a, possibly rather limited, longitude sector of the dayside magnetopause, as a result of the presence of a nonvanishing normal magnetic field component. In crossing the magnetopause the plasma is accelerated by the $\underline{I} \times \underline{B}_n$ force into two poleward-directed jets, one in each hemisphere. Here $\underline{I}$ is the magnetopause, or Chapman-Ferraro, current. These jets supply the boundary layers of the open model.

In the closed model the plasma flow is tangential and the associated electric field is normal to the magnetopause. Additionally, the magnetopause structure itself is likely to contain a normal electric field. In the open model, normal electric fields are also present. But in addition, there is a tangential component $\underline{E}_t$ at the magnetopause. This field leads to the drift of magnetosheath plasma into the magnetopause. It is associated with the occurrence of magnetic-field reconnection in or near the equatorial plane (reconnection in the cusps also remains a viable possibility), and its direction is such that $\underline{E}_t \cdot \underline{I} > 0$.

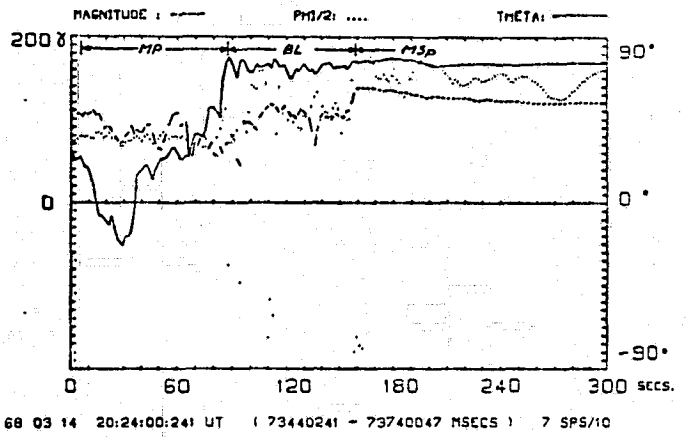

Figure 1. OGO-5 magnetometer record of crossing of the magnetopause (MP) and boundary layer (BL), showing the field magnitude (1γ = 1nt, dashed line), GSM latitude (θ, solid line) and longitude (φ, dotted line). Satellite location (GSM): X = 48130, Y = - 202040, Z = 3330 km.

3. OBSERVED TIME SIGNATURES

Figure 1 shows an OGO-5 magnetometer record of a traversal from the magnetosheath, across the magnetopause and boundary layer, and into the magnetosphere. The magnetic field is represented in terms of its magnitude, GSM latitude θ, and longitude φ. The latitude angle is initially positive (+25°), indicating that the magnetosheath field points somewhat north of the equatorial plane. The angle turns negative as the magnetopause is entered, and then positive again until it reaches the magnetospheric value (+85°) at the inner edge of the magnetopause. The field magnitude has a broad minimum during the 80 sec period comprising the magnetopause but it then remains low for another 60 sec. This latter period corresponds to the traversal of the boundary layer. The diamagnetic effect associated with the boundary-layer plasma is evident from the abrupt increase in field magnitude at the inner edge of the layer. It corresponds to a density change of 112 protons/cm^3 at an assumed temperature $T = 2 \times 10^6$°K. This unusually high density and the observed high field magnitude are associated with a magnetopause location at 8.2 R_E. Note also that the field magnitude has a substantial maximum just inside the inner edge of the boundary layer. Neugebauer et al. (Ref. 9) have associated this latter effect with the loss of magnetospheric trapped particles within a gyrodiameter of the magnetopause.

Large fluctuations of both field magnitude and direction are present, not only in the magnetopause,

but in the boundary layer as well. This is a characteristic feature of these regions (Ref. 21). Inside the boundary layer the field magnitude and latitude angle exhibit only slow variations. The longitude angle φ continues to fluctuate but since θ is near 90° the corresponding direction changes are relatively small.

It is noted that φ changes in a systematic way at the inner edge of the boundary layer. This change may correspond to a field-aligned current sheet flowing from the boundary layer into the ionosphere in the manner described by Eastman et al. (Ref. 21). An alternative explanation, which is less likely on account of the high fluctuation level in the field, is the finite ion-gyroradius effect described by Parker (Ref. 31, 32) and discussed further in Section 5.

If the magnetopause were stationary, the time duration of the magnetopause would correspond to a thickness of about 200 km. However, thickness estimates based on the analysis of multiple crossings and, more recently, on ISEE data (Ref. 14) indicate typical magnetopause thicknesses in the range of 500-1000 km, i.e., several proton gyrodiameters. In the present example it appears that the boundary layer was somewhat thinner than the magnetopause. In fact, unless one takes care to define the latter as the region where the main field direction change occurs, one may be tempted to incorporate the boundary layer into the magnetopause and thus fail to identify it as a separate region.

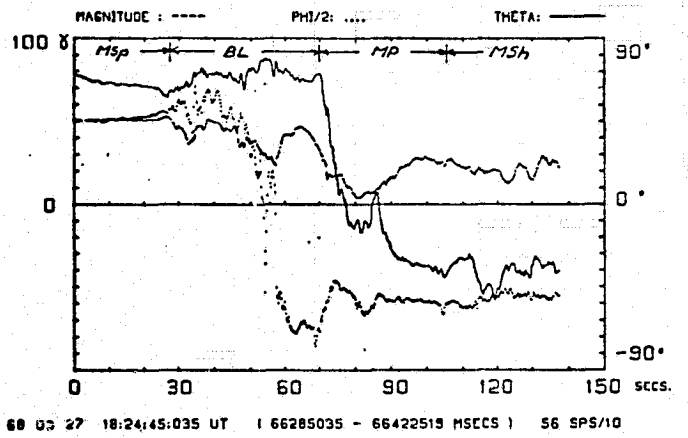

Figure 2. OGO-5 magnetometer record of boundary layer (BL) and magnetopause (MP) crossing. (For further information concerning the March 27, 1968, erosion event, see Ref. 7). (X = 54050, Y = - 45540, Z = 3590 km.)

Figure 2 shows another OGO-5 record, this time of an outbound crossing, which displays a clear magnetic signature of the boundary layer, namely a depressed field magnitude and large fluctuations. It should be noted, however, that in many cases the field depression in the boundary layer is weak or absent, presumably because the pressure in the hot tenuous ring-current plasma is about the same as the pressure in the cooler but denser boundary layer plasma. The deep field magnitude minimum in the magnetopause itself is a very common feature.

The field magnitude levels in Figure 2 are more representative of typical conditions at the magnetopause. Reference 11 gives average values of 28 nt outside the magnetopause and 42 nt inside the boundary layer, corresponding to a density change of 14 protons/cm^3 at 2×10^6°K.

Theoretical aspects of the electromagnetic structure of the boundary layer are discussed in a contributed paper (Ref. 33). In the remainder of the present report we shall focus on the magnetopause itself.

4. OBSERVED MAGNETOPAUSE STRUCTURES

It is of interest to ask whether the magnetopause structure is approximately one dimensional or intrinsically two or three dimensional. The former case implies that variations along the layer occur only on length scales much greater than its thickness. It then follows from $\nabla \cdot \underline{B} = 0$ that the magnetic field component normal to the magnetopause, B_n, remains very nearly constant across the layer at any location and instant. The latter case implies that variations along the sheet occur on length scales comparable to the thickness. In such circumstances B_n usually does not remain constant. If the magnetic vector data set taken during a magnetopause crossing has the property that a unique direction can be found along which all the vectors have one and the same component, B_n, then a strong case can be made to the effect that this direction is perpendicular to a one-dimensional sheet. Alternate possibilities are (i) that the two tangential derivatives in $\nabla \cdot \underline{B} = 0$ are large but equal and opposite; (ii) that time variations or variations in the attitude of the magnetopause exactly compensate for existing space variations in B_n. These alternatives require very special, and therefore highly unlikely, circumstances. A fourth and more likely alternative will be discussed at a later point. On the other hand, if one cannot find a direction having constant or nearly constant B_n from the data set, this does not necessarily imply that the local magnetopause structure was two or three dimensional. Time and attitude variations may have caused the nonconstancy.

In practice one usually cannot find a direction in space along with B_n is strictly constant. Instead one uses, as an approximation, that direction which yields minimum variance in the corresponding field component (Ref. 2). This direction is along the eigenvector $\underline{N}_3$ corresponding to the smallest eigen value (= variance λ_3) of the matrix

$$M_{ij} = \overline{B_i B_j} - \overline{B}_i \overline{B}_j \qquad (1)$$

which can be formed from the magnetopause magnetic vector data set by appropriate averaging (denoted by overhead bars). The vector $\underline{N}_3$ is taken to be directed away from the earth. The two other eigenvectors $\underline{N}_1$ and $\underline{N}_2$; corresponding to the largest and the intermediate eigenvalues, λ_1 and λ_2, are tangential to the local magnetopause surface and due approximately north and west, respectively. The right-handed orthogonal set ($\underline{N}_1$, $\underline{N}_2$, $\underline{N}_3$) provides a convenient natural coordinate system in which to examine the magnetic field data. Error estimate formulas for the normal vector $\underline{N}_3$ and the normal component $\overline{B}_3$ may be found in Ref. 8 and 11. These estimates represent lower limits because they do not include any systematic effects such as attitude or time changes during the crossing.

It is sometimes found that the matrix M_{ij} is nearly degenerate with λ_3 and λ_2 almost equal. In

that case an inaccurate determination of $\underline{N}_3$ results and the error estimates, containing terms of the form $(\lambda_2 - \lambda_3)^{-1}$, are correspondingly large. It is easy to show that such a state of affairs arises when the magnetopause current-density vectors are unidirectional or nearly unidirectional. As an illustration, consider the case of a two-dimensional tearing structure in the magnetopause. The current is unidirectional but not uniform, being concentrated to the centers of the tearing islands. The minimum variance analysis applied to such a structure gives $\lambda_3 = 0$, λ_2 small, and λ_1 large. The vector $\underline{N}_3$ is along the current, i.e., it is tangential, rather than normal, to the magnetopause surface!

When the minimum variance analysis is applied to an optimal segment of the magnetopause crossing in Figure 1, the eigen values $(\lambda_1, \lambda_2, \lambda_3)$ are found to be (1890, 338, 45) showing that the variance in the field component along $\underline{N}_3$ was large but still much smaller than the variances corresponding to $\underline{N}_2$ and $\underline{N}_1$. Thus, the magnetopause can be said to have been one-dimensional in an average sense, but with large superimposed two or three dimensional fluctuations.

The estimated normal vector $\underline{N}_3$ points in a reasonable direction, given the location of the spacecraft, and has an estimated error of ±6°. The normal magnetic field component, $B_n = \overline{B}_3 = 7.6 \pm 6.7°$, is not significantly different from zero. The crossing is shown in polar, or hodogram, form in Figure 3. The plot on the left represents the behavior of the tangential field (B_1, B_2), the one on the right shows the normal field B_3. A constant B_3 value corresponds to a vertical trace in the latter plot. The high level of turbulence peaking in the 0.01 - 0.10 Hz range is perhaps the most striking feature of the diagram.

Figure 4 shows a hodogram pair for the crossing in Figure 2. The eigen values are (480, 22, 5). The estimated error in $\underline{N}_3$ is only ±6° but it is seen that, apart from several minor excursions, the tangential hodogram indicates a fairly constant value of B_2, corresponding to a nearly unidirectional current along $-\underline{N}_2$. Thus, the normal direction is strongly influenced by the properties of the aforementioned minor field excursions and should not be trusted. Use of different data segments for the analysis also tends to give inconsistent results. This example illustrates the importance of examining the hodogram pairs before one draws conclusions about the reliability of the calculated normal vector and normal field component.

Figure 5 shows an example of a high quality determination of the normal vector, with an estimated angular error of only ±2.4°, and of the normal field component $B_n = \overline{B}_3 = 0.1 \pm 0.4$ nt. The set of eigen values for this case is (747, 82, 2) indicating that the layer is one-dimensional to a good approximation. Note that the fields on the two sides of the magnetopause are very nearly antiparallel, yet the magnetic trademark of reconnection, a B_n value substantially different from zero, is entirely absent. It seems clear that factors other than the orientation of the magnetosheath field relative to the earths field play an important role in controlling reconnection.

The nature of the tangential field in this outbound magnetopause crossing is remarkable. The field reverses direction by a rotation rather than by a decrease of the northward field to zero followed

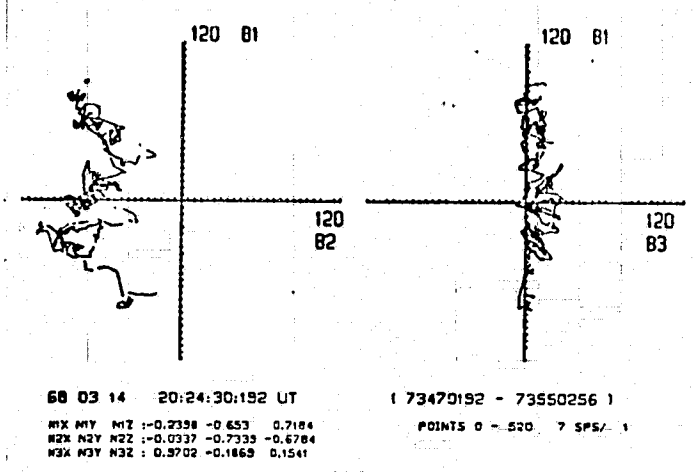

Figure 3. Hodogram representation, with field components in nt, of a portion of the magnetopause crossing in Figure 1. The magnetosphere has $B_1 > 0$. GSM projections of $(\underline{N}_1, \underline{N}_2, \underline{N}_3)$ on the lower left. (X = 48130, Y = - 20240, Z = 3330 km.)

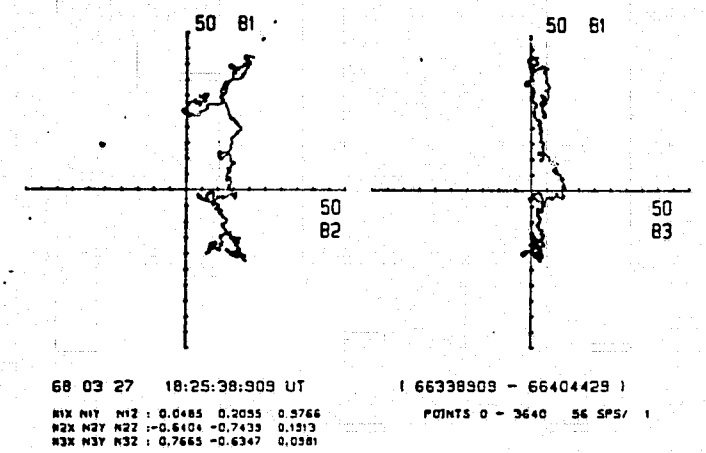

Figure 4. Hodogram representation of magnetopause crossing in Figure 2. (X = 54050, Y = - 45540, Z = 3590 km.)

by an increasing southward field as the magnetosheath side of the magnetopause is approached. Such behavior indicates the presence of substantial field-aligned, i.e., highly multidirectional, currents in the magnetopause. It is this field rotation, and the corresponding large variance λ_2 that helps produce an accurate normal vector determination.

The crossing in Figure 5 was extremely rapid, occurring in a time span of only 9 sec. Thus one may think that a snapshot picture of the magnetopause structure was obtained. However, the crossing was followed within less than 10 sec by a second even more rapid one back into the magnetosphere (see Ref. 11, Figs. 2 and 3). The structure of the second crossing was sufficiently different from Figure 5 to suggest that structural changes, presumably associated with rapid convection of magnetic structures along the magnetopause, occur on very short time scales. In other words, the hodogram obtained during a magnetopause crossing is often severely time aliased. It should be added that the normal vector orientations for the pair of crossings discussed above support the

interpretation that they were caused by an indentation in the magnetopause being swept downstream past the spacecraft.

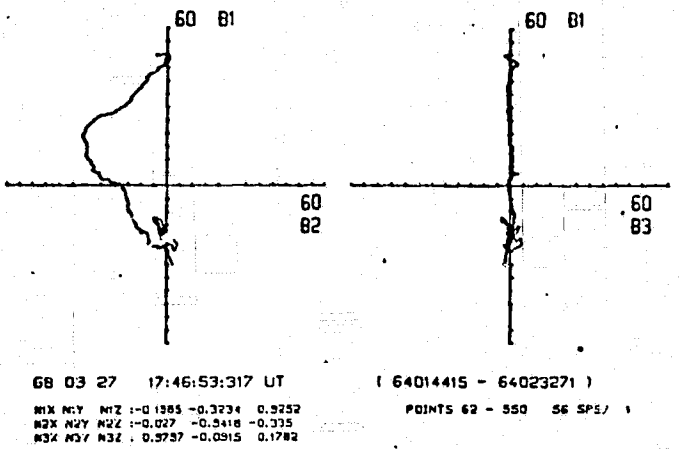

Figure 5. Hodogram representation of magnetopause crossing for which an accurate determination of $\underline{N}_3$ and $\overline{B}_3$ is obtained, and for which $\overline{B}_3 \approx 0$. (X = 56480, Y = - 50080, Z = 6590 km.)

Figure 6 shows another example of a good normal vector determination and a vanishingly small normal field component $B_n = \overline{B}_3 = 1.2 \pm 1.3$ nt. Again, the fields on the two sides are nearly antiparallel, but this time the structure of the tangential hodogram is rather more complicated.

As Reported in Ref. 11, values of $|\overline{B}_3|$ less than the error estimate are obtained in approximately 25% of the crossings. Values greater than three times the error estimate are also found about 25% of the time. Two examples of the latter situation are shown in Figures 7 and 8. In the former case $\overline{B}_3 = -5.1 \pm 0.9$ nt, in the latter $\overline{B}_3 = +8.1 \pm 0.4$ nt. Results of the minimum variance analysis for five data segments of the second crossing (Ref. 7, 13) are shown in Table 1. The consistency of the results, except for the shortest segment, the flatness of the B_1B_3 hodogram, and the extremely large separation between λ_3 and λ_2 for the optimal segment, provide convincing evidence that the magnetopause does indeed on occasion develop a substantial normal magnetic field component. This crossing occurred in a time span of only 4 seconds so that an approximate snapshot of the structure may have been obtained.

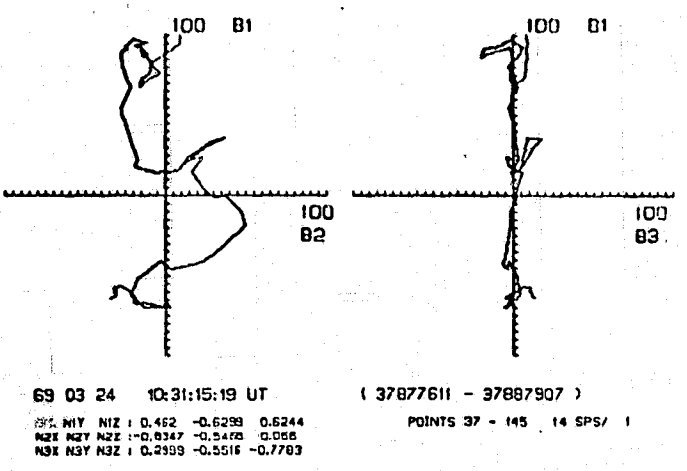

Figure 6. Hodogram representation of magnetopause crossing with $\overline{B}_3 \approx 0$. (X = 33550, Y = - 10950, Z = - 17730 km.)

5. TANGENTIAL DISCONTINUITIES

Current sheets having $B_n = 0$ are referred to as tangential discontinuities (Ref. 34). Self consistent one-dimensional Vlasov equilibria of such sheets can be generated by allowing the distribution function f to depend on the constants of motion of a particle: the total energy $\mathcal{E}$, and the two generalized linear momenta tangential to the sheet, P_1 and P_2.

$$f = f(\mathcal{E}, P_1, P_2) \tag{2}$$

$$\mathcal{E} = \tfrac{1}{2} mv^2 + e\phi \tag{3}$$

$$P_1 = mv_1 + eA_1 \tag{4}$$

$$P_2 = mv_2 + eA_2 \tag{5}$$

Here $\underline{v} = (v_1, v_2, v_3)$ is the velocity of a particle of mass m and charge e. Also, $\phi(x_3)$ and $\underline{A} = (A_1(x_3), A_2(x_3), 0)$ are the scalar and vector potentials, respectively, x_3 being the coordinate along the direction normal to the sheet.

During the last 20 years large numbers of equilibria of this type have been generated (for reviews see Ref. 35-37). The most recent work by Lee and Kan (Ref. 38) and by Roth (this conference) shows promise of being able to account for several observed magnetopause features. In general, by a sufficiently clever choice of the distribution functions, one

Table 1.

Segment	Number of $\underline{B}$ Vectors	Eigen Values γ^2			Normal Field	Error in N_3	
		λ_1	λ_2	λ_3	$\overline{B}_3 \pm \Delta B_3$, γ	$\Delta\underline{N}_3 \cdot \underline{N}_1$	$\Delta\underline{N}_3 \cdot \underline{N}_2$
1	48	76	1.5	0.15	3.4 ± 3.4	0.02	0.13
2	96	267	23	0.58	10.0 ± 1.2	0.02	0.06
3	144	463	83	1.3	8.1 ± 0.7	0.02	0.04
4	192	570	124	1.6	8.0 ± 0.5	0.02	0.03
5	240	722	130	1.9	8.1 ± 0.4	0.01	0.03

The five nested data segments are centered at 65938239 ms UT.
Fifty-six vector samples per second.

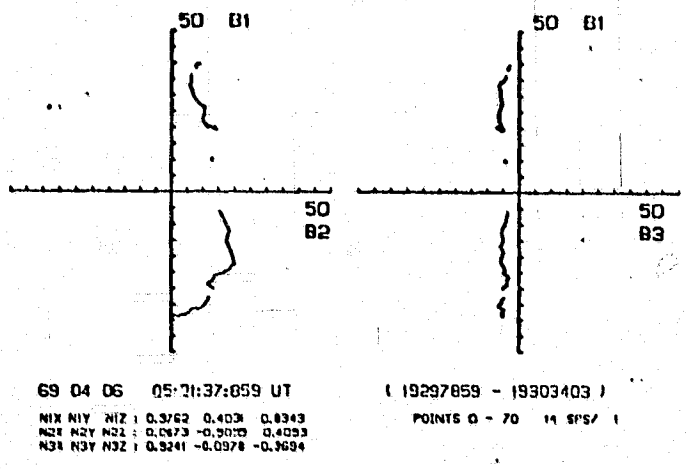

Figure 7. Hodogram representation of magnetopause crossing with $\overline{B}_3 < 0$ (X = 52000, Y = - 62080, Z = - 15270 km).

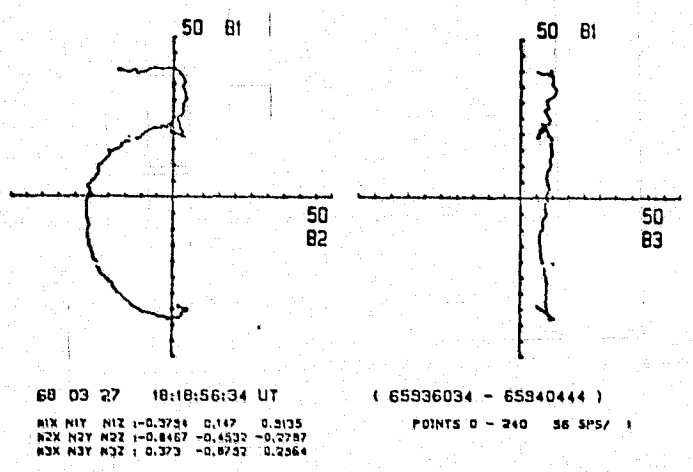

Figure 8. Hodogram representation of magnetopause crossing with $\overline{B}_3 > 0$ (X = 55000, Y = - 47000, Z = 4000 km).

can probably mimic the main magnetic features of many observed structures. However, it is unlikely that a one-one relationship exists between the magnetic structure and the distribution functions. Thus it is not clear what general conclusions can be drawn about the distributions from an examination of the magnetic structures.

There are two frequently observed features of the magnetopause which might be of interest in this regard. One is the occurrence of a rotation of the tangential magnetic field at the magnetospheric edge of the magnetopause leading to a hook-like appearance in the tangential hodogram, as shown in Figure 9 (see also Fig. 8, and Ref. 11 Fig. 4a). This feature may be a manifestation of an effect first described by Parker (Ref. 31, 32). In brief, Parker observed that field-aligned currents would occur near the inner edge of the magnetopause if magnetosheath ions with a net velocity along the field penetrate deeper into the magnetopause than magnetosheath electrons. In fact, even if the electrons penetrate to the same depth as the ions, as a result of fluctuations, say, they are unlikely to retain any memory of the external flow direction when they arrive at the inner edge of the magnetopause. Further discussion of Parker's effect will be given by L. R. O. Storey (this conference).

Another, as yet unexplained, effect is the common occurrence of an overswing of the tangential field rotation near the magnetosheath edge of the magnetopause. This feature is seen in Figure 1 where the latitude (θ) trace indicates an initial southward turning of the field as the satellite first enters the magnetopause. It seems possible that this feature too is associated with finite ion gyroradius effects in interpenetrating streaming plasmas.

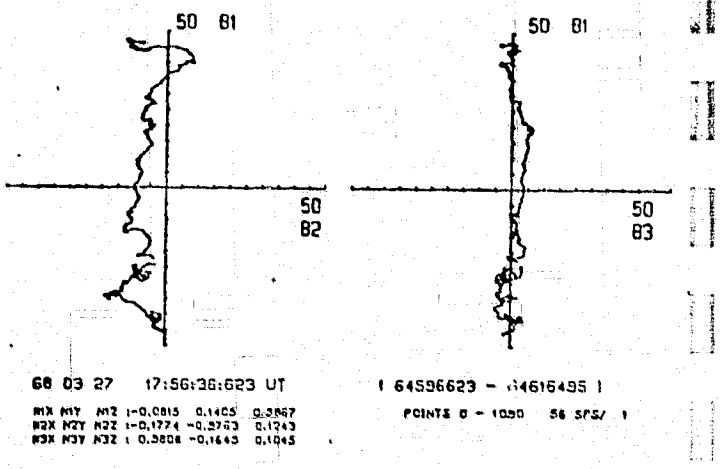

Figure 9. Field rotation near the magnetospheric side ($B_1 > 0$) of the magnetopause. (X = 55700, Y = - 49040, Z = 5840 km.)

In summary, the study of tangential-discontinuity Vlasov equilibria is an important activity for two reasons. First, such equilibria seem to be able to reproduce certain relatively frequently observed detailed features of the magnetopause structure. In such cases then, the current layer is presumably essentially laminar and diffusive particle transport across the magnetopause is small or absent. However, as we have seen, there are many other occasions when the magnetopause is highly turbulent. This fact provides a second reason for the examination of Vlasov equilibria: their stability should be studied in order to establish the circumstances in which the laminar and the turbulent states are to be expected.

6. ROTATIONAL DISCONTINUITIES: JUMP CONDITIONS

When a nonvanishing normal magnetic field component, B_n, is allowed for in a current sheet, the physics of the sheet changes dramatically. For $B_n = 0$ particles are permanently trapped in the sheet and can enter and leave only at its edges. When $B_n \neq 0$ they can enter and leave the sheet at any point by moving along the field lines. In this latter case, a critical question for the current sheet equilibrium is how to balance the net tangential Maxwell stress $\underline{T}_M = (B_n/\mu_o)\Delta\underline{B}_t$, where $\Delta\underline{B}_t$ is the change in the tangential magnetic field vector across the sheet. Viscous stresses and plasma pressure variations along the sheet can provide for the balance when B_n lies in the range <0.1-0.5nt. Such small normal components are in fact present in viscous magnetopause models (e.g. Ref. 39). But for B_n in the range 8-10nt (see Figures 7 and 8) these stresses are too small to be of importance.

The Maxwell stress, if left unbalanced, would lead to acceleration of the plasma in the magnetopause

at rates of 50-100 km/s^2. Such accelerations, even if operative only during the time it takes a spacecraft to cross the magnetopause, which would be an unlikely coincidence, leads to unacceptably high plasma velocities. The remaining possibilities are to balance $\underline{\tau}_M$ by changing the tangential momentum of magnetosheath plasma convecting across the current sheet or by utilizing the tangential component of the plasma pressure tensor which develops when the pressures $p_\parallel$ parallel and $p_\perp$ perpendicular to the magnetic field are unequal. This latter stress incorporates effects of particles reflected at the current sheet. The convective stress is $\underline{\tau}_c = -\rho v_n \Delta \underline{v}_t$, where ρ and v_n are the plasma density and flow component along $\underline{N}_3$, respectively, while $\Delta \underline{v}_t$ is the change in tangential flow velocity as the plasma crosses the sheet. The net tangential stress associated with $p_\parallel \neq p_\perp$ is $\underline{\tau}_\alpha = -\alpha \underline{\tau}_M$, where $\alpha = (p_\parallel - p_\perp)(\mu_o/B^2)$ is the pressure anisotropy factor.

The net tangential momentum balance now becomes (Ref. 40):

$$\rho v_n \Delta \underline{v}_t = (B_n/\mu_o)\Delta\{(1-\alpha)\underline{B}_t\} \qquad (6)$$

This equation applies to fast and slow shocks, for which $v_n \neq 0$ and $\Lambda_t = 0$, Λ_t being the angle formed between the tangential magnetic field components on the two sides of the sheet. It also applies to rotational discontinuities ($v_n \neq 0$, $0<\Lambda_t<\pi$) and to contact discontinuities ($v_n = 0$, $\Lambda_t = 0$, π). The rotational discontinuity is of key importance for the magnetopause application, because it is the only type of current layer with $B_n \neq 0$ that permits of a tangential field rotation by an arbitrary angle Λ_t. This important point was first recognized by Levy et al. (Ref. 41).

For the rotational discontinuity it may be shown (Ref. 40) that

$$\rho_1/\rho_2 = (1-\alpha_2)/(1-\alpha_1) \qquad (7)$$

where the subscripts 1 and 2 refer to conditions on the magnetosheath and magnetosphere sides of the magnetopause, respectively. Further, the normal flow speed is the Alfvén speed, modified by the pressure anisotropy factor:

$$|v_n| = (|B_n|/\sqrt{\mu_o \rho})\sqrt{1-\alpha} \qquad (8)$$

When plasma as well as magnetic field data are available for a magnetopause crossing, these formulas may be used to check the hypothesis that magnetosheath plasma flows across the magnetopause in the presence of $B_n \neq 0$. First, without knowledge of v_n and B_n, one may check whether the two vectors $\Delta \underline{v}_t$ and $\Delta\{(1-\alpha)\underline{B}_t\}$ are parallel (or antiparallel) as required by Equation (6). If that is the case, one may then obtain the ratio v_n/B_n from Equation (6) and compare it to the ratio obtained from Equation (8). Finally, if B_n can be reliably determined from the magnetic data by minimum variance analysis, one may check whether its sign agrees with that required by Equation (6). This type of analysis of ISEE plasma and magnetometer data may be found in the review by G. Paschmann (this conference).

It may be shown (Ref. 40) that for a rotational discontinuity the balance of normal stresses leads to the requirement

$$\Delta\{p_\perp + B^2/2\mu_o\} = 0 \qquad (9)$$

The general energy equation is of the form

$$\rho v_n \Delta\{\tfrac{1}{2}v^2 + \frac{1}{\rho}(\tfrac{1}{2}p_\parallel + p_\perp)\} + \Delta\{\underline{v}\cdot\underline{\underline{P}}\cdot\underline{n}\} + \Delta\{\underline{Q}\cdot\underline{n}\} = \underline{E}_t \cdot \underline{I} \qquad (10)$$

where $\underline{\underline{P}}$ is the pressure tensor, $\underline{Q}$ the heat-flow vector, and $\underline{I}$ the total magnetopause current. This latter equation shows that the electromagnetic power $\underline{E}_t \cdot \underline{I}$ associated with reconnection at the magnetopause may be converted into kinetic or internal energy associated with the plasma jets inside the magnetopause (first term on the left) or into flow work (second term) or into a net heat flow away from the layer (third term). All of these terms may be of relevance in resolving Heikkila's (Ref. 42) energy crisis.

In summary, it appears that an unambiguous identification of a rotational discontinuity at the magnetopause may be performed solely on the basis of the magnetic field data. The requirement is $B_n \neq 0$ and $0 < \Lambda_t < \pi$. In a nonisotropic plasma ($p_\parallel \neq p_\perp$) it is not in general required that $|\underline{B}_1| = |\underline{B}_2|$; changes in field magnitude can occur as a result of changes in α, provided Equation (9) remains satisfied. The energy equation and the condition that the entropy cannot decrease across the layer do, however, place certain constraints on possible changes across the discontinuity, as discussed by Hudson (Ref. 43, 44). In particular, when α has the same value on the two sides of the discontinuity then, in addition to $\rho_2 = \rho_1$ (Equation 7), one also finds, $p_{\parallel 2} = p_{\parallel 1}$, $p_{\perp 2} = p_{\perp 1}$, and $|\underline{B}_2| = |\underline{B}_1|$ (these latter results are obtained only if the heat flow term in Equation (10) can be neglected).

7. ROTATIONAL AND CONTACT DISCONTINUITIES: STRUCTURE

Vlasov equilibria for one-dimensional structures having $B_n \neq 0$ are difficult to construct analytically because the two generalized tangential momenta, Equations (4) and (5), now contain vector potential components which depend on the tangential coordinates x_1 and x_2. Thus any distribution function containing these momenta will lead to equilibria that are not one dimensional. Additionally, the construction of equilibria containing a net flow across the sheet require the use of a constant of motion $C(v_3)$ which is linear in the normal particle velocity v_3. In general such a constant is not readily available.

Exact symmetric hot-plasma equilibria with $\Lambda_t = \pi$ and $B_2 \equiv 0$ have been constructed numerically by Eastwood (Ref. 45) with application to the geomagnetic tail current sheet in mind. These solutions may perhaps be viewed as rotational discontinuities in the firehose limit ($\alpha = 1$) but more appropriately they should be classified as contact discontinuities.

Hot-plasma non-linear wave solutions exist (Ref. 46-48) corresponding to infinite wave trains of circularly polarized large-amplitude electron and ion whistlers. For this case a simple constant of motion $C(v_3)$ does exist.

Cold plasma solutions with a net flow across the layer yield either infinite wave trains or electron-polarized solitons (Ref. 49-52), the latter involving a net rotation of the tangential field of $\Lambda_t = 2\pi$. These results raise the fundamental question whether laminar time-independent equilibrium structures of the rotational discontinuity

type do in fact exist.

Finally, analytical cold-plasma Vlasov equilibria for asymmetric contact discontinuities have been found recently (Ref. 53). In these solutions, a cold plasma beam is incident from the magnetosheath and is magnetically reflected at the current layer. The existence of such equilibria serves to emphasize the possible importance of particle reflections in magnetopause structures with $B_n \neq 0$.

A question of considerable interest is the sense of polarization of magnetopause rotational discontinuities. Both the electron and the ion polarizations have been seen, but with a preference for the former (Ref. 4, 11). First-order orbit theory of the rotational discontinuity (Ref. 54) indicates that only the electron polarization should occur if the current layer is sufficiently thin. A more recent simple model (Ref. 13) suggests that the electron polarization should be expected in layers that are sufficiently thin so that electrons, but not ions, flow across the layer by sliding along the magnetic field lines. In this model, the electrons provide the field-aligned current that causes the rotation of the tangential field, while the ions provide an additional current that is more uniformly spread over the width of the layer. This simple idea was used in Reference 13 to account for the circular portion of the tangential hodogram in Figure 8. In general, for the earth's magnetopause, the electron polarization corresponds to a tangential hodogram with negative B_2 when B_3 is positive, as in Figure 8; with positive B_2 when B_3 is negative, as in Figure 7. For Jupiter's magnetopause the electron polarization yields $B_2 < 0$ for $B_3 < 0$ and $B_2 > 0$ for $B_3 > 0$.

8. FLUCTUATIONS

Table 2 contains a list of relevant natural frequencies for conditions typical of the magnetopause and boundary layer plasma. Theoretical suggestions for

Table 2.

Electron plasma frequency	$f_{pe} = 34.7 \times 10^3$ Hz
Electron gyrofrequency	$f_{ce} = 978$ Hz
Proton plasma frequency	$f_{pi} = 810$ Hz
Lower hybrid frequency	$f_{LH} = 22.8$ Hz
Proton gyrofrequency	$f_{ci} = 0.53$ Hz
Tearing convection frequency	$f_t = 0.16$ Hz

$n = 15$ cm^{-3}; $B = 35$ nt

the generation of noise at these frequencies include the electron-cyclotron drift instability, (f_{ce}; Ref. 55) the ion acoustic instability (f_{pi}; Ref. 56), the lower hybrid drift instability (f_{LH}; Ref. 57), the two-stream or current-driven ion-cyclotron instabilities (f_{ci}, Ref. 58, 16) and the tearing instability (f_t; Ref. 59). The two former require current-layer widths of the order of the electron inertial length ($\lambda_e = 1.4$ km) which is unrealistic; the latter may operate when the width is of the order of the ion inertial length ($\lambda_i = 59$ km) or more.

Experimental information concerning electric and magnetic oscillations in the magnetopause remains scarce. Neugebauer et al. (Ref. 9) and Fairfield (Ref. 16) have reported low-frequency magnetic oscillations near the proton gyrofrequency which they interpret as ion cyclotron waves. At higher frequencies (Ref. 9) the magnetopause appears as a boundary between magnetosheath-like ("lion's roars") and magnetosphere-like ("chorus") ELF noise, with occasional indications of emissions characteristic of the magnetopause itself. Recently, Gurnett et al. (Ref. 17; also, this conference) have found evidence of enhanced noise levels in the magnetopause and boundary layer at frequencies from a few Hz up to well beyond the electron plasma frequency, with power generally decreasing rapidly with increasing frequency (except for the occasional appearance of narrow-band electrostatic emissions near the electron plasma frequency).

Examination of high time resolution magnetometer data at the magnetopause indicates that most of the fluctuation power occurs at frequencies below the range measured by Gurnett and probably below the proton gyrofrequency as well. A substantial contribution to this low frequency noise may come from radial oscillations in the magnetopause position and from waves on the magnetopause surface (see review by D. Southwood, this conference). However, the possible importance of kinetic Alfvén waves (Ref. 60) and of the tearing mode needs to be examined in detail. In the following paragraph we comment briefly on the signatures of the latter at the magnetopause.

The tearing mode may in principle be detected from a single satellite, as a result of the convection of tearing islands along the magnetopause. The resulting path of the satellite relative to the islands is shown by the slanted dashed line on the lower left in Figure 10. For a convection speed of 200 km/s and a fastest growing wave length $L = 4\pi\ell$, $2\ell = 200$ km being the characteristic width of the magnetopause, we find a frequency of 0.16 H

In the local coordinate system (x, y, z) shown in Figure 10 the tearing mode produces no fluctuations in B_y. From the condition $\nabla \cdot \underline{B} = 0$ one may furth deduce that, away from the islands themselves, the ratio of the fluctuation amplitudes in B_z and B_x should be about $L/2\ell = 2\pi$. In other words, the prediction is that the largest fluctuations should occur in B_z, much smaller ones in B_x and none in B_y. The magnetopause crossing in Figure 11 (Ref. 10) displays three subsegments of oscillations having essentially this property, the peak power occurring at a frequency of 0.11 Hz.

If the magnetopause contains a single mode (which was not the case in Figure 11), then the tearing mode oscillations also display a characteristic polarization pattern as illustrated on the right in Figure 10.

This discussion indicates that a systematic search for tearing signatures at the magnetopause may be a worthwhile enterprise. A first step in this direction may be found in Reference 61.

9. CONCLUSION

In summary, the local electromagnetic structure of the magnetopause appears to be highly time variabl ranging from nearly laminar states to highly turbulent ones. To account for this situation, one may imagine a magnetopause surface consisting of many intermixed laminar and turbulent patches, of various sizes and in various proportions, which are being convected along the surface away from the subsolar region. Some of the patches may contain persistent normal field components, and it remains possible that occasionally the main features

of Dungey's classical reconnection model appear at the front side magnetopause. The field fluctuations, at all frequencies, in the magnetopause and boundary layer provide a promising area of further research, because these fluctuations contain essential information about local micro- and macroprocesses.

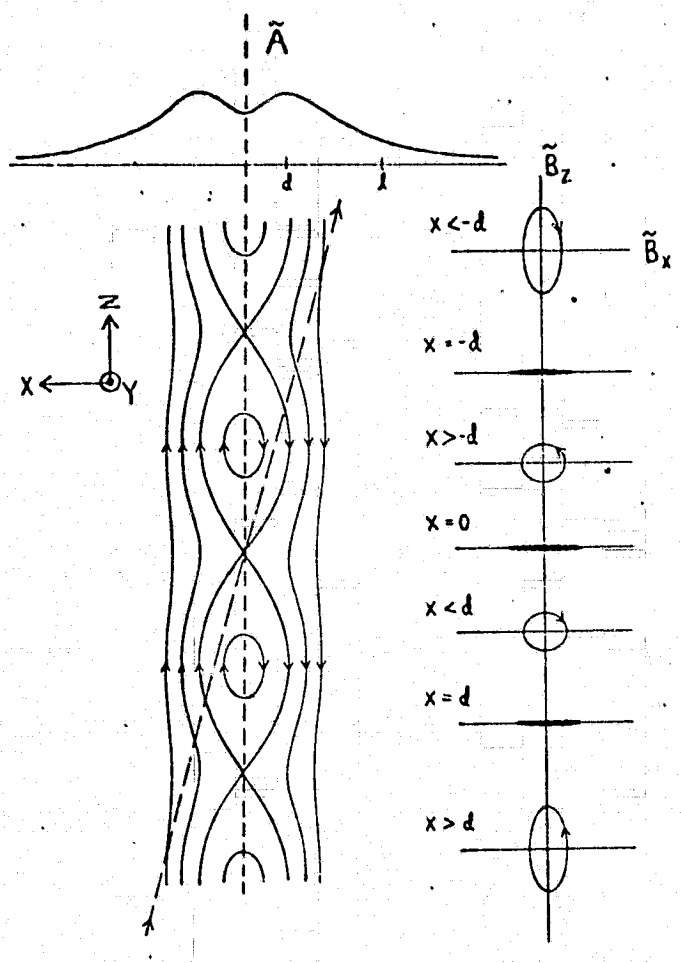

Figure 10. Signatures of the tearing mode. Upper left-hand diagram shows the perturbation vector potential Ã. On the lower left, the corresponding magnetic island structure is shown. Slanted dashed line represents satellite trajectory relative to the convecting islands. On the right, expected polarization properties of the perturbation magnetic field for different x values.

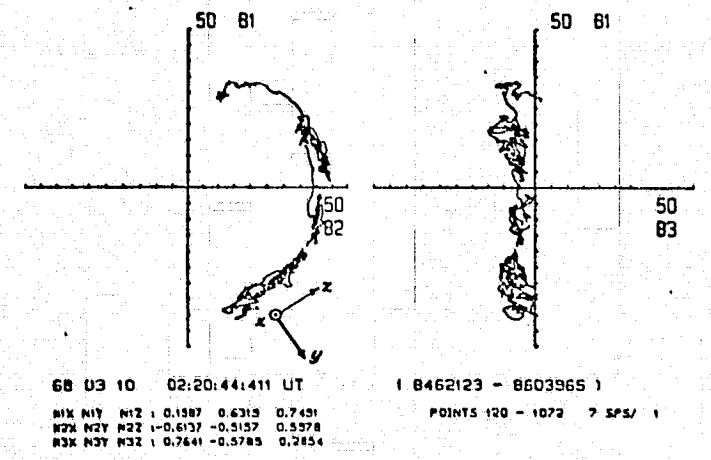

Figure 11. Hodogram representation of magnetopause crossing in which three separate tearing regions may have been encountered. (X = 21679, Y = - 77650, Z = 35052 km.)

10. ACKNOWLEDGEMENT

The research was supported by the National Aeronautics and Space Administration under grant NSG 7292 and by the National Science Foundation under grant ATM74-08223 A01 to Dartmouth College.

11. REFERENCES

1. Cahill L J & Amazeen P G 1963, The boundary of the geomagnetic field, J Geophys Res. 68, 1835-1943.

2. Sonnerup B U Ö & Cahill L J Jr 1967, Magnetopause structure and attitude from Explorer 12 observations, J Geophys Res. 72, 171-183.

3. Heppner J P, Sugiura M, Skillman T L, Ledley B G & Campbell M 1967, OGO-A magnetic field observations, J Geophys Res. 72, 5417-5471.

4. Sonnerup B U Ö & Cahill L J Jr 1968, Explorer 12 observations of the magnetopause current layer, J Geophys Res. 73, 1757-1770.

5. Cummings W D & Coleman P J Jr 1968, Magnetic fields in the magnetopause and vicinity at synchronous altitude, J Geophys Res. 73, 5699-5717.

6. Smith E J & Davis L 1970, Magnetic measurements in the earth's magnetosphere and magnetosheath, J Geophys Res. 75, 1233-1245.

7. Aubry M P, Kivelson M G & Russell C T 1971, Motion and structure of the magnetopause, J Geophys Res. 76, 1673-1696.

8. Sonnerup B U Ö 1971, Magnetopause structure during the magnetic storm of September 24, 1961, J Geophys Res. 76, 6717-6735.

9. Neugebauer M, Russell C T & Smith E J 1974, Observations of the internal structure of the magnetopause, J Geophys Res. 79, 499-510.

10. Sonnerup B U Ö & Ledley B G 1974, Magnetopause rotational forms, J Geophys Res. 79, 4309-4314.

11. Sonnerup B U Ö 1976, Magnetopause and boundary layer, in Physics of Solar Planetary Environments, Williams D J (ed.) Am Geophys U., Washington DC, 541-557.

12. Kaufmann R L & Cahill L J Jr 1977, The magnetopause at 5.2 R_E on August 4, 1972; Magnetopause shape and structure, J Geophys Res. 82, 1573-1584.

13. Sonnerup B U Ö & Ledley B G 1979, OGO-5 magnetopause structure and classical reconnection, J Geophys Res. 84, 399-405.

14. Russell C T & Elphic R C 1979, Initial ISEE magnetometer results: magnetopause observations, Space Sci Revs. 22, 681-715.

15. Mozer F S, Torbert R B, Fahleson U V, Fälthammer C-G, Gonfalone A, Pedersen A & Russell C T 1979, Direct observation of a tangential electric field component at the magnetopause, Geophys Res Lett. 6, 305-308.

16. Fairfield D H 1976, Waves in the vicinity of the magnetopause, in Magnetospheric Particles

Second and succeeding pages
and Fields, B M McCormac (Ed.), D Reider Publ Co Holland, 67-77.

17. Gurnett D A, Anderson R R, Tsurutani B T, Smith E J, Paschmann G, Haerendel G, Bame S J & Russell C T 1979, Plasma wave turbulence at the magnetopause, U Iowa Report 79-7, submitted to J Geophys Res.

18. Hones E W Jr, Asbridge J R, Bame S J, Montgomery M D, Singer S & Akasofu S-I 1972, Measurements of magnetotail plasma flow made with VELA 4B, J Geophys Res. 77, 5503-5522.

19. Akasofu S-I, Hones E W Jr, Bame S J, Asbridge J R & Lui A T Y 1973, Magnetotail and boundary layer plasmas at geocentric distance of 18 R_E: Vela 5 and 6 observations, J Geophys Res: 78, 7257-7274.

20. Rosenbauer H, Grünwaldt H, Montgomery M D, Paschmann G & Sckopke N 1975, HEOS 2 plasma observations in the distant polar magnetosphere: The plasma mantle, J Geophys Res. 80, 2723-2737.

21. Eastman T E, Hones E W Jr, Bame S J & Asbridge J R 1976, The magnetospheric boundary layer: Site of plasma, momentum and energy transfer from the magnetosheath into the magnetosphere, Geophys Res Lett., 3, 685-688.

22. Paschmann G, Haerendel G, Sckopke, N, Rosenbauer, H & Hedgecock P D 1976, Plasma and magnetic field characteristics of the distant polar cusp near local noon: The Entry Layer, J Geophys Res. 81, 2883-2899.

23. Crooker N U 1977, Explorer 33 entry layer observations, J Geophys Res. 82, 515-522.

24. Haerendel G, Paschmann G, Sckopke N, Rosenbauer H & Hedgecock P C 1978, The frontside boundary layer of the magnetosphere and the problem of reconnection, J Geophys Res. 83, 3195-3216.

25. Eastman T E & Hones E W Jr 1979, Characteristics of the magnetospheric boundary layer and magnetopause layer in high time resolution, Paper at 1978 Int Symp on Solar-Terr Phys, Innsbruck, Austria, 29 May-10 June, To appear Space Sci Revs.

26. Paschmann G, Sckopke N, Haerendel G, Papamastorakis I, Bame S J, Asbridge J R, Gosling J T, Hones E W Jr & Tech E R 1979, ISEE plasma observations near the subsolar magnetopause, Space Sci Revs. 22, 717-737.

27. Fairfield D H 1979, Structure of the magnetopause, observations and implications for reconnection, Paper at 1978 Int Symp on Solar-Terr Phys. Innsbruck, Austria, 29 May-10 June, 1978, To appear Space Sci Revs.

28. Chapman S & Ferraro V C A 1931, A new theory of magnetic storms, Terr Magnetism Atmosph Electr. 36, 77-97, 171-186.

29. Dungey J W 1961, Interplanetary magnetic fields and the auroral zones, Phys Rev Lett. 6, 47-48.

30. Podgorny I M, Dubinin E M & Potanin Yu N 1978, The magnetic field on the magnetospheric boundary from laboratory simulation data, Geophys Res Lett. 5, 207-210.

31. Parker E N 1967, Confinement of a magnetic field by a beam of ions, J Geophys Res. 72, 2315-2322.

32. Parker E N 1967, Small-scale nonequilibrium of the magnetopause and its consequences, J Geophys Res. 72, 4365-4374.

33. Sonnerup B U Ö 1979, Theory of the low-latitude boundary layer, this conference.

34. Landau L D & Lifshitz E M 1960, Electrodynamics of continuous media, Pergamon Press, New York, 224-229.

35. Willis D M 1971, Structure of the magnetopause, Rev Geophys Space Sci. 18, 953-985.

36. Willis D M 1975, The microstructure of the magnetopause, Geophys J R Astr Soc. 41, 355-389.

37. Willis D M 1978, The magnetopause: microstructure and interaction with magnetospheric plasma, J Atm Terr Phys. 40, 301-322.

38. Lee L C & Kan J R 1979, A kinetic model of the magnetopause, To appear J Geophys Res. 84.

39. Cassen P & Szabo J 1970, The viscous magnetopause, Planet Space Sci. 18, 349-366.

40. Hudson P D 1970, Discontinuities in an anisotropic plasma and their identification in the solar wind, Planet Space Sci. 18, 1611-1622.

41. Levy R H, Petschek H E & Siscoe G L 1964, Aerodynamic aspects of the magnetospheric flow AIAA J. 2, 2065-2076.

42. Heikkila W J 1975, Is there an electrostatic field tangential to the dayside magnetopause and neutral line?, Geophys Res Lett. 2, 154-15

43. Hudson P D 1971, Rotational discontinuities in an anisotropic plasma, Planet Space Sci. 19, 1693-1699.

44. Hudson P D 1973, Rotational discontinuities in an anisotropic plasma-II, Planet Space Sci. 21 475-483.

45. Eastwood J W 1974, The warm current sheet model and its implications on the temporal behavior of the geomagnetic tail, Planet Space Sci. 22, 1641-1668.

46. Bell T F 1965, Nonlinear Alfvén waves in a Vlasov plasma, Phys Fluids 8, 1829-1839.

47. Lutomirski R F & Sudan R N 1966, Exact nonlinear electromagnetic whistler modes, Phys Rev 147, 156-165.

48. Sonnerup B U Ö & Su S-Y 1967, Large amplitude whistler waves in a hot collision-free plasma, Phys Fluids 10, 462-464.

49. Saffman P G 1961, Propagation of a solitary wave along a magnetic field in a collision-free plasma, J Fluid Mech. 11, 16-20.

50. Saffman P G 1961, On hydromagnetic waves of finite amplitude in a cold plasma, J Fluid Mech. 11, 552-566.

51. Kellogg P J 1964, Solitary waves in a cold collisionless plasma, Phys Fluids 7, 1555-1571.

52. Kakutani T 1966, Nonlinear hydromagnetic waves propagating along a magnetic field in a cold collision-free plasma, J Phys Soc, Japan 21, 385-391.

53. Kirkland K B & Sonnerup B U Ö 1979, Contact discontinuities in a cold collision-free plasma, Preprint Radiophys Lab, Dartmouth College.

54. Su S-Y & Sonnerup B U Ö 1968, First-order orbit theory of the rotational discontinuity, Phys Fluids 11, 851-857.

55. Haerendel G 1978, Microscopic plasma processes related to reconnection, J Atm Terr Phys. 40, 343-353.

56. Coroniti F V & Eviatar A 1977, Magnetic field reconnection in a collision-free plasma, Astrophys J Suppl. 33, 189-210.

57. Huba J D, Gladd N T & Papadopoulos K 1977, The lower hybrid drift instability as a source of anomalous resistivity for magnetic field line reconnection, Geophys Res Lett. 4, 125-128.

58. Eviatar A & Wolf R A 1968, Transfer processes at the magnetopause, J Geophys Res. 73, 5561-5576.

59. Galeev A A & Zeleny L M 1978, Magnetic reconnection in a space plasma, in Theoretical and Computational Plasma Physics, Int Atomic Energy Comm, Vienna, 93-116.

60. Hasegawa A & Mima K 1978, Anomalous transport produced by kinetic Alfvén wave turbulence, J Geophys Res. 83, 1117-1123.

61. Greenly J B & Sonnerup B U Ö 1979, Tearing modes at the magnetopause, Preprint Radiophys Lab, Dartmouth College.

STRUCTURE OF JUPITER'S MAGNETOPAUSE

An Interim Report*

B.U.Ö. Sonnerup
Dartmouth College
Hanover, New Hampshire 03755

E.J. Smith and B.T. Tsurutani
Jet Propulsion Laboratory
Pasadena, California 91103

J.H. Wolfe
Ames Research Center
Moffet Field, California 94035

September 1979

Abstract

After a review of the time sequence of crossings of Jupiter's magnetopause by Pioneers 10 and 11, as identified in the plasma and magnetic field data, the detailed magnetic structures of a number of crossings are presented. Normal vectors are determined by minimum variance analysis, and the behavior of the normal and tangential field components is discussed. The normal vectors are compatible with a blunt model of Jupiter's magnetosphere. The normal magnetic field component is usually small. The observed structures and apparent thicknesses are compared to those of the earth's magnetopause.

*This report is based on a paper presented at S. Chapman Conference on Magnetospheric Boundary Layers, June 11-15, 1979, Alpbach, Austria.

1. Introduction

It is the purpose of this report to discuss the structure of Jupiter's magnetopause and to compare it with the terrestrial magnetopause. Data from the JPL helium vector magnetometers on board Pioneers 10 and 11 (Smith et al, 1976) will be used along with supporting evidence from the AMES plasma analyzer (Intriligator and Wolfe, 1976). The terrestrial magnetopause structures shown for comparative purposes were obtained from the GSFC flux-gate magnetometers onboard OGO-5 (J. Heppner, principal investigator).

2. Pioneer 10 Observations

Figure 1 shows the time sequence of magnetopause crossings during the Pioneer 10 encounter with Jupiter's magnetosphere. During the inbound leg of the trajectory, three magnetopause crossings were identified in the plasma data: November 27, 1973, at 20:35 UT (ground receipt time); December 1 at 03:18 and 14:20 (Intriligator and Wolfe, 1976). In the magnetic data the corresponding crossings appeared at 20:32, 03:20, and 13:56, respectively, indicating that the plasma was present somewhat inside the magnetopause. Several additional crossings, not apparent in the plasma data, may have occurred, as shown in the figure. In this report, we shall discuss the initial sequence of crossings (November 27 19:25, 19:40, 20:32) and the two crossings on December 1 at 03:20 and 13:56. Also, the final outbound crossing on December 14 at 19:36 will be examined. The other outbound crossings, identified in the plasma data, have yet to be uniquely associated with corresponding magnetic field structures.

Figure 2 shows a time record of the magnetic field during the initial three crossings. The field is represented by its magnitude (dashed line) its latitude angle θ in SJ coordinates (solid line) and its longitude angle φ (dotted line). The field outside the magnetopause is due slightly north. As the magnetopause is entered, the field first swings in the "wrong" direction, i.e. further north, and then turns south over a time span of 3 minutes to take on the direction typical of Jupiter's magnetosphere. However, the magnetopause starts moving back over the spacecraft almost immediately, and the field returns to the magnetosheath direction. The return is much slower and requires ~11 minutes. The excursion into the magnetosheath is brief and the third crossing is again a rapid one (~ 3 minutes). This time it is evident that an entry into the magnetosphere proper has occurred because the inner edge of the plasma boundary layer, marked by an abrupt field increase, is crossed at 20:41. This time should replace the approximate time 20:35 given by Intriligator and Wolfe (1976). From the change in field magnitude, with an assumed temperature $T = 5 \times 10^5 °K$, we conclude that the plasma density in the boundary layer was $n \geq 1.3$ cm^{-3} and that the beta value was $\beta > 1.6$ (β is the ratio of plasma to magnetic pressure).

Do the two first "so-called" crossings really represent traversals of the magnetopause or are they magnetic-field structures located in the magnetosheath outside the magnetopause? Figure 3 illustrates that both the normal vector orientations and the duration of the crossings are compatible with the interpretation of the time record as three distinct crossings, the multiplicity being caused by wave motion on the magnetopause. The normal vectors for the three cros-

sings, determined from minimum variance analysis, are given in terms of their solar-jovian X, Y, and Z components in Table 1.

Table 1 Normal vectors for the Pioneer 10 magnetopause crossings on Nov 27, 19:25, 19:40, 20:32 UT. θ_N is the latitude angle of the normal vector, and Δt is the duration of the crossing.

Crossing	N_X	N_Y	N_Z	θ_N°	Δt (sec)
1 (19:25)	.785	-.574	-.235	-13.6	180
2 (19:40)	.855	-.509	-.104	- 6.0	700
3 (20:32)	.943	-.224	-.247	-14.3	190

All three vectors point approximately in the direction expected for a forenoon crossing occurring slightly below the equatorial plane (longitude $\varphi = 325°$, latitude $\Lambda = -6°$). The monotonic increase in N_Y as time progresses may be the result of a very long wave length ondulation of the magnetopause surface. The change in N_Z is not monotonic. It is much greater than estimated errors, and it is compatible with the wave model shown in figure 3 on the left. The wave travels south and is responsible for the triple crossing of the magnetopause. Assuming the wave to sit still and the spacecraft to move north along the magnetopause instead, with the wave speed, v, and across it with the spacecraft speed ($v_s \sim 10$ km/s), we see that the first crossing should have a relatively large negative N_Z and a short crossing time Δt. The second crossing should have a smaller negative N_Z and a long crossing time, and the third one again a larger negative N_Z and a short crossing time. As shown in the table, this is exactly what occurs.

The right-hand part of figure 3 shows that the model can also be used to estimate the actual magnetopause thickness h_{MP}. Assuming small angles, three equations relating h_{MP}/v to the angles θ_N, θ_{MP}, and δ are obtained.

$$h_{MP}/(v\Delta t_1) = -\theta_{N1} - (-\theta_{MP} - \delta)$$

$$h_{MP}/(v\Delta t_2) = -\theta_{N2} - (-\theta_{MP} - \delta) \quad \Big\} \; h_{MP} = 32.1v \sim 3850 \text{ km}$$

$$h_{MP}/(v\Delta t_3) = -\theta_{N3} - (-\theta_{MP} - \delta) \quad \Big\} \; h_{MP} = 37.8v \sim 4540 \text{ km}$$

Here $\theta_N = \sin^{-1} N_Z$ is the measured tilt of the normal vector, $\delta \sim v_s/v$ is the angle associated with the skew traversal of the spacecraft across the wave, and θ_{MP} is the average tilt of the magnetopause. Also, Δt is the time duration of a crossing, measured from peak northward to peak southward field, or vice versa. From the three equations, by elimination of $(-\theta_{MP} - \delta)$, two estimates for h_{MP} are obtained. Given the crude nature of the model, the agreement between the two estimates is satisfactory. Assuming wave speed of $v = 120$ km/s, the thickness is $h_{MP} \sim 4200$ km, i.e., about 4 R_{Li} ($R_{Li} = 1077$ km for a 500 Volt particle in a 3 γ field). On the other hand, for $n = 1.3$ cm^{-3} the ion inertial length $\lambda_i = (m_i/\mu_o ne^2)^{\frac{1}{2}} = 200$ km so that $h_{MP} \sim 21\ \lambda_i$. This result supports the view that the relevant scale length for the thickness of a tangential-discontinuity type magnetopause is R_{Li} rather than λ_i. As a comparison, for a typical terrestrial magnetopause crossing the thickness may be $h_{MP} \sim 400$ km while $R_{Li} = 90$ km, $\lambda_i = 40$ km ($\varepsilon = 500$ Volt, $B = 35\gamma$, $n = 30$ cm^{-3}). Since the jovian magnetosphere on this occasion was more than 100 times larger than the terrestrial one, it is also

evident that the magnetopause was not proportional to the size of the magnetosphere.

The thickness h_{BL} of the plasma boundary layer may also be estimated. For v = 120 km/s one finds $h_{BL} \sim 6600$ km. The ratio h_{BL}/h_{MP} is comparable to the terrestrial values at corresponding locations on the magnetopause. Finally, the average tilt of the magnetopause relative to the Z axis may be calculated. For v = 120 km/s it is $\theta_{MP} \sim 8°$. Given the latitude of the crossing ($\Lambda = -6°$) this result corresponds to a relatively blunt magnetopause shape.

The sequence of three crossings can also be accounted for by assuming periodic radial motion of the magnetopause. In such a case too, the middle crossing is expected to have a longer penetration time. In a simple model with magnetopause motion either inwards or outwards with speed v_{MP} one may then use the observed penetration times to find $v_{MP} = 17$ km/s, $h_{MP} = 5000$ km. The nature of the model is such that it overestimates the thickness h_{MP}. The conclusion that R_{Li} rather than λ_i, or a constant fraction of the size of the magnetosphere, is the appropriate scale length remains valid.

We shall now examine the structure of the three crossings more in detail. Figure 4 shows a polar plot of the tangential field components ($B_1 B_2$) on the left, and of the normal field component B_3 on the right, for the first of the three crossings. Note that the tangential component B_2 remains negative in the crossing. Note also that the average normal field B_3 is nearly zero (although the ring-shaped structure in the middle of the crossing apparently has an orientation different from that of the main magnetopause). The structure is, on the whole, consistent with a tangential disconti-

nuity. The second crossing, shown in figure 5, displays a complicated turbulent structure. In reality it may not have been more turbulent than the first one. Rather it is the much longer crossing time in the second crossing that allows one to see more of the turbulent changes in the structure. Note that B_2 remains negative as in the first crossing, and that the average normal field component B_3 remains essentially zero. The third crossing, shown in figure 6, is again relatively rapid and displays less turbulence. The component B_2 is negative and $B_3 \sim 0$, as in the previous cases. The internal consistency ($B_2 < 0$, $B_3 \sim 0$) of the three observed structures supports the interpretation of the outer two structures as true magnetopause crossings.

Figure 7 shows a comparison of the time record for the last of the three Jupiter crossings above and for a terrestrial magnetopause crossing observed by the GSFC magnetometer on board OGO-5. There is a striking qualitative similarity between the two records. First, the inner edge of the plasma boundary layer is seen clearly in both records (although in the terrestrial case with $T = 10^6$°K the boundary layer density was $n \geq 225$ cm^{-3}). The field direction changes can be compared only after one of the two θ traces has been mirror imaged in the time axis to compensate for the fact that in the equatorial plane Jupiter's field is due south, while the earth's field is due north. When this has been done, it is seen that both records display an initial direction change in the "wrong" sense (as mentioned already in connection with figure 2) near the outer edge of the magnetopause. This behavior is seen frequently at the earth's magnetopause and can probably be accounted for in terms of

a finite gyroradius effect. Clearly, Jupiter's and the earth's magnetopause are occasionally remarkably similar.

Figure 8 shows, in polar form, the magnetopause structure during the next exit of Pioneer 10 from the magnetosphere. In this case too there may have been a sequence of three crossings, but the case for such an interpretation is less convincing than for the earlier sequence. Thus, only the innermost crossing is shown here. It had $B_2 > 0$ and contained a fairly large amount of turbulence. On the average the normal field component B_3 remained approximately zero. The penetration time was about 10 minutes.

Figure 9 shows the polar plots for the last crossing on the inbound leg of the Pioneer 10 orbit. Its structure was complicated, but again one notes a tendency for the normal component to average to zero. The penetration time was about 5 minutes.

Finally, figure 10 shows the last outbound crossing observed by Pioneer 10. This was a very rapid crossing with a penetration time of less than one minute. The structure was remarkably simple and contained a portion that we identify as a rotational discontinuity. The normal magnetic field component is $-0.82\gamma \pm 0.26\gamma$; in other words, it is significantly different from zero. The negative sign is what is expected in an open magnetosphere model for a crossing south of the reconnection line. The spacecraft latitude was small ($\Lambda = +8.2°$) so that a location south of a hypothetical reconnection line is entirely possible. The sense of rotation of the tangential field vector is remarkable. In a model discussed by Sonnerup and Ledley (1979) the field rotation in a thin rotational discontinuity is produced by the electrons in the magnetosheath plasma flowing

across the discontinuity. These electrons move adiabatically and essentially along the field thus causing a field-aligned current. In the present case, this model works only if the flow is from the magnetosphere into the magnetosheath, rather than vice versa. There is another piece of evidence that suggests the same thing, namely the field magnitude increase at the outer edge of the magnetopause, followed by a small field rotation. In the OGO-5 crossing of the earth's magnetopause shown in figure 11 (Sonnerup and Ledley, 1979), the same structure is present, but now at the inner edge of the magnetopause instead. This feature has been discussed by Sonnerup and Ledley in terms of a slow expansion fan, as proposed by Levy et al (1964), followed by a field direction change of the type discussed by Parker (1967 a, b). The general configuration shown in figure 11 is compatible with reconnection, with flow from the magnetosheath into the magnetosphere. Does the Jupiter crossing indicate reconnection with a reverse flow direction? We do not insist that this must be so. But the remarkable similarity between the Jupiter crossing and the terrestrial one indicates the importance of developing a better understanding of rotational field structures at the magnetopause.

3. Pioneer 11 Observations

We turn now to a brief discussion of the Pioneer 11 magnetopause crossings. The time sequence of possible crossings on both the inbound and outbound legs is shown in figure 12 for plasma as well as magnetic field data. The following comments should be made. The first inbound crossing at 02:08 on November 27, 1974, is gradual and poorly defined in the magnetic data. A second crossing (from

the magnetopause back into the magnetosheath) is found at 08:19. This crossing is well defined (although of 20 - 30 minutes duration) but, paradoxically, it occurs substantially before the crossing time indicated by the plasma data. A reexamination of plasma and magnetic field data is underway for this case. The final entry into the magnetosphere at 13:30 on November 29 was in all likelihood preceded by a brief entry of 1 hour duration. We shall discuss only the final crossing (figure 13).

On the outbound leg, the situation is initially complicated in that there is much magnetic field activity in a region identified via the plasma results as being the magnetosphere. Included is one field change at 06:42 on December 6 which has many of the features of a regular magnetopause crossing (figure 15). The crossings at 08:47 (figure 16) and at 19:07 on the same day are well defined but involve only small field direction changes. The final outbound crossing is also well defined (figure 17).

Figure 13 shows the polar representation of the magnetic field during the last crossing on the inbound leg. The duration of the crossing was 20 minutes, yet it does not display a grossly turbulent structure. Rather, small scale turbulence seems to occur in patches. This turbulence has considerable structure with alternating regions of circular and linear polarization. The frequency range centers around 0.05 Hz. One possible interpretation is in terms of tearing bubbles being convected past the spacecraft (Greenly and Sonnerup, 1979). The gross structure of the crossing is that of a rotational discontinuity. The normal field component is + 0.71γ ± 0.43γ, and the relationship between the sense of rotation and the sign of the normal field com-

ponent is that expected from the model by Sonnerup and Ledley (1979), this time assuming flow across the magnetopause from the magnetosheath into the magnetosphere.

For purposes of comparison, figure 14 shows an OGO-5 crossing of the earth's magnetopause which displays essentially the same features as the crossing in figure 13. In this case too, an interpretation in terms of a rotational discontinuity with flow from the magnetosheath into the magnetosphere and with convecting tearing structures appears reasonable (Greenly and Sonnerup, 1979).

Figure 15 shows a magnetic field structure observed on December 6, 1974 at 06:42 during the outbound portion of the Pioneer 11 trajectory. The structure occurred in a region identified via the plasma data as the magnetosphere. However, it is hard to believe that it is not a bona fide magnetopause crossing. It has the basic features of a rotational discontinuity. The normal field component, which appears positive on the slide, is in fact found to be slightly negative ($- 0.20\gamma \pm 0.26\gamma$) when the minimum variance analysis is performed on the main field rotation data segment alone. Thus, the main rotation is in the right sense, assuming plasma flow from the magnetosheath into the magnetosphere. Furthermore, the magnetic field increase and final field rotation at the inner edge of the crossing appear to be the exact counterparts of the features shown in figure 11 for an OGO-5 crossing of the earth's magnetopause.

Figure 16 shows a time record of the outbound magnetopause crossing at 08:47 on December 6, 1974. Here the field direction change is quite small; yet it is clear that the magnetopause is an effective barrier for the plasma. With $T = 5 \times 10^5$°K, the field magnitude

change indicates a density change $\Delta n \sim 3.9\ cm^{-3}$ across the magnetopause. The normal magnetic field component is near zero for this crossing.

The last outbound crossing by Pioneer 11 is shown in figure 17. It has a duration of ~7 minutes, and the structure is complicated. The B_1B_3 diagram suggests that the magnetopause attitude may have changed during the crossing. For this reason the Y component of the normal vector N_{3Y} (which should be ~-0.12 given the location: $\varphi = 353°$, $\Lambda = 31.2°$) is unreliable.

4. Shape of Jupiter's Magnetopause Surface

Figure 18 summarizes information concerning the gross shape of Jupiter's dayside magnetopause, extracted from the normal vector calculations. The angles θ_N and φ_N are the latitude and longitude angles of the normal vectors, while Λ and φ are the corresponding quantities for the spacecraft position vector. The 45° line in the two figures helps one compare the data to a model consisting of a centered sphere.

The most striking feature of the diagrams, when compared to corresponding ones for the earth's magnetosphere, is the large spread in the data. Presumably, this larger scatter is the result of a jovian magnetosphere that is far more "floppy" than the terrestrial one. The data do not provide support for a sharp-nosed (in the noon-midnight meridional plane) model of Jupiter's magnetopause. On the average, the shape may be about as blunt as a sphere.

5. Conclusion

We have shown that there is a striking similarity between the magnetic structures of the jovian and the terrestrial magnetopause. Our estimate of the magnetopause thickness supports the view that normally the ion gyroradius R_{Li} is the relevant scale size, rather than the ion inertial length, or some constant fraction of the magnetosphere radius. Thus, one should not expect to find thicknesses less than one or two R_{Li}. The possibility that the magnetopause thickness sometimes is many R_{Li} and perhaps even proportional to the size of the magnetosphere cannot be excluded, since such extremely thick structures have been found at the earth's magnetopause on rare occasions.

6. Acknowledgement

The research at Dartmouth College was supported by National Aeronautics and Space Administration under grant NSG 7292.

7. References

Greenly, J.B., and B.U.Ö. Sonnerup, Tearing modes at the magnetopause, Preprint 28 pages, Dartmouth College, July, 1979.

Intriligator, D.S., and J.H. Wolfe, Results of the plasma analyzer experiment on Pioneers 10 and 11, in Jupiter, T. Gehrels, ed., Univ. Arizona Press, pp. 848-869, 1976.

Levy, R.H., Petschek, H.E., and G.L. Siscoe, Aerodynamic aspects of the magnetospheric flow, AIAA J., 2, 2065-2076, 1964.

Parker, E.N., Confinement of a magnetic field by a beam of ions, J. Geophys. Res., 72, 2315, 1967a.

Parker, E.N., Small-scale nonequilibrium of the magnetopause and its consequences, J. Geophys. Res., 72, 4365, 1967b.

Smith, E.J., Davis, L., Jr., and D.E. Jones, Jupiter's magnetic field and magnetosphere, in Jupiter, T. Gehrels, ed., Univ. Arizona Press, pp. 788-829, 1976.

Sonnerup, B.U.Ö., and B.G. Ledley, OGO-5 magnetopause structure and classical reconnection, J. Geophys. Res., 84, 399-405, 1979.

8. Figure Captions

Fig. 1 Pioneer 10 crossings of Jupiter's magnetopause in 1973, as recorded by the JPL magnetometer and the AMES plasma analyzer.

Fig. 2 Time record of magnetic field observations during the first, triple, inbound magnetopause crossing by Pioneer 10. Theta and phi are the SJ latitude and longitude angles of the magnetic field vector, respectively. Jupiter's magnetosphere has $\theta \sim -90°$. The field magnitude is measured in nT (1nT = 1γ).

Fig. 3 Schematic of magnetopause wave motion model to account for the normal vector variation and the penetration times for the three crossings in figure 2.

Fig. 4 Polar representation (hodograms) of the magnetic field during the first of the three magnetopause crossings in figure 2. The field components B_1 and B_2, measured in nT, are tangential to the magnetopause surface, with the former due approximately north and the latter approximately west. Thus B_1 is negative in Jupiter's magnetosphere. The

component B_3 is perpendicular to the magnetopause and is positive when directed away from the planet. The matrix in the lower left-hand corner of the figure gives the components of the corresponding unit vectors $\underline{N}_1$, $\underline{N}_2$, and $\underline{N}_3$, along these three directions, in SJ coordinates. $\underline{N}_3$ is the magnetopause normal vector.

Fig. 5 Hodogram for the second crossing in figure 2.

Fig. 6 Hodogram for the third crossing in figure 2.

Fig. 7 Comparison of time record of the third crossing in figure 2 (top) with a terrestrial magnetopause crossing by the satellite OGO-5 (bottom).

Fig. 8 Hodogram of Pioneer 10 inbound magnetopause crossing on December 01, 1973, 03:20 UT.

Fig. 9 Hodogram of Pioneer 10 final inbound magnetopause crossing on December 01, 1973, 13:56 UT.

Fig. 10 Hodogram of Pioneer 10 final outbound magnetopause crossing on December 14, 1973, 19:36 UT.

Fig. 11 Hodogram of OGO-5 crossing of the earth's magnetopause. Note that $B_1 > 0$ in the earth's magnetosphere while $B_1 < 0$ in Jupiter's magnetosphere. Compare to figures 10 and 15.

Fig. 12 Pioneer 11 crossings of Jupiter's magnetopause in 1974, as recorded by the JPL magnetometer and the AMES plasma analyzer.

Fig. 13 Hodogram of Pioneer 11 final inbound magnetopause crossing on November 29, 1974, 13:30 UT.

Fig. 14 Hodogram of OGO-5 crossing of the earth's magnetopause. Compare to figure 13.

Fig. 15 Field structure observed by Pioneer 11 on December 06, 1974, 06:42 UT. Compare to figures 10 and 11.

Fig. 16 Time record of Pioneer 11 outbound magnetopause crossing on December 06, 1974, 08:47 UT.

Fig. 17 Hodogram of Pioneer 11 final outbound magnetopause crossing on December 08, 1974, 01:22 UT.

Fig. 18 Shape of Jupiter's magnetopause surface. The angles Λ and φ are the SJ latitude and longitude of the spacecraft during penetration of the magnetopause. The angles θ_N and φ_N are the SJ latitude and longitude of the magnetopause normal vector $\underline{N}_3$, determined from minimum variance analysis. The terms "sharper" and "blunter" refer to the magnetopause shape relative to a centered sphere (= 45° line).

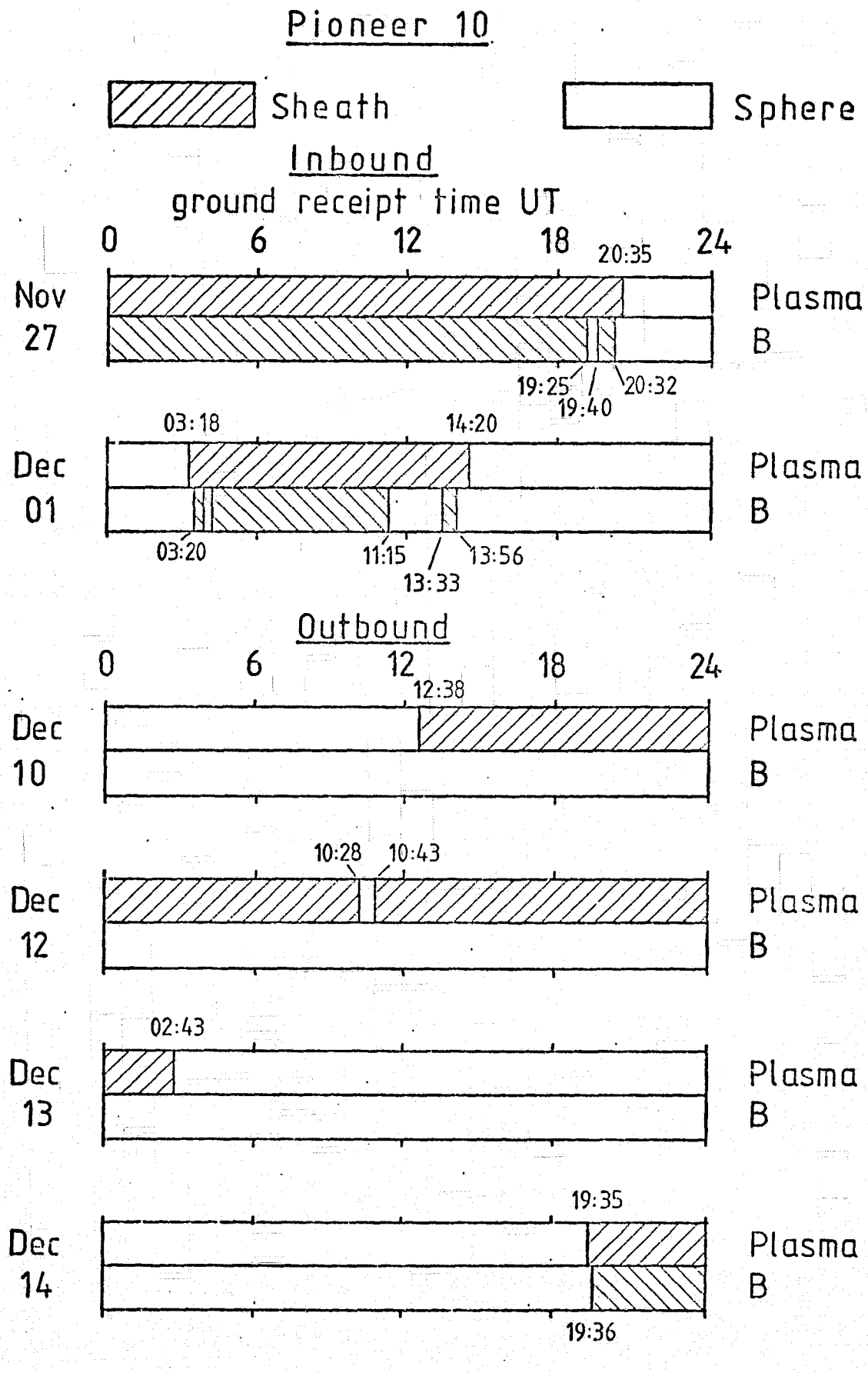
Pioneer 10
Sheath
Sphere
Inbound
ground receipt time UT
0
6
12
18
24
Nov 27
20:35
19:25
19:40
20:32
Plasma B
Dec 01
03:18
14:20
03:20
11:15
13:33
13:56
Plasma B
Outbound
Dec 10
12:38
Plasma B
Dec 12
10:28
10:43
Plasma B
Dec 13
02:43
Plasma B
Dec 14
19:35
19:36
Plasma B

Figure 1

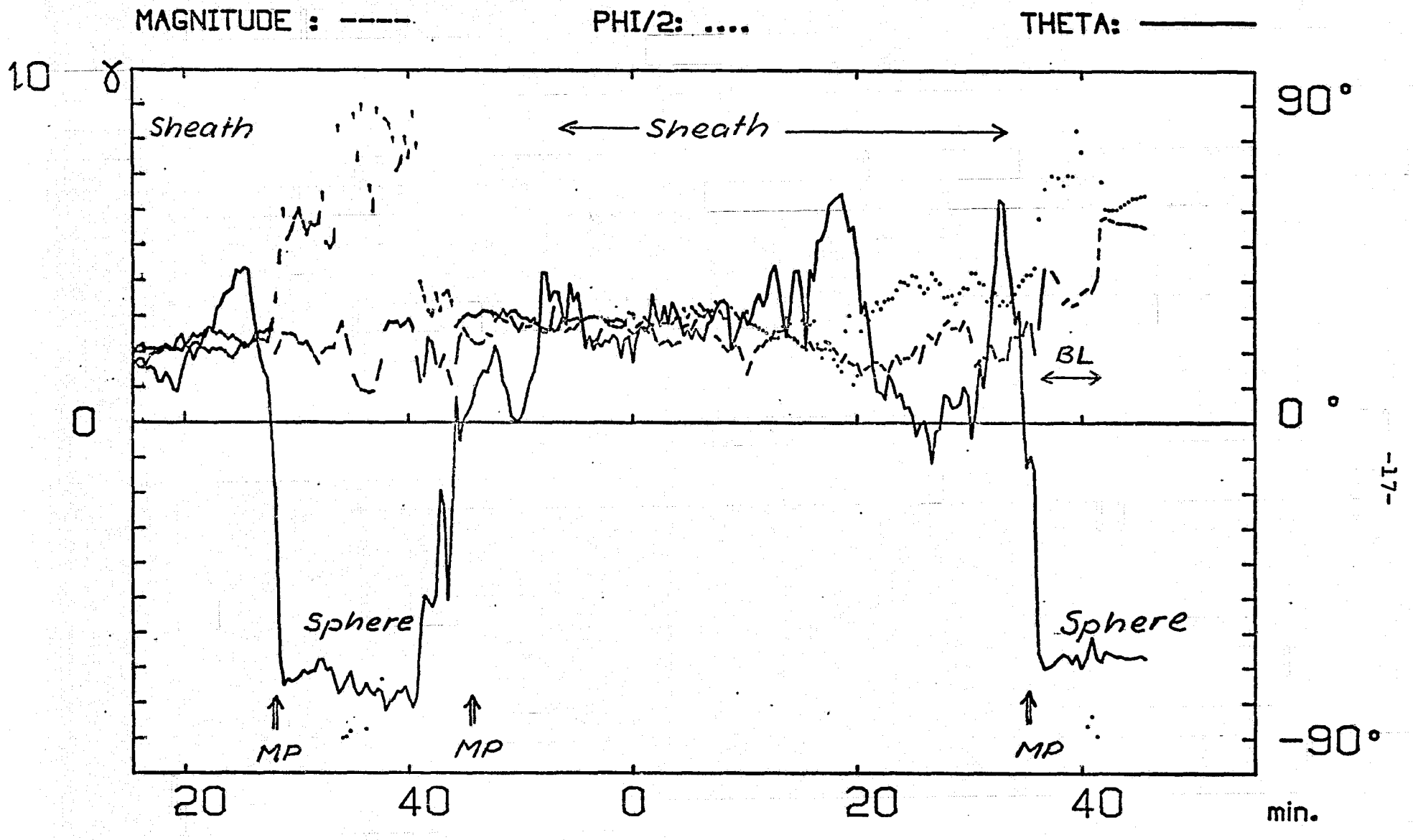

73 11 27 19:15:20.574 UT (69320574 - 74744844 MSECS) 2.7 SPS/56

Figure 2

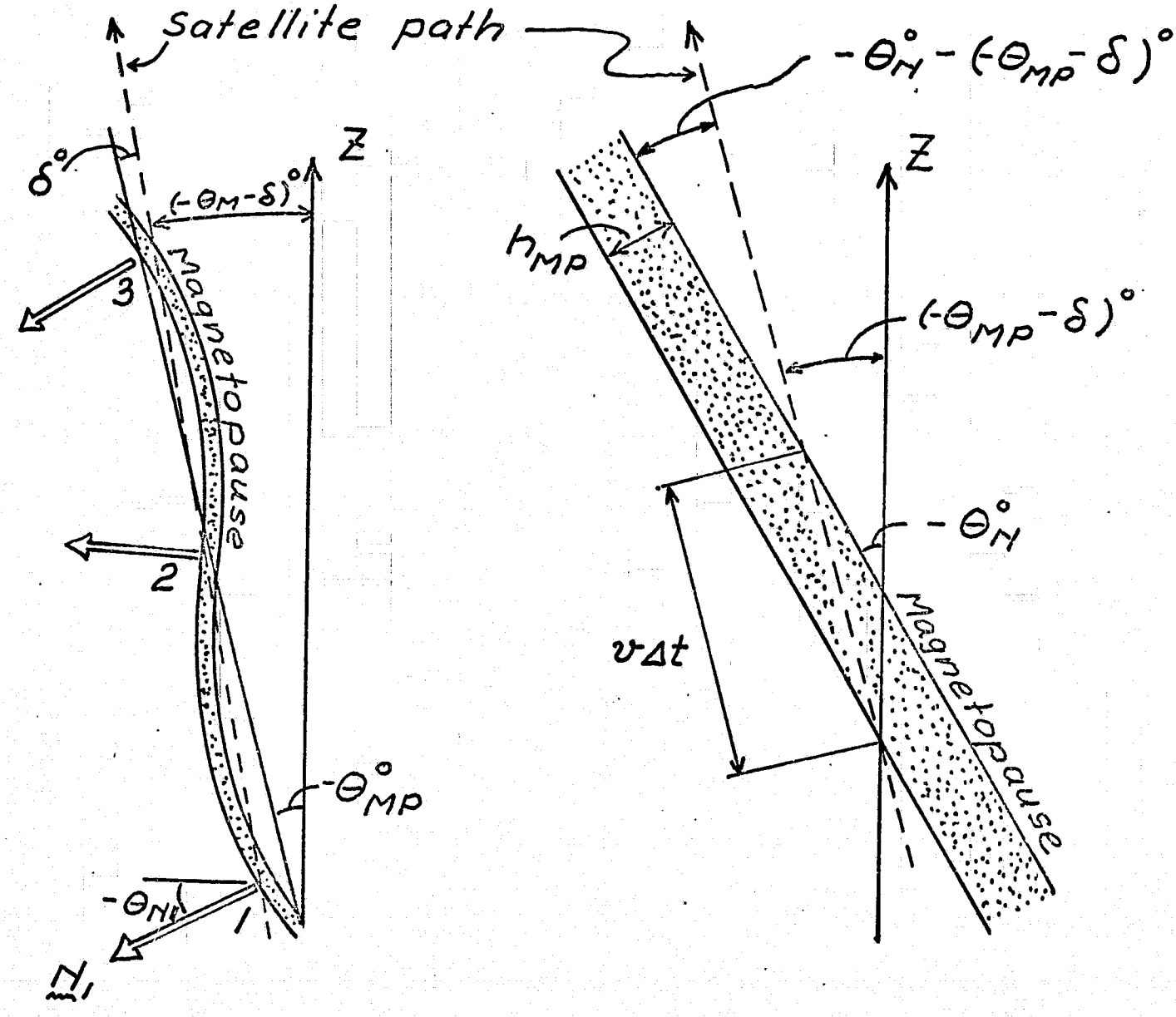
Satellite path
δ°
(-θM-δ)°
Z
3
Magnetopause
2
-θMP°
-θM1
M1
-θM° - (-θMP - δ)°
Z
hMP
(-θMP-δ)°
-θM°
vΔt
Magnetopause

Figure 3

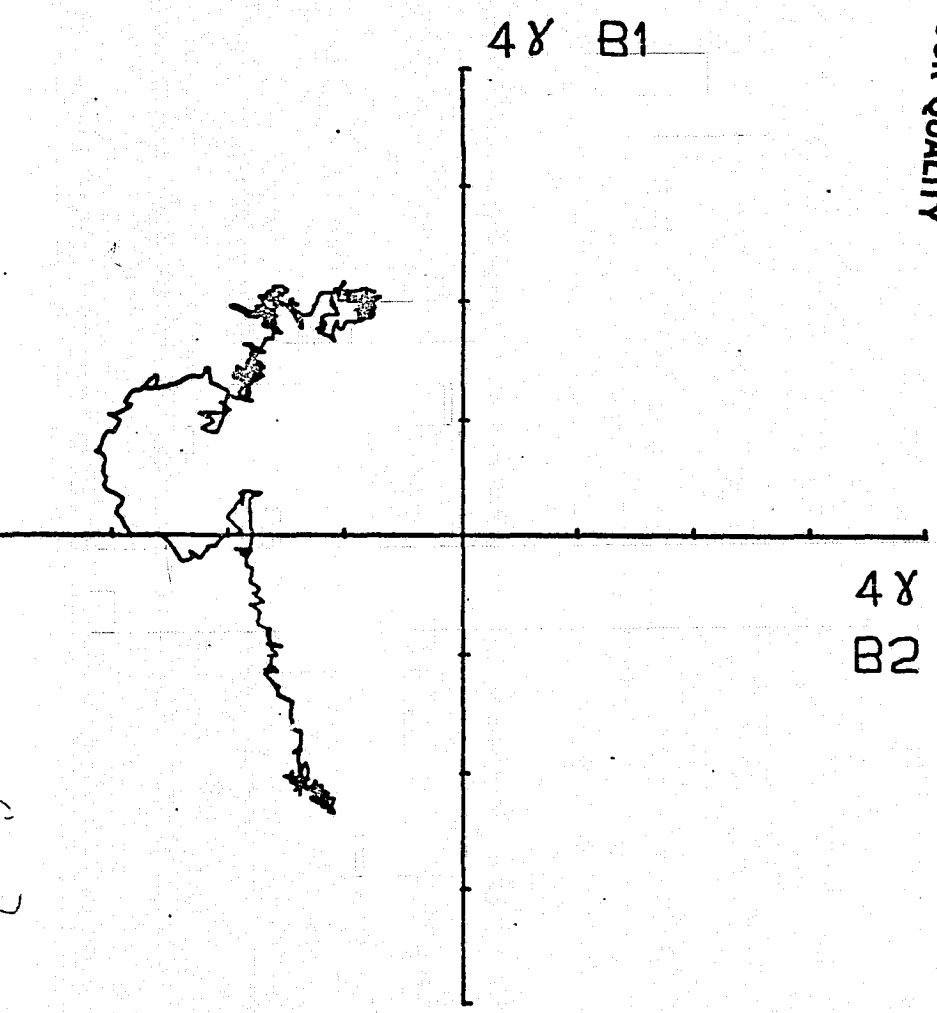

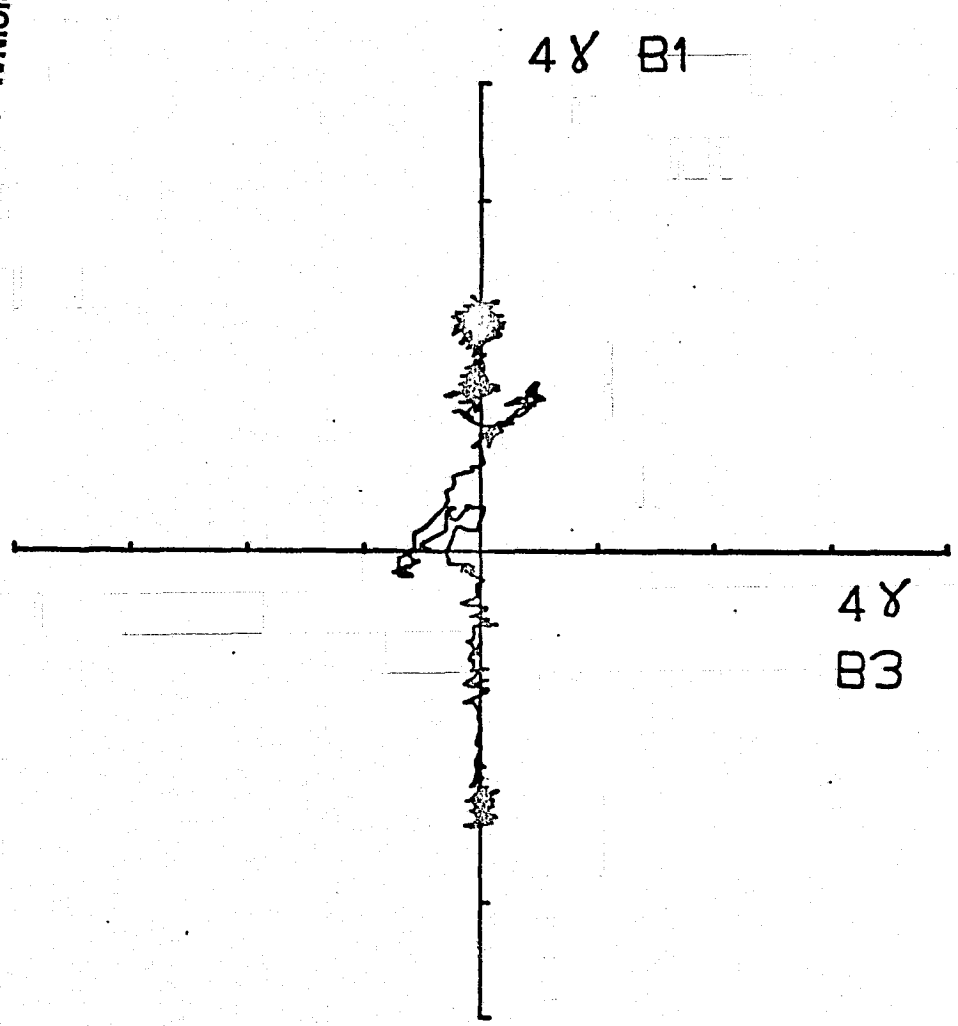

73 11 27 19:24:53.643 UT (69893643 - 70159548)

N1X N1Y N1Z : 0.3973 0.175 0.9009
N2X N2Y N2Z :-0.4755 -0.8003 0.3652
N3X N3Y N3Z : 0.7849 -0.5735 -0.2347

POINTS 0 - 710 2.7 SPS/ 1

Figure 4

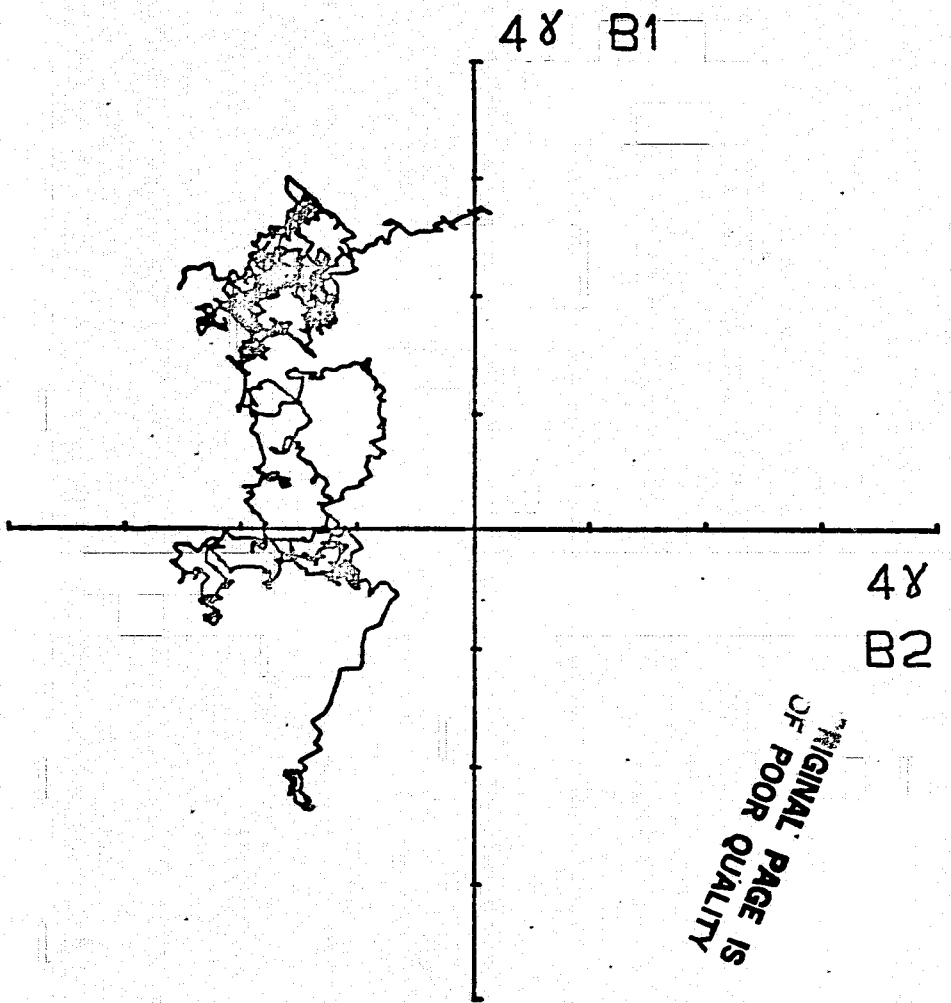

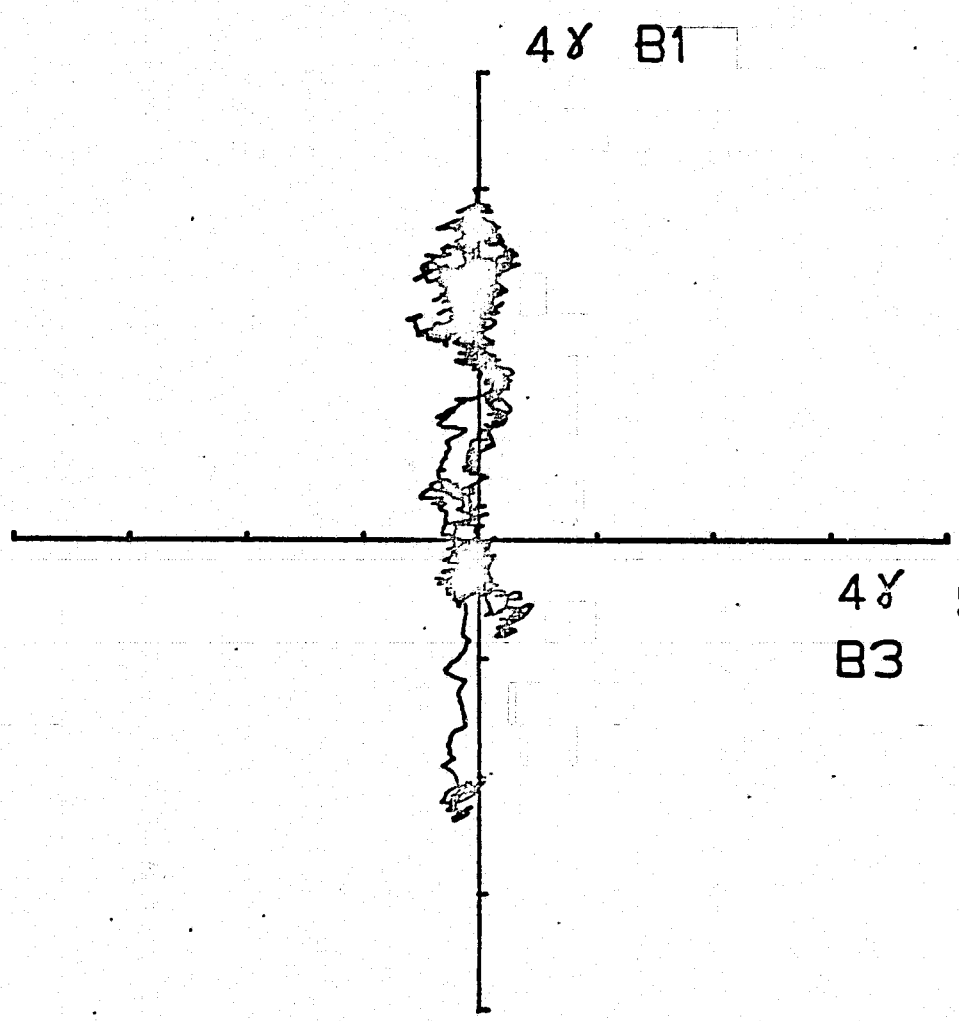

73 11 27 19:40:22.999 UT (70822999 - 71520957)

N1X N1Y N1Z : 0.4051 0.5275 0.7467
N2X N2Y N2Z :-0.3248 -0.6804 0.6563
N3X N3Y N3Z : 0.8546 -0.5087 -0.1043

POINTS 0 - 1860 2.7 SPS/ 1

Figure 5

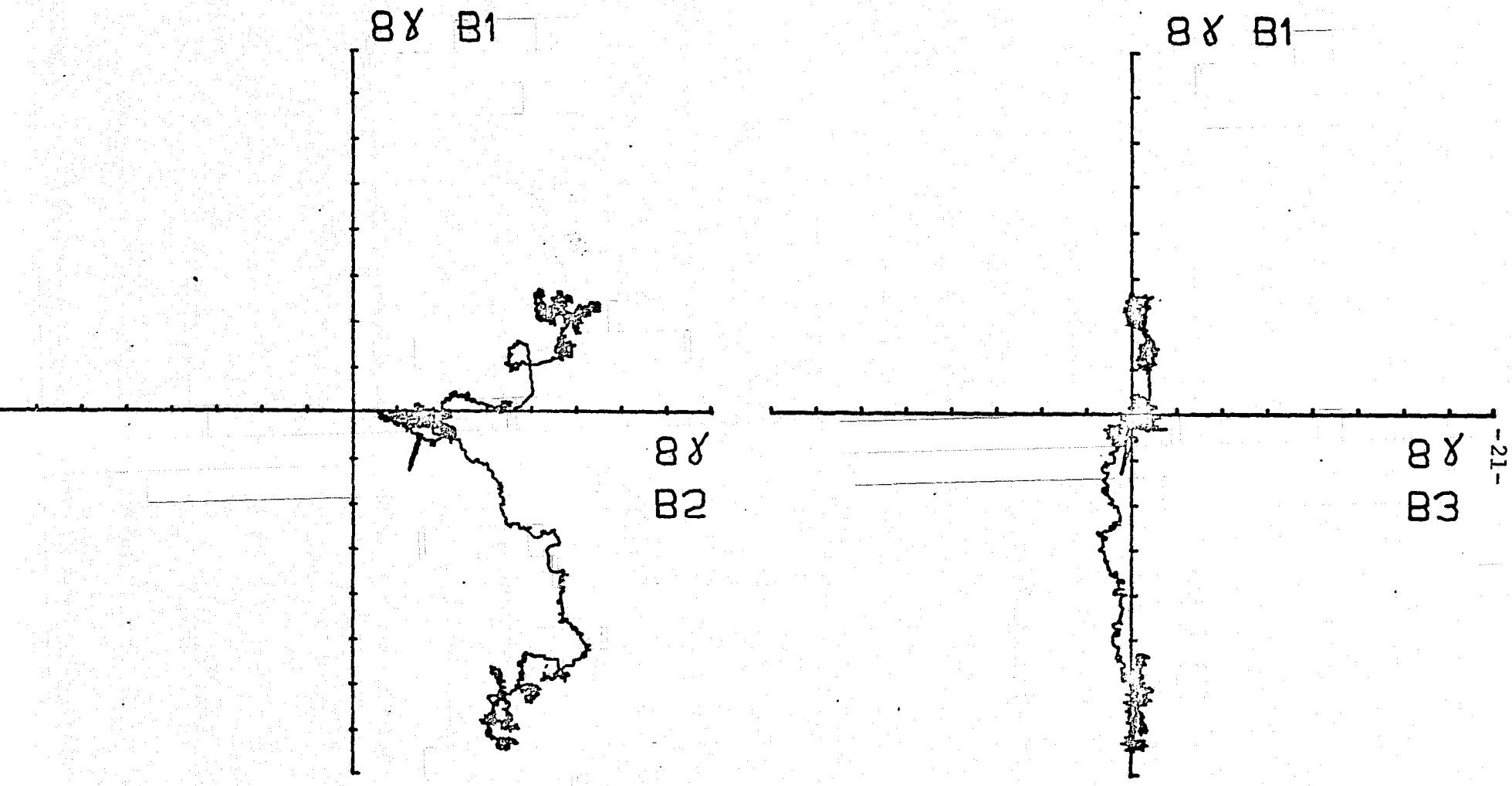

74 12 08 01:21:35.850 UT (5016046 - 5395190)

N1X N1Y N1Z :-0.2488 -0.0672 0.9662
N2X N2Y N2Z : 0.1437 -0.9891 -0.0317
N3X N3Y N3Z : 0.9578 0.1309 0.2558

POINTS 1283 - 5129 10.7 SPS/ 1

Figure 6

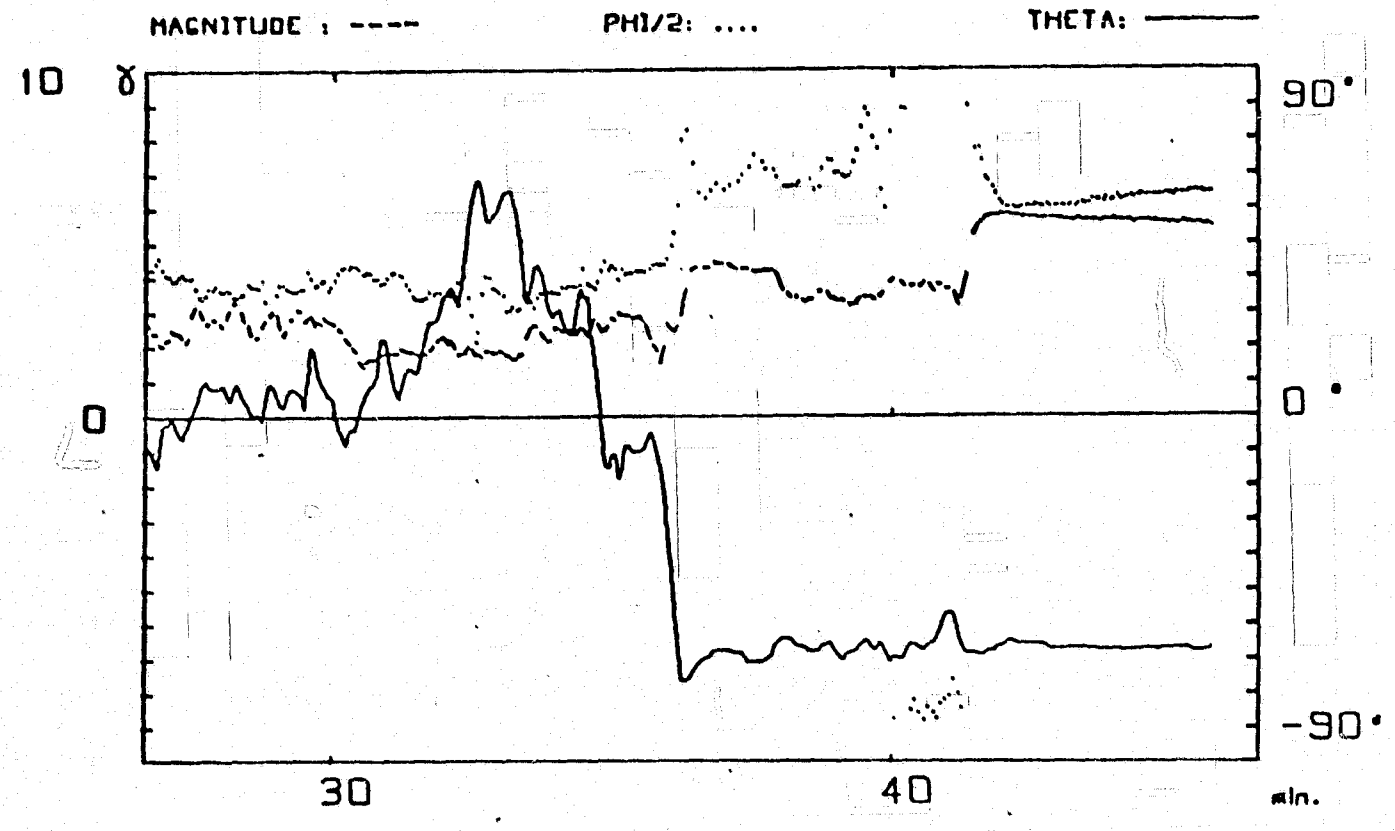

73 11 27 20:26:33.072 UT (73593072 - 74744833 MSECS) 2.7 SPS/10

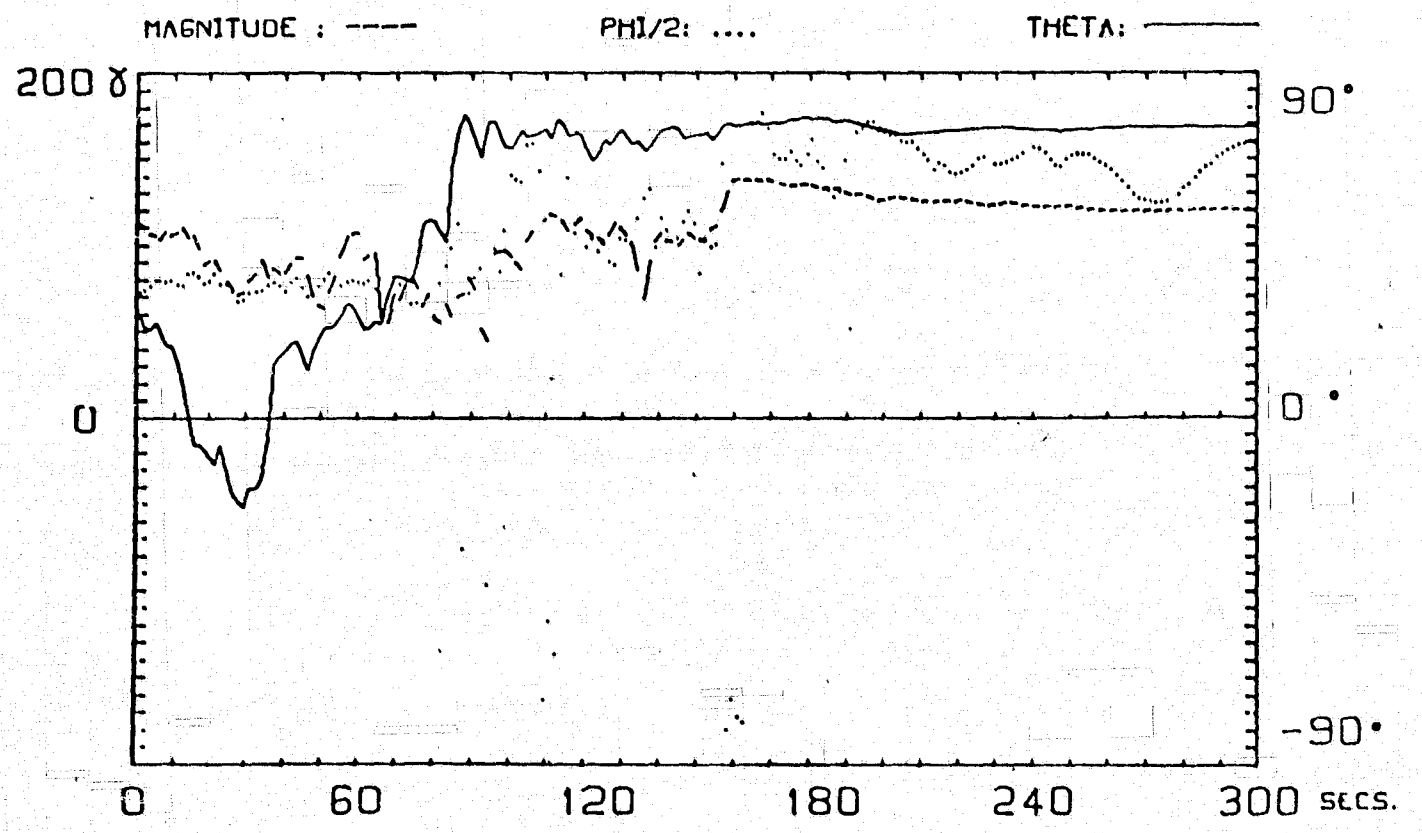

68 03 14 20:24:00:241 UT (73440241 - 73740047 MSECS) 7 SPS/10

Figure 7

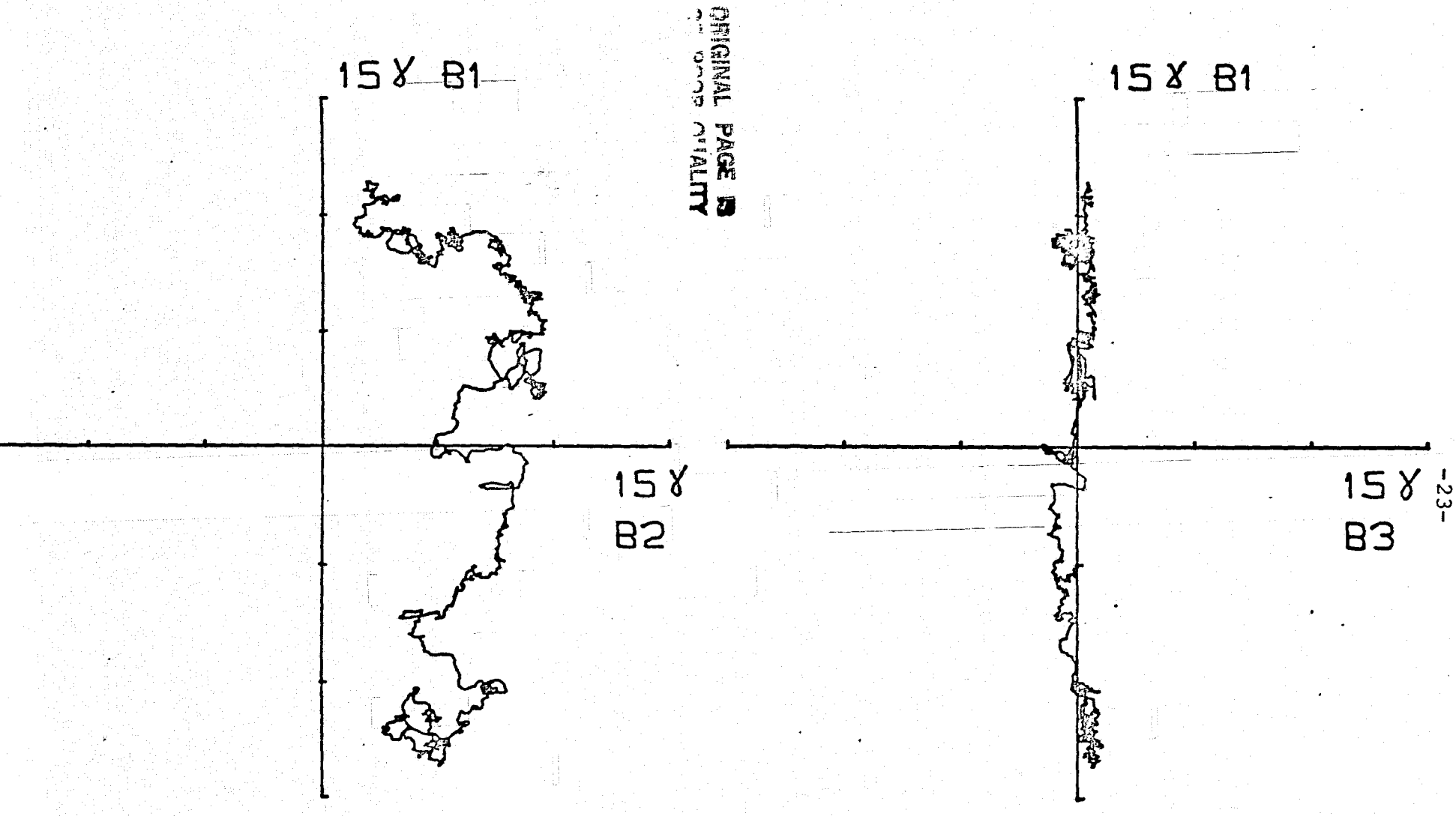

73 12 01 03:19:35.626 UT (12068638 - 12812349)

N1X N1Y N1Z :-0.023 -0.267 0.9634
N2X N2Y N2Z :-0.0733 -0.9606 -0.268
N3X N3Y N3Z : 0.997 -0.0768 0.0026

POINTS 249 - 2233 2.7 SPS/ 1

Figure 8

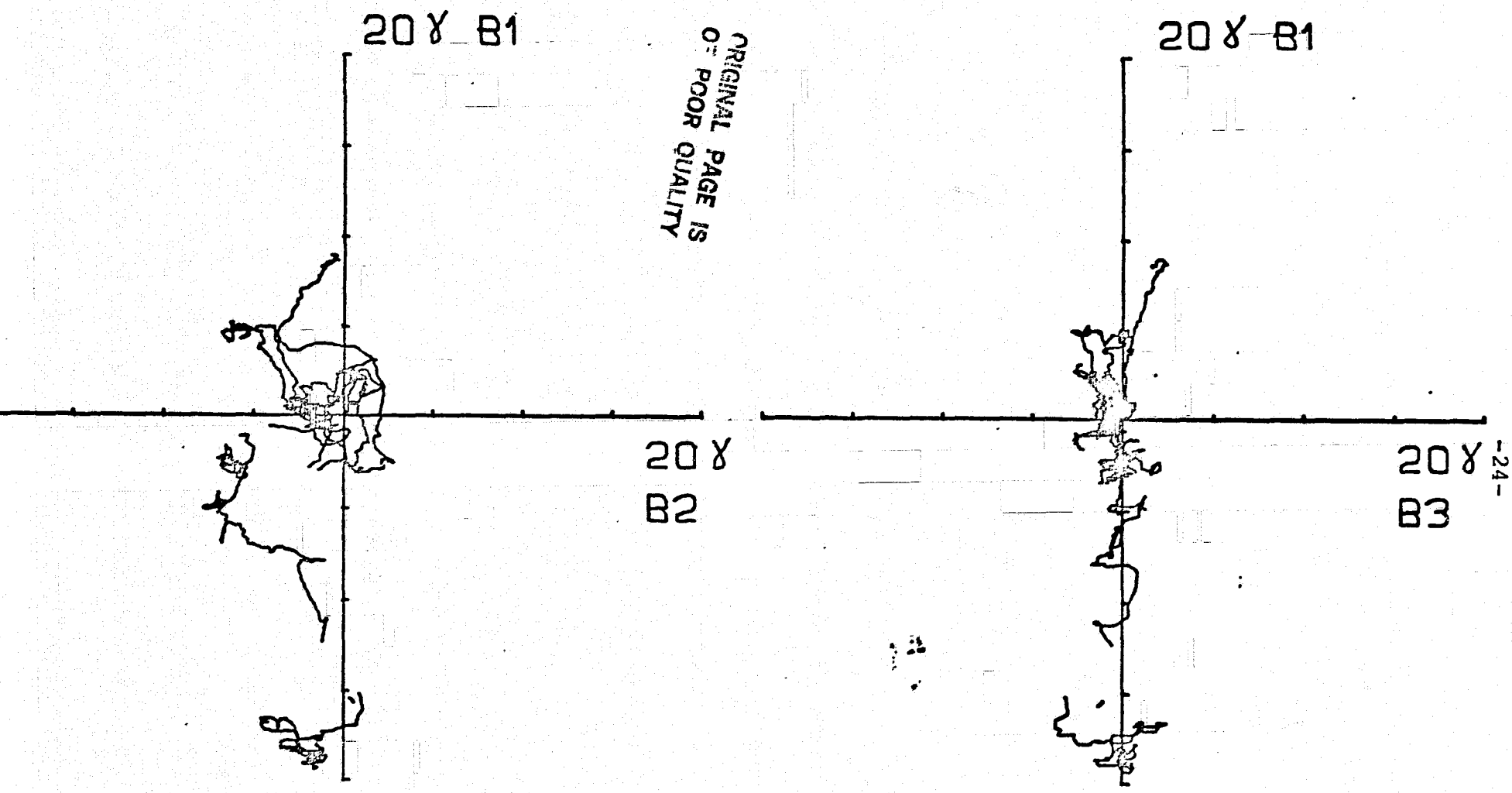

73 12 01 13:55:47.838 UT (50147838 - 50578762)

N1X N1Y N1Z : 0.0724 0.4647 0.8825
N2X N2Y N2Z :-0.3173 -0.8281 0.4621
N3X N3Y N3Z : 0.9455 -0.3135 0.0875

POINTS 0 - 1130 2.7 SPS/ 1

Figure 9

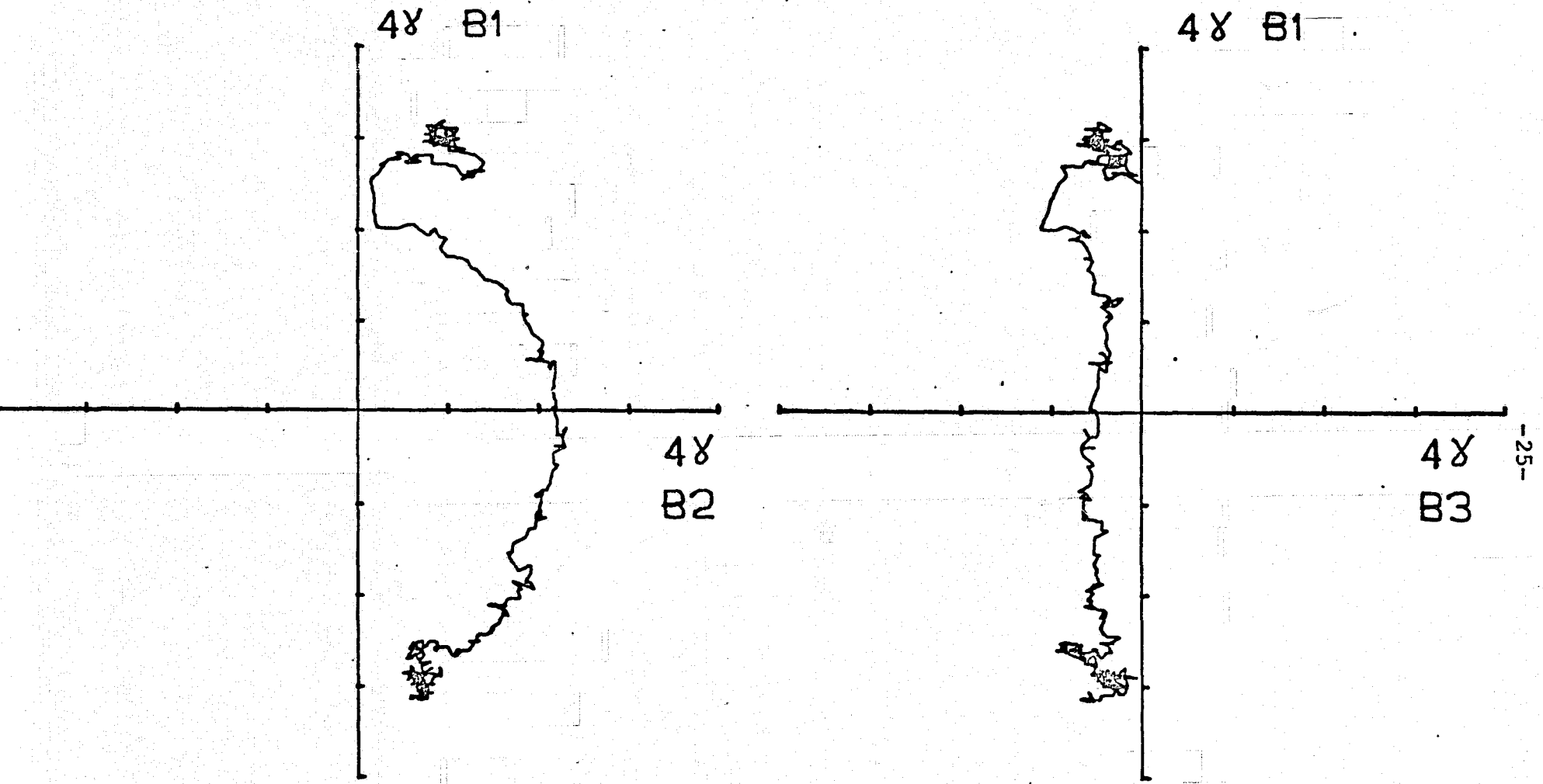

73 12 14 19:36:08.266 UT (70578767 - 70662585)

N1X N1Y N1Z :-0.0374 0.1561 0.987
N2X N2Y N2Z :-0.6007 -0.7929 0.1026
N3X N3Y N3Z : 0.7986 -0.5891 0.1234

POINTS 57 - 505 5.3 SPS/ 1

Figure 10

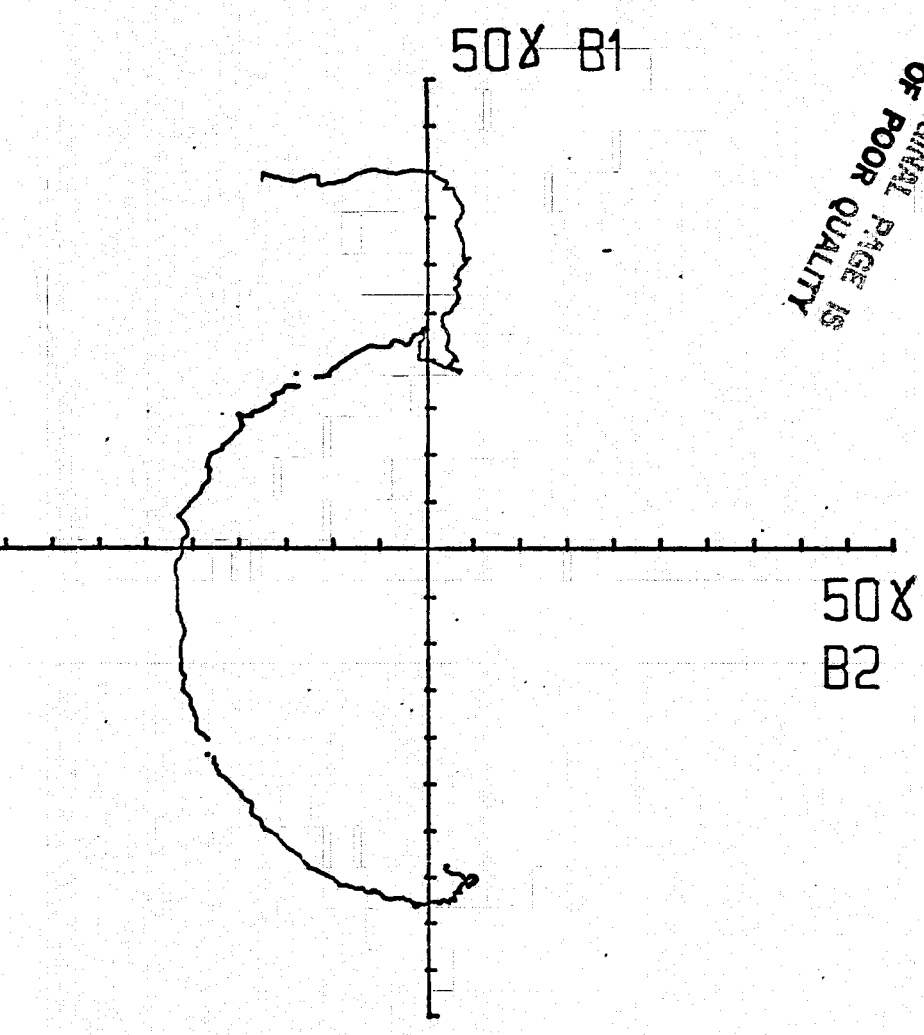

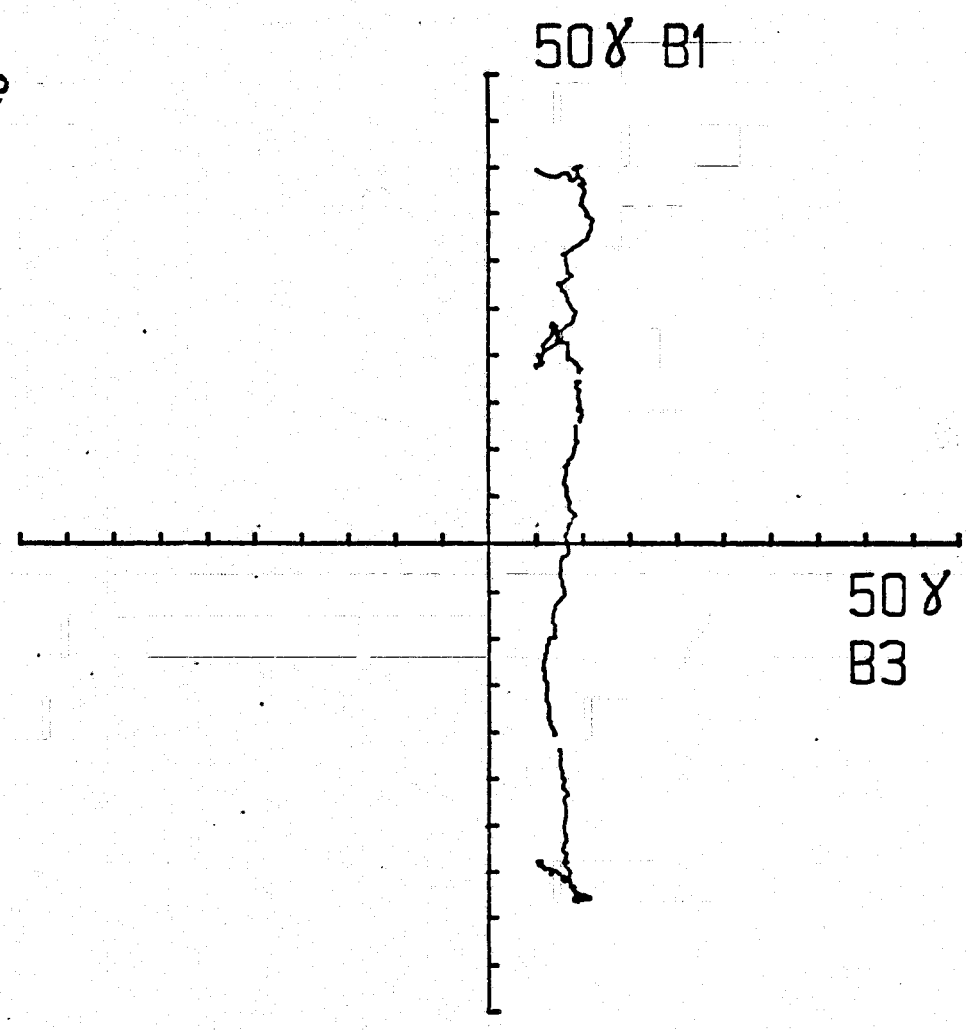

68 03 27 18:18:56:34 UT (65936034 - 65940444)

N1X N1Y N1Z :-0.3794 0.147 0.9135
N2X N2Y N2Z :-0.8467 -0.4532 -0.2787
N3X N3Y N3Z : 0.373 -0.8732 0.2964

POINTS 0 - 240 56 SPS/ 1

Figure 11

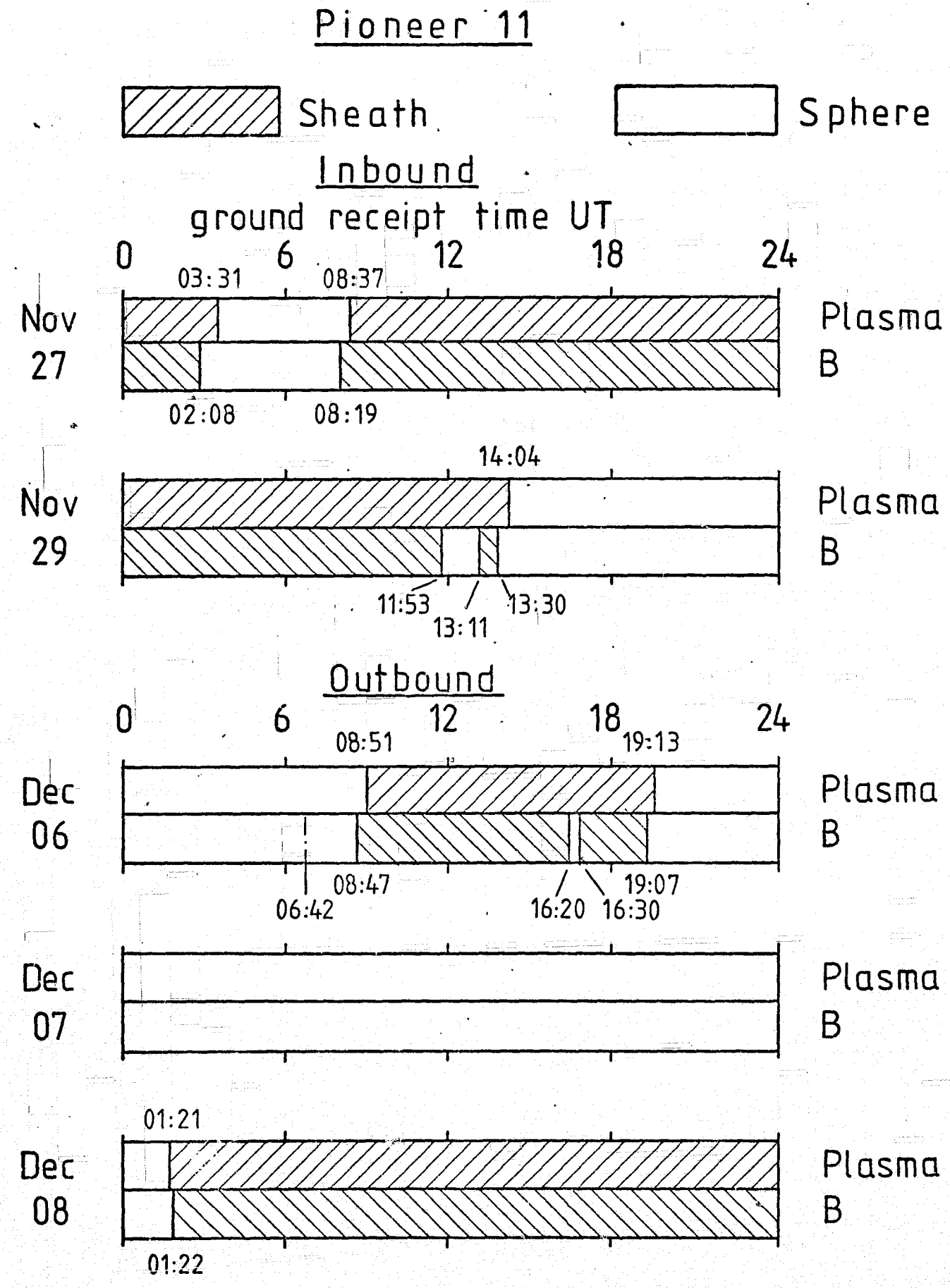
Pioneer 11
Sheath
Sphere
Inbound
ground receipt time UT
0
6
12
18
24
03:31
08:37
Nov 27
Plasma B
02:08
08:19
14:04
Nov 29
Plasma B
11:53
13:11
13:30
Outbound
0
6
12
18
24
08:51
19:13
Dec 06
Plasma B
06:42
08:47
16:20
16:30
19:07
Dec 07
Plasma B
01:21
Dec 08
Plasma B
01:22

Figure 12

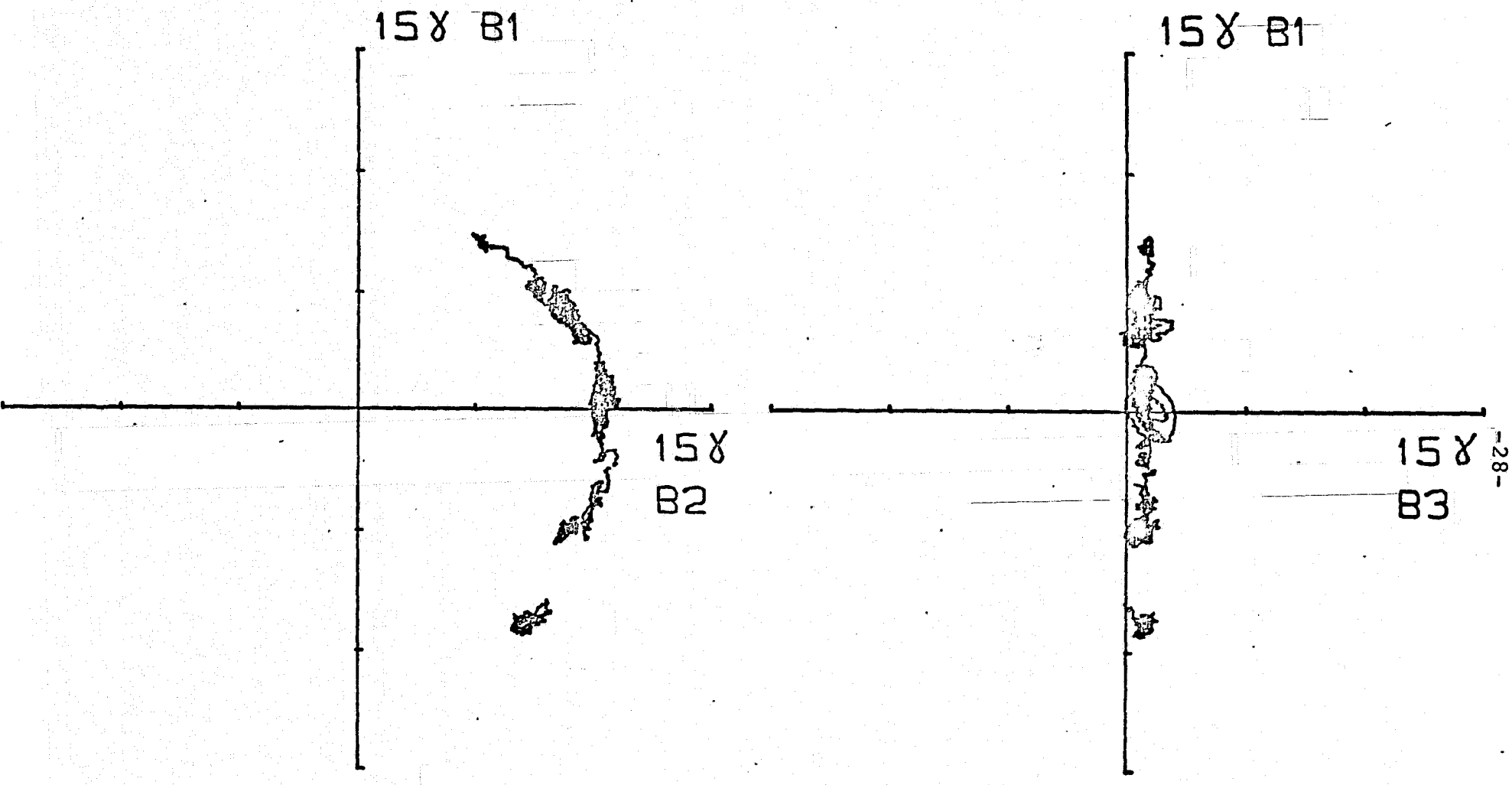

74 11 29 13:30:18.310 UT (48618310 - 49800088)

N1X N1Y N1Z :-0.0941 -0.6064 0.7896
N2X N2Y N2Z :-0.5213 -0.5457 -0.558
N3X N3Y N3Z : 0.8482 -0.4641 -0.2553

POINTS 0 - 4490 5.3 SPS/ 1

Figure 13

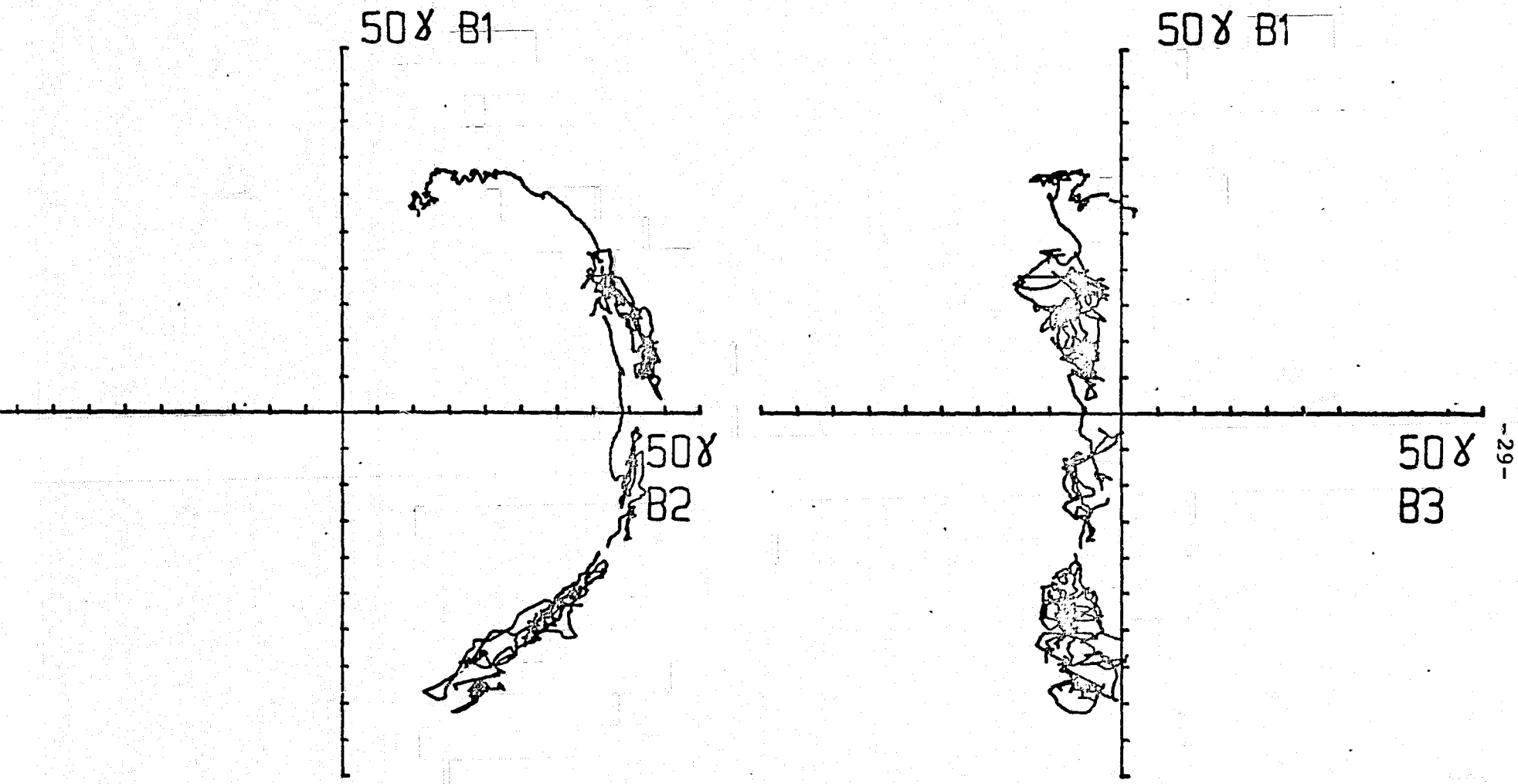

68 03 10 02:20:44:411 UT (8462123 -- 8603965)

N1X N1Y N1Z : 0.1987 0.6319 0.7491
N2X N2Y N2Z :-0.6137 -0.5157 0.5978
N3X N3Y N3Z : 0.7641 -0.5785 0.2854

POINTS 120 - 1072 7 SPS/ 1

Figure 14

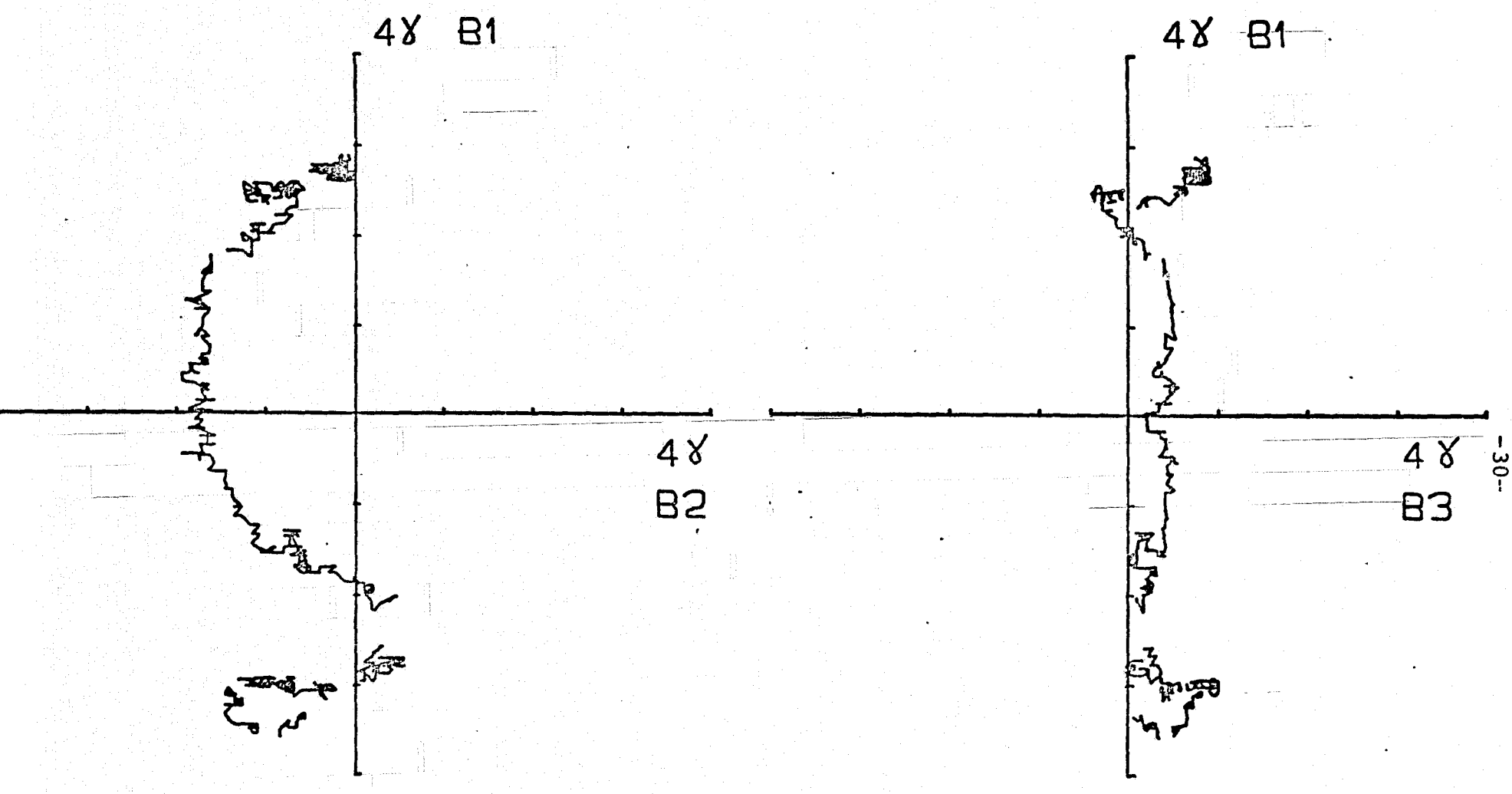

74 12 06 06:42:08.495 UT (24128495 - 24304943)

N1X N1Y N1Z : 0.0225 -0.095 0.9952
N2X N2Y N2Z :-0.9749 -0.2228 0.0007
N3X N3Y N3Z : 0.2216 -0.9702 -0.0976

POINTS 0 - 730 5.3 SPS/ 1

Figure 15

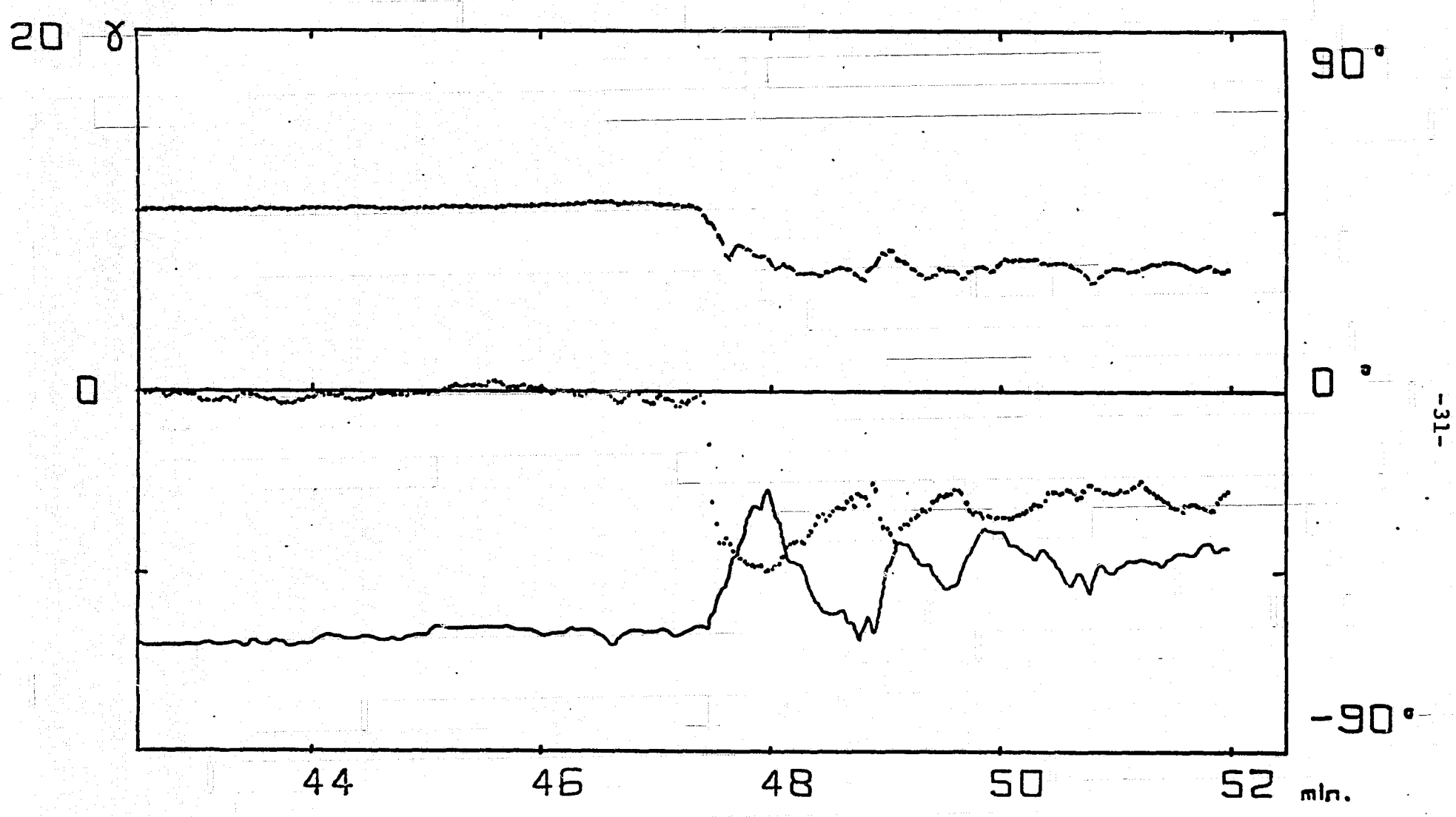

74 12 06 08:42:28.418 UT (31348418 - 31919580 MSECS) 5.3 SPS/10

Figure 16

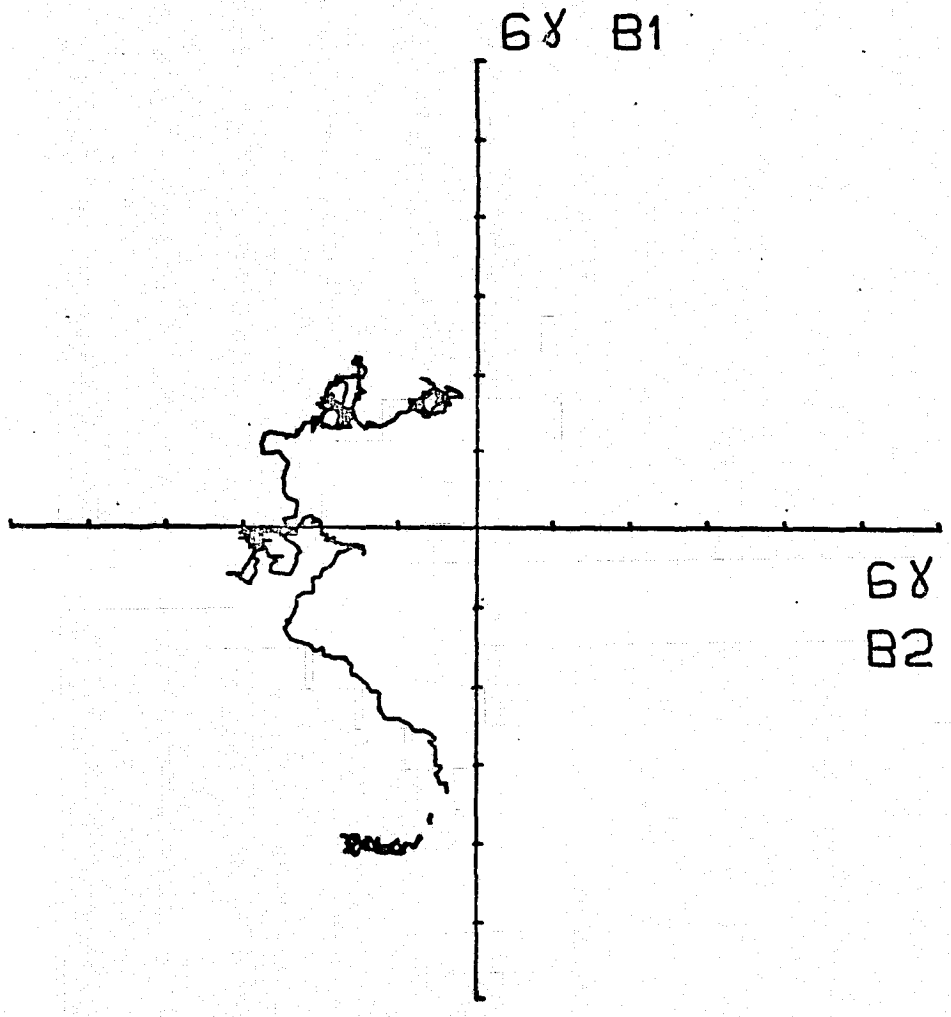

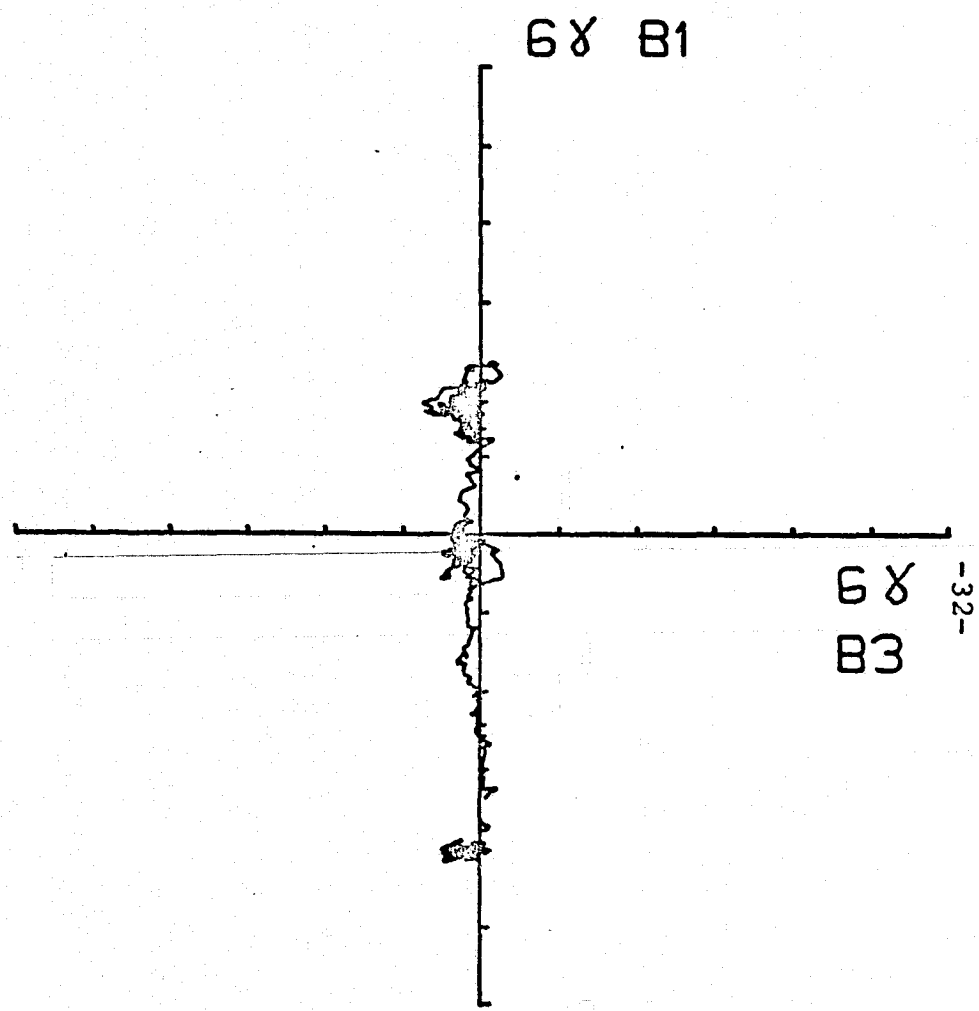

73 11 27 20:32:27.487 UT (73947487 - 74274526)

N1X N1Y N1Z : 0.274 0.0965 0.9569
N2X N2Y N2Z :-0.1907 -0.9697 0.1524
N3X N3Y N3Z : 0.9426 -0.2242 -0.2473

POINTS 0 - 760 2.7 SPS/ 1

Figure 17

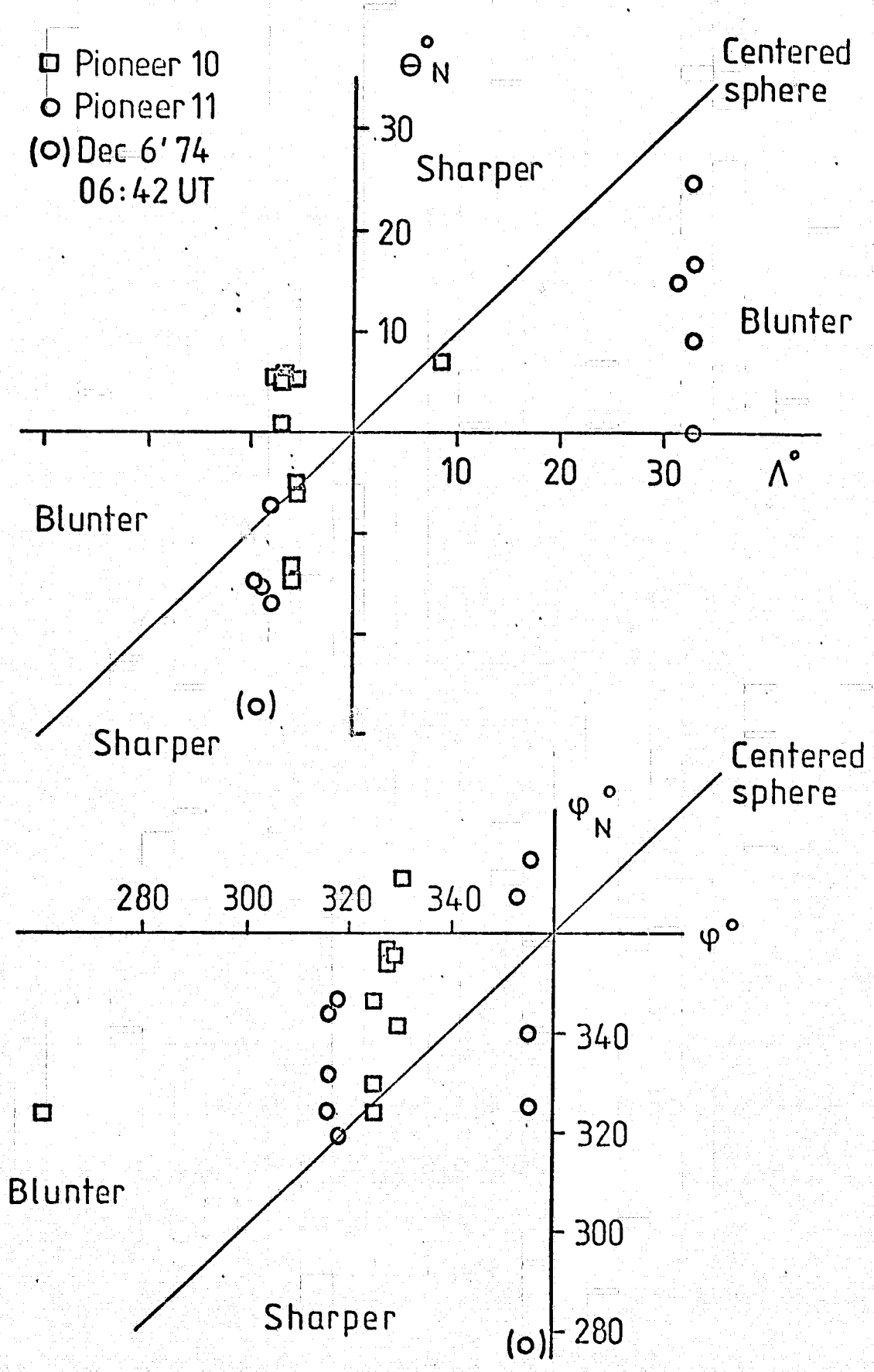
Pioneer 10
Pioneer 11
(o) Dec 6' 74
06:42 UT
Θ°N
Centered sphere
30
Sharper
20
10
Blunter
10
20
30
Λ°
Blunter
(o)
Sharper
Centered sphere
φ°N
280
300
320
340
φ°
340
320
300
280
Blunter
Sharper
(o)

Figure 18

TEARING MODES AT THE MAGNETOPAUSE

J. B. Greenly* and B. U. Ö. Sonnerup
Dartmouth College, Hanover, New Hampshire 03755

Abstract

This paper examines the possible occurrence of collisionless tearing modes in the dayside magnetopause. The expected magnetic signature of tearing is obtained from existing theory. Magnetometer data from one terrestrial magnetopause crossing, and one crossing of Jupiter's magnetopause are then examined in detail. Magnetic field oscillations are found in three subsegments of the terrestrial crossing at a frequency of 0.1-0.2 Hz and with peak amplitudes of 5-10 nanotesla (nt), and in one segment of the Jovian crossing at .05-.1 Hz and with 2 nt amplitude. The frequency range as well as the orientation of the magnetic field perturbation vectors agree with a model in which tearing-produced magnetic islands are convected past the satellite with the plasma flow in the current layer. In both cases the magnetopause structure was of the rotational discontinuity type with a nonvanishing normal magnetic field component . Hence, if the tearing structures were active, i.e., growing, at the observation site, ion tearing must be invoked. But it is also possible that the structures were passive, consisting of "debris" from active tearing elsewhere on the magnetopause surface, this debris being convected along the magnetopause past the observation site.

*Present address: Laboratory of Plasma Studies
Upson Hall
Ithaca, New York 14853

August, 1979

1. Introduction

The structure of the magnetopause current layer has been the subject of many investigations, both theoretical and observational (see, e.g. Willis, 1971, 1975, 1978; Sonnerup, 1976; Sonnerup and Ledley, 1979). The most obvious and striking characteristic of the magnetopause as observed during spacecraft crossings is its variability. Steady-state one-dimensional models may help explain certain average basic features of the current layer, although their success to date has been limited. But, in order to account for observations in detail, one must include temporal as well as two and three dimensional spatial variations.

It is our purpose here to examine the possibility that the collision-free tearing mode may be operative in the magnetopause as suggested by Galeev and Zeleny (1978). To do so we first describe some of the basic magnetic field signatures associated with tearing and then compare these signatures with substructures in the earth's magnetopause, observed by the Goddard Space Flight Center magnetometer onboard OGO-5, and in Jupiter's magnetopause, observed by the Jet Propulsion Laboratory vector helium magnetometer onboard Pioneer 11.

2. Tearing Mode Signatures

The basic unperturbed magnetic field geometry assumed in tearing mode analyses is of the form:

$$\underline{B} = \hat{\underline{e}}_x B_{ox} + \hat{\underline{e}}_y B_{oy} + \hat{\underline{e}}_z B_{oz} \tanh\left(\frac{x}{\ell}\right) \qquad (1)$$

Here ℓ is the characteristic width of the region of the magnetopause in which tearing occurs. It is referred to as the shear length. Also, $B_x = B_{ox}$ is the constant magnetic field component perpendicular

to the magnetopause, $B_y = B_{oy}$ a constant field component in the plane of the magnetopause and parallel to the current. Finally, B_z is the reversing field component which takes on the values $\pm B_{oz}$ when $|x| >> \ell$.

The tearing mode perturbation of the above field has a vector potential of the form

$$\underline{\tilde{A}} = \underline{\hat{e}}_y \, \tilde{A}(x) e^{\gamma t + ikz} \tag{2}$$

where γ and k are the growth rate and wave number, respectively, and $\tilde{A}(x)$ is an unknown function of x, the coordinate perpendicular to the layer, to be determined along with the growth rate from the Vlasov-Maxwell equations. When such a field is superposed upon the unperturbed field, the resulting field line configuration is as shown in Figure 1. The behavior of $\tilde{A}(x)$ is qualitatively as shown in the figure. Note that, apart from the phase factor, $\tilde{B}_x \sim k\tilde{A}(x)$ while $\tilde{B}_z \sim d\tilde{A}/dx$.

Detailed expressions for $\tilde{A}(x)$ and for the growth rate γ have been derived under a variety of assumptions, none of which are entirely applicable to the present situation. However, the following two results are of interest:

(i) In a collision-free plasma with B_{ox}, the unperturbed magnetic field component perpendicular to the current layer, equal to zero, Galeev and Zeleny (1978) found a linear growth rate

$$\gamma = \frac{k \, v_{th_e}}{\sqrt{\pi}} \left(\frac{B_{oz}}{B_{oy}}\right)\left(\frac{\lambda_e}{\ell}\right)^2 (1 - k^2 \ell^2) \tag{3}$$

In this formula v_{th_e} is the electron thermal velocity and $\lambda_e \equiv (m_e/\mu_o n e^2)^{\frac{1}{2}}$ is the electron inertial length (m_e being the electron mass and n the particle density). This formula describes a purely growing mode,

dominated by the electron dynamics in a region of width comparable to λ_e around $x = 0$, and therefore referred to as electron tearing. In arriving at Equation (3) the assumption $B_{oy}/B_{oz} >> (R_{Li}/\ell)^{\frac{1}{2}}$ was made, where R_{Li} is the ion gyroradius in the field B_{oz}. This assumption is at best marginally satisfied at the magnetopause where, in usual circumstances, B_{oy} is comparable to B_{oz} and ℓ to R_{Li}. Even more seriously, the normal magnetic field component B_{ox} at the magnetopause is often sufficiently large so as to suppress the electron tearing mode.

When γ is evaluated from (3) at the earth's magnetopause, where $B_{oz} = B_{oy}$, $n = 10\ cm^{-3}$, $kT_e = 25eV$, and $\ell = 50$ km, one obtains a maximum growth rate $\gamma_{max} = 1/50\ sec^{-1}$ for a wave length $\lambda = 2\pi/k = 4\pi\ell = 600$ km.

(ii) In a collision-free plasma with $B_{ox} \neq 0$ but $B_{oy} = 0$ Galeev (1978) finds

$$\gamma = \frac{v_{th_i}}{\sqrt{\pi}\ell} \left(\frac{R_{Li}}{\ell}\right)^{3/2} \left(1 + \frac{T_e}{T_i}\right)(1 - k^2\ell^2) \qquad (4)$$

In this mode, referred to as ion tearing, the ions provide the essential dynamics and it is required that $B_{ox}/B_{oz} < \gamma\, m_i/eB_{oz}$. (A lower limit on B_{ox}/B_{oz} also exists; see Galeev (1978).) The assumption $B_{oy} = 0$ is usually not satisfied at the magnetopause.

In a proton electron plasma at the earth's magnetopause with $kT_i = 170$ eV, $B_{oz} = 35$ nt, $T_e/T_i = 0.15$, $\ell = 50$ km, and $k = 1/2\ell$ one finds from (4): $\gamma = 1\ sec^{-1}$, and $B_{ox}/B_{oz} < \gamma m_i/eB_{oz} = 0.28$.

Neither of the two cases discussed above is strictly applicable to the magnetopause situation. For example, the influence of velocity

shear in the magnetopause is not included in either case. Additionally, for magnetopause crossings with a nonvanishing normal field component, plasma flow across the magnetopause is likely to occur, and it is not known how such an effect influences the ion tearing. Killeen and Shestakov (1978) have shown, in the high-conductivity limit of resistive MHD tearing theory, that nonsymmetric modes may be strongly destabilized by diffusive flow across the current layer. Their analysis, however, is again not directly applicable to the magnetopause. Furthermore, in most observed magnetopause structures B_y is not zero and does not remain constant throughout the layer. Thus, the results given above must be considered as illustrative rather than as quantitatively applicable. They nevertheless suggest that the following statements are likely to be relevant to magnetopause tearing:

(a) Ion as well as electron tearing leads to the formation of magnetic islands which do not propagate relative to the plasma. The fastest growth occurs at a wavelength of the order of $4\pi\ell$ where ℓ is comparable to the width of the current layer (compare Eq. (1)).

(b) At least for thin current layers, the growth rates may be sufficient to permit the tearing modes to yield finite magnetic perturbations before the island structures are swept away from the front side magnetopause by the solar wind. For the terrestrial magnetosphere, the time scale for the latter process is of the order of 5-10 minutes. However, the growth rate decreases rapidly with increasing layer thickness, so that active tearing may not be seen

in thick magnetopause structures. At any rate, tearing should be more easily observable away from the sub-solar point than near it.

The results of nonlinear tearing analysis are limited at present, but several investigators have found, by analytical means or by numerical simulation (Dickman et al, 1969; Biskamp et al, 1970; Rutherford, 1973; Schindler, 1974; Drake and Lee, 1977; White et al, 1977; Galeev and Zeleny, 1977), that single modes can grow to large amplitudes. One recent analysis (Galeev et al, 1978) even indicates explosive growth in the nonlinear stage of ion tearing. On the other hand, Pellat (1978) has argued that collision-free ion tearing is not possible except in very special circumstances. However, resistive tearing in a current sheet with a finite normal magnetic field remains possible, the resistivity being provided by for example the lower hybrid drift instability (Huba et al, 1977). On the whole, there appears to be no strong theoretical reason to doubt that magnetopause tearing modes may occur and may grow to amplitudes of at least several nanotesla. A quantitative description of such large amplitude tearing structures in the magnetopause field is not yet available, a fact that limits the possibilities for detailed comparison between theory and observed signatures (see point (e) below).

(c) The convection of magnetic tearing structures along the magnetopause can make the tearing mode observable from a single satellite crossing the magnetopause. If the convection speed is denoted by v_c, a Doppler shifted frequency of $f = (v_c k/2\pi)\cos\theta$ is obtained.

Here θ is the angle between the convection velocity vector and the z axis (the direction of the "propagation" vector $\underline{k}$). For $v_c \approx 200$ km/s (e.g., Aubry et al, 1971) and with $k = 1/2\ell = 10^{-2}m^{-1}$ (corresponding to the most rapidly growing wavelength) we find $f = (0.3 \cos\theta)$ Hz for $\ell = 50$ km. Because of the short wavelength cutoff at $k = 1/\ell$ (see (3) and (4)), frequencies above 0.6 Hz should not occur.

The angle θ also requires comment. If $\theta = \pi/2$ no Doppler shift occurs and the tearing mode remains unobservable from a single satellite. For example, if the convection velocity vector is taken to point approximately away from the subsolar point, $\theta = \pi/2$ occurs in the equatorial plane of the magnetosphere when the magnetosheath field is antiparallel to the earth's field.

The velocity of a satellite relative to the magnetopause may vary greatly because of radial motion of the magnetopause itself. At the terrestrial magnetopause, relative velocities of the order of $v = 5 - 10$ km/sec (normal to the magnetopause) are typical. Thus, with a convection speed of 200 km/s, the motion of the satellite relative to the tearing structure in Figure 1 is at a rather skew angle as indicated in the figure. During a crossing a satellite would be expected to transverse $N = (v_c \cos\theta / v)(\ell k/2\pi)$ wavelengths. For $v_c/v = 40$, $\theta = 0$, and $k = 1/2\ell$ we find $N = 3$. The conclusion is that under favorable circumstances, i.e., when v_c/v is large and θ is sufficiently small, tearing should be observable in the magnetic field records taken during magnetopause crossings.

(d) All tearing theories to date are such that they leave the B_y component entirely unperturbed. In other words, the magnetic field perturbations are confined to the xz plane. This characteristic signature should be helpful in identifying tearing oscillations during magnetopause crossings. It is perhaps somewhat surprising that B_y should remain constant in the tearing mode. Such a result requires the macroscopic ion and electron motions in the xz plane to be identical so that no Hall current loops develop in that plane. A more refined analysis is likely to reveal the presence of such loops and associated small variations in B_y.

(e) For a single mode, the tearing perturbations in B_x and B_z are out of phase by $\pi/2$. Furthermore the amplitude ratio is

$$\frac{|\tilde{B}_x|}{|\tilde{B}_z|} = \frac{|k\tilde{A}|}{|d\tilde{A}/dx|} \simeq \frac{|k\tilde{A}|}{|\tilde{A}/\ell|} = k\ell. \qquad (5)$$

Since $k\ell < 1$ always, the B_z oscillation should have larger amplitude than the B_x oscillation. However, as shown in Figure 1, $\tilde{B}_z$ vanishes at $x = 0$ and at $x = \pm d$. An observer at fixed x position, watching the tearing structure convected in the z direction, would see various polarizations of the $\tilde{B}_x$, $\tilde{B}_z$ field oscillations, as shown in the figure. For $|x| > d$, the polarization is elliptical with $|B_z| > |B_x|$, but for $|x| \leq d$, a complicated polarization dependence on x occurs. The scale length d is independent of mode amplitude and depends on k for small amplitude (linear) modes, and $d \to 0$ as $k\ell \to 1$. The size of d for large amplitude modes at the magnetopause is not known, but should be of the order of the island width, as shown in the figure. In principle, it appears possible, then, that the complex polarization

changes for $|x| \leq d$ could be observed. In practice the situation may be more complicated for two reasons. First, the x value of the satellite changes as it crosses the magnetopause, leading to a relatively rapid transition from one polarization pattern to another. Second, more than one wavelength is likely to be present. Thus one would not expect to easily observe the polarization ellipses discussed above. However, since these ellipses have their major axis along the z direction except in a layer, probably narrow compared to ℓ, around $x = 0$, one would expect the perturbations to have $|\tilde{B}_z| > |\tilde{B}_x|$ except in that layer.

The phase (polarization) relation between $\tilde{B}_x$ and $\tilde{B}_z$ is antisymmetric about $x = 0$. A spacecraft traversing the $x = 0$ plane of a single tearing mode must observe elliptical polarization of opposite sense at equal distances on either side of $x = 0$. This antisymmetry would be strong evidence of having passed through $x = 0$ even if the complex behavior for $|x| \leq d$ is not seen. Conversely, if at the beginning and end of an observation of oscillations in $\tilde{B}_x$ and $\tilde{B}_z$ the sense of the polarization is not reversed, then the observer has not passed through $x = 0$. The polarization antisymmetry is not unique to tearing modes, but is a necessary property of any perturbation with the same symmetry as the unperturbed magnetopause field of Eq. (1), that is, symmetry under 180° rotation about the y axis. We thus have a criterion for traversal of the $\underline{k} \cdot \underline{B} = 0$ ($x = 0$) plane that is independent of the assumed mode type. Unless this overall polarization antisymmetry is observed, one should not expect to see any of the detailed structure near $x = 0$.

(f) In actual observed magnetopause crossings, a constant or nearly constant value of B_y (corresponding to a magnetopause current that is directed entirely along the y axis) is seldom observed. Rather the B_y value may change in a systematic manner as the satellite passes through the magnetopause. For example, in a rotational form the quantity $(B_y^2 + B_z^2)$ remains approximately constant (see e.g., Sonnerup and Ledley, 1974). In order to apply existing tearing mode analyses and much of the previous discussion to such crossings it is necessary to examine subsegments of a crossing, selected such that one magnetic field component tangential to the magnetopause remains nearly constant during the subsegment. A local Cartesian coordinate system is then constructed with the y axis along the constant field, with the x axis remaining perpendicular to the magnetopause surface, and with the z axis completing the right-handed orthogonal triad. It is in this local system that Figure 1 is to be applied. The angle θ under point (c) above is then the angle between the local convection velocity (which may differ from the magnetosheath flow velocity) and the local z axis. Note also that the characteristic width ℓ is associated with the subsegment rather than with the entire magnetopause.

As is evident from the previous discussion, it is important for the observational study of magnetopause tearing to have precise information about the direction (x) normal to the magnetopause. Such information is obtained from minimum variance analysis of the magnetopause magnetic field vector data set (Sonnerup and Cahill, 1967). It is known that, because of degeneracy of the variance ellipsoid, this method fails to give an accurate determination of the normal direction when the current in the magnetopause is unidirectional as it is in the model in Figure 1. Indeed, if minimum-variance analysis

were applied to a crossing in which the structure is exactly as in Figure 1, the normal (i.e., the minimum variance) direction would be selected along the y axis rather than the x axis. Thus, it is desirable to examine actual magnetopause crossings in which the current is not unidirectional. Rotational forms would appear ideal for this purpose.

(g) It would of course be of interest to examine not only the magnetic signature of magnetopause tearing but the particle signature as well. However, we have found that existing collisionless tearing theory has for the most part not reached a stage of development where reliable or reasonably reliable predictions may be made concerning the spectra of energized electrons and ions. For example, while simple tearing analysis leads to a purely growing mode, more detailed studies are likely to yield overstability instead (e.g., Drake and Lee, 1977). Such a change may influence the particle acceleration in a profound way. Thus, the observed layer of energetic electrons at the magnetopause (Meng and Anderson, 1970; Baker and Stone, 1977) may possibly provide important information concerning tearing, but at present we have no way of taking advantage of the information.

3. OGO-5 Crossing on March 10, 1968 at 02:20 UT

In order to illustrate the ideas discussed in the previous section, we now examine in detail one OGO-5 crossing of the earth's magnetopause where we think tearing mode signatures may have been present. Its gross magnetic structure is that of a rotational form so that a good determination of the normal direction is obtained in spite of the fluctuation in the normal field component, presumably

associated with the tearing. The crossing also occurred at a substantial distance from the subsolar point: the solar magnetospheric latitude and longitude were 23.5°N and 74.4°W, respectively. This crossing has been studied previously by Sonnerup and Ledley (1974). Information about the results of the minimum variance analysis may be found in their paper.

A polar (hodogram) representation of the magnetic field during the crossing is shown in Figure 2. In this figure the axes labeled B1, B2, and B3 are aligned with the directions of maximum, intermediate, and minimum variance, respectively. The latter (B3) represents the direction normal to the magnetopause. Thus, the field component B3 is identical with B_x. The right-hand hodogram indicates that an average magnetic field component $B3 = B_x = -8nt$ is present, with a large amount of superimposed noise. The two field components B1 and B2 are tangential to the magnetopause so that the left-hand hodogram shows the rotational behavior of the tangential field $\underline{B}_t = (B_y\hat{\underline{e}}_y + B_z\hat{\underline{e}}_z)$.

We observe three subsegments in this crossing, denoted by I, II and III, where a substantial amount of magnetic noise is present. By direct inspection, it is evident that the noise is not isotropic: the amplitudes in the direction along the tangential hodogram trace and in the B3 direction are much larger than those in the direction perpendicular to the tangential hodogram trace. Since the electric current in a rotational discontinuity is directed essentially perpendicular to the tangential hodogram trace (i.e., it is approximately radial in the left-hand hodogram), it is evident that the magnetic perturbation along the current direction is small for each

subsegment, a result that agrees with the constancy of B_y in the tearing mode model of Figure 1. Since the normal field component is different from zero, the tearing, if it is locally active, should be of the ion type. But we cannot exclude the possibility that tearing "debris", produced elsewhere, is being convected past the satellite. The ratio B_{ox}/B_{oz} is of the order of 0.2 which may be in the unstable range (compare (ii) in the previous section).

For each of the subsegments, I, II, III we have selected a local (y, z) coordinate system such that the fluctuation in B_y is a minimum. These local systems are shown in Figure 2. In each case, the third coordinate (x) remains along B3.

The orientation of the convection velocity vector $\underline{v}_{co}$ on the magnetosheath side of the layer is assumed to be tangent to the curve of intersection of the magnetopause surface and the plane containing the earth's center, the sun and the satellite. Within the magnetopause structure, the convection velocity is presumably directed somewhat differently and has different magnitude. If the magnetosheath plasma flows across the magnetopause, as one must assume for a rotational discontinuity, then the tangential velocity and magnetic field changes in the magnetopause are proportional, i.e., $\Delta\underline{v}_t = \pm\Delta\underline{B}_t/\sqrt{\mu_o\rho}$, where ρ is the mass density. The choice of sign depends on the sign of B3. For each of the subsegments in Figure 2, we have added a corresponding $\Delta\underline{v}_t$ to $\underline{v}_{co}$ (assuming v_{co} = 200 km/s and a density of 10 protons/cm^3) in order to obtain the local convection velocity $\underline{v}_c$. The orientations of $\underline{v}_c$ and the angle θ between $\underline{v}_c$ and the local z axis (section 2c) are shown in Figure 2. It is noted that in a few recent cases the velocity change $\Delta\underline{v}_t$ of the plasma has been directly measured. (Paschmann et al, 1979.)

Table 1 gives a summary of results of detailed analysis of the three subsegments. A Fast Fourier Transform (FFT) was made of the data for each field component of the subsegment, giving a discrete power spectrum whose points are multiples of the basic frequency $f_o = (N\tau)^{-1}$, where τ is the sampling interval and N the number of data points. Spectra of the three components for subsegment I are shown in Figure 3. The large peak at f_o in B_z and smaller peaks in B_x and B_y correspond to the shear in the magnetopause field across the layer. It is not of interest here. The other major peak, at .11-.1375 Hz in all components, contains essentially all of the power in the field oscillations evident in the hodogram. No other significant peaks appear up to the Nyquist frequency $f_N = (2\tau)^{-1} = 3.5$ Hz. The ratios of areas under the major peaks in the three components give the power ratios among the field components (see Table 1). For subsegment I the corresponding amplitude ratios are $|\tilde{B}_z|/|\tilde{B}_x|/|\tilde{B}_y| = 10/4.6/1.4$. The angle θ for segment I is about 40°, and the local convection speed is $v_c = 275$ km/s. Thus the inferred wavelength is

$$\lambda = v_c \cos\theta / f_{observed} = (275 \text{ km/s})(\cos 40°)/0.125 \text{ Hz} \simeq 1685 \text{ km}$$

When the observed amplitude ratio $|\tilde{B}_x|/|\tilde{B}_z| = 0.46$ is substituted into Eq. (5) there results

$$\ell \simeq 0.46/k = 0.46\lambda/2\pi \simeq 125 \text{ km}$$

The interpretation of this magnetopause substructure in terms of a tearing mode thus gives a realistic estimate for the scale length of the magnetic field shear in this portion of the layer. Similar calculations for subsegments II ($\theta \simeq 65°$, $v_c = 400$ km/s) and III

($\theta \simeq 80°$, $v_c = 455$ km/s) yield ℓ values of 60 km and 35-65 km, respectively (see Table 1).

None of the subsegments has significant phase coherence in the $B_x B_z$ plane so that no conclusion can be drawn from detailed comparison with the tearing-mode polarization structure described earlier in the paper.

4. Pioneer 11 Crossing on Nov 29, 1974 at 13:30 UT

This crossing of Jupiter's magnetopause is the last one on the inbound leg of the Pioneer 11 trajectory. This crossing too occurred a substantial distance away from the subsolar point: the solar-jovian latitude and longitude were 9.5°S and 44°W, respectively, and $R = 64.7 R_j$.

The hodogram of the crossing is shown in Figure 4. Except for the field magnitude, which is much lower in the jovian case, the overall features of this crossing are similar to the terrestrial crossing in Figure 2. The Jupiter magnetopause is a clear case of a rotational form with a nonzero normal field component and it contains several subsegments of magnetic fluctuations similar in character to those in Figure 2.

Table 1 gives results of the analysis of the subsegment I in Figure 4. These results show the presence of a mode of the same type as above, with a somewhat lower frequency, and a smaller amplitude, but similar ratio of amplitude to total field strength. In this subsegment there is also definite phase coherence between B_x and B_z, as shown in Figure 5. B_x generally leads B_z by $\frac{\pi}{2}$ during the whole subsegment, although clearly there are significant fluctuations in this relation, and especially complex behavior near the center of the subsegment. Although the time plot of Figure 5 might suggest

that the observer had passed through x = 0 near the middle of the subsegment, there is not an overall polarization antisymmetry, and the frequency is actually slightly higher in the second half of the subsegment. It is therefore probable that two separate structures, rather than the two sides of a single mode, are crossed here. This segment is nevertheless the clearest example we have yet found of the type of magnetic oscillation we are describing here.

For the segment I the local convection velocity $\underline{v}_c$, directed as shown in Figure 4, has a magnitude of 190 km/s and forms an angle $\theta \simeq 58°$ with the z axis of the local coordinate system. In obtaining these results we used v_c = 200 km/s and a density of 2 protons/cm^3. Performing the same calculation as before we then find the wavelength $\lambda \simeq 1680$ km and the shear length $\ell \simeq 170$ km. These numbers appear somewhat too small when compared to an estimated thickness of Jupiter's magnetopause of ~4000 km (Tsurutani et al, 1979). However, it should be remembered that ℓ is associated with the width of the substructures, and not with the total magnetopause thickness.

Other segments of this crossing also show magnetic oscillations of the same character, in the frequency range .03-.1 Hz, but have several superposed frequencies, or are very short intervals, so they are not examined in detail.

5. Discussion

An important common feature of the four data segments we have analyzed is that the z axis of the local coordinate system, chosen for minimum variation in B_y, is always approximately perpendicular to the local tangential field direction at the time of observation of the magnetic oscillations. This means that, although we have not

found evidence of actually crossing the $\underline{k} \cdot \underline{B} = 0$, i.e. the $x = 0$, plane of any of the structures, the oscillations, if produced by tearing, are all observed fairly close to that plane. It is a basic feature of the tearing perturbations that they decay exponentially with increasing distance away from $x = 0$. Thus they should be easily observable only relatively near $x = 0$.

Examination of five other OGO-5 crossings has shown more than twenty subsegments of large amplitude oscillations similar to those described here. The local coordinate system for each subsegment is always such that the z axis is nearly perpendicular to the local field.

Although we have not been able to show clear evidence of the polarization behavior (Fig. 1) associated with tearing-mode magnetic islands it appears that the observed oscillations are consistent with tearing in the following ways:

i) The magnetic oscillations are very nearly two-dimensional with virtually no oscillations in the B_y component.

ii) The observations are comparable with the hypothesis that the oscillations are confined to a relatively narrow region about the $\underline{k} \cdot \underline{B} = 0$ plane.

iii) The oscillations fall in a frequency range (0.05-0.4 Hz) which, with typical magnetopause convection velocities, gives reasonable inferred values of the wavelength.

iv) The ratio of the amplitudes of the two oscillating field components is consistent with reasonable values of the shear length ℓ which is representative of the thickness of the tearing substructures.

Two alternative interpretations should be mentioned. First, oscillatory radial motion of the magnetopause would produce B_z oscil-

lations in a local coordinate system with its z axis perpendicular to the local tangential field. But it would not generate an associated oscillation in the normal component B_x. This latter objection may be removed in a second model in which the radial oscillation is the result of small amplitude wave motion of the entire magnetopause, with the wave vector $\underline{k}$ having a substantial component along the local tangential field in the magnetopause. Without actual observations of the polarization reversal at $x = 0$ in the tearing mode it is not easy to discriminate between tearing structures and this type of wave motion. However, if the wave propagation direction $\underline{k}$ remains fixed (along $\underline{v}_{co}$ say), the wave model predicts that the amplitude of the B_x oscillation should be a maximum for subsegments where the local magnetic field is parallel to $\underline{k}$. No such effect is seen either in Figure 2 or 4. Thus we feel that the tearing mode interpretation is stronger than the wave interpretation for the cases analyzed here. However, study of a much larger number of events is required in order to discriminate in a reliable way between the two possibilities.

It also remains possible that some other instability or wave motion might be responsible for these magnetic oscillations. Progress must be made in the theory of both tearing and other instabilities and wave modes in strongly sheared, thin collision-free current layers with plasma flow, as well as in the observations of such structures at planetary magnetopauses, before definite conclusions may be drawn. The most important observational improvement will be simultaneous measurements from separated points in space, which the ISEE mission is now providing. Independent and unambiguous information about the magnetopause thickness and other basic parameters will be important

in deciding among possible modes. In particular, the growth of tearing modes is controlled by the layer thickness (the shear length ℓ) and by the size of the normal component. Since it is somewhat unlikely that sufficiently clear signatures of phase and polarization will be found to permit of an unambiguous identification of the mode, correlation of its occurrence with magnetopause parameters may be the strongest evidence that can be added toward identification.

In summary, we have shown evidence of the existence of a particular two-dimensional low-frequency oscillation of the magnetic field in the dayside magnetopause current layer of the earth and of Jupiter. This oscillation has been shown to be consistent, in its location, orientation, amplitude and frequency with our present understanding of the tearing mode. However, the tearing mode interpretation is not necessarily unique.

Acknowledgement

The authors thank Brian G. Ledley of the Goddard Space Flight Center for use of the OGO-5 data and Edward J. Smith of the Jet Propulsion Laboratory for use of the Pioneer 11 data. The research was supported by the National Aeronautics and Space Administration under grant NSG 7292 and by the National Science Foundation under grant ATM 74-08223 A01 to Dartmouth College.

References

Aubry, M.P., M.G. Kivelson, and C.T. Russell, Motion and structure of the magnetopause, J. Geophys. Res. 76, 1673, 1971.

Baker, D.N., and E.C. Stone, The magnetopause electron layer along the distant magnetotail, Geophys. Res. Lett. 4, 133, 1977.

Biskamp, D., R.Z. Sadeev, and K. Schindler, Nonlinear evolution of the tearing instability in the geomagnetic tail, Cosm. Electrodyn. 1, 297, 1970.

Dickman, D.O., R.L. Morse, and C.W. Nielson, Numerical simulation of axisymmetric collisionless finite-β plasma, Phys. Fluids 12, 1708, 1969.

Drake, J.F., and Y.C. Lee, Kinetic theory of tearing instabilities, Phys. Fluids 20, 1341, 1977.

Galeev, A.A., Reconnection in the magnetotail, Space Research Institute, Academy of Sciences, USSR, Report D-260, 1978.

Galeev, A.A., and L.M. Zeleny, Magnetic reconnection in a space plasma, in Theoretical and Computational Plasma Physics, International Atomic Energy Agency, Vienna, p. 93, 1978.

Galeev, A.A., F.V. Coroniti, and M. Ashour-Abdalla, Explosive tearing mode reconnection in the magnetospheric tail, Geophys. Res. Lett. 5, 707, 1978.

Huba, J.D., N.T. Gladd, and K. Papadopoulos, The lower-hybrid-drift instability as a source of anomalous resistivity for magnetic field line reconnection, Geophys. Res. Lett. 4, 125, 1977.

Killeen, J., and A.L. Shestakov, Effect of equilibrium flow on the resistive tearing mode, Phys. Fluids 21, 1746, 1978.

Meng, C.-I., and K.A. Anderson, A layer of energetic electrons (E > 40 keV) near the magnetopause, J. Geophys. Res. 75, 1827, 1970.

Paschmann, G., B.U.Ö. Sonnerup, I. Papamastorakis, N. Sckopke, G. Haerendel, S.J. Bame, J.R. Asbridge, and C.T. Russell, Plasma acceleration at the magnetopause: evidence for reconnection, Preprint, Max Planck Inst. Extraterr. Phys., Garching, 1979.

Pellat, R., About "Reconnection" in a collisionless plasma Report PPG-370, Center for Plasma Physics and Fusion Engineering, U. Cal. Los Angeles, 1978.

Rutherford, P.H., Nonlinear growth of the tearing mode, Phys. Fluids 16, 1903, 1973.

Schindler, K., A theory of the substorm mechanism, J. Geophys. Res. 79, 2803, 1974.

Sonnerup, B.U.Ö., Magnetopause and boundary layer, in Physics of Solar-Planetary Environments, D.J. Williams ed., Am. Geophys. Union, p. 541, 1976.

Sonnerup, B.U.Ö., and L.J. Cahill, Magnetopause structure and attitude from Explorer 12 observations, J. Geophys. Res. 72, 171, 1967.

Sonnerup, B.U.Ö., and B.G. Ledley, Magnetopause rotational forms, J. Geophys. Res. 79, 4309, 1974.

Sonnerup, B.U.Ö., and B.G. Ledley, Electromagnetic structure of the magnetopause and boundary layer, Proc. Chapman Conf. on Magnetospheric Boundary Layers, Alpbach, Austria, 1979.

Tsurutani, B.T., E.J. Smith, J.H. Wolfe, and B.U.Ö. Sonnerup, Structure of Jupiter's magnetopause, Proc. Chapman Conf. on Magnetospheric Boundary Layers, Alpbach, Austria, 1979.

White, R.B., D.A. Monticello, M.N. Rosenbluth, and B.V. Waddell, Saturation of the tearing mode, Phys. Fluids 20, 800, 1977.

Willis, D.M., Structure of the magnetopause, Rev. Geophys. Space Sci. 18, 953, 1971.

Willis, D.M., The microstructure of the magnetopause Geophys. J. R. Astr. Soc. 41, 355, 1975.

Willis, D.M., The magnetopause: microstructure and interaction with magnetospheric plasma, J. Atm. Terr. Phys. 40, 301, 1978.

Table 1. Frequency and wavelength information for three OGO-5 data segments and one Pioneer 11 segment.

Segment	Duration (sec)	$f_o=(N\tau)^{-1}$ Hz	Spectral peaks (f f_o)Hz B_x	B_y	B_z	Peak amplitude $\|B_z\|$nt	Power in spectral peaks $B_z:B_x:B_y$	Inferred λ (km)	Inferred ℓ (km)
OGO-5 I	36.6	0.0275	0.11-0.1375	0.1375	0.11	10-15	10:2.1:0.2	1685	125
OGO-5 II	18.3	0.055	0.16	0.22	—	10	10:1.5:<0.1	1055	65
OGO-5 III	36.6	0.0275	0.11 and 0.165	0.11 and 0.165	0.11	5	10:3:1.1	720	65
					—		10:2:<0.1	480	35
Pioneer 11 I	96	0.01	0.06	0.06	0.06	1.5-2	10:4:0.4	1680	170

Figure Captions

Fig. 1. Schematic representation of tearing mode perturbation. Central x = 0 ($k \cdot B = 0$) plane is shown by dotted line. Diagonal dotted line represents path of a spacecraft crossing the layer as the structure is convected past it. Plots of B_z vs B_x indicate polarizations of oscillations which would be observed at the fixed x positions indicated. $\tilde{A}$ is the vector potential.

Fig. 2. Polar (hodogram) representation of OGO-5 magnetopause crossing. The left hand diagram shows the behavior of the magnetic field components B1 and B2 tangential to the magnetopause; the right-hand diagram shows the normal component B3. The axes are the principal axes obtained from minimum variance analysis and shown in GSM coordinates in lower left-hand corner. Three subsegments, I, II, and III, of field oscillations are present. For each of these local x, y, z coordinate system, corresponding to the one in Figure 1 is identified. Also shown is the local convection velocity vector and angle θ for each subsegment.

Fig. 3. Fast Fourier transform power spectra of the three components for OGO-5 segment I. Vertical scale is arbitrary, horizontal scales are in units of .11 Hz. All spectra continue to decrease beyond the frequency range shown, up to the Nyquist frequency at 3.5 Hz.

Fig. 4. Hodogram representation of Pioneer 11 crossing of Jupiter's magnetopause. See Figure 2 for details. The principal axes are given in the solar jovian (SJ) system.

Fig. 5. B_z (solid line) and B_x (dashed line) oscillations for a 150 sec. interval of the crossing of Jupiter's magnetopause. Polar plots are for the three subintervals indicated.

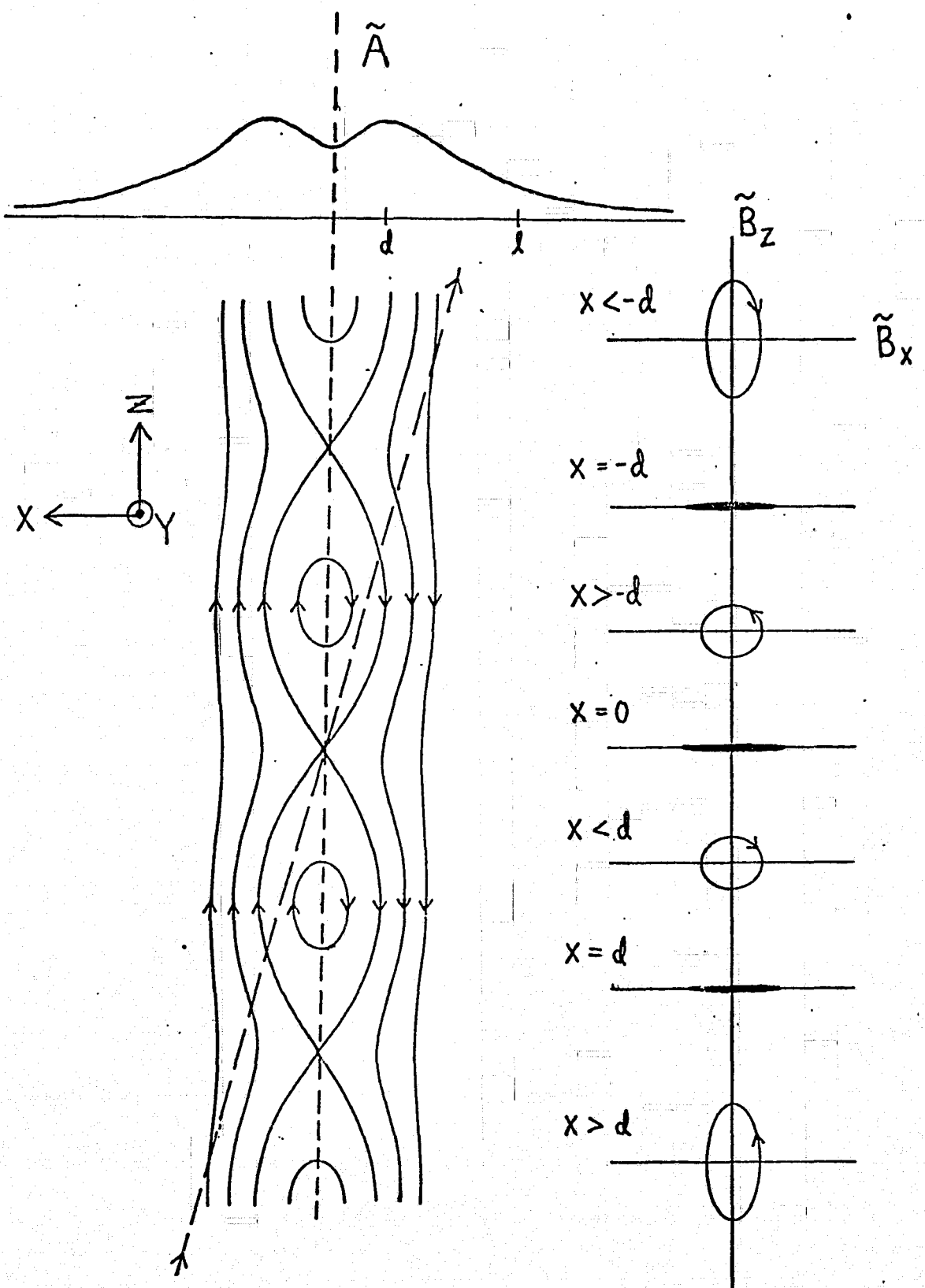

Fig. 1

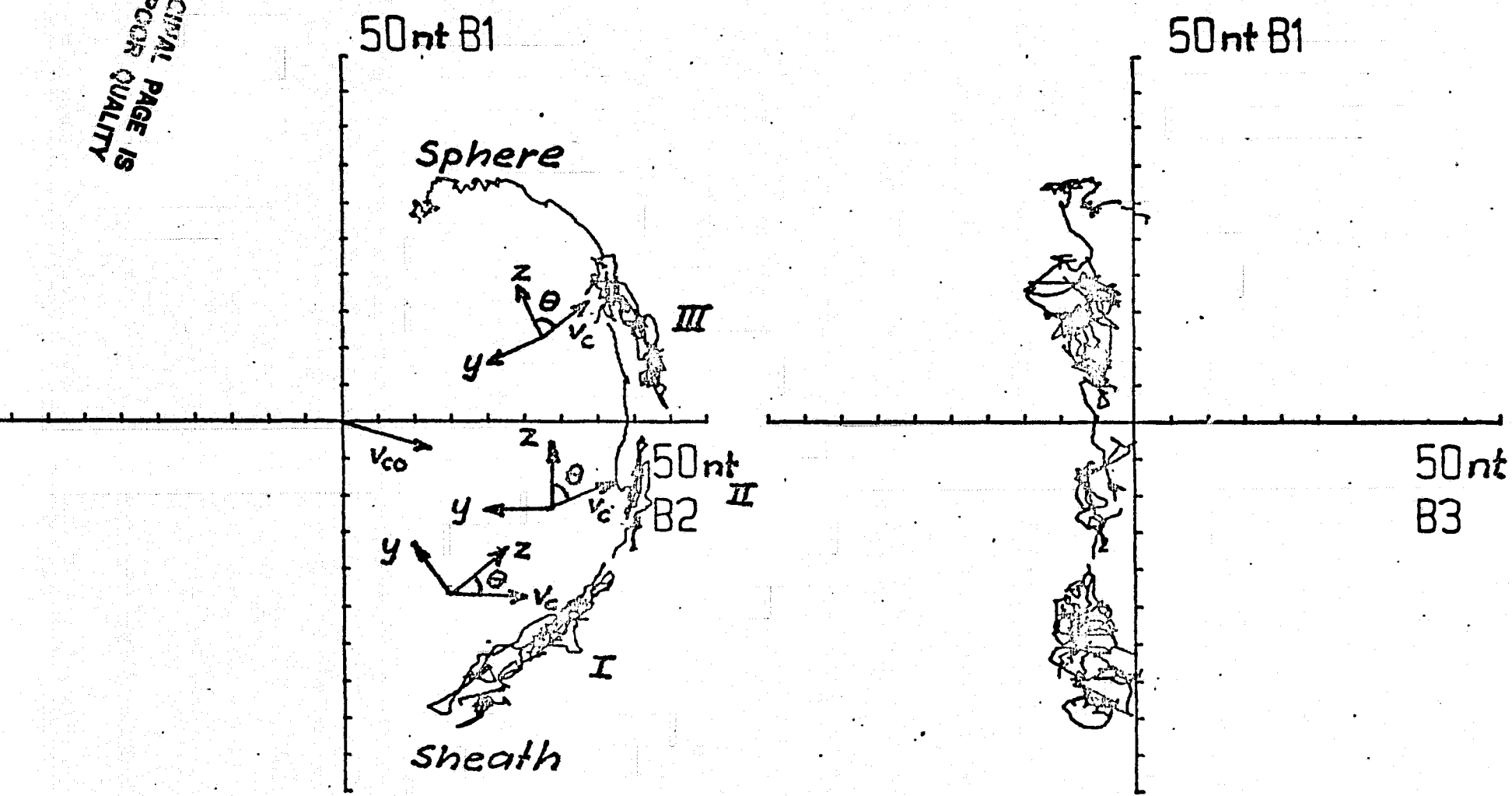

68 03 10 02:20:44:411 UT (8462123 - 8603965)

N1X N1Y N1Z : 0.1987 0.6319 0.7491
N2X N2Y N2Z :-0.6137 -0.5157 0.5978
N3X N3Y N3Z : 0.7641 -0.5785 0.2854

POINTS 120 - 1072 7 SPS/ 1

Fig. 2

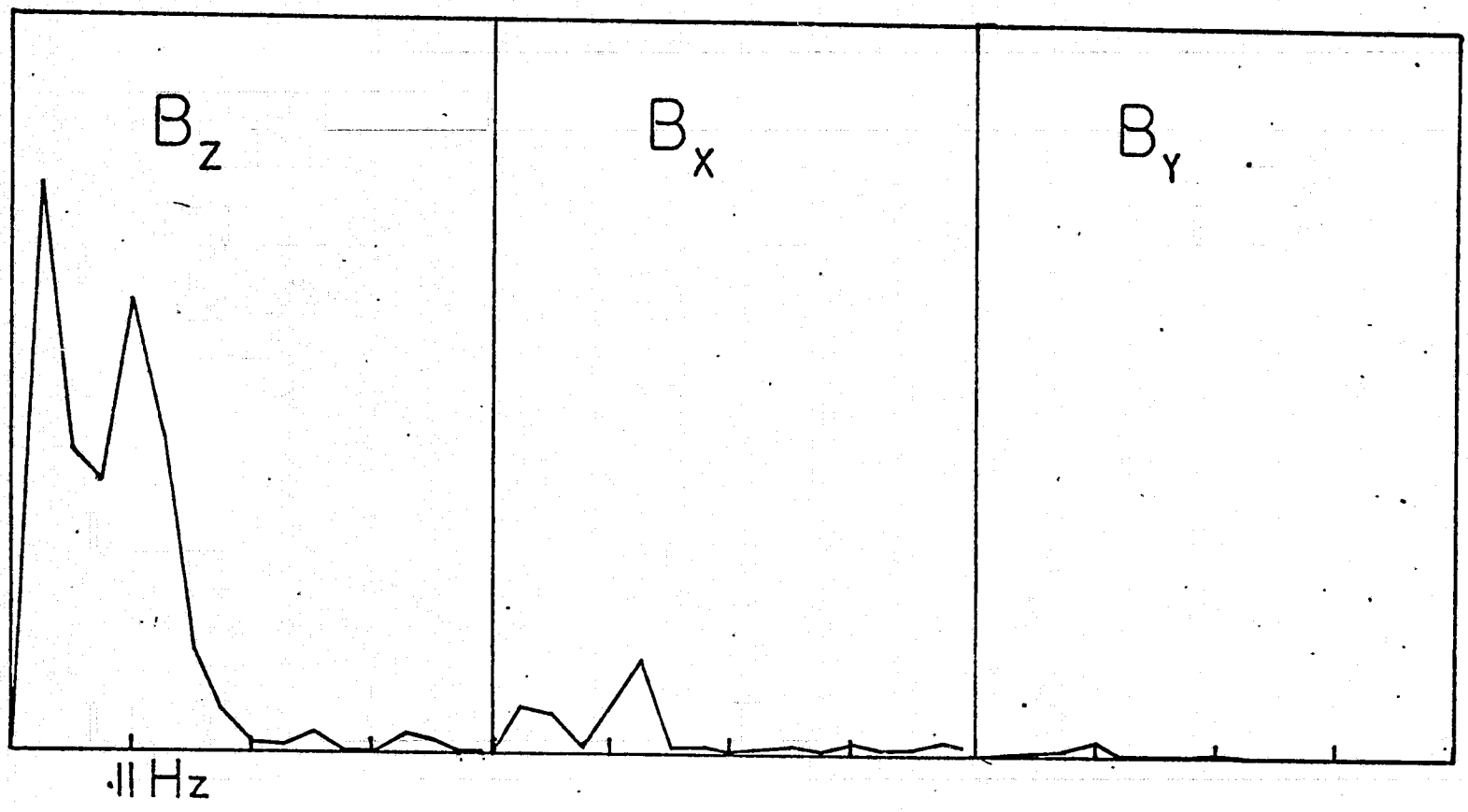

Fig. 3

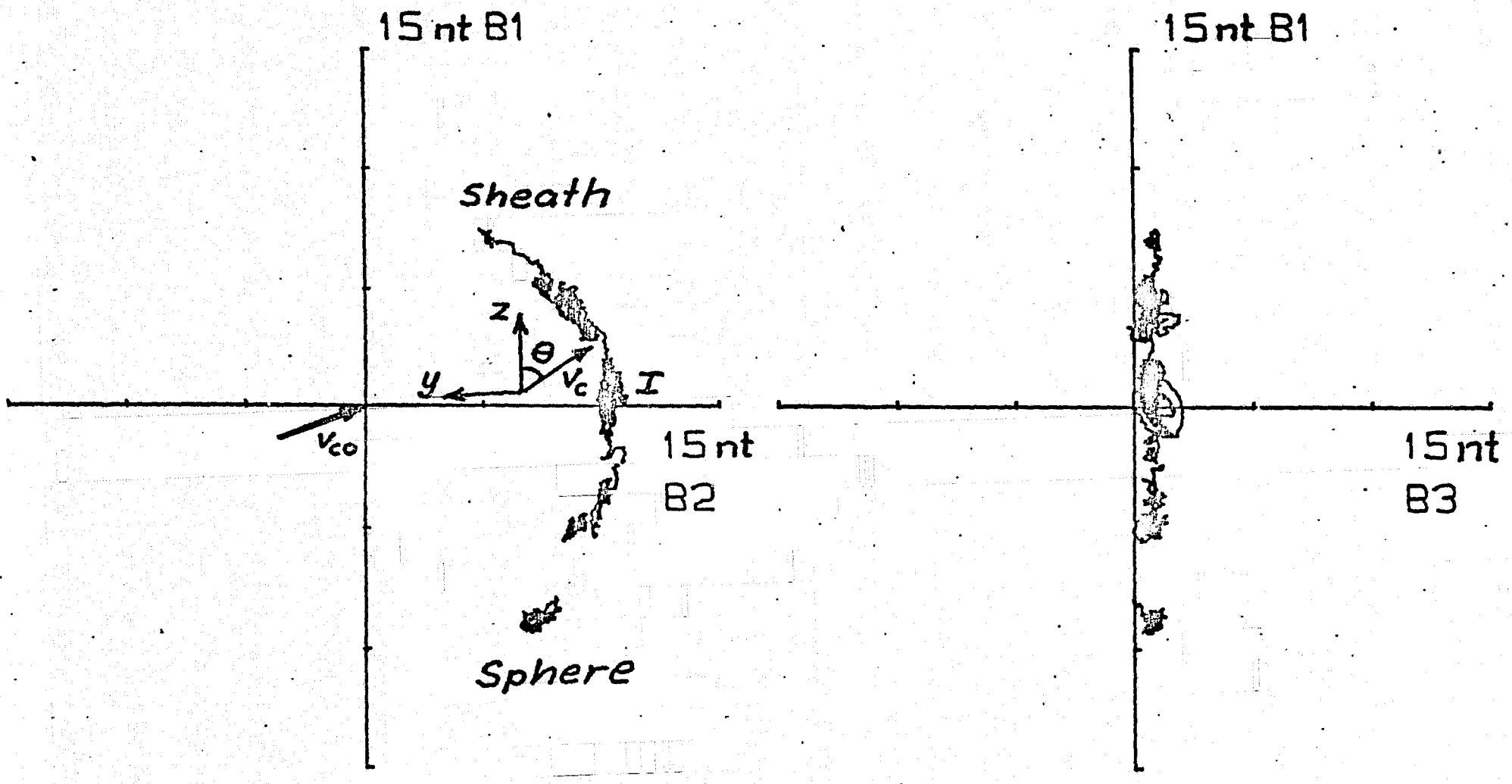

74 11 29 13:30:18.310 UT (48618310 - 49800088)

N1X N1Y N1Z :-0.0941 -0.6064 0.7896
N2X N2Y N2Z :-0.5213 -0.6457 -0.558
N3X N3Y N3Z : 0.8482 -0.4641 -0.2553

POINTS 0 - 4490 5.3 SPS/ 1

Fig. 4

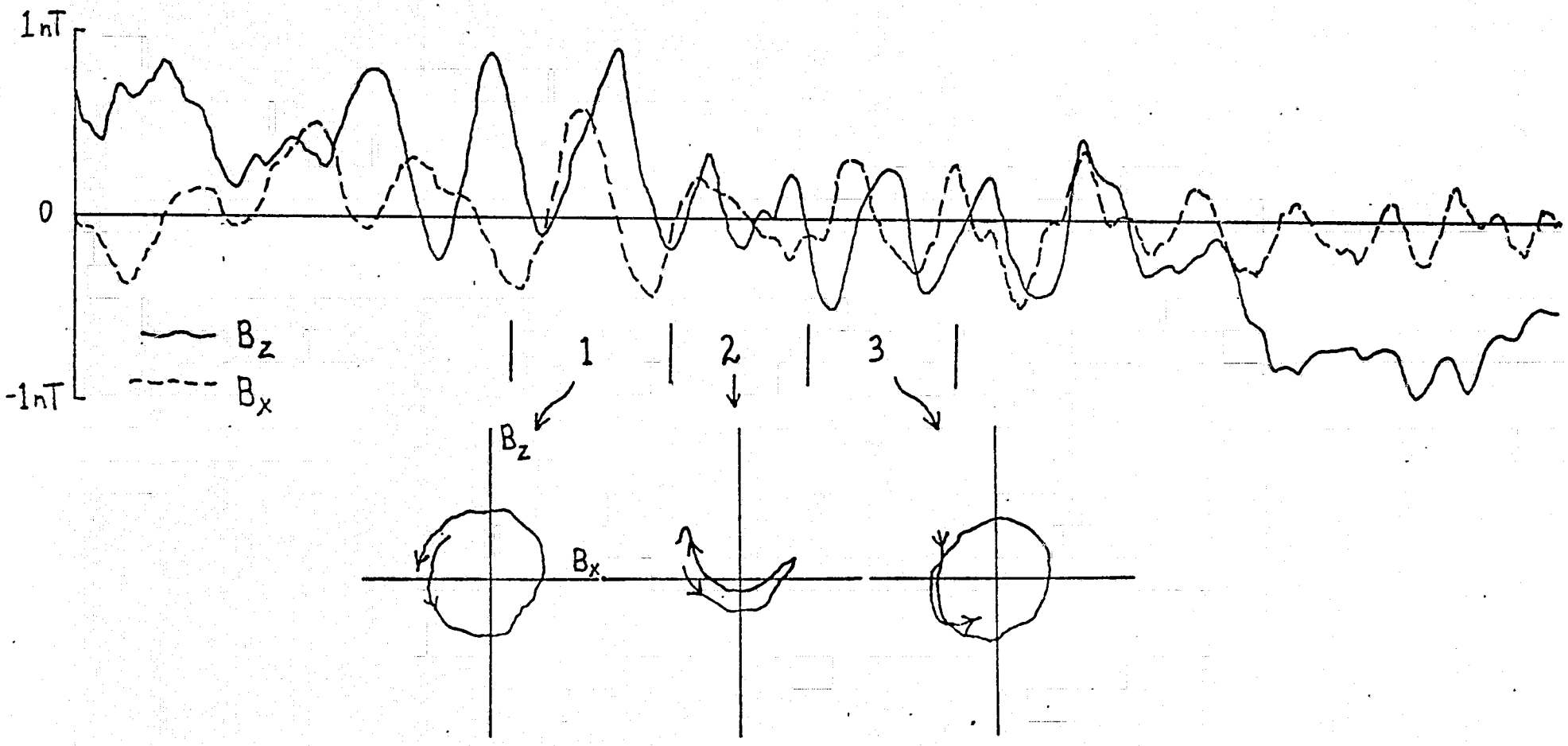

Fig. 5